Synthesis of Fluorescent Probes for Specific Recognition and Imaging Applications

Thesis Submitted to AcSIR for the Award of the Degree of

DOCTOR OF PHILOSOPHY

In Chemical Science

(Academy of Scientific and Innovative Research)

By

Anila H A

(Reg.No. 10CC14J26001)

Under the guidance of

Dr. Amitava Das

CSIR-National Chemical Laboratory
Pune, Maharashtra, India– 411008

February 2018

Dedicated

To

My Parents

And

Prof. A M Starwin

CANDIDATE'S STATEMENT

I hereby declare that the work incorporated in the present thesis is original and it has not been submitted to any University/Institution for the award of a Diploma or a Degree. Research material obtained from other sources has been duly acknowledged in the thesis. I further declare that the results presented in the thesis and the considerations made therein, contribute in general to the advancement of knowledge in Chemistry and in particular to "**Synthesis of Fluorescent Probes for Specific Recognition and Imaging Applications**".

Anila H A

CERTIFICATE

This is to certify that the work incorporated in this Ph.D. thesis entitled "**Synthesis of Fluorescent Probes for Specific Recognition and Imaging Applications**" submitted by **Mr. Anila H A** to Academy of Scientific and Innovative Research (AcSIR) in fulfillment of the requirements for the award of the Degree of Doctor of Philosophy embodies original research work under my supervision. I further certify that this work has not been submitted to any other University or Institution in part or full for the award of any degree or diploma. Research material obtained from other sources has been duly acknowledged in the thesis. Any text, illustration, table etc., used in the thesis from other sources, have been duly cited and acknowledged.

Student

Supervisor
Amitava Das

Acknowledgements

*I would like to express my gratitude to my research supervisor **Dr Amitava Das**. I am extremely grateful to him for his continuous encouragement and motivation. His sincerity and hard work have deeply inspired me. I greatly appreciate the freedom he gave to me to find my own path and the support he offered whenever I needed the most.*

*I would like to thank **Prof. A M Starwin**, one of the best Chemistry teachers I have ever had. He taught me the Chemistry in a simple and clear way, without him, I couldn't have reached this level.*

*I wish to convey my sincere thanks to **Dr Andrey Klymchenko** from the University of Strasbourg who supported my application for Raman-Charpak fellowship and hosted me at Strasbourg for six months.*

*I wish to thank our collaborators **Dr Samit Chattopadhyay,** from the Indian Institute of Chemical Biology, **Prof. Jim A Thomas** and **Prof. Carl G Smythe** from the University of Sheffield for fruitful discussions on research problems, appreciative comments. I thank them for providing the access to the cell culture and microscopy facilities.*

*I wish to express my sincere thanks to my doctoral advisory committee members **Dr D Srinivasa Reddy, Dr H V Thulasiram, Dr Shafeek A R Mulla,** and **Dr S Mayadevi** (former advisory committee member) for their time and insightful questions.*

*I am grateful to **Dr Ashwini K Nangia (**Director, NCL), **Dr Sourav Pal** (Former Director, NCL), **Dr Subhash P Chvan** Head, Division of Organic Chemistry and **Dr Pradeep Kumar Tripathi** (Former Head, Organic division) for providing me the opportunity and all the necessary facilities to carry out my research work.*

*My sincere thanks to **Dr Santhosh B Mhaske, Dr Santhosh Babu Sukumaran, Dr Sakya Singha Sen**, **Dr R. A. Joshi,** and all other scientists of NCL for their motivation, constant encouragement and support.*

*I would like to express my special thanks to my seniors and post doctoral fellows of my lab **Dr Gandra Upendar Reddy**, **Dr Vadde Ramu** and **Dr Hridesh Agarwalla**, **Dr Praveen L., Dr Sovan Roy**, they all helped me in the initial days of my research carrier.*

*I am fortunate enough to have a wonderful group of colleagues **Dr Suman Pal, Dr Ajoy Pal, Dr Shilpi Kushwaha, Dr Ketan Patel, Dr Monalisa, Dr Firoj, Arunava, Sunil, Ananta, Koushik and Sanjukta** with whom I worked all these four years. Each one of them equally contributed in different way to take up my course so fruitfully throughout these four years. I thank all of them individually from the bottom of my heart.*

*I am extending my thanks to the master students **Jayesh**, **Pavan Kumar** and **Riyanka** whom I co-mentored for their master's project.*

Acknowledgement

*My Sincere thanks to my friends and collaborators **Dr Nandaraj Taye** and **Mohsina Khan** from the National Centre for Cell Sciences and **Sreejesh Sreedharan** from the University of Sheffield. They helped me with imaging and bio studies.*

*I am grateful to **Dr Ashok Kumar** from the University of Strasbourg who gave me hands on training on the cell culture and microscopy handling. Thanks for your time and patience. I also thank **Dr Mayeul Collot** who taught me some of the key synthesis and purification techniques.*

*My sincere thanks to **Dr Philippe Chabert,** who provided a space in his lab to carry out some synthesis work. A special thanks to him for the wonderful weekend trekking.*

*I wish to thank **UGC** for funding and **AcSIR** for allowing me to submit my work in the form of thesis. I am also grateful to **CEFIPRA** for Raman-Charpak fellowship, which allowed me to carry out a part of my PhD research at the University of Strasbourg.*

*I wish to convey my thanks to AcSIR coordinators **Dr M Shashidhar**, **Dr Mahesh Kulkarni**, and student academic office staffs, **PV Iyer**, **Kohle**, **Vaishali**, **Komal** and **Purnima** for their help and cooperation. I also thank **Catherine** from the Organic Division for her continuous help and support.*

*My time at CSIR-NCL was made enjoyable due to many friends. My sincere thanks to my former roommates **Mr. Krishnaprasad** and **Mr. Vijay Koshti** and of course to all my NCL friends for their support and to make my journey joyful and a memorable one.*

*I am extremely thankful to my beloved friend **Goudappagouda** with whom I spent a lot of time in these four years. Thanks for many unforgettable memories. I also wish to thank some of my best friends **Dr Prashanth**, **Dr Sangeetha**, **Chidananda**, **Madhu**. You guys keep on giving the moral support for me for more than eight years.*

*I wish to thank a wonderful bunch of friends and colleagues from Strasbourg, **Dr Krishna**, **Dr Jagannath**, **Dr Adarsh**, **Dr Koteeshwari**, **Dimitro**, **Kyong**, **Nina**, **Bilal**, **Asad**, **Wahid**, **Kamal** for many unforgettable moments.*

*At this moment, I invariably feel short of words to express my sincere thanks to My Grand Parents **Thimmappaiah** and Late **Katyayini**, my father **Ashok** and my beloved mother **Nirmala** for all the sacrifices you have made on my behalf. I am thankful to my sister **Shruthi** for her love and support. I would like to thank all my extended family members for their continuous encouragement and support in completion of this tough task.*

*It is a privilege for me to thank my best friend **Medhashree Bhat**. Thanks for being with me in all the ups and downs of my research career. I am extremely grateful to you for your support and thanks for your time and patience in reading my thesis.*

I am also thankful to Almighty God for all your blessings to me and for the strength you give me each day.

Anil

List of abbreviations

CD_2Cl_2	Deuterated dichloromethane
$CDCl_3$	Deuterated chloroform
CD_3OD	Deuterated Methanol
DMSO-d_6	Deuterated Dimethyl sulfoxide
CD_3CN	Deuterated acetonitrile
DMF	N,N'-dimethylformamide
DMSO	Dimethyl sulfoxide
THF	Tetrahydrofuran
ACN	Acetonitrile
ESI	Electrospray Ionization
ET	Energy Transfer
HOMO	Highest Occupied Molecular Orbital
LUMO	Lowest Unoccupied Molecular Orbital
CT	Charge Transfer
ICT	Intramolecular Charge Transfer
TICT	Twisted Intramolecular Charge Transfer
PET	Photo-induced Electron Transfer
ESIPT	Excited State Intramolecular Proton Transfer
ESICT	Excited State Intramolecular Charge Transfer
FRET	Fluorescence Resonance Energy Transfer
NIR	Near Infrared

List of abbreviations

HEPES	4-(2-hydroxyethyl)-1-piperazineethanesulfonic acid
NMR	Nuclear Magnetic Resonance
FTIR	Fourier Transform Infrared
MTT	3-(4,5-dimethylthiazol-2-yl)-2,5-diphenyltetrazolium bromide
CLSM	Confocal Laser Scanning Microscope
LRMS	Low Resolution Mass Spectrometry
HRMS	High Resolution Mass Spectrometry
HPLC	High Performance Liquid Chromatography
SIM	Structured Illumination Microscopy
SRM	Super-Resolution Microscopy
ACY-1	Aminoacylase-1
QY	Quantum Yield
LUV	Large Unilamellar Vesicle
GUV	Giant Unilamellar Vesicle
DOPC	1,2-Dioleyl-*sn*-glycero-3-phosphocholine
SM	Sphingomyelin
PBS	Phosphate Buffer Saline
NEM	N-ethylmaleimide
NAC	N-acetylcystiene
BSO	L-Butathionine-sulfoximine

CHAPTER 1

INTRODUCTION

FLUORESCENT PROBES - A tool box to unravel the hidden facts

Small molecules as synthetic dyes are the indispensable tools for detection and visualization of various analytes in biological systems in real time. Followed by the discovery of the first synthetic dye, mauvine in 1856 by William Perkin, vast majorities of synthetic chromophore were discovered and currently been used in many fields.[1,2] Fluorescence-based detection and imaging require fluorescent tools, so-called fluorescent probes. The major building block of a probe is a signaling unit, a dye. The principal feature of the fluorescence-based technique is its compatibility with living systems. The standard analytical methods like high-performance liquid chromatography (HPLC), titrimetry, voltammetry, potentiometry, etc., could only be used for the in vitro analysis. Most of these methods require long analysis time, sample derivatization. Moreover, these analytical instruments are quite expensive and need expertise handling.

In view of these limitations, fluorescence based methods gained more attention because of the simplicity and its ability to light up the biological objects. All the chemical species undergo certain transformations or changes within the biological milieu. An ideal strategy to monitor such transformations is by developing fluorescent probes to recognize the species of interest in the complex biological environment by exploiting the difference in the reactivity. Such reaction based approach provides specificity without altering the biological activity of cells and tissues of the living organisms.[3]

The biologists now have a spectrum of fluorophores for visualizing and tracking the biological transformations. Development of the modern microscopy techniques like two-photon, super-resolution microscopy revolutionized the application of fluorophores in imaging. In the same way, the demand for the more photostable and brighter dyes to meet the ‘photon budget’ (the number of fluorophores in each sample multiplied by the number of photons emitted by each fluorophore before photobleaching) requirement of the modern microscopy techniques is rapidly increasing.[1,2] Only the chemists can fulfill the demand by the application of modern synthetic methods.

The aim of this thesis is to develop new fluorescent probes to address some of the fundamental issues related specific analyte detection as well as imaging by the applying modern synthetic methods. Much emphasis has been paid to improve the

optical properties of the fluorophores in order to meet the requirements of the modern microscopic techniques. In addition to this, much attention is given to the probe design in order to achieve higher selectivity and sensitivity.

1A. Synthetic small molecule probes for Cysteine

1A.1. Introduction

Cysteine (Cys), a sulphur containing amino acid plays many important roles in living organisms. It is frequently found in the majority of the proteins, wherein it is involved in the structural modification of proteins through the formation of intra and inter-chain disulfide bonds between the protein chains.[4] Along with glycine and glutamine, Cys is one of the main precursors required for glutathione (GSH) synthesis; the latter is crucial for providing the redox immunity to human physiology.[5] It is also involved in redox signaling through the formation of sulfenic acid intermediates and mixed disulfides.[5] Any abnormality in Cys level is closely related to many diseases. For example slow growth in children, depigmentation of hair, edema, skin lesions etc. are due to the deficiency of Cys. Whereas, the elevated level is responsible for neurotoxicity and cardiovascular diseases.[6]

Owing to the biological and clinical importance of this small molecule thiol, it is not surprising that there has been immense interest in developing novel reagents and methodologies for the detection and quantification of Cys level in biological fluids. Methods like high-performance liquid chromatography (HPLC), mass spectrometry, and electrophoresis were reported for the detection and quantification.[5,6] However, these methods have many limitations such as derivatization of the samples, long running time, involvement of expensive instruments and skilled manpower, etc. Moreover, these techniques are only limited to in vitro studies.[6]

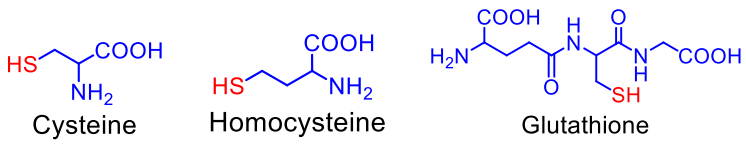

Figure 1A.1. Molecular structures of Cys, Hcy, and GSH.

In this context, fluorescence based methods offer many advantages such as high speed, cost-effective, operational simplicity, and most importantly biocompatibility. So, the development of optical probes for thiols has become an active area of

research in the recent years. However, the development of the probes for the discrimination among biothiols such as Cys, Homocysteine (Hcy) and GSH is challenging owing to the structural similarities (Figure 1A.1). All the three biothiols have –SH functionality and give the similar type of reactions.

Since these biothiols play different roles in various crucial biological processes, selective discrimination among these biothiols is crucial. For the past two decades, significant effort has been put forward by many research groups to develop specific probes to discriminate among these biothiols. A spectrum of new probes with different sensing mechanisms has been reported in recent years. This chapter focuses on the small molecule probes that are developed for the detection and quantification of Cys. The discussion in this dissertation will be limited to design strategies and their interesting biological applications.

1A.2. Various probes for Cysteine

1A.2.1. Probes based on conjugate addition and cyclization with acrylates

Conjugate addition of Cys to acrylates was known since 1966, for the synthesis of 1,4 thiazepines.[7] This reaction involves 1,4 addition by -SH group of Cys to acrylate to form thioether, then it cyclises to form 7-membered, substituted 1,4 thiazepines. This strategy was successfully exploited by Strongin's group to develop a new sensing methodology for Cys. The general mechanism is shown in Figure 1A.2. Initially, the photoinduced electron transfer (PET) involving the dye moiety as donor and alkene moiety as an acceptor would account for the observed quenching of the fluorescence. Conjugate addition of Cys to acrylate followed by cyclization nullifies the possibility of such a PET process and this account for the observed turn-on fluorescence response (Figure 1A.2). As shown in the Figure 1A.2, PET is an excited state electron transfer process in which the excited electron is transferred from the electron rich donor to the electron deficient acceptor and causes fluorescence quenching. In the case of Hcy and GSH, conjugate addition is possible. However, the relative rate of the subsequent intramolecular cyclization is very slow. Moreover, Hcy forms an 8-membered cyclic product, which is thermodynamically unstable. While GSH, being a tripeptide does not have the adjacent free amine functionality to participate in the cyclization reaction. So, this strategy provides absolute selectivity to Cys.[8] Subtle changes in the pK_a values for these biothiols could also contribute to the observed differences in the reactivity towards an acrylate derivative.

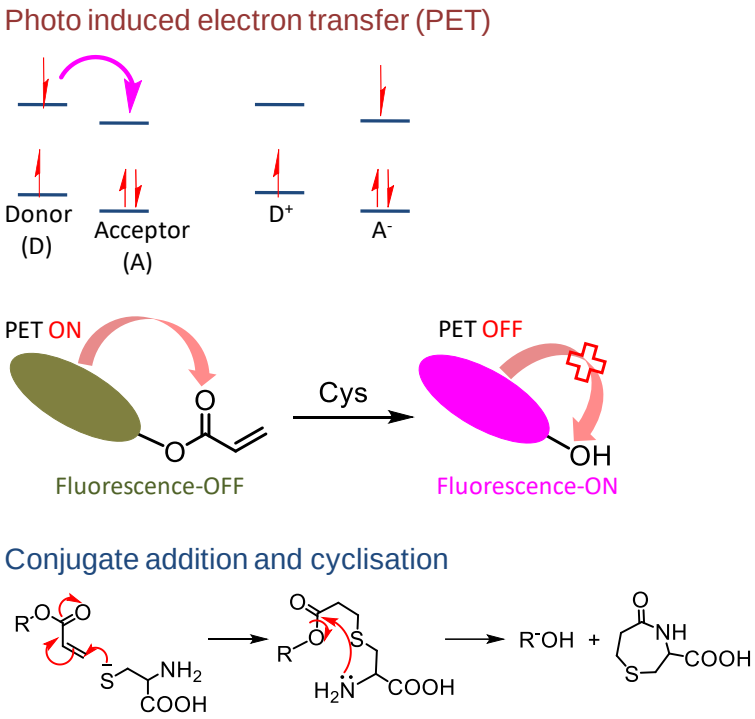

Figure 1A.2. The general mechanism of conjugate addition and cyclization and PET mechanism responsible for quenching in acrylate based probes.

Strongin and co-workers in their pioneering work designed a dual emissive excited state intramolecular proton transfer (ESIPT) probe **1**.[8] The hydroxyl group of the parent fluorophore was masked by acrylate moiety that blocks the ESIPT process and emission was observed only from the enol-like form. Upon addition of Cys, the emission band at 377 nm was found to bleach with concomitant growth of a new emission band at 487 nm, which was attributed to the generation of the corresponding keto form. Cys was subjected to nucleophilic addition to the acrylate moiety through conjugate-addition to form a thioether, which followed an intramolecular cyclization process to release the acrylate moiety with subsequent formation of the corresponding hydroxyl fluorophore that participated in the ESIPT process. This enabled the reagent to exhibit dual emission bands. In case of Hcy, this cyclization process is much slower, and reaction with Hcy would have resulted in the thermodynamically unfavourable 8-membered ring. Relative difference in the rates of intramolecular cyclization helped to distinguish Cys from Hcy.[8]

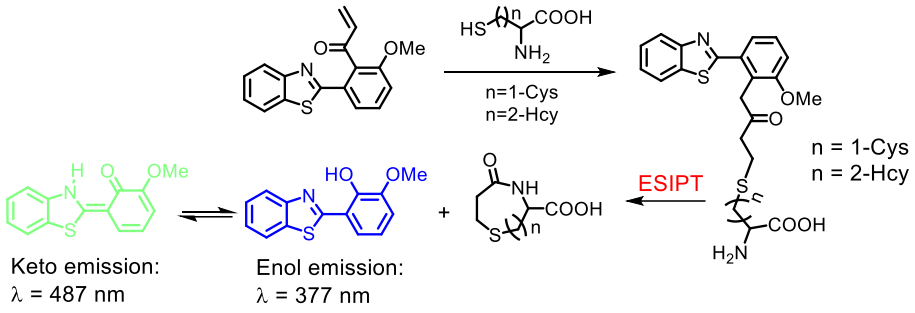

Figure 1A.3. Acrylate-based dual emissive ESIPT probe **1**. Cys forms a 7-membered thiazepine type ring. Whereas Hcy forms an 8-membered ring, which is slow and thermodynamically not favourable.

Organelle-specific probes are very important in biology to acquire the information about the analyte in the particular organelles. Das et al. reported a BODIPY-acrylate based probe ER-F, capable of detecting Cys in the endoplasmic reticulum (ER) region of the cells (probe **2**).[9] BODIPY emission was extended to the red region by the condensation of the acidic methyl group of the BODIPY core with electron-rich phenolic functionality. Hydroxyl group of the extended BODIPY was protected with acrylate moiety, which acted both as Cys recognition site as well as a moiety responsible for fluorescence quenching. Upon addition of Cys, acrylate functionality was cleaved and free hydroxyl compound was released, with subsequent fluorescence ON response. Reagent **2** was found to be specifically localised in ER regions of the cells and was used to detect the intracellular Cys distributed in the ER region of cells. Also, the probe was successfully utilized to develop simple and cost-effective test strips for the on-spot detection and quantification of Cys (Figure 1A.4) in human blood plasma.[9]

Molecular probes that are capable of mapping distribution of Cys in other organelles were also explored. Two NIR probes **3** and **4** were designed based on hemicyanine signalling moiety functionalized with acrylate for Cys recognition.[10,11] Probe **3** showed emission band at 735 nm whereas the probe **4** showed emission band at 697 nm. These two probes were specifically designed for targeting mitochondria. The cationic indolinium functionality in these probes was responsible for mitochondrial localization (Figure 1A.5).

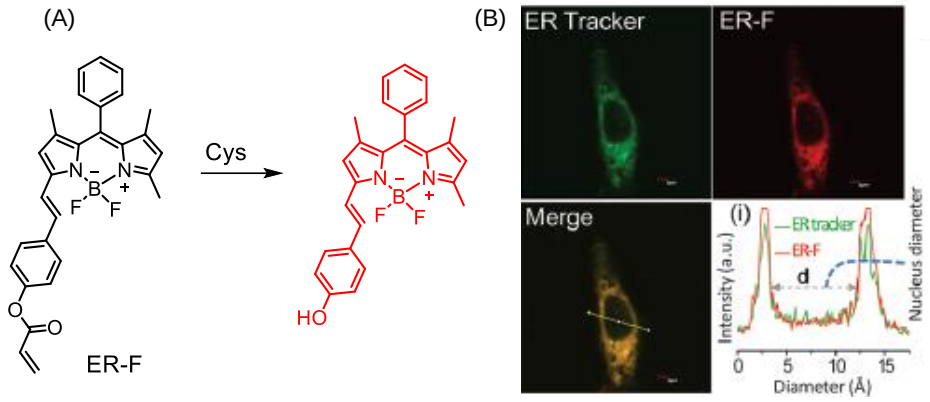

Figure 1A.4. (A) Molecular structure of the probe **2** (ER-F) and its reaction with Cys. (B) Confocal micrographs of Hct116 cells treated with ER-F and ER-tracker green. (i) The intensity profile of a region of interest across the cell; red line represents the intensity of ER-F and green line indicates the intensity of ER tracker green. (Reprinted with permission from ref. 9. Copyright the Royal Society of Chemistry).

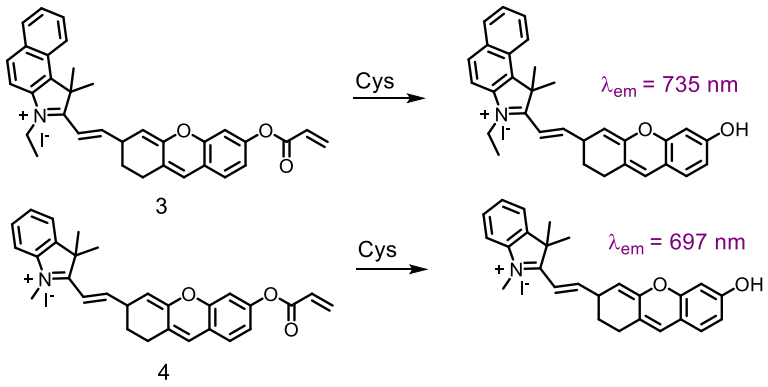

Figure 1A.5. The molecular structure of mitochondria-specific molecular probes **3** and **4** and their reaction with Cys.

Ratiometric probes are very useful for the quantification of an analyte. Here the observed emission response is independent of analyte concentration. So it is possible to quantify the analyte by taking the ratio of the two emission bands. Yoon and co-workers developed one such ratiometric probe (probe 5) for Cys.[12] A near-infrared emissive hydroxyl cyanine was used as a ratiometric signaling moiety. The hydroxyl group of the parent fluorophore was masked with the Cys specific α,β-unsaturated acrylate functionality. Initially, the probe showed an absorption and emission band at 770 and 780 nm, respectively. The reaction of Cys with acrylate accounted for the release of the hydroxyl cyanine fluorophore with the associated shifting of the absorption and emission bands to 515 and 570 nm, respectively. This probe was successfully utilized to image the intracellular Cys in living cancer cells.

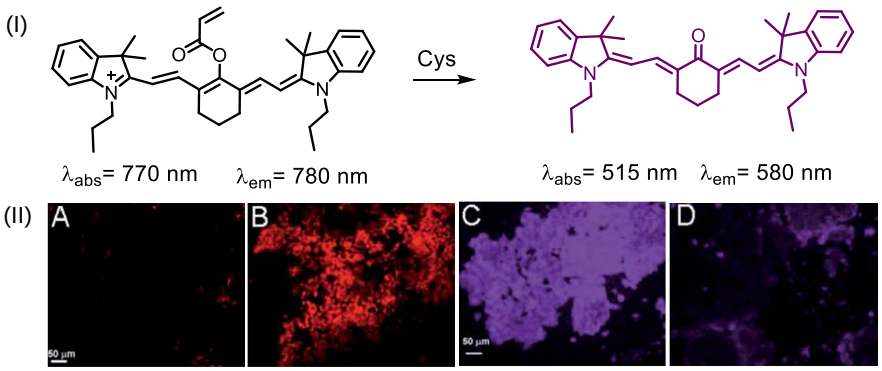

Figure 1A.6. (I) The molecular structure of the ratiometric probe **5** and its reaction with Cys. (II) Fluorescence imaging in MCF-7 cells incubated with CyAC (5 mM) for 30 min in an EtOH: HEPES (1: 9, 0.01 M, pH 7.4) solution. (A) and (B) the excitation wavelength is 510– 560nm and the emission were collected at 590 nm; (C) and (D) the excitation wavelength is 660–750 nm and the emission was collected at 760–855 nm. (Reprinted with permission from ref. 12. Copyright the Royal Society of Chemistry).

Probes based on acrylate trigger was found to be a promising strategy because of its excellent selectivity and relative ease in synthesis. This strategy was extensively utilized to develop a spectrum of probes; each showed interesting photophysical properties and biocompatibility (Figure 1A.7).[13-19]

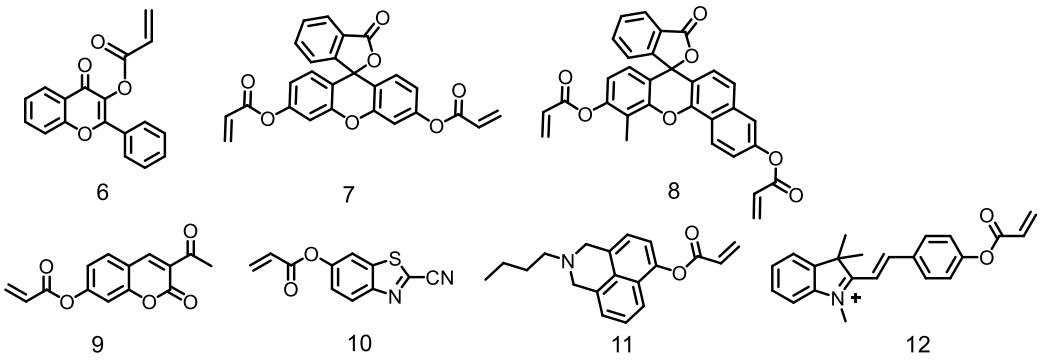

Figure 1A.7. The molecular structures of acrylate-based Cys probes.

With the development of new microscopy technique like Two-photon microscopy (TPM), now it is possible to achieve deep tissue imaging with appropriate resolution. Two-photon microscopy uses two NIR radiation pulses as the excitation source. Since the auto fluorescence from the biological samples is minimum at NIR window and NIR photons can penetrate deeper in tissues and cells, so deep tissue imaging is possible with TPM. Less energetic NIR photons in TPM studies also help in curbing the common phenomena like photobleaching and tissue damage. Probe **13** developed by Wong and co-workers was found to be compatible for TPM studies.[20] This probe was derived from merocyanine based signaling unit functionalized with

α,β-unsaturated acrylate group. This probe could detect Cys in ratiometric manner. It could detect the Cys present in mitochondria of the cells. This reagent also allowed ratiometric imaging of the Cys present in mitochondria. In addition to this, this probe showed two-photon action cross section of 65.2 GM at 740 nm and 72.6 GM at 760 nm in an aqueous medium. TPM imaging of Cys in tissue slices was demonstrated (Figure 1A. 8).

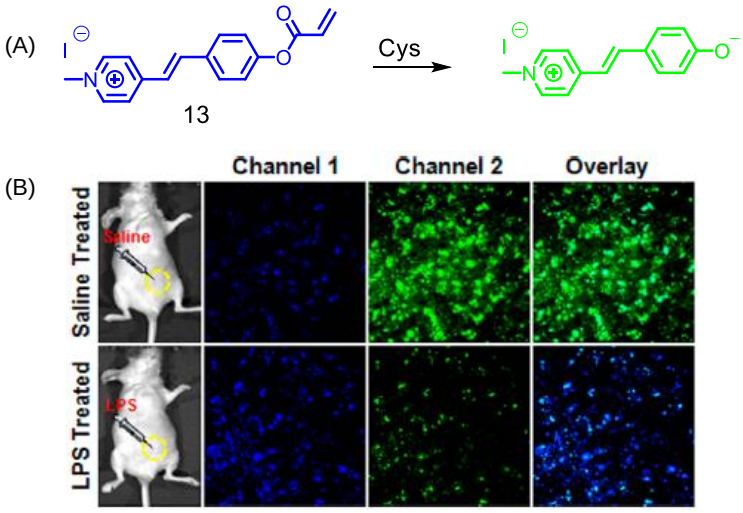

Figure 1A.8. (A) Molecular Structure of TP-acrylate probe **13** and its reaction with Cys. (B) Two-photon confocal microscopic fluorescence images in tissue slices injected with probe **13** (50 μM) after pre-treatment with saline (200 μL) and LPS (200 μL, 1.0 mg/mL), respectively. From left to right: Channel 1: λ_{em} = 430−470 nm, Channel 2: λ_{em} = 490−530 nm, overlay. λ_{ex} = 750 nm. (Reprinted with permission from ref. 20. Copyright American Chemical Society).

1A.2.2. Probes based on cyclization with aldehydes

Thiol containing amino acids undergo 1, 1 addition reaction with carbonyls and forms rings. This type of reaction was utilized to develop probes for thiols wherein a fluorophore containing aldehyde functionality undergo 1,1 addition reaction with thiols and forms a thiazolidine ring (Figure 1A. 9).

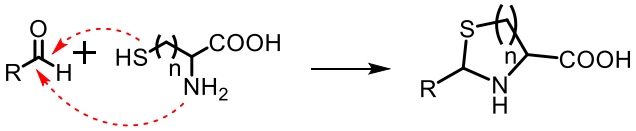

Figure 1A.9. A general mechanism for the cyclization of thiols with aldehydes.

But Cys and Hcy can undergo a similar type of reaction with aldehydes and typically can not be utilized for discriminating Cys and Hcy. Strongin and co-workers first reported that 3-(4-(dimethylamino)phenyl) acrylaldehyde probe (**14**) could

discriminate Cys and Hcy efficiently.[21] However, this probe showed only colorimetric response. Peng and co-workers were the first to develop a rhodamine-based fluorescent probe for the selective detection of Cys.[22] As shown in figure 1A.10 (ii), **15** formed a 5-membered thiazolidine intermediate, which was subjected to hydrolysis to form a highly emissive rhodamine derivative. Whereas in the case of Hcy, reaction with **15** resulted a stable non-cyclic adduct, that failed to participate in hydrolysis reaction and remain colourless. This probe was further utilized for imaging Cys in MCF and PC 12 cells.

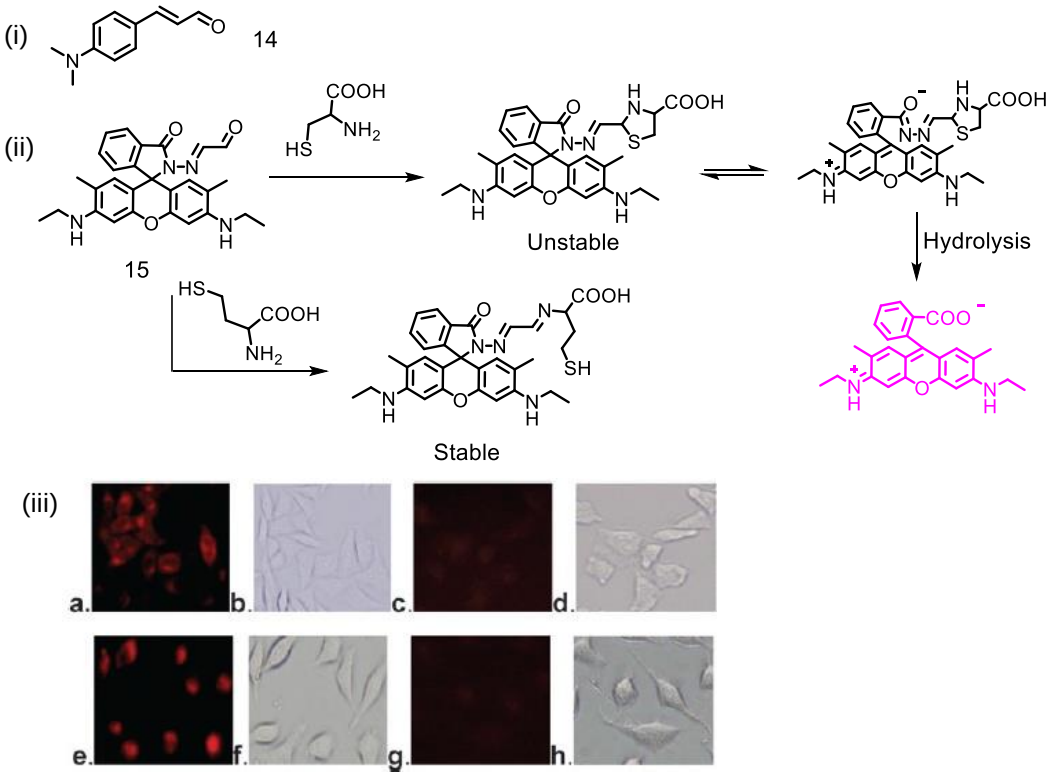

Figure 1A.10. (i) The molecular structure of Cys selective aldehyde probe **14**. (ii) Structure and mechanism of Cys sensing by probe **15**. (iii) Confocal micrographs of MCF (a-d) and PC 12 (e-h) cells. (a, e) cells treated with 60 µM of **15**. (c, g) cells treated with 30 µM N-ethyl maleimide (NEM, a thiol blocker). (b & f, d & h) bright field images. (Reprinted with permission from ref. 22. Copyright the Royal Society of Chemistry)

A coumarin-based ratiometric probe **16** having an aldehyde recognition site was designed by taking advantage of a specific cyclization reaction of Cys with the aldehyde.[23] Initially, the probe showed an emission band at 557 nm with a quantum yield of 0.12. Upon reaction with Cys, emission band at 557 nm was found to decrease gradually with a dramatic enhancement of emission band intensity at 487 nm, which qualify this probe as a ratiometric receptor for Cys. Quantum yield was evaluated as 0.25 at 487 nm after binding to Cys. A bathochromic shift of 70 nm with

a change in solution colour from green to blue was observed indicating the possibility of naked eye detection. Upon addition of Cys, a dramatic 115 fold increase in the fluorescent intensity was observed (Figure 1A. 11).

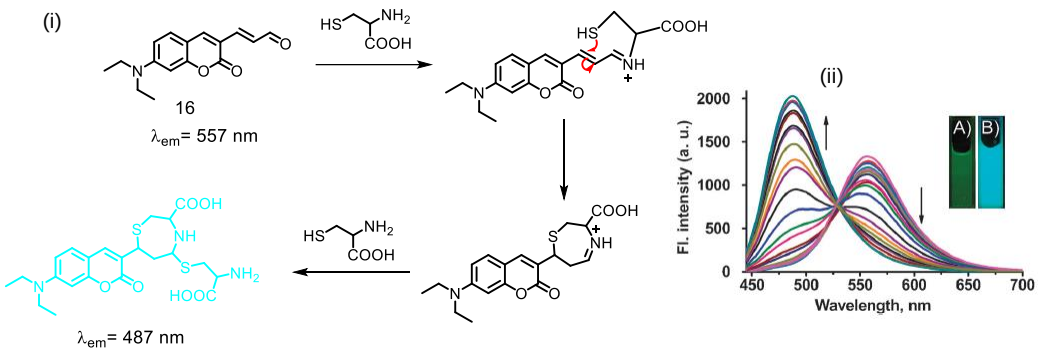

Figure 1A.11. (i) The molecular structure of probe **16** and its reaction with Cys. (ii) Ratiometric response of the probe towards Cys and the corresponding change in solution luminescence (A & B). (Reprinted with permission from ref. 23. Copyright the Royal Society of Chemistry).

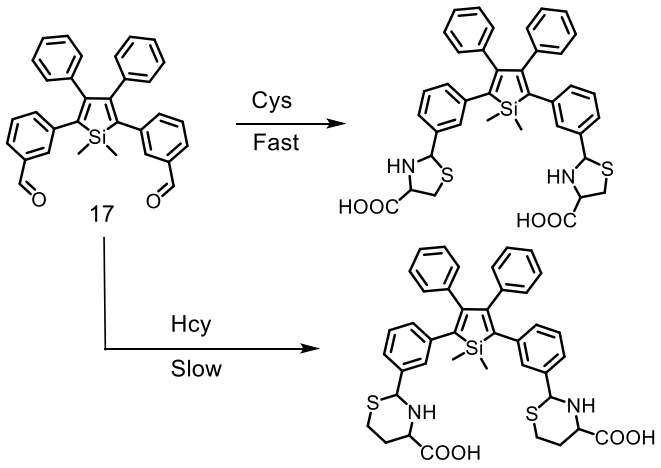

Figure 1A.12. The molecular structure of the AIE based Cys probe **17** and its reaction with Cys and Hcy.

An aggregation Induced emission (AIE) based probe **17** was reported by Tang and co-workers.[24] This probe was comprised of two aldehyde recognition sites and a dimethyltetraphenyl silole core as signaling unit. Upon reaction with Cys in aq. DMSO buffer medium, this probe lost its solubility and formed molecular aggregates with a prominent emission band at ~ 424 nm. Subsquent increase in emission intensities was observed upon increasing the Cys concentration. The solution turned completely turbid after the Cys addition. In the case of Hcy, the cyclization reaction was sluggish, and thus the probe proved to be suitable for Cys detection.

1A.2.3. Probes based on Michael-addition

1,4 addition of a nucleophile to α, β- unsaturated carbonyl group is termed as Michael-addition. In the year 1981, Sippel first reported a Michel acceptor-maleimide functionalised probe for thiol recognition.[25] Since then this reaction strategy was extensively used by the researchers to develop thiol specific probes. Many excellent Michael acceptors like α,β-unsaturated aldehydes, and ketones, squaraines, quinones, malononitriles have been utilized to develop fluorogenic thiol probes. Most of these probes were designed to detect the thiols like Cys, Hcy, and GSH. However, some of the probes showed excellent selectivity towards Cys. Such probes were designed by considering the steric factor and the pKa values of Cys, Hcy and GSH (8.2, 10.0 and 9.2, respectively).

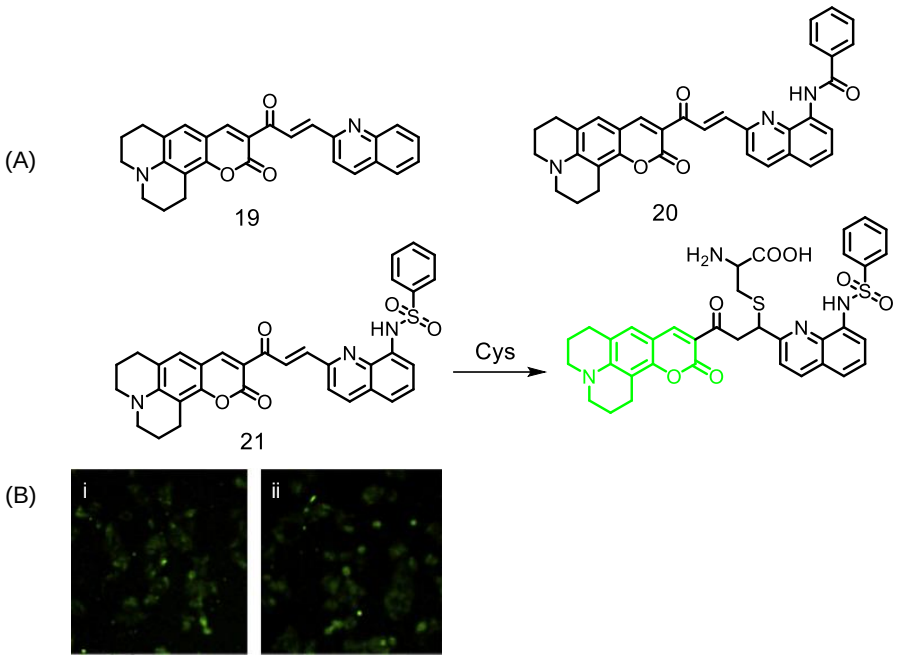

Figure 1A.13. (A) The molecular structures of probe **19, 20** and **21** and reaction of **21** with Cys. (B) Confocal micrographs of HepG2 cells incubated with 2 μM of **21** for 30 minutes. (Prior to the incubation with **21**, the cells were treated with NEM (0 and 0.2 mM, i & ii respectively) to block the intracellular Cys for 1 hour). (Reprinted with permission from ref. 26. Copyright Elsevier).

Since Cys has lower pKa value than other thiols, at near neutral pH the probability of thiolate/thiol ratio must be higher for Cys when compared to Hcy and GSH. Literature reports suggest that this subtle variation in pK_a resulted in the higher reactivity and higher selectivity of Cys with the probes.[26]

Kim and co-workers developed a series of coumarin-based probes based on Michael-addition strategy.[26] Probes were designed by combining a coumarin signaling moiety with a quinoline quencher fragment linked by a α,β-unsaturated carbonyl functionality as thiol recognition site.

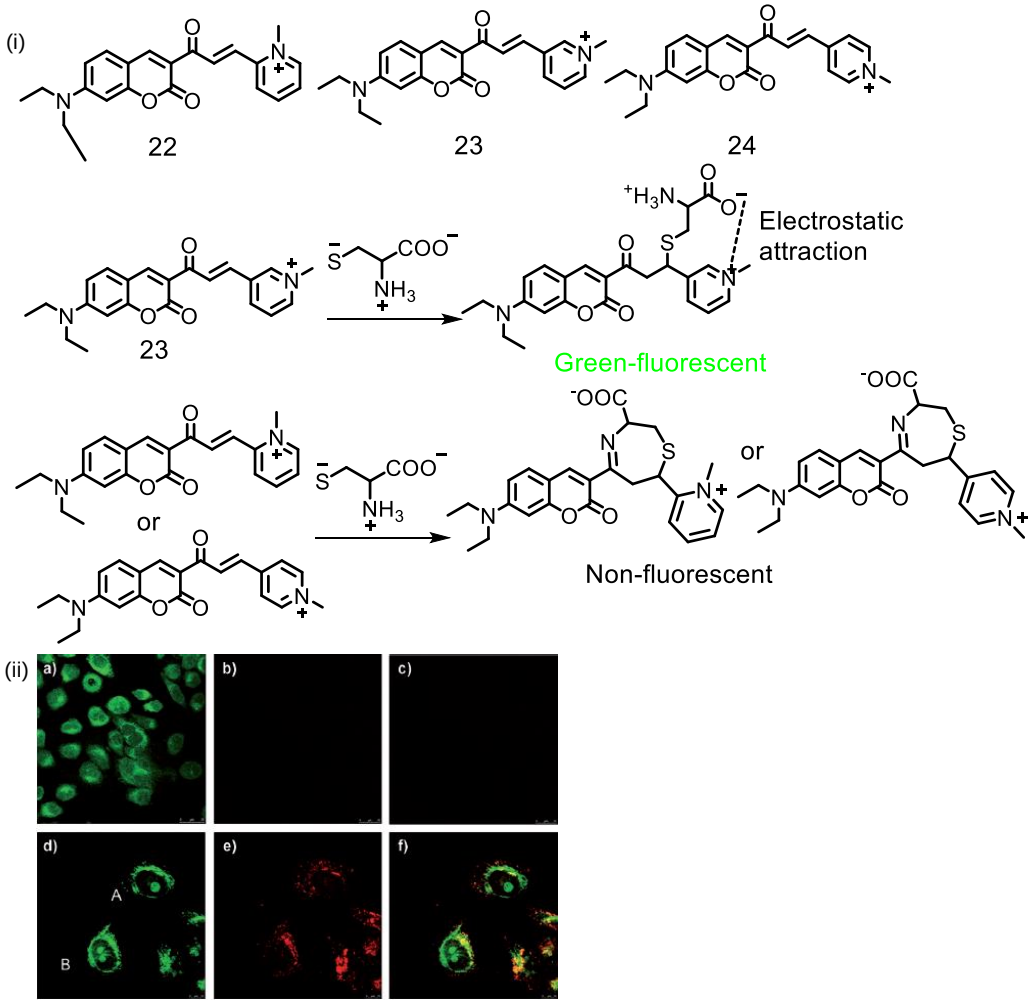

Figure 1A.14. (i) The molecular structures of coumarin probes functionalized with ortho-, meta- and para-substituted pyridinium moiety (**22, 23** and **24)** and their reaction with Cys; (ii) confocal micrographs of HeLa cells stained with probes (5 μM) a) **23**, b) **22**, and c) **24** respectively. These cells were incubated with probes for 1 h at 37° C before imaging. Individual HeLa cells were also co-stained with probe **23** (5 μM) and Mito tracker (2 μM): c) green emission for probe **23**, d) red emission for Mito-tracker, and f) merged. (A & B in image d represents different stages of cell division). (Reprinted with permission from ref. 27. Copyright John Wiley and Sons)

Among the chemodosimetric probes **18**, **19**, **20** and **21**, molecular probe **21** showed excellent selectivity to Cys over Hcy and GSH. **21** was initially non-fluorescent due to an intramolecular charge transfer (ICT) process involving the coumarin moiety and conjugated benzene sulfonamide. Michael-addition of Cys to α, β-unsaturated

carbonyl group disrupted the conjugation, and this interrupted the ICT process that was otherwise operational. This resulted in fluorescence ON response**.** The –SH proton of Cys is more acidic compared to the –SH protons of Hcy and GSH due to the lower pK_a value of Cys compare to other thiols. This favoured a higher population of the thiolate species over the corresponding thiol species for Cys, as compared to Hcy and GSH. Apart from a relatively significant difference in pK_a for Cys and GSH, a steric factor could also have played a role in getting the selectivity. This Cys specific probe was further utilized to image the intracellular Cys present in HepG2 cells.

Xue Wu and co-workers developed molecular probes **22**, **23**, **24** for efficient recognition of Cys. Derivative of coumarin was covalently coupled to ortho, meta- and para-substituted methyl pyridinium moiety through a α,β-unsaturated carbonyl linker.[27] Among the probes, the meta-substituted one (probe **23**) displayed selectivity to Cys based on Michael addition and electrostatic attraction. Michael addition of Cys with ortho and para substituted probes resulted in a 7-membered cyclic non-fluorescent product (Figure.1A.14). Whereas in the case of meta-substituted one, because of the electrostatic attraction, cyclization cannot occur, this resulted in the bright green fluorescence. To confirm this, authors synthesised neutral probes of coumarin conjugated to pyridine. But these neutral probes participated in similar reaction without having any preference for Cys. Further, this reagent was used in live cell imaging in HeLa cells. This cell membrane permeable reagent could recognize Cys in the cytoplasm, nucleus and mitochondria.

1A.3. References

1. L. D. Lavis, *Biochemistry*, 2017, **56**, 5165-5170.
2. J. B. Grimm, A. K. Muthusamy, Y. Liang, T. A. Brown, W. C. Lemon, R. Patel, R. Lu, J. J. Macklin, P. J. Keller, N. Ji and L. D. Lavis, *Nat. Methods*, 2017, **14**, 987-994.
3. J. Chan, S. C. Dodani and C. J. Chang, *Nat. Chem.*, 2012, **4**, 973-984.
4. S. M. Marino and V. N. Gladyshev, *J. Biol. Chem.*, 2012, **287**, 4419-4425.
5. S. García-Santamarina, S. Boronat and E. Hidalgo, *Biochemistry*, 2014, **53**, 2560-2580.
6. L.-Y. Niu, Y.-Z. Chen, H.-R. Zheng, L.-Z. Wu, C.-H. Tung and Q.-Z. Yang, *Chem. Soc. Rev.*, 2015, **44**, 6143-6160.
7. N. J. Leonard and R. Y. Ning, *J. Org. Chem.*, 1966, **31**, 3928-3935.
8. X. Yang, Y. Guo and R. M. Strongin, *Angew. Chem., Int. Ed.*, 2011, **50**, 10690-10693.
9. F. Ali, A. H. A, N. Taye, R. G. Gonnade, S. Chattopadhyay and A. Das, *Chem. Commun.*, 2015, **51**, 16932-16935.
10. J. Zhang, J. Wang, J. Liu, L. Ning, X. Zhu, B. Yu, X. Liu, X. Yao and H. Zhang, *Anal. Chem.*, 2015, **87**, 4856-4863.
11. C. Han, H. Yang, M. Chen, Q. Su, W. Feng and F. Li, *ACS Appl. Mater. Interfaces*, 2015, **7**, 27968-27975.
12. Z. Guo, S. Nam, S. Park and J. Yoon, *Chem. Sci.*, 2012, **3**, 2760-2765.
13. B. Liu, J. Wang, G. Zhang, R. Bai and Y. Pang, *ACS Appl. Mater. Interfaces*, 2014, **6**, 4402-4407.
14. H. Wang, G. Zhou, H. Gai and X. Chen, *Chem. Commun.*, 2012, **48**, 8341-8343.
15. X. Yang, Y. Guo and R. M. Strongin, *Org. Biomol.Chem.*, 2012, **10**, 2739-2741.
16. X. Dai, Q.H. Wu, P.C. Wang, J. Tian, Y. Xu, S.Q. Wang, J.Y. Miao and B.X. Zhao, *Biosen.Bioelectron.*, 2014, **59**, 35-39.
17. M. Zheng, H. Huang, M. Zhou, Y. Wang, Y. Zhang, D. Ye and H.-Y. Chen, *Chem.Eur. J.*, 2015, **21**, 10506-10512.
18. B. Zhu, B. Guo, Y. Zhao, B. Zhang and B. Du, *Biosen.Bioelectron.*, 2014, **55**, 72-75.
19. Q. Han, Z. Shi, X. Tang, L. Yang, Z. Mou, J. Li, J. Shi, C. Chen, W. Liu, H. Yang and W. Liu, *Org. Biomol.Chem.*, 2014, **12**, 5023-5030.
20. W. Niu, L. Guo, Y. Li, S. Shuang, C. Dong and M. S. Wong, *Anal. Chem.*, **88**, 1908-1914.

21. O. Rusin, N. N. St. Luce, R. A. Agbaria, J. O. Escobedo, S. Jiang, I. M. Warner, F. B. Dawan, K. Lian and R. M. Strongin, *J. Am. Chem. Soc*., 2004, **126**, 438-439.

22. H. Li, J. Fan, J. Wang, M. Tian, J. Du, S. Sun, P. Sun and X. Peng, *Chem. Commun.*, 2009, 5904-5906.

23. L. Yuan, W. Lin and Y. Yang, *Chem. Commun.*, 2011, **47**, 6275-6277.

24. J. Mei, Y. Wang, J.Tong, J. Wang, A. Qin, J. Z. Sun and B. Z. Tang, *Chem. Eur. J*., 2013, **19**, 613-620.

25. T. O. Sippel, J. Histochem. Cytochem., 1981, **29**, 314–316.

26. H. S. Jung, J. H. Han, T. Pradhan, S. Kim, S. W. Lee, J. L. Sessler, T. W. Kim, C. Kang, J. S. Kim, *Biomaterials*, 2012, **33**, 945-953.

27. X. Zhou, X. Jin, G. Sun and X. Wu, *Chem. Eur. J.*, 2013, **19**, 7817-7824.

1B. Enzyme Recognition and Quantification in bio fluids

1B.1. Introduction

The Detection and monitoring of crucial biomarkers using fluorescent labels are vital in clinical diagnostics. One such biomarker of interest is the enzyme aminoacylase-1 (ACY-1). Aminoacylases are the mono nuclear or binuclear zinc(II)-based enzymes that catalyse the hydrolysis of N-acetylated amino acids.[1] Among various acylases, ACY-1 is abundant in humans physiology and it is highly expressed in kidney.[2] ACY-1 plays a major role in the metabolism of drug N-acetylcysteine (NAC) in intestine and liver. NAC, an acetylated form of cysteine is used to treat the patients suffering from acetaminophen overdose, HIV, glutathione replenishment, oxidative stress etc.[3] ACY-1 deficiency causes rare inborn metabolic disorder mainly associated with neurologic symptoms such as intellectual disability, motor delay, seizures, lack of speech development, growth delay etc.[2] Patients with ACY-1 deficiency excrete N-acetylated amino acids in urine.[2] Besides its biological roles, aminoacylases are largely used in industries for the synthesis of optically pure amino acids. N-acetylated amino acids were optically resolved to D and L forms with the help of these enzymes.[4] Hence, reliable detection, quantification and monitoring of its enzymatic activity have relevance for clinical diagnostic, therapeutic follow up as well as for monitoring crucial industrial processes. More recently, ACY-1 is identified as a novel biomarker in blood serum samples of patients with delayed graft function (DGF). ACY-1 level in serum samples of patients with DGF markedly increases after renal transplantation.[5] Delayed graft function (DGF) is one of the major complications associated with renal transplantation. Patients with DGF have to undergo dialysis after the kidney transplantation.[6] DGF increases the risk of graft failure, acute rejection, and arterial hypertension etc.[7] Hence, its estimation in blood serum (BS) is decisive in clinical diagnosis for the recovery and treatment of such patients.[5-7] Such quantification in the serum sample is conventionally achieved by immune depletion and label-free single dimensional liquid chromatography-tandem mass spectrometry analysis.[8] This technique involves the removal of abundant proteins from serum samples with the help of HPLC and then analysis of samples by using mass spectrometry.[9] But this method is expensive, time consuming and it requires expertise for execution. This suggests the need of simple and reliable methods for the detection and quantification of ACY-1.

As discussed in the earlier paragraph, even though ACY-1 plays many important roles in human physiology, but there are not many methods available for the detection and

quantification of ACY-1. Except HPLC based method, there are some ELISA based reagents. The commercially available assay kits for ACY-1 mostly rely on enzyme linked immunosorbent assay (ELISA) technique. These techniques have many limitations. ELISA based methods are highly complicated and the analysis involves multiple steps. Moreover, it takes minimum of 4 to 5 hours for the analysis. The reagents involved in ELISA need sophisticated storage and expertise handling. All these add to the cost and overall process is expensive. Appropriate reagent and the methodology that allow optical measurements/ quantification of ACY-1 is an unexplored area. Reason might be the lesser bio availability of the enzyme and lack of biocompatible, sensitive and selective molecular probes or methods that could detect and quantify the small quantity of ACY-1present in bio fluids.[10] Due to the lack of many optical probes for ACY-1, the discussion is only limited to the two of the commercially available reagents called fluorescamine and 2,4,6-trinitrobenzenesulfonic acid.

1B.2.1. Fluorescamine assay for ACY-1

4-phenylspiro[furan-2(3H),1`-phthalan]-3,3`-dione, commonly known as fluorescamine is a fluorogenic reagent that reacts with amines to yield a new compound that has high fluorescence quantum yield.[10] In fluorescamine assay, first the N-acetyl amino acids were allowed to react with ACY-1 and the product of the reaction (deacetylated amino acids) reacts with fluorescamine to give specific turn ON fluorescence response.The amount of product formed from the reaction of known ACY-1 is used to develop the calibration plot. Unknown ACY-1 can be quantified from the calibration plot (Figure 1B.1).

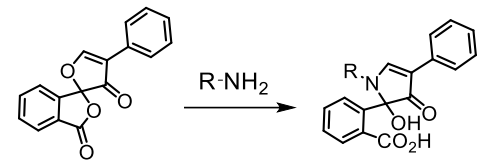

Figure 1B.1. The molecular structure of fluorescamine and its reaction with free amine.

Even though it is the only available fluorescent based reagent for ACY-1, it has some limitations. Fluorescamine can react with the free amines of proteins, peptides and amino acids. Complex biological fluids like blood serum or plasma will have various proteins and amino acids and all these can react with fluorescamine. This would lead to an inaccurate measurement or quantification of ACY-1. This limits the use of this reagent for quantification of ACY-1 in complex biological fluids.

1B.2.2. Assay based on 2, 4, 6-trinitrobenzenesulfonic acid (TNBS)

2,4,6-trinitrobenzenesulfonic acid is a colorimetric reagent that gives specific colour change upon reaction with the free amines.[11] This method is also based on the analysis of reaction product between ACY-1 and N-acetylated amino acids.

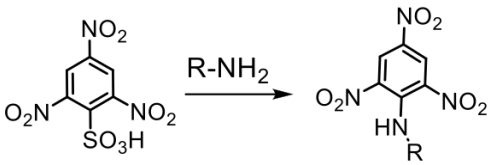

Figure 1B.2. The molecular structure of 2,4,6-trinitrobenzenesulfonic acid and its reaction with ACY-1

The amine derivative of the deacylated amino acid reacts with the TNBS to yield a yellow colour product that could be measured colorimetrically. ACY-1 was quantified from the calibration plot (Figure 1B.2). This reagent also had several limitations such as interference from proteins, and other amino acids that could be present in biological samples/biofluids.

1B.3. References

1. V. Uttamsingh, R. B. Baggs, D. M. Krenitsky and M. W. Anders, *Drug Metab. Dispos.*, 2000, **28**, 625-632.

2. L. Ferri, S. Funghini, A. Fioravanti, E. G. Biondi, G. la Marca, R. Guerrini, M. A. Donati and A. Morrone, *Clin.Genet*, 2014, **86**, 367-372.

3. S. C. De Rosa, M. D. Zaretsky, J. G. Dubs, M. Roederer, M. Anderson, A. Green, D. Mitra, N. Watanabe, H. Nakamura, I. Tjioe, S. C. Deresinski, W. A. Moore, S. W. Ela, D. Parks, L. A. Herzenberg and L. A. Herzenberg, *Eur. J. Clin. Invest.*, 2000, **30**, 915-929.

4. S. V. Story, A. M. Grunden and M. W. W. Adams, *J. Bacteriol.*, 2001, **183**, 4259-4268.

5. M. P. Welberry Smith, A. Zougman, D. A. Cairns, M. Wilson, T. Wind, S. L. Wood, D. Thompson, M. P. Messenger, A. Mooney, P. J. Selby, A. J. P. Lewington and R. E. Banks, *Kidney Int.*, 2013, **84**, 1214-1225.

6. R. Sola, A. Alarcón, C. Jiménez and A. Osuna, *Nephrol Dial Transplant*, 2004, **19**, iii32-iii37.

7. S. G. Yarlagadda, S. G. Coca, R. N. Formica, E. D. Poggio and C. R. Parikh, *Nephrol Dial Transplant*, 2009, **24**, 1039-1047.

8. M. P. W. Smith, S. L. Wood, A. Zougman, J. T. C. Ho, J. Peng, D. Jackson, D. A. Cairns, A. J. P. Lewington, P. J. Selby and R. E. Banks, *Proteomics*, 2011, **11**, 2222-2235.

9. V. V. Snitynskyĭ, L. I. Solohub, H. L. Antoniak, D. M. Kopachuk, M. H. Herasymiv, *Ukr Biokhim. Zh*, 1999, **71**, 5.

10. S. Udenfriend, S. Stein, P. Bohlen, W. Dairman, W. Leimgruber and M. Weigele, *Science*, 1972, **178**, 871-872.

11. V. Uttamsingh, D. A. Keller and M. W. Anders, *Chem. Res. Toxicol.*, 1998, **11**, 800-809.

1C. Probes for the detection Polysulfides

1C.1. Introduction

Reactive sulfur species (RSS) such as Cysteine (Cys), Homocysteine (Hcy), Glutathione (GSH), Hydrogen sulfide (H_2S) etc. participate in many crucial biochemical transformations/ enzymatic processes in human physiology. Recent reports reveal that hydrogen polysulfide (H_2S_n, n > 1) is another important RSS species that plays key roles in signaling and other biochemical transformations.[1] One important function of H_2S_n is protein sulfuration wherein a sulfur atom is added to the cysteine residue of the protein causing the modification in protein structure and hence reactivity.[2] Earlier, it was believed that H_2S was the active species for protein sulfuration. Recently is has been identified that H_2S_n is the active species involved in protein sulfuration.[2] Recent studies also suggest that H_2S_n is actually the active species for many other biological transformations associated with H_2S. In astrocytes, H_2S_n induces Ca^{2+} influx 300 times more efficiently than H_2S.[3,4] Moreover, H_2S_n is also regulates the activity of tumour suppressors, transcription factors etc.[3] Even though it plays many important roles, but there are not many methods to detect and monitor the activity of H_2S_n because of the poor understanding of the chemistry and reactivity of H_2S_n. There are some traditional methods like monitoring the absorbances at 290-300 nm and 370 nm.[5] However, such measurement technique is not sensitive and also not suitable for studies with biological samples. So, there is an urgent need to develop some sensitive methods for detection and monitoring of H_2S_n. In this regard, the fluorescence-based reagent and a methodology could be better suited for studies with biological samples as these would offer a higher sensitivity and biocompatibility. Following the first report on fluorescent polysulfide probe[6] by Prof. Xian's group in 2014, there is a growing interest in developing molecular probes in the subsequent years. Some of the important developments in this field are briefly summarized in the subsequent paragraphs. Probes were subdivided into different categories based on the differenene in methodologies adopted for the sensing process.

1C.2. Various probes for H_2S_n

1C.2.1. Probes based on activated aromatic nucleophilic substitution and cyclization

H_2S_n is a combination of polysulfide species. Upon dissolution, it gives H_2S_2 as one of the active species. There exists a dynamic equilibrium between H_2S_n and H_2S_2 in solution. The sulphur atoms in H_2S_2 (H-S-S-H) can participate in the nucleophilic substitution reaction. So, if a bis-electrophilic group is attached to a fluorophore, it could capture H_2S_2 through activated aromatic nucleophilic substitution followed by cyclization to release the benzodithialone and the fluorophore with fluorescence ON response (Figure 1C.1).[6]

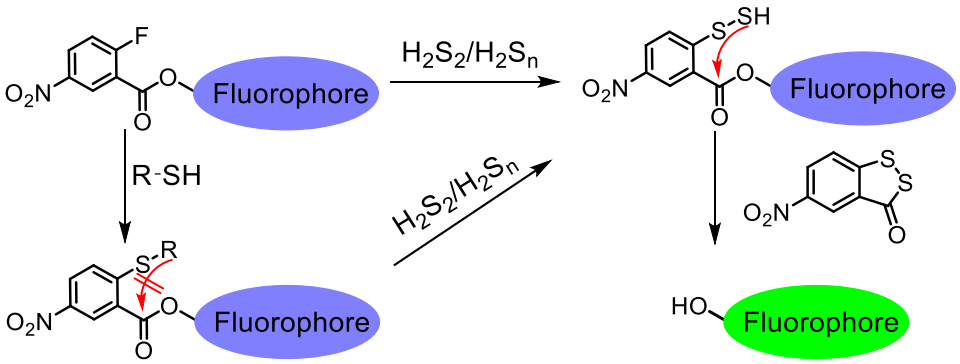

Figure 1C.1. General mechanism for H_2S_n sensing based on activated aromatic nucleophilic substitution and cyclization.

Based on this idea, Xian's group first developed three probes (probe **1**, **2** & **3**) having fluorescein moiety as fluorophore and 2-fluoro-5-nitro benzoate moiety as the recognition site.[6] Hydroxyl group of the fluorescein was protected by 2-fluoro-5-nitrobenzoate moiety, which also ensured that the lactone form of fluorescein (fluorescence OFF state) existed. Upon reaction with Na_2S_2 (H_2S_2 donor), fluorobenzoate participated in a nucleophilic substitution reaction to yield an intermediate as persulfide. This intermediate further participated in cyclization to yield benzodithiolone and free fluorescein with fluorescence ON response. However, the only concern about this kind of design is that these fluorobenzoates can also participate in nucleophilic substitution with other biothiols (Figure 1C.1), which results in a large amount of probe consumption. Nevertheless, such reactions would not turn ON the fluorescence of the probe. Among the three probes, **3** showed excellent response with a lower detection limit of 71 nM. It was further utilized to image H_2S_n in HeLa cells.

Based on this general idea, several other research groups used the same template with different fluorophores and reported many probes with interesting photophysical properties in the subsequent years. Probes **4-10** were designed based on the 2-fluoro-5-nitrobenzoate recognition moiety.[7-13]

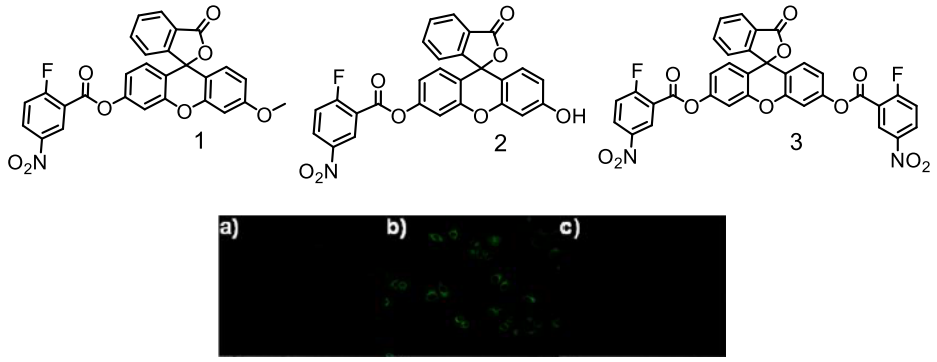

Figure 1C.2. The molecular structure of polysulfide probes. Confocal images of HeLa cells treated with probe **3** (10 μM). (a) Probe **3** only, (b) 100 μM Na_2S_2, (c) 100 μM Na_2S. (Reprinted with permission from ref. 6. Copyright American Chemical Society)

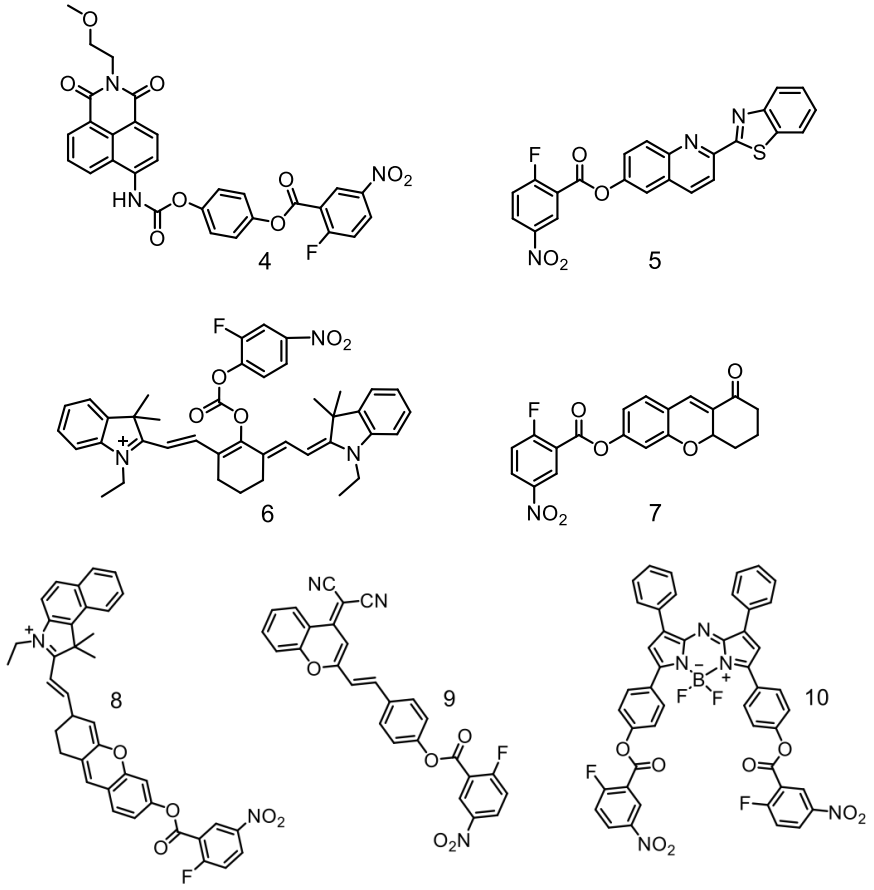

Figure 1C.3. The molecular structures of polysulfide probes designed based on the 2-fluoro-5-nitrobenzoate recognition moiety.

1C.2.2. Probe based on aziridine ring opening by H_2S_n

A specific nucleophilic attack by H_2S_n on aziridines was used to develop a polysulfide probe by Xian's group.[14] Probe **11** showed excellent selectivity to H_2S_n and the fluorescent product exhibited excellent two-photon properties. However, the attempts to use this probe in the biological medium were not successful. Probe **11** was reported to be useful only for solution studies.

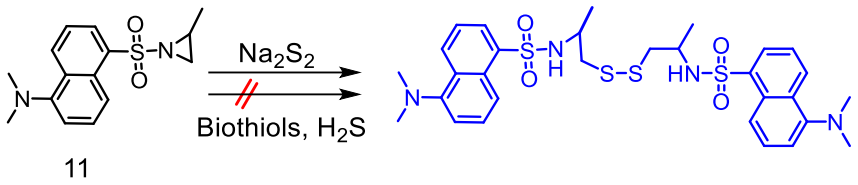

Figure 1C.4. The molecular structure of **11** and its reaction with H_2S_n.

1C.2.3. Probes based on 2-(benzoylthio)benzoate trigger group

So, significant effort has been put forward by many research groups to develop H_2S_n specific probes in order to overcome the limitations associated with the existing probes. In the year 2015, Prof. Xian and co-workers came up with few H_2S_n selective chemodosimetric probes using 2-(benzoylthio)benzoate as the recognition moiety.[15] They had utilized the dual reactivity of polysulfides (both as electrophile and nucleophile) to develop H_2S_n specific probes. The idea behind this design involves the nucleophilic attack of H_2S_n on thioester functionality to yield a thiolate intermediate, which further reacts with H_2S_n (now acts as electrophile) to undergo a spontaneous cyclization process to release free probe with turn ON fluorescence response.

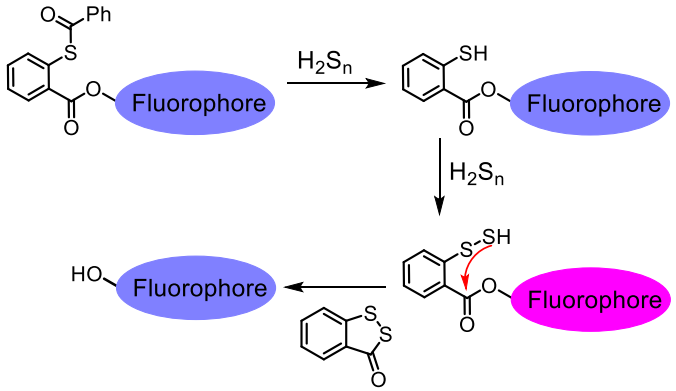

Figure 1C.5. Schematic representation of the general mechanistic pathway for reaction of H_2S_n through intermediate formation of thioester and the spontaneous cyclization process.

Probes **12**, **13** and **14** were designed by protecting the hydroxyl group of fluorescein with 2-(benzoylthio)benzoate functionality. **R** group at thioester functionality was varied with methyl, tertiary butyl and phenyl groups in order to check the steric effect on the reactivity of H_2S_n with the probe. Among the three probes, **14** with phenyl substituted thioester showed excellent sensitivity and selectivity. This probe was further utilized for endogenous detection of H_2S_n in lipopolysaccharide (LPS) stimulated COS 7 cells.[15]

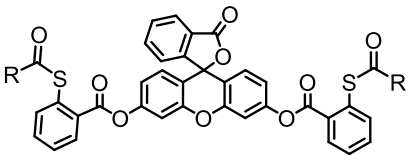

R= -CH_3 (Probe 12)
-$C(CH_3)_3$ (Probe 13)
-Phenyl (Probe 14)

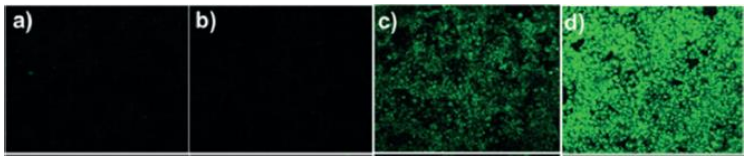

Figure 1C.6. The molecular structures of polysulfide probes **12**, **13** and **14**. Fluorescence images of endogenous H_2S_n in COS 7 cells (a-d). (a) Cells only, (b) Cells treated with **14**1(5 μM), (c) LPS stimulated cells treated with **14**, (d) Cells treated with 20 μM Na_2S_2. (Reprinted with permission from ref. 15. Copyright John Wiley and Sons)

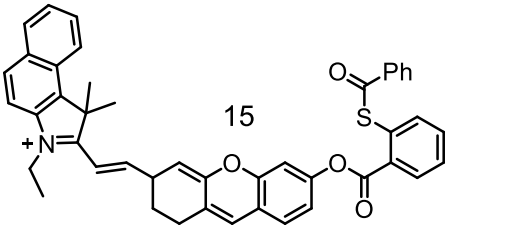

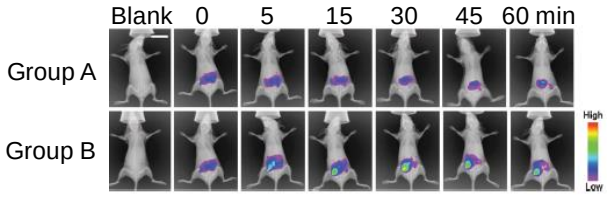

Figure 1C.7. The molecular structure of polysulfide probe **15**. NIR fluorescence images of H_2S_n in BALB/c mice. Both groups A and B were subjected to an i.p. cavity injection with probe **15** (50 μM, 50 μL in 1: 99 DMSO/saline, v/v) for 15 min; then group A was given an i.p. cavity injection with 50 μL saline as control, and group B was given an i.p. cavity injection with Na_2S_2 (100 μM, 50 μL in saline), followed by recording the fluorescence images at different time points. Scale bar, 1 cm. (Reprinted with permission from ref. 16. Copyright Royal Society of Chemistry)

Huimin Ma and co-workers recently reported an NIR active molecular probe using similar sensing platform. Probe **15** was a cyanine derivative that was functionalized with 2-

(benzoylthio)benzoate trigger group. This probe showed excellent selectivity to H_2S_n with a lower detection limit of 35 nM. It was utilized for in vivo imaging in BALB mice.[16]

1C.3. References

1. H. Kimura, *Proc. Jpn. Acad., Ser. B*, 2015, **91**, 131.

2. A. K. Mustafa, M. M. Gadalla, N. Sen, S. Kim, W. Mu, S. K. Gazi, R. K. Barrow, G. Yang, R. Wang and S. H. Snyder, *Sci. Signal.*, 2009, **2**, ra72.

3. Y. Kimura, Y. Mikami, K. Osumi, M. Tsugane, J.-i. Oka and H. Kimura, *FASEB J.,* 2013, **27**, 2451.

4. T. Ida, T. Sawa, H. Ihara, Y. Tsuchiya, Y. Watanabe, Y. Kumagai, M. Suematsu, H. Motohashi, S. Fujii, T. Matsunaga, M. Yamamoto, K. Ono, N. O. Devarie-Baez, M. Xian, J. M. Fukuto and T. Akaike, *Proc. Natl. Acad. Sci. U.S.A*, 2014, **111**, 7606.

5. R. Greiner, Z. Pálinkás, K. Bäsell, D. Becher, H. Antelmann, P. Nagy and T. P. Dick, *Antioxid. Redox Signal.,* 2013, **19**, 1749.

6. C. Liu, W. Chen, W. Shi, B. Peng, Y. Zhao, H. Ma and M. Xian, *J. Am. Chem. Soc.,* 2014, **136**, 7257.

7. W. Chen, X. Yue, H. Zhang, W. Li, L. Zhang, Q. Xiao, C. Huang, J. Sheng and X. Song, *Anal. Chem.,* 2017, **89**, 12984.

8. M. Gao, F. Yu, H. Chen and L. Chen, *Anal. Chem.,* 2015, **87**, 3631.

9. L. Zeng, S. Chen, T. Xia, W. Hu, C. Li and Z. Liu, *Anal. Chem.*, 2015, **87**, 3004.

10. Q. Han, Z. Mou, H. Wang, X. Tang, Z. Dong, L. Wang, X. Dong and W. Liu, *Anal. Chem.,* 2016, **88**, 7206.

11. Y. Huang, F. Yu, J. Wang and L. Chen, *Anal. Chem.,* 2016, **88**, 4122.

12. K.-B. Li, F.-Z. Chen, Q.-H. Yin, S. Zhang, W. Shi and D.-M. Han, *Sens. Actuators, B*, 2018, **254**, 222.

13. J. Ma, J. Fan, H. Li, Q. Yao, F. Xu, J. Wang and X. Peng, *J Mater Chem B*, 2017, **5**, 2574.

14. W. Chen, E. W. Rosser, D. Zhang, W. Shi, Y. Li, W.-J. Dong, H. Ma, D. Hu and M. Xian, *Org. Lett.,* 2015, **17**, 2776.

15. W. Chen, E. W. Rosser, T. Matsunaga, A. Pacheco, T. Akaike and M. Xian, *Angew. Chem., Int. Ed*., 2015, **54**, 13961.

16. Y. Fang, W. Chen, W. Shi, H. Li, M. Xian and H. Ma, *Chem. Commun.,* 2017, **53**, 8759.

1D. Probes for the plasma membrane imaging

1D.1. Introduction

Visualization of molecular targets using fluorescent biomarkers is vital in clinical diagnosis and real time imaging. Various fluorescence imaging techniques have attracted great attention due to their obvious advantages in terms of the availability of biocompatible imaging reagents with high temporal resolution and sensitivity.[1] Key component of fluorescence imaging is appropriate fluorescent tool, the so-called fluorescent molecular probes. One of the most attractive targets in cellular imaging is plasma membranes. It is the very first cellular barrier that is easily accessible to molecules from the extracellular medium. Being the outer envelope of cells, it regulates the movement of various ions or molecules in and outside the cells. Cell membrane is exposed to extracellular environment and it is a prime target for many drugs.[2,3] Lipid bilayer of the mammalian plasma membrane is made up of different polar lipids and proteins. Plasma membrane shows the asymmetric distribution of the polar lipids, which is described by the lipid raft hypothesis.[4] Cell membrane possesses liquid ordered (Lo) and liquid disordered (Ld) phases. Lo consists of cholesterol and saturated phospholipids whereas Ld phase is made up of unsaturated lipids. These lipid rafts are believed to be behind many membrane and/or cellular processes such as formation of protein clusters, signal transduction, pathogen invasion, cholesterol homeostasis, neurodegenerative diseases, apoptosis and angiogenesis.[1,4] Membrane imaging provides a clear cellular contour allowing delimitation of the cells and studying their morphology. The classical approach for developing a membrane probe relies on functionalizing appropriate fluorophore with a long hydrophobic alkyl chain.[5] However; such probes are not always efficient in monitoring the biophysical properties such as lipid order, fluidity, hydration and electrostatics. This leaves us with a distinct opportunity for developing efficient molecular probes for studying the lipid order, fluidity, polarity and hydration. Brief discussions on classical molecular probes developed for cell membrane targeting are described in this section.

1D.2. Various probes for cell membrane imaging

1D.2.1. Classical membrane probes having appended long alkyl chains

As discussed earlier, one of the best and easy ways to develop fluorescent probes for membrane is to incorporate long, hydrophobic alkyl chains in fluorophores. These long hydrophobic chains help to partition the probes in the cell membrane. However, these probes fail to provide information about the biophysical properties of the membrane. Presence of the long hydrophobic chains makes these probes rather insoluble in aqueous medium, which hinders the practical utility of such probes in membrane imaging. Moreover, these hydrophobic dyes are known to bind to some of the non-membrane components like proteins of serum and limit their usages for *in-vitro* imaging (probe **1**). Moreno and co-workers developed a series of molecular probes having different alkyl chain lengths (from 4 - 16) based on 7-nitrobenz-2-oxa-1,3-diazol-4-yl (NBD) fluorophore. These probes (Figure 1D.1) were developed based on the classical approach by modifying the fluorophore with long hydrocarbon chains. Partition behaviour of the probes was studied in an aqueous medium and model bilayer vesicles composed of 1-palmitoyl-2-oleoyl phosphatidylcholine (POPC). They could find a linear dependence in the distribution of probes between the aqueous medium and POPC vesicles as a function of the alkyl chain length.[6]

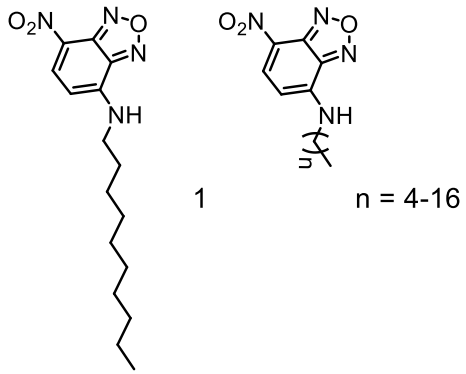

Figure 1D.1. The molecular structures of the long-alkyl chain membrane probes based on NBD fluorophore.

1D.2.2. Molecular rotor based membrane probes

Membrane viscosity plays a key role in many important cellular processes such as cell division, cell death, motility and membrane fusion. So, monitoring the viscosity of the membrane in non-invasive manner is of paramount importance.[7,8] Fluorescence probes called ‘molecular rotors’ are a class of twisted intramolecular charge transfer (TICT)

active molecules wherein their emission properties are dependent on the surrounding environment.[8] Molecular rotors and the associated TICT process of these molecular probes are generally sensitive to the surrounding medium viscosity. Molecular rotors are typically non-emissive in the aqueous medium and their emission intensity dramatically enhances in the viscous environment. Such molecular rotors with long hydrophobic alkyl chains could be the best candidates to report the viscosity of the membranes. Probe **2** and **3** are the two unique examples of molecular rotors that are extensively used for viscosity measurement in the membrane micro environment. Probe **2** is based on 9-(dicyanovinyl)-julolidine commonly known as DCVJ[9] and probe **3** is difluoroborondipyrromethene, commonly known as BODIPY .[10,11]

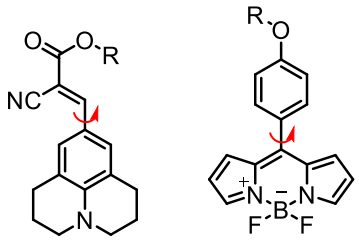

2 3

Figure 1D.2. Structures of molecular rotors derived from DCVJ and BODIPY.

In the case of DCVJ, the free rotation of the C-C bond between julolidine unit and the vinyl group was responsible for the formation of twisted structure. Whereas in the case of BODIPY, the free rotation of meso phenyl group was responsible for the twisted structure. These rotors were found to exhibit very poor emission quantum yield in a non-viscous medium. However, a gradual increase in their emission intensity was registered with increase in the viscosity of the surrounding environment. By utilizing this property, various membrane viscometers with these rotors were developed by modifying the –R group with hydrophobic alkyl chains, polyethylene glycol, and cholesterol moieties etc.

1D.2.3. Environment sensitive probes for membrane

Environment sensitive dyes are a class of fluorophores wherein their emission intensity or the colour changes with respect to the surrounding environment. Environment sensitive dyes are generally highly fluorescent in apolar membrane environment and their emission is effectively quenched in the polar aqueous environment. A series of 3-hydroxyflavone based environmental sensitive probes were developed to monitor the polarity and hydration of the cell membrane (Figure 1D. 3). All these probes showed dual emission bands around 500 nm and 600 nm, as ESIPT process was operational for these

molecular probes. These probes showed a dramatic increase in their emission intensity when incorporated into the large unilamellar vesicles (LUVs). These probes exhibited polarity dependent blue shift in their emission band in the bilayer. The change in the intensity ratio of the two bands was found to vary linearly with the local hydration of the membrane. So, in principle, these probes were found to be useful for monitoring both the polarity and hydration properties of the membrane.[12]

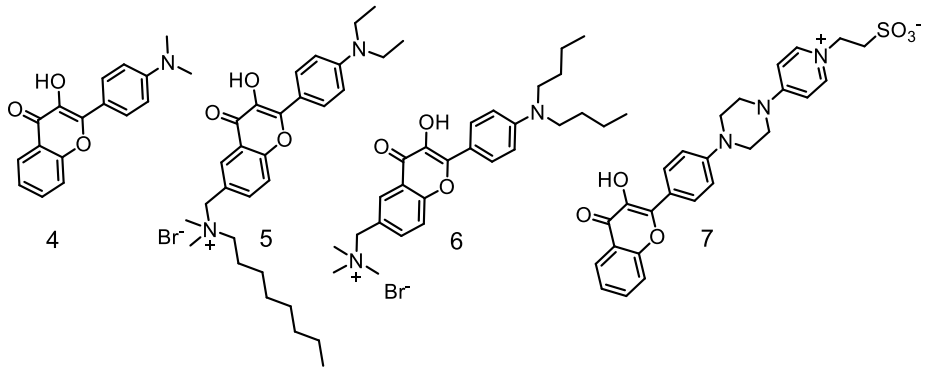

Figure 1D.3. The molecular structures of environment sensitive membrane probes **4** - **7**.

1D.2.4. Membrane probes for lipid order monitoring

As explained in the introduction, plasma membrane shows the asymmetric distribution of the lipids in the bilayer. Outer leaflet of the membrane contains a large amount of sphingomyelin (SM) (up to 40%) whereas only a fraction of it is present in the inner leaflet.[1,4] Probes which are specific to any of these leaflets have immense application potentials. For example, the programmed cell death (popularly known as apoptosis) is associated with the change in the lipid composition at the outer leaflet of the membrane.[1] So, probes which are selective to outer leaflet could be useful to monitor the apoptosis process. One such molecular probe specific to the outer leaflet of the membrane was developed by Klymchenko and co-workers.[13] This probe was designed by modifying the environmental sensitive fluorophore, Nile-red with an amphiphilic anchor group (Figure 1D. 4). This probe was exclusively bound to the outer membrane leaflet of the model vesicles as well as living cells. Moreover, this probe showed a significant blue shift for the liquid ordered phase,[13] hence one could monitor the lipid order with the help of this probe. Moreover, emission response of **8** correlates well with the cholesterol content of the cell membrane.

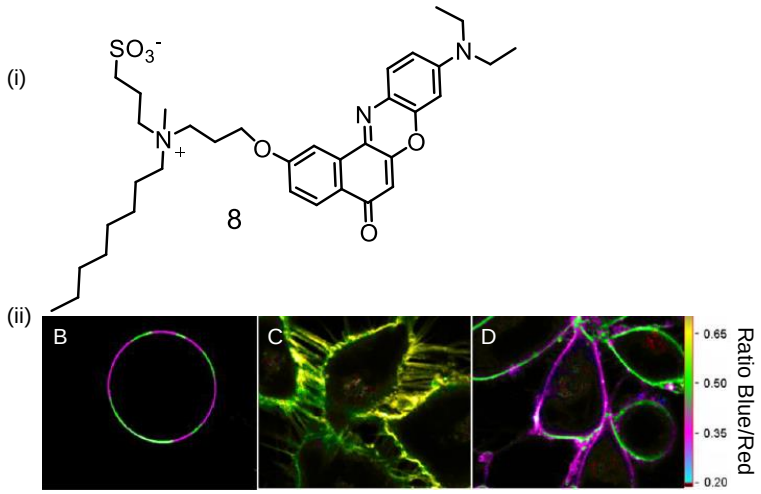

Figure 1D.4. (i) The molecular structure of the Nile-Red based membrane probe. (ii) its application for fluorescence ratiometric imaging of giant lipid vesicles (B) and living cells (astrocytoma). Giant vesicles were composed of Lo and Ld domains as visualized by **8**. Intact cells (C) and cells after cholesterol extraction with MβCD (D) show different color in the ratiometric images. (Reprinted with permission from ref.13. Copyright American Chemical Society)

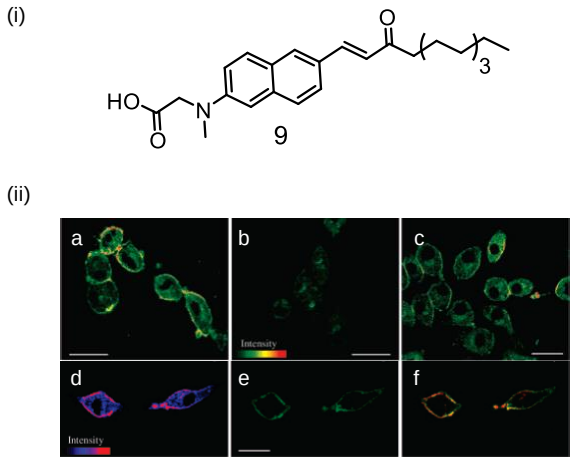

Figure 1D.5. (i) The molecular structure of TP lipid raft probe. (ii) (a-c) Pseudo colored TPM images of **9** labeled (2 μM) macrophages before (a) and after (b) treatment with 10 mM MβCD for 30 min at 37 °C. (c) TPM image of cholesterol depleted macrophages after repletion with 50 μM cholesterol for 1 h at 37 °C. The cells were labeled with 2 μM **9**. (d) The domains with high two-photon fluorescence intensity on macrophages labeled with **9**, (e) fluorescence image in the macrophages labeled with BODIPY-GM_1 and (f) merged image. Excitation wavelengths are 800 nm (a-d) and 488 nm (e), respectively. (Reprinted with permission from ref.14. Copy right American Chemical Society)

This enabled researchers for monitoring the cholesterol depletion process with methyl-β-cyclodextrin by fluorescence microscopy. This probe also has one additional attractive feature; one can use it for membrane imaging under 'no wash' conditions. Because of these features, this reagent was commercialized by Invitrogen.[13]

Naphthalene based two-photon (TP) turn ON probe (probe **9**) for lipid raft was reported by Cho and co-workers.[14] This probe could distinguish lipid ordered and disordered domains through TP microscopy in model membranes. TP microscopy experiments with live macrophages clearly showed bright regions (Figure 1D. 5) indicating the lipid raft. These regions disappeared following treatment with methyl- *β*-cyclodextrin (lipid raft destroying agent) and returned to nearly normal level after the treatment with cholesterol. A co-staining experiment with BODIPY-GM_1 (a well-known lipid raft probe) further confirmed the binding of **9** to lipid rafts.[14]

1D.2.5. Probes to report membrane potential

Electrostatic surface potential is another important property of the membrane that warrants mentioning in this discussion.

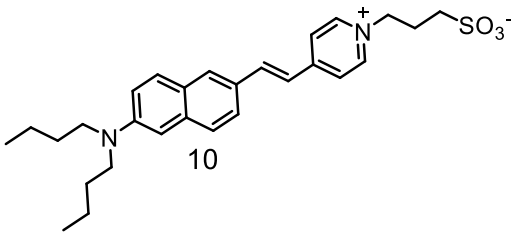

Figure 1D.6. The molecular structure of potential sensitive probe **10**.

In order to monitor membrane potential, electrochromic fluorophores with vertical orientation in the membrane are required. These probes should have a charged group on one side in order to bind the probe to polar head groups. On the other side such molecular probes should have long hydrophobic chains to ensure its strong insertion in the hydrophobic part of the bilayer.[15] Leow and co-workers developed a series of probes based on conjugated aminostyryl pyridinium analogue. These probes showed specific response on change in the membrane potential and were found to be useful for monitoring the potential of the membrane surface.[16]

1D.3. References

1. A. S. Klymchenko, *Acc. Chem. Res.*, 2017, **50**, 366-375.
2. K. R. Kampen, *J. Membr. Biol*, 2011, **242**, 69-74.
3. L. D. Bergelson, J. G. Molotkovsky and Y. M. Manevich, *Chem. Phys. Lipids*, 1985, **37**, 165-195.
4. K. Simons and E. Ikonen, *Nature*, 1997, **387**, 569-572.
5. Y. Niko, P. Didier, Y. Mely, G.-i. Konishi and A. S. Klymchenko, *Sci. Rep.*, 2016, **6**, 18870.
6. R. M. S. Cardoso, H. A. L. Filipe, F. Gomes, N. D. Moreira, W. L. C. Vaz and M. J. Moreno, *J. Phys. Chem. B*, **114**, 16337-16346.
7. M. K. Kuimova, G. Yahioglu, J. A. Levitt and K. Suhling, *J. Am. Chem. Soc.*, 2008, **130**, 6672-6673.
8. M. A. Haidekker and E. A. Theodorakis, *Org. Biomol.Chem.*, 2007, **5**, 1669-1678.
9. M. A. Haidekker, T. P. Brady, D. Lichlyter and E. A. Theodorakis, *Bioorg. Chem.*, 2005, **33**, 415-425.
10. M. R. Dent, I. Lopez-Duarte, C. J. Dickson, N. D. Geoghegan, J. M. Cooper, I. R. Gould, R. Krams, J. A. Bull, N. J. Brooks and M. K. Kuimova, *PCCP*, 2015, **17**, 18393-18402.
11. Y. Wu, M. Stefl, A. Olzynska, M. Hof, G. Yahioglu, P. Yip, D. R. Casey, O. Ces, J. Humpolickova and M. K. Kuimova, *PCCP*, 2013, **15**, 14986-14993.
12. A. S. Klymchenko, Y. Mely, A. P. Demchenko and G. Duportail, *Biochim. Biophys. Acta*, 2004, **1665**, 6-19.
13. O. A. Kucherak, S. Oncul, Z. Darwich, D. A. Yushchenko, Y. Arntz, P. Didier, Y. Mély and A. S. Klymchenko, *J. Am. Chem. Soc.*, 2010, **132**, 4907-4916.
14. H. M. Kim, B. H. Jeong, J.-Y. Hyon, M. J. An, M. S. Seo, J. H. Hong, K. J. Lee, C. H. Kim, T. Joo, S.-C. Hong and B. R. Cho, *J. Am. Chem. Soc.*, 2008, **130**, 4246-4247.
15. A. P. Demchenko, Y. Mely, G. Duportail and A. S. Klymchenko, *Biophys. J.*, 2009, **96**, 3461-3470.
16. E. Fluhler, V. G. Burnham and L. M. Loew, *Biochemistry*, 1985, **24**, 5749-5755.

1E. Probes for the detection of Apoptosis

1E.1. Introduction

The lipid bilayer of the mammalian plasma membrane is made up different polar lipids and proteins. Plasma membrane shows the asymmetric distribution of the polar lipids in the bilayer wherein the zwitterionic phosphatidylcholine (PC) is present in the outer leaflet of the bilayer, while the anionic phosphatidylserine (PS) exclusively located in the inner leaflet.[1] This asymmetric distribution is maintained by the intracellular translocases enzymes.[2] During the apoptosis or 'programmed cell death', translocases activity is diminished, leading to the exposure of the negatively charged PS on the cell surface. Presence of the negative charge on the cell surface is a hallmark of apoptosis. This is a natural phenomenon responsible for daily clearance of dead cells in the body.[2] The appearance of anionic PS on the cell surface is a key biomarker of many disease states, namely activation of coagulation factors, clot formation during injury, fiber formation on arterial walls in cardiovascular diseases. These are all due to PS exposure on cell surface.[2] Moreover, the therapeutic efficacy of any cancer treatment is judged by the apoptosis.[3] So, apoptosis detection is very important from the biological and clinical standpoint. Apoptosis process could be in many ways, prominent methodologies are based on DNA fragmentation, caspase activation, etc.[4,5] However, the most extensively methodology involves monitoring the appearance of negatively charged PS on the cell surface by the reagent Annexin V.[2] Annexin V is a fluorescently labelled antibody that specifically binds to the negatively charged PS. Even though Annexin V is extensively used in the apoptosis detection, this reagent has many limitations.[6] Annexin V has a short shelf life and this protein is not stable. Annexin V activity solely depends upon the extracellular Ca^{2+} concentration.[2,6] Presence of a millimolar concentration of extracellular Ca^{2+} is required for this enzyme is to be an active one. There are some phospholipid transport proteins in membranes called scramblases. These proteins are responsible for the non-specific movement of the phospholipids in the bilayers. Scramblases are activated in the presence of micromolar Ca^{2+}, which add to an error in the measurement by Annexin V.[2,6] In addition to this, Annexin V binding kinetics is very slow and this accounts for an incubation time of 1 hour for complete binding.[6] So, there is a distinct scope for developing appropriate reagents to overcome all these limitations. Significant effort has been put forward by many research groups to develop the reagents. Among the various strategies, reagents based on positively charged Zn(II)-complexes seem to be a better alternative for Annexin V. Various probes designed for the apoptosis detection

were briefly summarized here. The discussion in this part of this dissertation is mainly focused on probe design and their interesting biological applications.

1E.2. Various probes for Apoptosis

1E.2.1. Probes based on Zinc(II)-complexes

Cationic zinc-dipicolylamine (ZnDPA) complexes with an appended fluorescence active fragment are designed and extensively studied for the detection of apoptosis.[2] These cationic complexes form a strong association with the negatively charged phosphate and carboxylate residues of the PS head group and this serves as the basis for the targeting of apoptotic cells (Figure 1E.1). ZnDPA-based probes are superior to conventional Annexin V in many aspects. These probes show fast response, excellent water solubility, and high specificity.[2] Moreover, these probes are independent of Ca^{2+} concentration, a major drawback of Annexin V based measurement. Based on this strategy many probes with different reporter units were developed and utilized as apoptosis reporters.

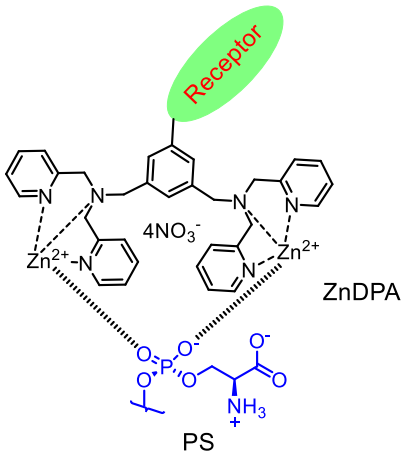

Figure 1E.1. The schematic representation of the association between anionic PS and ZnDPA receptor.

A ZnDPA derivative probe (**1**), appended with anthracene as the fluorophore was reported by Smith et al.[7] Probe **1** showed a 10-fold increase in the emission intensity in the presence of 50% of anionic phospholipids. Moreover, this probe could detect apoptotic cells as efficiently as Annexin V-FITC (Fluorescein isothiocyanate), a commercially available apoptosis marker. The drawback of this probe is that it needs the excitation in the blue region (380 nm), which is not suitable for bio studies.[7]

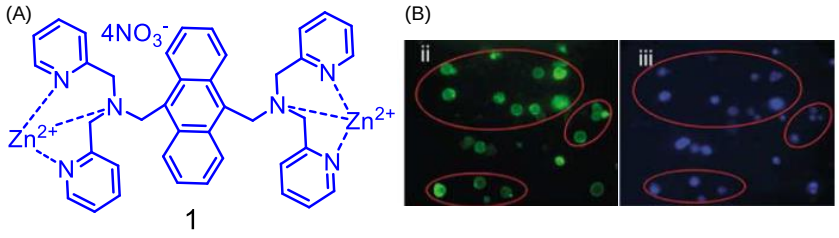

Figure 1E.2. (A) The molecular structure of anthracene-ZnDPA probe. (B) Jukart cells stained with Annexin V FITC (II). Jukart cells stained with **1** (iii) (Reprinted with permission from ref. 6. Copyright Springer Nature).

Nitrobenzoxadiazole (NBD) is an environment sensitive fluorophore, which is known to be poorly emissive in the hydrophilic environment and strongly emissive in the hydrophobic environment.[8] Exploiting this property, two ZnDPA complexes having appended NBD fragments were designed for PS sensing with different linker groups. Probe **2** had a butyl linker and Probe **3** had a long tris(ethyleneoxy) linker.[8] Both the probes showed fluorescence enhancement in the presence of PS-rich vesicles, however, the latter one showed more enhancement in the emission than the former one. Because of the broad emission of NBD, these probes could not be utilized for studying apoptosis.

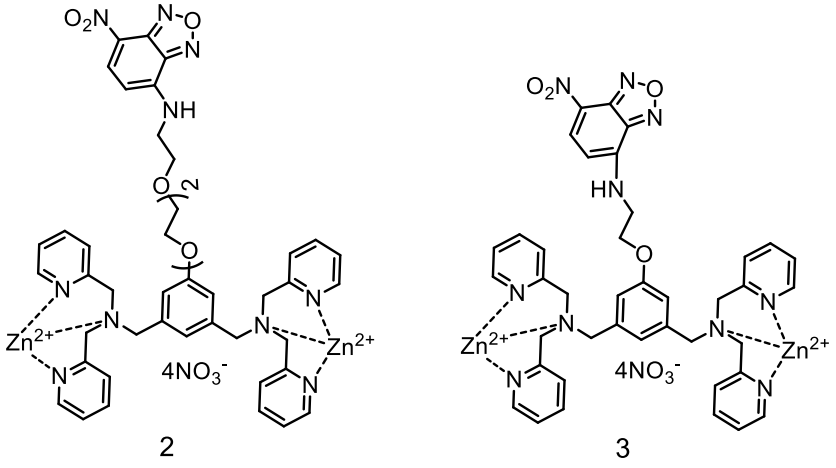

Figure 1E.3. The molecular structures of NBD-ZnDPA probes.

Increase in the number of Zn-DPA units in a single probe could increase the affinity of the probe to PS, which in turn could be useful for in vivo targeting. To realize this, two far-red fluorescent probes having cyanine reporter functionalities were derived using a phenoxide bridged bis-dipocolylamine Zn(II)-complexes by Bradley Smith and co-workers.[9] Among these two probes, one was a bivalent version with 4 Zn(II)-centres (probe **4**) and the other one was the monovalent version with two Zn(II)-centres (probe **5**). They utilized a FRET-based assay method by using $DiIC_{18}$, a cyanine-based fluorophore as FRET donor. Upon

addition of liposomes with different concentration of PS, a bleaching of the donor fluorophore intensity at 568 nm was observed (following λ_{Ext} = 480 nm) with concomitant growth in emission intensity at 660 nm. As anticipated, the bivalent probe showed strong affinity to PS-rich membrane.

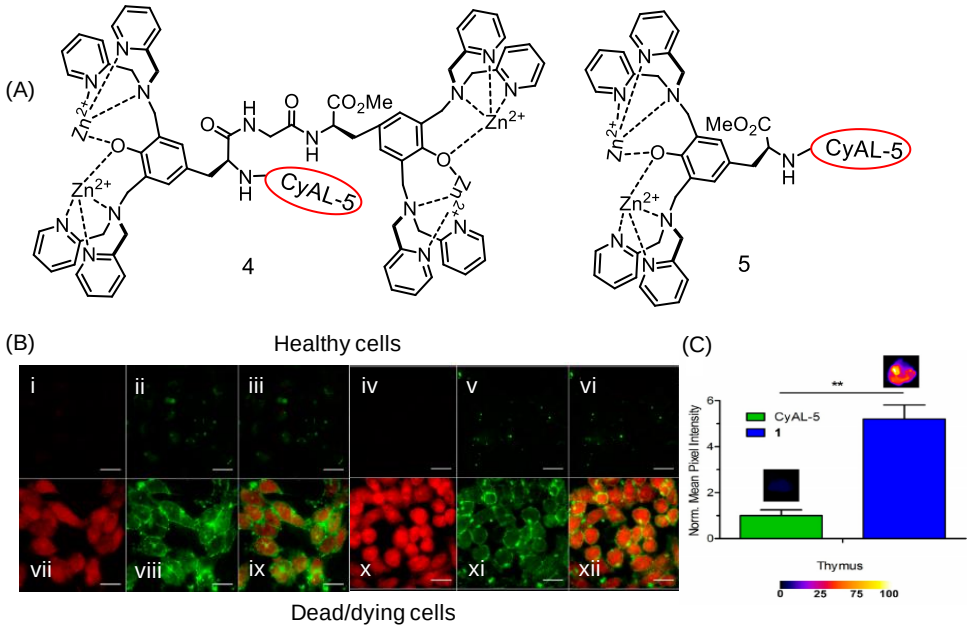

Figure 1E.4. (A) The molecular structures of receptors **4** and **5**. (B) Fluorescence micrographs of healthy (Top row) and dead/dying (Bottom row) CHO-K1 cells stained with probe **4** (I & vii), Annexin V Alexafluor 488 (ii & viii, v & xi), probe **5** (iv & x). (iii & ix represents the merged images of i& ii and vii & viii respectively. vi & xii represents merged images of iv & v and x & xi respectively. (C) In vivo imaging; Intensity profile plot of the mice organ slice treated with probe **5** (Reprinted with permission from ref. 9 Copyright American Chemical Society).

However, this probe exhibited self quenching on the membrane surface, whereas the monovalent version showed bright fluorescence and was found to be best suited for apoptosis imaging. Apoptosis imaging in CHO-K1 cells was performed and compared with a standard Annexin V Alexafluor 488. Both the probes showed strong affinity to dead and dying cells. Moreover, these Zn(II)-based probes internalized in cells whereas Annexin V localized preferentially on the apoptotic cell membrane. Further, the probe **5** was used for in vivo imaging in mice. Apoptosis in mice was induced by dexamethasone injection for 24 hours. Further, mice were injected with the probe and organ slices were imaged. This was the first attempt to use Zn-DPA probes for in vivo imaging.[9] Smith et.al reported three PS probes using the receptor-spacer-reporter concept. Probe **6** was functionalized with fluorescein reporter, the probe **7** was functionalized with biotin and the third one (probe **8**) was conjugated to CdSe/CdS quantum dots. All these probes showed

good affinity to PS-rich domains on the apoptotic cell surface. These probes could work under Ca^{2+} free conditions.[10]

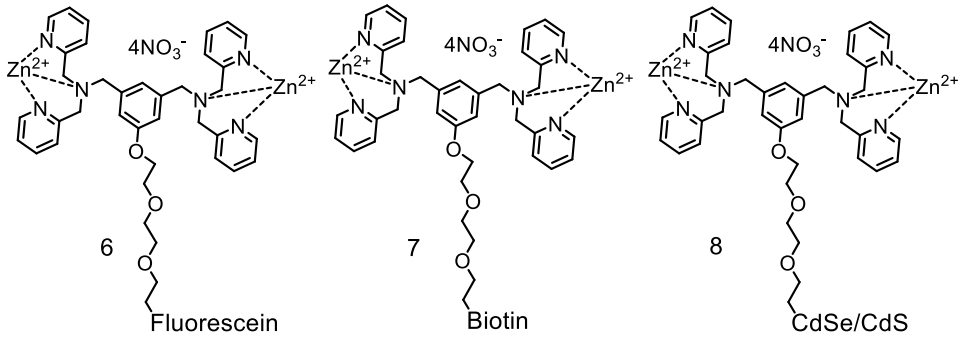

Figure 1E.5. The molecular structures of ZnDPA complexes appended with fluorescein **6,** biotin **7** and CdSe/CdS quantum dots **8**.

Bin Liu and coworkers reported an Aggregation Induced Emission (AIE) based Zn(II)-DPA probe (probe **9**).[11] This probe showed no affinity to healthy cells but could bind specifically to the negatively charged membrane in early stages of apoptosis and to DNA in the late stages of apoptosis. Moreover, the molecular probe without Zn(II)-center was found to find specifically to lipid droplets inside the cells. This molecular probe showed week emission at 483nm on excitation at 365 nm. Upon addition of the probe to a mixture of (1:1) POPS and POPC vesicles, enhancement in the fluorescence with an observed red shift from 483 to 563 nm was observed due to an effective ESIPT process. Interestingly, this probe showed large Stokes shift of 190 nm. Its application in the apoptosis detection in HeLa cells was demonstrated and efficiency was compared with the standard Annexin V 488 reagent.[11]

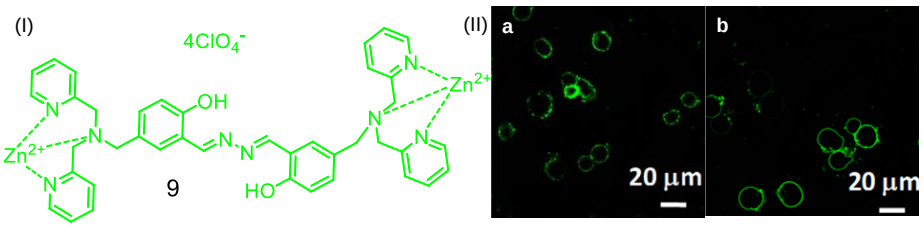

Figure 1E.6. (I) The molecular structure of ZnDPA based AIE probe. Confocal micrographs of apoptotic HeLa cells (a) treated with **9** (20 µM) and (b) treated with Alexa Fluor 488 Annexin V. Apoptosis in these cells were induced by the treatment with 250 µM of H_2O_2 for 6 hours. (Reprinted with permission from ref.11. Copyright American Chemical Society).

1E.2.2. Ratiometric probe for Apoptosis

Ratiometric probes are very useful for the accurate measurement. As discussed earlier, ratiometric emission response is independent of analyte concentration. Hence, one can determine/ quantify the analyte concentration more accurately when compare to those probes having single emission band. Klymchenko et. al reported the first ratiometric probe for apoptosis detection.[3]

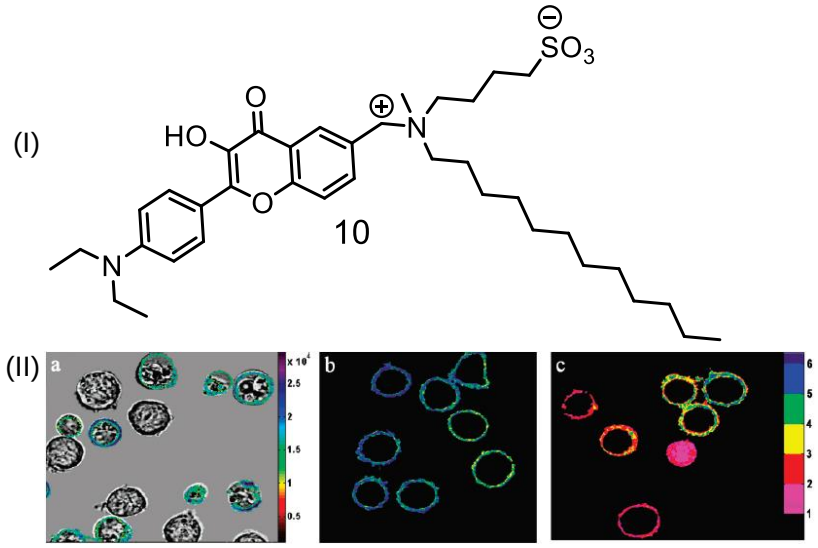

Figure 1E.7. (I) The molecular structure of the ratiometric molecular probe **10**. (II) Confocal micrographs of T lymphocytes stained with annexin V-FITC (a) and **10** (b and c). (a). FITC intensity is displayed in pseudocolor by using the color code on the right scale. (b and c) Ratiometric images of normal (b) and actinomycin D-treated (c) cells stained with 0.2 μM **10**. The ratios of intensities of the two bands are displayed in pseudocolor by using the color code on the right scale. Apoptosis was induced by Actinomycin D treatment for 18 h. (Reprinted with permission from ref. 3 Copyright American Chemical Society).

Probe **10** consisted of a hydroxyflavone based fluorophore unit functionalized with a zwitterionic anchor group having a long hydrophobic tail.[3] This probe could sense the loss of plasma membrane integrity occurring during the early stages of the apoptosis. This probe exhibited ESIPT process and resulted two-band emission that were found to be highly sensitive to apoptosis process. This enabled molecular probe **10** to be used for ratiometric imaging of apoptosis.[3]

1E.3. References

1. O. A. Kucherak, S. Oncul, Z. Darwich, D. A. Yushchenko, Y. Arntz, P. Didier, Y. Mély and A. S. Klymchenko, *J. Am. Chem. Soc.*, 2010, **132**, 4907-4916.

2. D. R. Rice, K. J. Clear and B. D. Smith, *Chem. Commun.*, 2016, **52**, 8787-8801.

3. V. V. Shynkar, A. S. Klymchenko, C. Kunzelmann, G. Duportail, C. D. Muller, A. P. Demchenko, J.-M. Freyssinet and Y. Mely, *J. Am. Chem. Soc.*, 2007, **129**, 2187-2193.

4. Y. Wu, D. Xing, S. Luo, Y. Tang and Q. Chen, *Cancer Lett.*, 2006, **235**, 239-247.

5. P. R. Walker, J. Leblanc, B. Smith, S. Pandey and M. Sikorska, *Methods*, 1999, **17**, 329-338.

6. A. V. Koulov, K. A. Stucker, C. Lakshmi, J. P. Robinson and B. D. Smith, *Cell Death Differ.*, 2003, **10**, 1357.

7. B. A. Smith, W. J. Akers, W. M. Leevy, A. J. Lampkins, S. Xiao, W. Wolter, M. A. Suckow, S. Achilefu and B. D. Smith, *J. Am. Chem. Soc.*, 2010, **132**, 67-69.

8. C. Lakshmi, R. G. Hanshaw and B. D. Smith, *Tetrahedron*, 2004, **60**, 11307-11315.

9. K. J. Clear, K. M. Harmatys, D. R. Rice, W. R. Wolter, M. A. Suckow, Y. Wang, M. Rusckowski and B. D. Smith, *Bioconjugate Chem.*, 2016, **27**, 363-375.

10. R. G. Hanshaw, C. Lakshmi, T. N. Lambert, J. R. Johnson and B. D. Smith, *ChemBioChem*, 2005, **6**, 2214-2220.

11. Q. Hu, M. Gao, G. Feng, X. Chen and B. Liu, *Acs Appl. Mater. Interfaces*, 2015, **7**, 4875-4882.

CHAPTER 2

REAGENT FOR SPECIFIC RECOGNITION OF CYSTEINE IN AQUEOUS BUFFER AND IN NATURAL MILK: IMAGING STUDIES, ENZYMATIC REACTION AND ANALYSIS OF WHEY PROTEIN

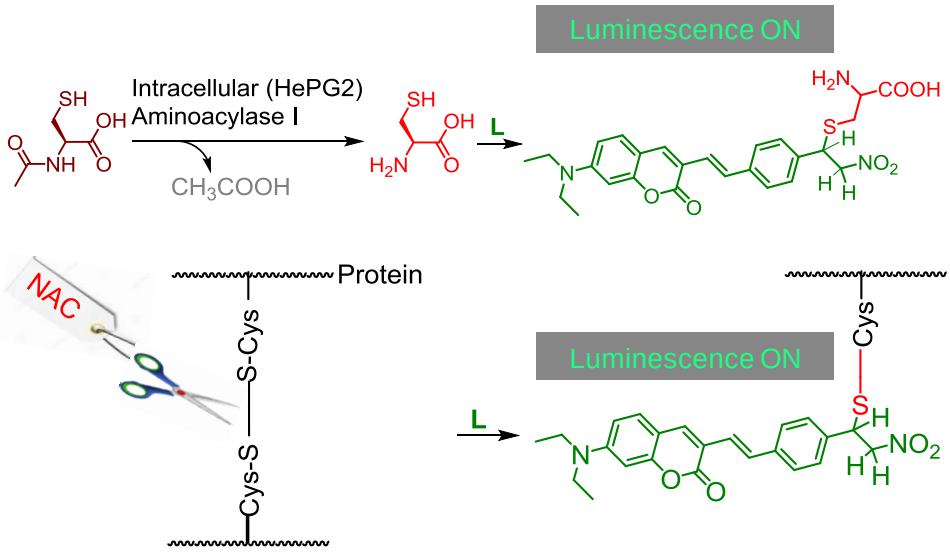

Publication:
Chem. Commun., 2015, **51**, 15592-15595

2.1. Introduction

Post-translational modifications of specific amino acids play major roles in regulating protein function.[1] Major functional sites of proteins that typically respond to redox perturbations contain cysteine (Cys) residue.[1] Glutathione (GSH) plays a pivotal role in maintaining cellular antioxidant defense system.[1e,1f,2a] Abnormal levels of GSH is linked to many diseases such as HIV, aging, neurodegenerative diseases and cancer.[2a] Cys is one of the three main precursors that are required for GSH synthesis.[1b,e,f] Apart from this crucial role in human physiology, deficiency of Cys also has adverse influences on child growth, depigmentation of hair, edema, liver damage, skin lesions, and weakness.[1c,d] Literature reports also suggest that free Cys is not ideally suited for human physiology for its toxicity and facile oxidation.[2b] Thus, appropriate and stable Cys-derivatives are prescribed as supplements, which participate in an enzymatic reaction to liberate Cys for maintaining its optimum concentration in human blood plasma (HBP). Whey protein (WP) concentrate is also used as an effective Cys supplement for GSH replenishment in its immune deficient state.[3a]

Thus, specific detection and estimation of Cys and its derivatives have significance in clinical research and diagnostics. However, interference from Hcy (Homocysteine) and GSH makes it difficult owing to the similarities in structure and reactivity. Also, some of the reagents, which are commonly adopted for different chemodosimetric detection of Cys, also react with CN^-, an efficient nucleophile with relatively low hydration enthalpy.[3b,4] All these add to the challenge in designing a reagent for specific detection and estimation of Cys in biofluids. HPLC is the most conventional methodology that is being adopted for Cys estimation in biofluids. However, such a procedure involves intricate sample preparation process and more importantly requires a post-column derivatization technique.[4] Considering the complexity involved in such process, recent efforts are focused in designing fluorescence-based molecular probes for selective estimation of Cys in biofluids as well as for use as an imaging reagent for detection of intracellular distribution of Cys.[1c,d] Strategies like chemodosimetric procedure or metal-Cys coordination has usually been adopted for specific recognition of Cys in aqueous medium.[5] Barring some reports,[6] examples for specific detection of Cys or its residues in the presence of above referred competing biothiols are limited. Moreover, none of these reagents was utilized for developing an assay for enzyme

like Aminoacylase-1 for *in-situ* generation of Cys from a prescribed drug N-acetyl cysteine (NAC), which is generally used for treating psychiatric and many other disorders[7] or for estimation of Cys/ Cystine residues in cow's milk whey.

Keeping these in mind, we have designed a chemodosimetric probe (**L**) for specific reaction with Cys in the presence of all other amino acids (including Hcy and GSH), all common anions and cations (alkali, alkaline earth and transition metal ions that are common in human physiology) in physiologically relevant aq. medium. Using the specificity of this reagent **L** towards Cys, we could estimate Cys residues with free sulfhydryl functionality in whey protein as well as we could develop an efficient methodology for probing the release free Cys from NAC by Aminoacylase-1, an important enzyme for human physiology. Such example is scarce in the contemporary literature.

2.2. Experimental Section

2.2.1. Materials

Vinyl acetic acid, 4-(diethylamino)salicylaldehyde, *N,N'*-dicyclohexylcarbodiimide (DCC), 4-dimethylaminopyridine (DMAP), CS_2CO_3, 4-bromobenzaldehyde, sodium acetate, triphenylphosphine, Pd(OAc) and Cysteine, were obtained from Sigma Aldrich and were used as received. Nitro methane, ammonium acetate, N-acetyl Cysteine, Histidine, Glutathione, Arginine, Isoleucine, Proline, Methionine, Glycine, Alanine, Serine, Threonine, Tryptophan, Tyrosine, Valine, Leucine were purchased from SD Fine Chemicals, India. Solvents used for the synthesis of various intermediates and final compound were of AR grade (S.D. Fine Chemicals) and were dried using standard procedures. HPLC grade (S.D. Fine Chemicals) solvents were used for all spectroscopic studies.

2.2.2. Analytical Methods

^{1}H and ^{13}C NMR spectra were recorded on Bruker 400/500 MHz FT NMR (Model: Advance-DPX 400/500) using TMS as an internal standard. High-resolution mass spectra were recorded on JEOL JM AX 505 HA mass spectrometer. IR spectra were recorded on Bruker Alpha FT IR spectrometer. UV-Vis spectra were recorded using Shimadzu UV-1800 spectrometer. Fluorescence measurements were carried out on quanta master-400 fluorescence spectrometer. Microplate reading experiment was performed in a Varioskan

flash multimode reader. Confocal images were acquired in Olympus Fluoview microscope.

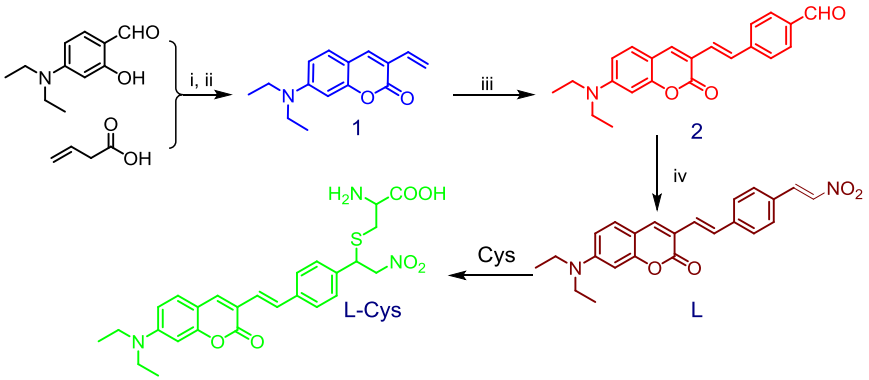

i. DCC, DMAP, CH_2Cl_2, 0° C, 4h; ii. Cs_2CO_3,12h; iii. 4-bromobenzaldehyde, $Pd(OAc)_2$, PPh_3, NaOAc, DMF, 80°C, 16h; iv CH_3NO_2, NH_4OAc, 85°C, 3h.

Scheme 2.1. The methodology adopted for the synthesis of **L**.

2.2.3. General experimental procedure for UV-Vis and Fluorescence studies

A stock solution of **L** was prepared in acetonitrile and the same solution was used for all the studies after appropriate dilution. Unless and otherwise mentioned, 10mM and pH 7 solution of aq. HEPES buffer was used for all spectroscopic studies. All amino acid solutions of $1X10^{-1}$M were prepared in HEPES buffer (pH 7). For spectroscopic measurements, the stock solution of the probe was further diluted by using HEPES: ACN (9:1) mixture and the effective final concentration were made as 10 μM. All luminescence measurements were done using λ_{Ext} = 445 nm with an emission slit width of 2 nm. The fluorescence quantum yield was determined according to literature method using fluorescein (in 0.1 M NaOH) as a reference (Φ_f = 0.92).

2.2.4. Preparation of TLC test strips

TLC test strips were prepared by coating 5 μM of probe solution in acetonitrile on silica TLC plates. 5μl of Cys ($1x10^{-1}$M) in 10 μM aq.HEPES buffer (pH7) was added to it, dried and the visual, as well as fluorescence colour changes, were observed after 5 min. The same was repeated for Hcy and GSH as well. To detect Cys in blood plasma, 20 μl of blood plasma was (diluted with 20 μl buffer) added on probe quoted TLC plate. The same methodology was repeated for enzymatic reaction on TLC plate by using 10 μl of NAC and aminoacylase-1 enzyme.

2.2.5. General procedure for enzymatic study

Cipla made effervescent tablets of N-Acetyl-Cysteine (mucinac 600) were purchased from commercially available sources. Based on the quantity of NAC present in the tablet, $1X10^{-1}$M tablet solution was prepared in 10 mM aq.HEPES buffer solution (pH7). The enzyme solution was prepared according to the requirement by dissolving 1mg/ml in 10 mM aq.HEPES buffer solution (pH7). A fixed concentration of NAC (200 equiv.) was added to the 10 μM probe in HEPES: ACN (9:1). Since 1mg of the solid enzyme contains 3301 units of protein, and 1 unit can hydrolyse 1 μM of the substrate, accordingly enzyme concentration was varied with respect to the substrate concentration.

2.2.6. General procedure for detecting Cysteine from raw milk

Raw milk was subjected to fermentation and the liquid whey which was settled above after the fermentation process was separated by filtration. 500 μl whey was added to probe **L** (10 μM) in HEPES: ACN at pH 7. A varying amount of N-Acetyl Cysteine (0-500 μl) was added to each of the above solutions to hydrolyse the bound Cysteine present in whey protein (NAC solution was prepared by dissolving NAC tablets in a buffer as mentioned in the enzymatic study). A control experiment was performed by pre-treating the whey with 2 mM NEM prior to the addition of **L**. Luminescence changes were recorded after 45 minutes of incubation at room temperature. Luminescence measurements were also done by partially denaturing the protein at 60^{o} C for 1 hr.

2.2.7. General procedure for confocal studies

For confocal studies, HEPG2 cells (3×10^{5}) were seeded on coverslips placed in 6 well plates. After 24 hours, the cells were treated with 2 mM NEM for 30 minutes. Cells were then washed with buffer and treated with 20 μM of NAC and incubated for 1 hour. Further, cells were incubated with **L** (10 μM) for 30 minutes. Cells were then washed thrice with Phosphate Buffer Saline (1X PBS) and fixed with 4% PFA for 20 minutes and washed again with 1X PBS. Nail paint was used to seal the coverslips mounted on the glass slides. To make sure that the fluorescence was not from the intracellular cysteine; control experiment was performed by treating the cells with NEM followed by further incubation with **L** for 30 min. No fluorescence was observed from these cells, which indicates the complete blocking of intracellular cysteine and the observed fluorescence after incubation with NAC and **L** was due to the metabolism of NAC inside the cells. Images were acquired in Olympus Fluoview Microscope.

The *in vitro* cytotoxicity of **L** on HEPG2 cells were determined by conventional MTT (3-(4, 5-Dimethylthiazol-2-yl)-2, 5-diphenyltetrazolium bromide, a yellow tetrazole) assay. HEPG2 cells (7 x 10^3) were seeded in each well of a 96 well plate and cultured in a 37°C incubator supplied with 5% CO_2. Cells were maintained in DMEM medium, supplemented with 10% Foetal Bovine Serum and 100 Units of Penicillin-Streptomycin antibiotics. After 24 hours, the cells were treated with different concentrations of the **L** in triplicates for 12 hours. After treatment cells were added with 0.5 µg/ml of MTT reagent. The plate was then incubated for 4 hours at 37°C. 100 µl of Isopropyl Alcohol was added to each well. Optical density was measured at 570nm using Multiskan Go (Thermo Scientific) to find the concentration of the cell inhibition. IC_{50} value has been calculated to be 100 µM. The formula used for the calculation of the MTT assay for evaluation of the cell viability was as follows: Cell viability (%) = (means of Absorbance value of treated group/ means of Absorbance Value of untreated control) X 100.

2.2.8. Determination of detection limit

The detection limit was calculated based on the fluorescence titration. To determine the S/N ratio, the emission intensity of **L** without Cys was measured 10 times and the standard deviation of blank measurements was determined. The detection limit (DL) of **L** for Cys was determined from the following equation: DL = K * Sb1/S. Where K = 2 or 3 (we took 3 in this case); Sb1 is the standard deviation of the blank solution; S is the slope of the calibration curve. From the graph, we get slope = 1.2097x 10^8, and the Sb1 value was found to be 427.5843. Thus by using the above formula detection limit = 26.01 x 10^{-9} M.

2.3. Synthesis and Characterisation

2.3.1. Synthesis of 1

Under N_2 atmosphere, to a solution of vinyl acetic acid (0.28 mL, 3.23 mmol) in dry CH_2Cl_2 , DCC (667.45 mg, 3.23 mmol) was added and stirred at 0^oC for 1 hr. To this, 4-(diethylamino) salicylaldehyde (500 mg, 2.58 mmol) and DMAP (40 mg, 0.32 mmol) were added and it was stirred at room temperature for 2 hr. The reaction was monitored by TLC. Once the reaction was completed, the solid was filtered and to the filtrate CS_2CO_3 (843 mg, 2.58 mmol) was added and it was stirred for 12 hr to complete the reaction. The mixture was washed with H_2O, dried, concentrated under vacuum. The crude product was purified by column chromatography to give vinylcoumarin as greenish yellow solid. Since the compound is labile, it was stored in cold condition. Yield-56%. IR (film) ν_{max} (cm^{-1}) :

1707 (CO), 1597 (C=C), 3017 (-C=C-H).^{1}H NMR ($CDCl_3$, 400 MHz): δ (ppm) 1.19 (6H, t, CH_3), 3.38 (4H, q, CH_2), 5.26 (1H, d, *J*=11.45Hz, CH), 5.98 (1H, d, *J*=17.40Hz), 6.65 (1H, *J*=17.80Hz, CH), 7.55 (1H, s), 6.55 (1H, dd, *J*=8.7Hz and *J*=2.75Hz), 6.45 (1H, d), 7.23 (1H, S). ^{13}C NMR ($CDCl_3$, 125 MHz): δ (ppm) 12.48, 44.83, 97.09, 109, 115.75, 117.86, 128.87, 131.16, 135.54, 150.50, 155.80, 161.35. HRMS (ESI): m/z calculated for $C_{15}H_{18}NO_2$ [M+H] 244.1332 found 244.1331.

2.3.2. Synthesis of 2

Vinylcoumarin (75 mg, 0.30 mmol) was taken in dry DMF, to this 4-bromobenzaldehyde (64 mg, 0.36 mmol), sodium acetate (28 mg, 0.33 mmol) and triphenylphosphine (64.67 mg, 0.24 mmol) was added and it was purged with N_2 and was added $Pd(OAc)_2$ (14 mg, 0.06 mmol). It was refluxed for 12 hr at 80^{o} C under an inert atmosphere; the completion of the reaction was monitored by TLC. Reaction mass was washed with H_2O and brine solution, dried, concentrated under vacuum. The crude product was purified by column chromatography to give compound 2 as an orange red solid. Yield- 80%. IR (film) ν_{max} (cm^{-1}): 1696 (-CHO), 1612 (C=C), 3021 (-C=C-H). ^{1}H NMR ($CDCl_3$, 400 MHz): δ (ppm) 1.25 (6H, t, CH_3), 3.46 (4H, q, CH_2), 6.52 (1H, d, *J*=1.96 Hz), 6.63 (1H, dd, *J*=8.8Hz), 7.20 (1H, *J*=16.14Hz), 7.28 (1H, t, *J*=8.80 Hz), 7.55 (1H, d, *J*=16.38 Hz), 7.65 (2H, d, *J*=8.07Hz), 7.73 (1H, s), 7.85 (2H, d, *J*=8.07 Hz), 9.99 (1H, s, CHO). ^{13}C NMR ($CDCl_3$, 100 MHz): δ (ppm) 12.49, 44.93, 97.11, 109.30, 116.83, 126.87, 128.58, 129.15, 130.21, 135.16, 139.77, 143.98, 150.90, 155.89, 161.15, 191.63. HRMS (ESI): m/z calculated for $C_{22}H_{21}N_2O_3$ [M+H] 348.1594 found 348.1591.

2.3.3. Synthesis of L

Compound 2 (80 mg, 0.23 mmol) was dissolved in nitromethane (8 mL) and was added ammonium acetate (170 mg, 2.30 mmol). It was refluxed for 3hr and reaction was monitored by TLC. After the completion of the reaction, it was concentrated under vacuum and purified by column chromatography to give compound 3 as red solid. Yield- 49%. IR (film) ν_{max} (cm^{-1}) : 1701 (CO), 1506 (N-O), 1615 (C=C), 3024 (-C=C-H).^{1}H NMR (DMSO-d_6, 400 MHz): δ (ppm) 1.14 (6H, t, CH_3), 3.45 (4H, q, CH_2), 6.57 (1H, s), 6.74 (1H, d, *J*=8.80 Hz), 7.27 (1H, d, *J*=16.14 Hz), 7.47(1H, d, *J*=8.80 Hz), 7.53 (1H, d, *J*=16.38 Hz), 7.64 (2H, d, *J*=8.07 Hz), 7.84 (2H, d, *J*=8.07 Hz), 8.10 (1H, s), 8.14 (1H, d, *J*=15.45 Hz), 8.22 (1H, *J*=13.45 Hz). ^{13}C NMR (DMSO-d_6, 100 MHz): δ (ppm) 12.83, 44.64, 96.74, 108.85, 109.99, 116.08, 126.78, 127.30, 128.40, 129.66, 130.16, 130.96137.85,

139.43, 141.25, 141.78, 151.21, 155.93, 160.59. HRMS (ESI): m/z calculated for $C_{23}H_{22}N_2O_4$ [M+H] 391.1652 found 391.1651.

2.4. Results and Discussions

Kim and co-workers reported the role of pKa in achieving the desired specificity to Cys (in presence of Hcy & GSH) for participating in Michael-type reactions.[6d] We have adopted this methodology for designing an efficient chemodosimetric probe (**L**, Scheme 2.1) for Cys. Choice of nitro olefin not only helped in achieving a favorable intramolecular charge transfer (ICT) transition but also offered us the desired functionality for participating in the Michael-type reaction.[5j]

The synthetic methodology adopted for the synthesis of **L** is given in Scheme 2.1. Analytical and spectroscopic data confirmed the formation of product **L** with the desired purity. Electronic spectrum of **L** (10 μM) in aq. HEPES buffer:CH_3CN (9:1, v/v; pH 7) showed a λ_{Max} of 468 nm in the visible region and this was attributed to an ICT process with Me_2N- functionality as a donor and -NO_2 as acceptor. Observed redshift of this absorption band upon an increase in the solvent polarity [Figure. 2.1 (I)] confirmed the predominant ICT nature of this band.

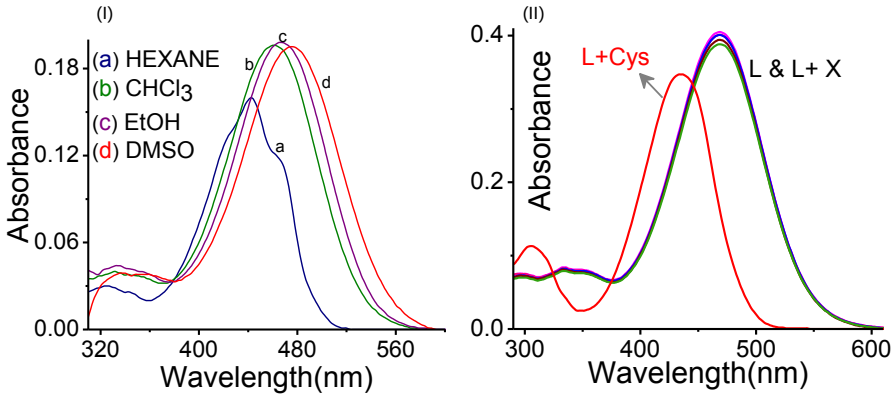

Figure 2.1. (I) Absorption spectra of probe in different solvents of varying polarity. (II) Absorption spectra of probe in the presence of different analytes and cysteine.

Spectrum for **L** (10 μM) remained unchanged when it was recorded in the presence of 100 equiv. of all common anions (X: F^-, Cl^-, $H_2PO_2^-$, CH_3COO^-, HSO_4^-, CN^-), cations (Na^+, Ca^{2+}, Mg^{2+}, $Fe^{2+/3+}$, Cu^{2+}, Cr^{3+}, Ni^{2+}, Zn^{2+}, Hg^{2+}) [Figure 2.1 (II)] and natural amino acids (AAs: Histidine (His), Leucine (Leu), Methionine (Met), Isoleucine (Ile), Phenyl alanine (Phe), Tryptophon (Trp), Tyrosine (Tyr), Valine (Val), Serine (Ser), Alanine (Ala), Arginine (Arg), Glycine (Gly), Aspartame

(Asp), Glutamine (Gln), Proline (Pro), Aspartic acid (Asp), Glutamic (Glu) acid, Threonine (Thr), Lysine (Lys), Methionine (Met), GSH and Hcy), except for Cys. For Cys, a distinct hypsochromic shift of ~ 30 nm [Figure 2.1 (II)] was observed with a visually detectable change in solution colour from reddish brown to light green (Figure 2.2 A). Systematic titration with **L** (10 μM) in the presence of varying [Cys] (0-100 equiv.) in aq. HEPES-CH_3CN medium (9:1, v/v; pH 7) revealed a ratiometric response with gradual bleaching of the ICT band for **L** at 468 nm and a concomitant growth of a new absorption band with λ_{Max} at 438 nm (Figure 2.2 A).

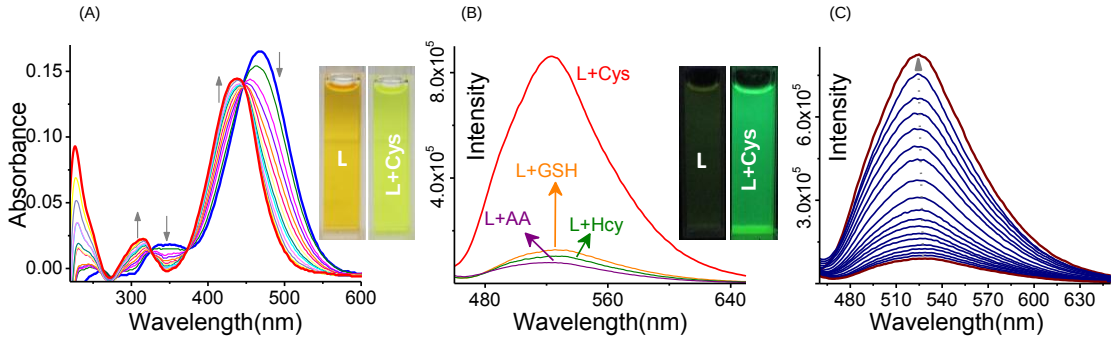

Figure 2.2. (A) UV-Vis titration profile for **L** (10 μM) in the absence and presence of varying [Cys] (0-1 mM) (B) Emission spectra of **L** in absence and presence of various AAs. (C) Emission titration profile for **L** (10 μM) in the absence and presence of varying [Cys] (0-100 equiv.).

Titration profile revealed three simultaneous isosbestic points at 325, 372 and 445 nm, which confirmed the presence of only two species in equilibrium. Luminescence band maximum for reagent **L** (10 μM) appeared at ~ 520 nm on excitation at 445 nm (λ_{Max} ICT). Spectral pattern essentially remains unchanged upon addition of 200 mole equiv. of all natural AAs (except Cys) and all other common anionic/cationic analytes. Emission titration profile clearly revealed that a switch *ON* luminescence response with an emission maximum of 520 nm (Φ_f **L** ~ 0.06 & Φ_f **L**+Cys = 0.32; using fluorescein with Φ_f = 0.92 as standard) was observed for varying [Cys] (0-100 mole equiv., Figure 2.2 C). Simultaneously, a visually detectable change in solution luminescence (Figure 2.2 B) was observed. To confirm the Michael addition reaction between **L** and Cys, ^{1}H NMR spectra were recorded for **L** and **L** + Cys in $DMSO_{d6}$ (Figure 2.3) after the solution mixture of **L** and Cys was allowed to equilibrate for 20 min at RT. The olefin peaks at 8.25 ppm (H_a) and 8.15 ppm (H_b) for **L** disappeared, while the appearance of two new peaks was observed at 5.29 ppm and 4.77 ppm, respectively, for H_{a1}/H_{a2} and H_b, protons in **L**-Cys. Little upfield shifts were observed for aromatic protons and this

was attributed to a reduced electron withdrawing influence of -NO_2 functionality in **L**-Cys due to a lesser extent of extended conjugation. Formation of the proposed **L**-Cys adduct was further confirmed from an isolated reaction product of **L** and Cys using HRMS [ESI-Ms] (Figure 2.4). Formation of **L**-Cys is also expected to disfavour the ICT process and enhances the energy gap between the frontier orbitals (HOMO & LUMO), which agree well with the observed hypsochromic shift of ~ 30 nm in the UV-Vis spectra. Presumably, this enhanced HOMO-LUMO energy gap interrupted the non-radiative deactivation pathway of the ICT based excited state and accounted for the observed luminescence.

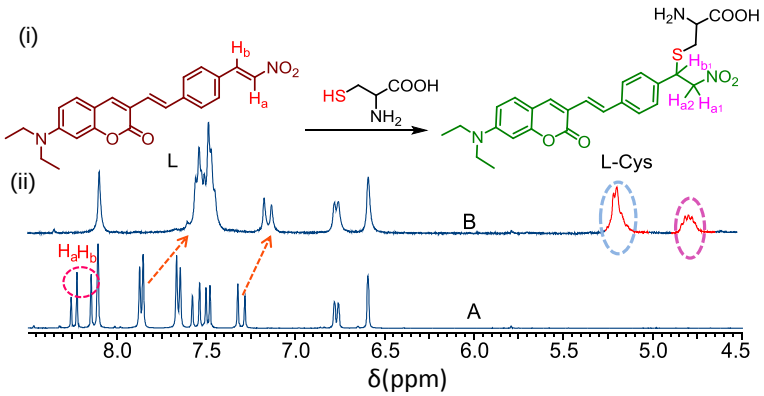

Figure 2.3. (i) Proposed mode of binding in between **L** and Cys; (ii) Partial ^{1}H NMR spectra of compound (A) **L** only and (B) **L** + Cys in DMSO-d_6.

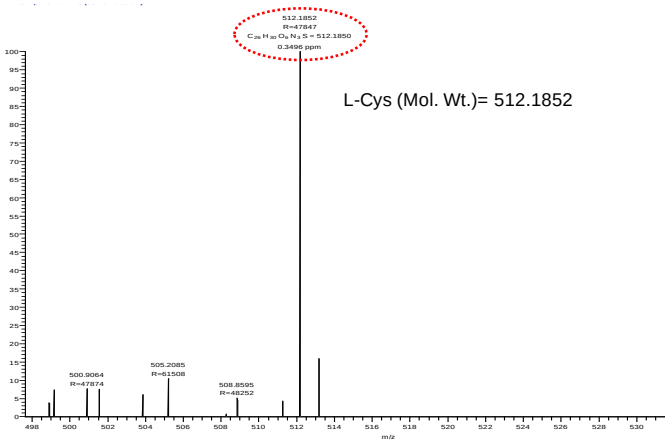

Figure 2.4. HRMS spectra of **L**+ Cys adduct.

Under identical conditions, other AAs and common anionic/cationic analytes did not show any detectable change in the absorption and luminescence spectra.

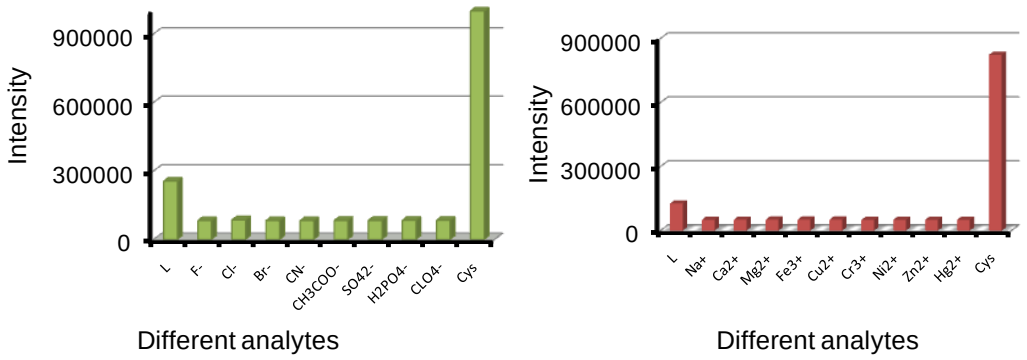

Figure 2.5. Fluorescence response of L upon addition of common cations, anions and Cys (100 equiv) in 10 mM HEPES: ACN (9:1) v/v at pH7, λ_{Ext} = 445nm

Examples of the molecular probes for specific recognition and estimation of Cys and its protein residues with free sulfhydryl$_{Cys}$ group in an ensemble of several other AAs are scanty and considering this, the result described in this article has significance.[1c] The switch ON luminescence response of the probe at 520 nm showed a good linear relationship with varying [Cys] (0 to 1000 μM; Figure 2.6 A). The lowest detection limit of Cys was determined as 23.65 nM based on signal to noise ratio of 3 at 520 nm (Figure 2.6 B).

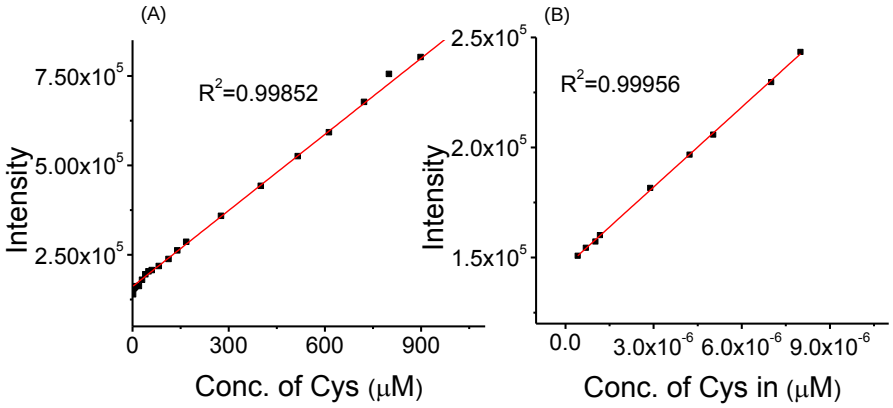

Figure 2.6. (A) Fluorescence intensity at 524 nm upon addition of Cys (0-1000μM) in10 mM HEPES: ACN (9:1) v/v at pH7,λ_{Ext} 445 nm. (B) Intensity vs. concentration plot for detection limit calculation.

Studies with Cys, Hcy and GSH (pKa values of 8.22, 10.00 and 9.20, respectively)[8,6d] at different pH were performed to examine the influence of pH on the observed specificity of the reagent towards Cys (Figure 2.7 A). pH studies clearly demonstrates the higher sensitivity and selectivity of the reaent **L** towards Cys at pH 7. Interference from GSH became noteworthy only at pH ≥ 8.

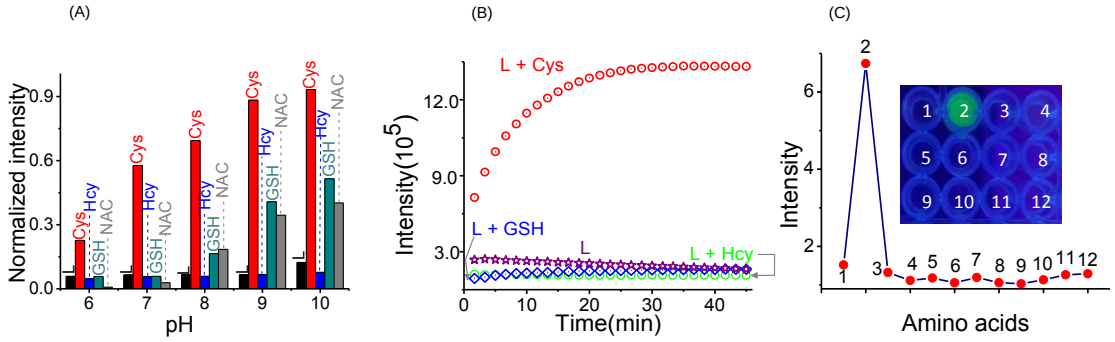

Figure 2.7. (A) Changes in fluorescence response (λ_{Ext} = 445 nm) of **L** (10 μM) with Cys, Hcy, GSH and NAC at varying solution pH; (B) Time-dependent fluorescence response of **L** (10 μM) with 200 mole equiv. of Cys, Hcy, and GSH. (C) Micro plate fluorescence reading of **L** with different AAs and corresponding plots of relative changes in emission intensities.(From 1-12- **L** only, Cys, Hcy, GSH, Met, His, Tryp, Ph-al, Gly, Val, Tyr, Ser) Inset: change in solution fluorescence on irradiation with 365 nm UV lamp in the presence of different AA. All studies were performed in 10 mM aq. HEPES: CH_3CN (9:1, v/v; pH 7.0)

Due to the lowest pKa value, the thiolate/thiol ratio was higher for Cys at pH 7.0, as compared to Hcy and GSH, which resulted in the higher reactivity and the desired specificity of **L** towards Cys. Figure 2.7 B further reveals that this chemodosimetric reaction takes approximately 25 minutes to complete. A comparison study further revealed that the possibility of any interference from GSH and Hcy was minimal under the identical experimental conditions. The microplate reading experiment with 0.2 μM of **L** and respective AAs (200 mole equiv.) in aq. HEPES: CH_3CN (9:1, v/v) solution further confirmed that only Cys could induce a detectable change in solution fluorescence (Figure 2.7 C).

After confirming that this reagent could detect Cys in an essentially aq. buffer medium (aq. HEPES: CH_3CN; 9:1, v/v) at pH 7.0, we explored the possibility of using this reagent for monitoring the release of free Cys from NAC by aminoacylase-1, an important mammalian enzyme. NAC is widely used as a pro-drug and Cys supplement for the treatment of acetaminophen overdose, glutathione replenishment, HIV patients etc.[7] Aminoacylase-1 generates Cys inside the cells from NAC.[9a] Although NAC has a free sulfhydryl group, our control experiment with **L** and 200 mole equiv. of NAC revealed no change in the luminescence response of **L** [Figure 2.8 (i)]. This confirmed that NAC failed to participate in any reaction with **L** at pH 7.0 Figure 2.8 (ii)]. This was presumably due to the higher pKa value of NAC (pKa = 9.5)[9b], which did not favour the reaction with **L** at pH 7. This finding nullified the possibility of any interference from NAC in our studies on the release of Cys from NAC by aminoacylase-1.

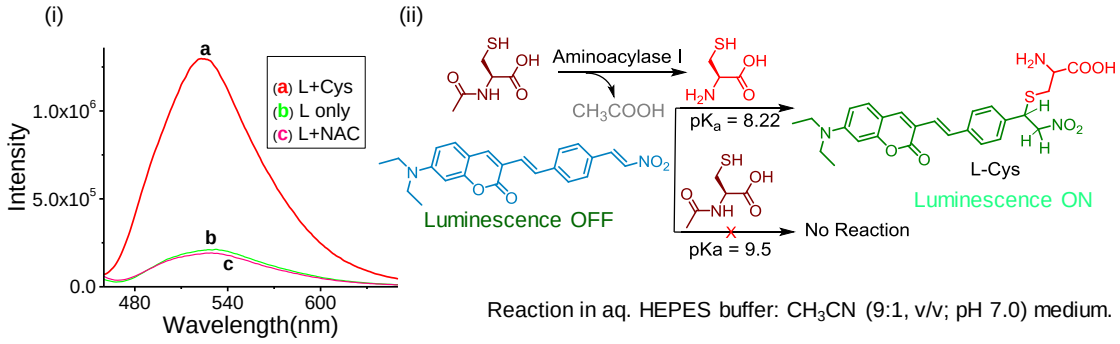

Figure 2.8. (i) Fluorescence response of probe (10 μM) with Cys and N-Acetyl Cysteine (200 equiv. each) in 10 mM HEPES: ACN(9:1) v/v at pH7, λ_{Ext} 445 nm (ii) Hydrolysis of NAC by aminoacylase-1 and subsequent reaction of in-situ generated Cys with **L**.

Aminoacylase-1 is a binuclear Zn(II)-dependent metallopeptidase, which hydrolyses acetylated cysteine.[10] Coordination to the Zn(II)-center(s) enhances the electrophilicity at the C-center of –CONHNAC functionality and lowers the activation barrier for N-C bond cleavage of the amide moiety in NAC and generation of Cys.[10] In the current study, we utilized the luminescence ON response for **L**-Cys formation due to a reaction between **L** and Cys, released by enzymatic action of aminoacylase-1 on NAC [Figure 2.8 (ii)]. Methodologies adopted for this experiment are discussed in the materials section. In absence of aminoacylase-1, no change in emission intensity was observed at 520 nm [Figure 2.9 (i)]. However, analogous studies with definite concentration of aminoacylase-1 showed gradual increase in emission intensity at 520 nm with time [Figure 2.9 (ii)] and confirmed a reaction between Cys (generated in-situ) and the reagent **L** for the formation of **L**-Cys. Increase in luminescence intensities with increase in [Aminoacylase-1] (0 to 2000 units) was also observed [Figure 2.9 (i)]. In-situ generation of Cys in the live HepG2 cells was demonstrated successfully by utilizing the facile reaction between Cys released from NAC by intracellular aminiacylase-1. HePG2 cells were particularly chosen for the following reasons. Aminoacylase-1 is abundant in HePG2 cells and its activity is maximum in liver cells.[10] The preliminary target of NAC is the liver and it is known to metabolize in liver cells.[7-9] Comparison of the Figures 2.10 (b & e) or (c & f) clearly revealed that the reagent **L** could react with Cys, generated within these HepG2 cells from NAC by enzymatic reaction of aminoacylase-1.

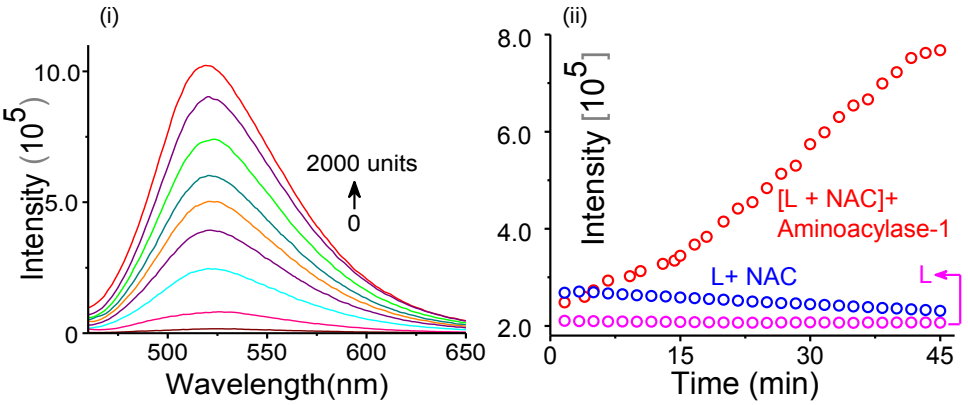

Figure 2.9. (i) Changes in luminescence spectra on incubation of [**L** + NAC (200 equiv.)] with varying [aminoacylase-1] (0 -2000 units) for 45 minutes; (ii) Fluorescence response of **L** (10 μM), **L** + NAC and [**L** + NAC (200 equiv.)] + aminoacylase-1 (1000 units) with time at 37^{o}C.

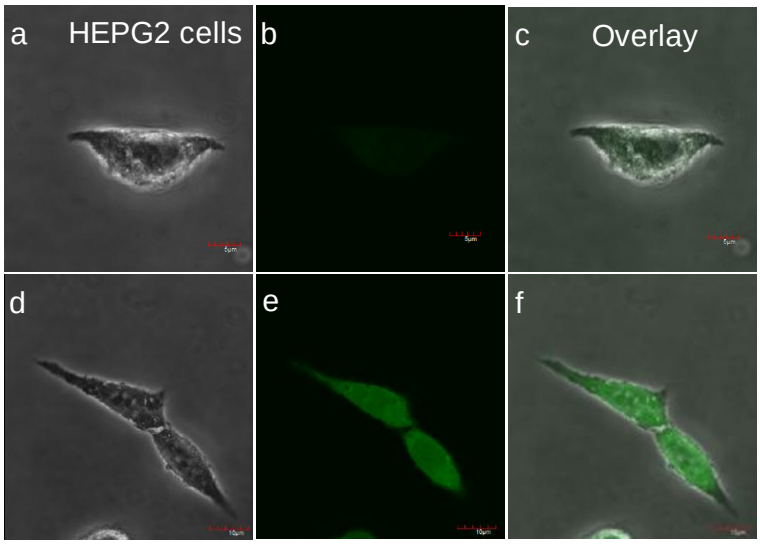

Figure 2.10. Confocalal images of live HepG2 cells: (a) - (c): bright field, dark field and overlay images of cells treated first with 2 mM NEM and then with 10 μM of **L**, respectively; (d) – (f): analogous images for cells treated with 2 mM NEM, and then these cells were washed after incubation of 20 min—followed by exposure of these washed cells to 20 μM NAC. Comparison of Figures (b & e) or (c & f) establish the bright green luminescence for the formation of **L**-Cys due to a reaction between **L** and Cys, produced *in-situ* by reaction of NAC and intracellular aminoacylase-1. For emission studies, λ_{Ext} = 445 nm was used. Scale bar 5 μm (a-c) and 10 μm (d-f).

These experiments also confirmed the cell membrane permeability and usefulness of **L** as an imaging reagent. Further, MTT assay studies with live HepG2 cells confirmed the insignificant toxicity of the reagent (Figure 2.11). Suitability of this reagent for specific recognition and estimation of Cys-residues present in natural milk proteins was also explored. For this, WP was isolated from cow's milk was

used. Experimental protocols were given in the experimental section. Three important constituents of natural cow's milk whey are α- lactalbumin, β-lactoglobulin and Bovine serum albumin. The ratio of Cys-residues present in monosulfide and disulfide forms are 2:23 and among these disulfides, few are not accessible to external reagents.[11a,b] Earlier literature reports also reveal that NAC can cleave disulfide bonds.[11c]

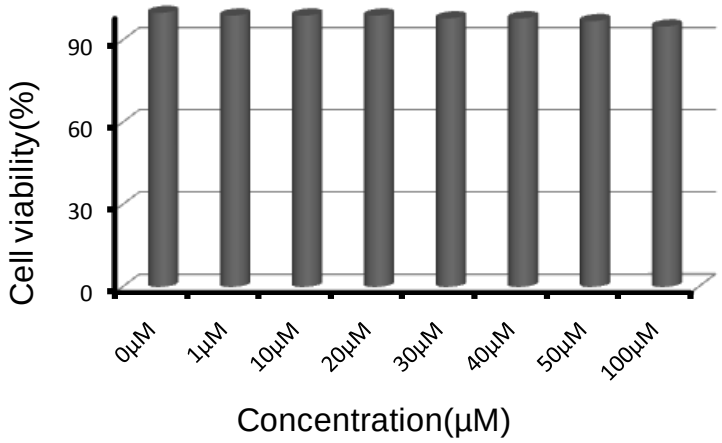

Figure 2.11. MTT assay to determine the cell viability percentage in HepG2 cells. IC_{50} has been calculated to be 100 μM.

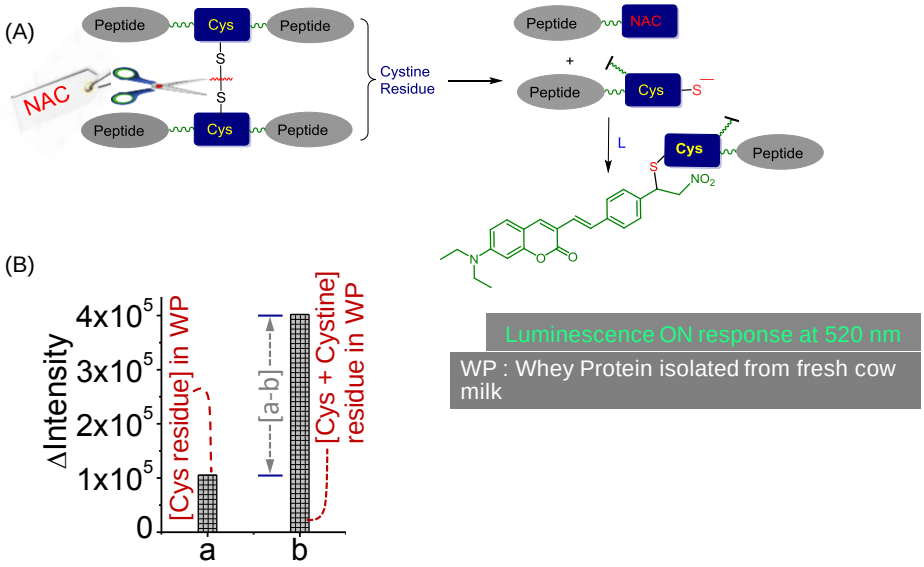

Figure 2.12. (A) Scheme showing the cleavage of –S—S– bond in WP in presence of NAC; (B) Difference in the emission responses for **L** (10 μM) in presence of WP (500 μl) and WP (500 μl) pre-treated treated with NAC (500 μl) at 37°C as compared to the emission response for free **L**. Studies were performed in 10 mM aq.HEPES: CH_3CN (9:1, v/v at pH 7.0) using λ_{Ext} = 445 nm and λ_{Ems} = 520. All the measurements were performed after 45 minutes of incubation at 37°C.

This was utilized for estimation of Cys-residues that could be present in WP in monosulfide and disulfide forms (Figure 2.12). Change in emission intensity observed at column-a (Figure 2.12 B) represents the enhancement in emission for the formation of L-Cys-P, and this was attributed to Cys-residues with the free sulfhydryl$_{Cys}$ group in native WP, exposed to the solvent. While the difference in column-b and column a was attributed to the Cystine-residue of the native WP present in the disulfide form and are accessible to reagent NAC and **L** under the experimental condition. These results revealed that fluorescent tags like **L** could be utilized for detection of Cys or Cystine residues present in WP and are exposed to the solvent and external reagents.[12] To test the efficacy of probe **L** as an imaging reagent for intracellular cysteine present in live cells, confocal laser microscopic studies were carried out. Live Hct116 cells were incubated with **L** (10 μM) for 30 min at 37^{o} C.

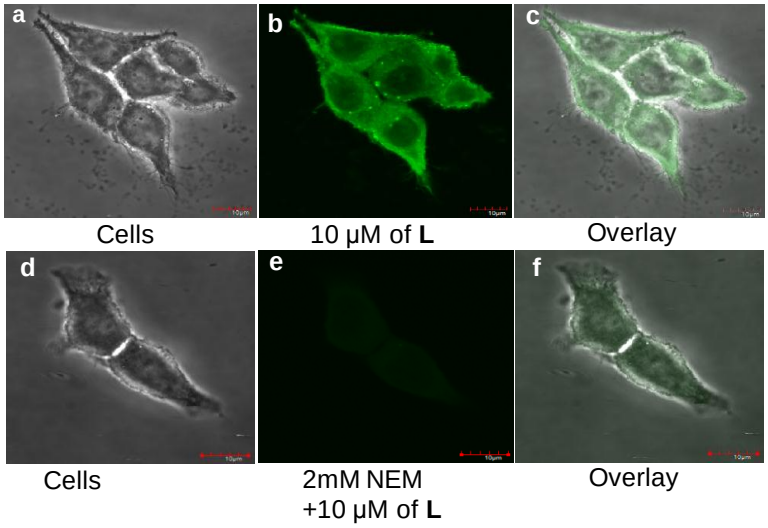

Figure 2.13. Confocal laser microscopic images of Hct116 cells. (a & d) cells only, (b) Cells with 10 μM of **L** (e) cells with 2 mM NEM and 10 μM of **L**. (c & f) overlay images. Scale bar 10 μm.

Bright green fluorescence was observed from cells indicating the cell membrane permeability of **L** and its ability to react with intracellular Cys (Figure 2.13). In order to confirm the fluorescence turn-on response was due to reaction of **L** with intracellular Cys, control experiment was performed by pre-incubating the cells with 2 mM of NEM (a known thiol blocking agent) for 30 minutes prior to the incubation with **L.** The results showed a remarkable decrease in fluorescence intensity because intracellular Cys were blocked by NEM. These results confirmed the

potential utility of **L** as a viable cellular imaging agent for detection of intracellular Cys.

To establish a simple method for real-time monitoring of Cys, we have prepared TLC test strips. Preparation methods were explained in the experimental section. With the addition of Cys, the colour of probe coated TLC plates changes from red to yellowish green and became highly fluorescent when observed under 365nm UV lamp (Figure 2.14). But Hcy and GSH do not give any observable visible as well as fluorescence changes. The same strategy was further extended to detect Cys in blood plasma and the Cys released in an enzymatic reaction as well. This method is of much practical significance in real time monitoring as it could be done without the aid of any instruments.

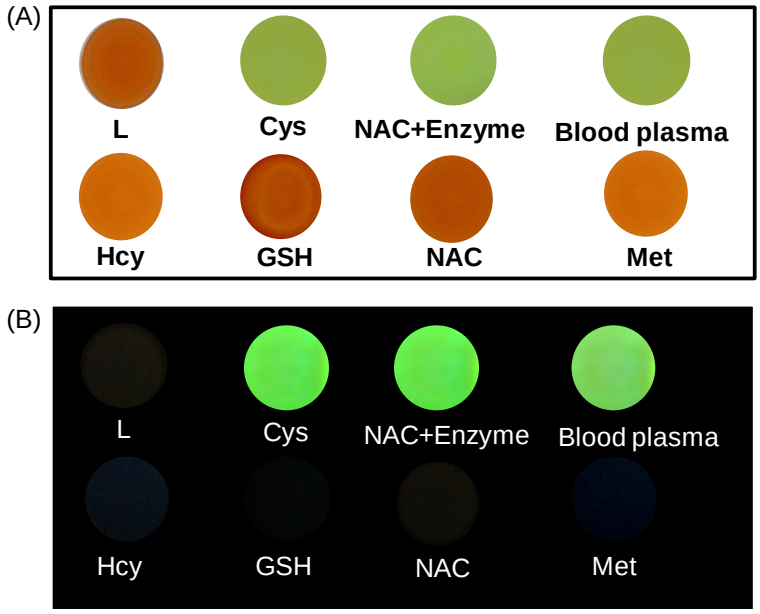

Figure 2.14. (A) Visual and (B) Fluorescent color changes of **L** (5 μM) coated on TLC plates upon addition of different analytes. Fluorescent color changes were observed under hand held 365 nm UV lamp.

2.5. Conclusion

We have demonstrated that a new chemodosimetric reagent (**L**) could be used for detection of free Cys as well as Cys-residues with free sulfhydryl$_{Cys}$ group present in protein structures. Visually detectable change in solution colour and fluorescence allowed a naked eye detection of Cys in the presence of all natural AAs, common anions and cations at pH 7 in an essentially aq. buffer medium. This non toxic reagent could also be used for probing the enzymatic hydrolysis of NAC,

a common prescribed drug used as Cys-supplement, in aq. Buffer as well as within the live HepG2 cells. Additionally, the probe was tested for detection of Cys on silica based TLC test strips. Considering the specificity, luminescence on response and cell membrane permeability, this reagent (**L**) has immense application potential as an imaging reagent for Cys. Moreover, it could be used for protein labeling.

2.6. References

1. (a) S. M. Marini, V. N. Gladyshev, *J. Biol. Chem*, 2012, **287**, 4419-4425; (b) R. O. Ball, G. Courtney-Martin and P. B. Pencharz, *J. Nutr*, 2006, **136**, 1682S-1693S; (c) H. S. Jung, X. Chen, J. S. Kim and J. Yoon, *Chem. Soc. Rev.*, 2013, **42**, 6019-6031; (d) C. Yin, F. Huo, J. Zhang, R. Martinez- Manez, Y. Yang, H. Lv and S. Li, *Chem. Soc. Rev*., 2013, **42**, 6032-6059; (e) L. A. Herzenberg, S. C. De Rosa, J. G. Dubs, M. Roederer, M. T. Anderson, S. W. Ela, S. C. Deresinski and L. A. Herzenberg, *Proc. Natl. Acad. Sci.*, 1997, **94**, 1967-1972. (f) F. J. T. Staal, S. W. Ela, M. Roederer, M. T. Anderson, L. A. Herzenberg and L. A. Herzenberg, *The Lancet*, 1992, **339**, 909-912.

2. J. B. Schulz, J. Lindenau, J. Seyfried and J. Dichgans, *Eur. J. Biochem.*, 2000, **267**, 4904-491. (b) M. H. Stipanuk, J. E. Dominy, J.-I. Lee and R. M. Coloso, *J. Nutr*, 2006, **136**, 1652S-1659S

3. (a) E. Haa and M. B. Zemel, *J. Nutr. Biochem,* 2003*,* **14***,* 251–258; (b) S. K. Kwon, S. Kou, H. N. Kim, X. Chen, H. Hwang, S.-W. Nam, S. H. Kim, K. M. K. Swamy, S. Park and J. Yoon, *Tetrahedron Lett.*, 2008, **49**, 4102-4105.

4. W. Wang, O. Rusin, X. Xu, K. K. Kim, J. O. Escobedo, S. O. Fakayode, K. A. Fletcher, M. Lowry, C. M. Schowalter, C. M. Lawrence, F. R. Fronczek, I. M. Warner and R. M. Strongin, *J. Am. Chem. Soc*., 2005, **127**, 15949-15958.

5. (a) X.-F. Yang, Q. Huang, Y. Zhong, Z. Li, H. Li, M. Lowry, J. O. Escobedo and R. M. Strongin, *Chem. Sci.*, 2014, **5**, 2177-2183; (b) X. Zhou, X. Jin, G. Sun and X. Wu, *Chem. Eur. J.*, 2013, **19**, 7817-7824; (c) A. N. Shao, J. Y. Jin, S. M. Cheung, R. H. Yang, W. H. Chan and T. Mo, *Angew. Chem., Int. Ed*, 2006, **118**, 5066-5070; (d) J. Liu, Y.-Q. Sun, H. Zhang, Y. Huo, Y. Shi and W. Guo, *Chem. Sci.*, 2014, **5**, 3183-3188; (e) C. S. Lim, G. Masanta, H. J. Kim, J. H. Han, H. M. Kim and B. R. Cho, *J. Am. Chem. Soc*., 2011, **133**, 11132-11135; (f) P. Das, A. K. Mandal, U. Reddy G, M. Baidya, S. K. Ghosh and A. Das, *Org. Biomol. Chem.*, 2013, **11**, 6604-6614; (g) M. H. Lee, J. H. Han, P.-S. Kwon, S. Bhuniya, J. Y. Kim, J. L. Sessler, C. Kang and J. S. Kim, *J. Am. Chem. Soc.*, 2011, **134**, 1316-1322; (h) J. H. Lee, C. S. Lim, Y. S. Tian, J. H. Han and B. R. Cho, *J. Am. Chem. Soc.*, 2010, **132**, 1216-1217; (i) P. Das, A. K. Mandal, N. B. Chandar, M. Baidya, H. B. Bhatt, B. Ganguly, S. K. Ghosh and A. Das, *Chem. Eur. J.*, 2012, **18**, 15382-15393; (j) M. Isik, T. Ozdemir, I. S. Turan, S. Kolemen and E. U. Akkaya, *Org. Lett*., 2012, **15**, 216-219; (k) X. Chen, S.-K. Ko, M. J. Kim, I. Shin and J. Yoon, *Chem. Commun*., 2010, **46**, 275-2753; (l) U. G. Reddy, H. Agarwalla, N. Taye, S. Ghorai, S. Chattopadhyay and A. Das, *Chem. Commun*., 2014, **50**, 9899-9902; (m) L.-Y. Niu, Y.-Z. Chen, H.-R. Zheng, L.-Z. Wu, C.-H. Tung and Q.-Z. Yang, *Chem. Soc. Rev.*, 2015, DOI 10.1039/C5CS00152H; (n) S. Sreejith, K. P. Divya, and A. Ajayaghosh; *Angew. Chem. Int. Ed*. 2008, **47**, 7883 –7887.

6. (a) H. Li, J. Fan, J. Wang, M. Tian, J. Du, S. Sun, P. Sun and X. Peng, *Chem. Commun.*, 2009, 5904-5906; (b) X. Yang, Y. Guo and R. M. Strongin, *Angew. Chem., Int. Ed.*, 2011, **50**, 10690-10693; (c) Z. Guo, S. Nam, S. Park and J. Yoon, *Chem. Sci.*, 2012, **3**, 2760-2765; (d) H. S. Jung, J. H. Han, T. Pradhan, S. Kim, S. W. Lee, J. L. Sessler, T. W. Kim, C. Kang and J. S. Kim, *Biomaterials*, 2012, **33**, 945-953; (e) B. Liu, J. Wang, G. Zhang, R. Bai and Y. Pang, *Acs Appl Mater Inter*, 2014, **6**, 4402-4407; (f) H. Wang, G. Zhou, H. Gai and X. Chen, *Chem. Commun.*, 2012, **48**, 8341-8343; (g) X. Zhou, X. Jin, G. Sun, D. Li and X. Wu, *Chem. Commun.*, 2012, **48**, 8793-8795; (h) J. Zhang, J. Wang, J. Liu, L. Ning, X. Zhu, B. Yu, X. Liu, X. Yao and H. Zhang, *Anal. Chem.*, 2015, **87**, 4856-4863;

7. (a) O. Dean, F. Giorlando and M. Berk, *J. Psy. Neuro,* 2011, **36**, 78l ; (b) H.A. Lindner, V.V. Lunin, A. Alary, R. Hecker, M. Cygler and R. Ménard, *J. Biol. Chem.*, 2003, **278**, 44496-44504.

8. R. E. Benesch and R. Benesch, *J. Am. Chem. Soc.*, 1955, **77**, 5877-5881.

9. (a) V. Uttamsingh, R. B. Baggs, D. M. Krenitsky and M. W. Anders, *Drug Metab. Dispos.*, 2000, **28**, 625; (b) C. A. S. Regino and D. E. Richardson, *Inorg. Chim. Acta*, 2007, **360**, 3971-3977.

10. (a) S. V. Story, A. M. Grunden and M. W. W. Adams, *J. Bacteriol.*, 2001, **183**, 4259-4268; (b) A. Sommera, E. Christensenb, S. Schwengerc, R. Seuld, D. Haase and H. Olbrich; *Biochim. Biophys. Acta,* 2011, **1812,** 685- 690; (d) M. Hernick and C. A. Fierke, *Arch. Biochem. Biophys.*, 2005, **433**, 71-84.

11. (a) E. D. Chrysina, K. Brew and K. R. Acharya, *J. Biol. Chem.* 2000, **275**, 37021-37029; (b) K. Sakurai, T. Konuma, M. Yagi and Y. Goto, *Biochim. Biophys. Acta*, 2009, **1790,** 527-537; (c) G. S. Kelly, *Altern Med. Rev*, 1998, **3**, 114-127.

12. (a) E. Branigan, C. Pliotas, G. Hagelueken and J. H. Naismith, *Nat. Protocols*, 2013, **8**, 2090-2097; (b) M. Fernández-Suárez, H. Baruah, L. Martínez-Hernández, K. T Xie, J. M Baskin, C. R Bertozzi and A. Y Ting, *Nat. Biotechnol*. 2007, **25**, 1483-1487.

CHAPTER 3

A CYSTEINE SPECIFIC FLUORESCENT SWITCH FOR MONITORING OXIDATIVE STRESS AND QUANTIFICATION OF AMINOACYLASE-1 IN BLOOD SERUM

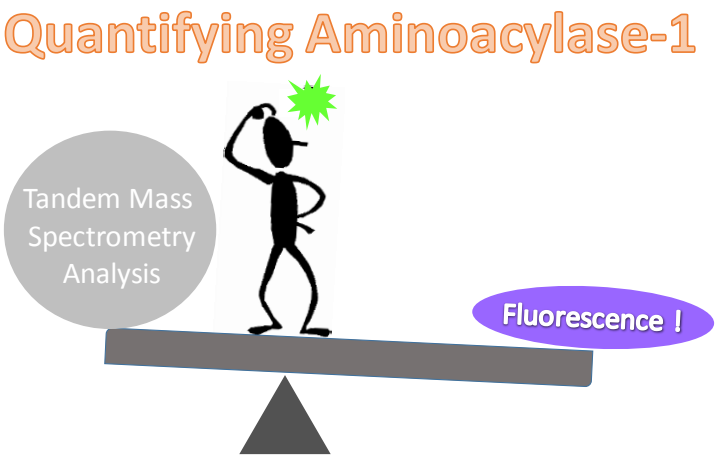

Publication:
Anal.Chem. 2016, **88**, 12161−12168

3.1. Introduction

Recognition and visualization of molecular targets using fluorescent markers are vital in clinical diagnosis and real-time monitoring of analytes of biological importance. Cysteine (Cys) is one such analyte of interest because of its thumping roles in human physiology. Being one of the reactive sulfur species (RSS), Cys is often found in the majority of the proteins and is involved in various catalytic and regulatory functions.[1] Reversible oxidation of Cys residues is known to play a key role in intracellular signalling mechanism and understanding the thiol-redox chemistry in cellular processes is crucial for developing a better insight in this issue.[2] Anticipated concentration of Cys in human blood plasma (HBP) sample for a healthy person is 240 - 360 μM.[3] Any abnormality in Cys level is a marker for many diseases. Deficiency of Cys has adverse influences on child growth, depigmentation of hair, edema, liver damage, skin lesions etc. Also, Cys is responsible for maintaining the optimum glutathione (GSH) concentration in human physiology.[1] While it is believed that the elevated level of Cys is responsible for neurotoxicity and Alzheimer's diseases.[4] So, estimation of Cys in biofluids, like HBP is crucial for understanding the occurrence of many diseases. Reactive oxygen species (ROS) cause oxidative stress in cells. ROS like hydrogen peroxide (H_2O_2) causes oxidation of Cys residues into sulfenic acid intermediates or disulphides.[5,6] Cys residues not only act as an antioxidant but also regulate H_2O_2 induced signal transduction. It has been argued that understanding the reactivity of H_2O_2 with the sulfhydryl functionality of Cys is key to understand the thiol-mediated redox processes and how this species engages in signaling.[2]

ACY-1 is an important and endogenous mammalian enzyme that plays an important role in the hydrolysis of N-acetylcysteine and releases free Cys.[7] Interestingly, ACY-1 is also an important biomarker with potential prognostic utility in patients with delayed graft function (DGF) following renal transplantation. ACY-1 level in serum samples of patients with DGF markedly increases after kidney transplantation, and its estimation in blood serum (BS) is decisive in clinical diagnosis for the recovery and treatment of such patients.[8-10] Such quantification in the serum sample is conventionally achieved by label-free single dimensional liquid chromatography-tandem mass spectrometry analysis.[11] Till date, no literature report suggests the use of any optical spectroscopic method for such purpose.

From the past few decades, significant attention has been paid to develop methods for the detection/quantification of Cys either in biological fluids or for mapping distribution of

endogenous Cys in live cells. Most commonly adopted methods include high-performance liquid chromatography (HPLC), electrochemical and colorimetric techniques. A methodology involving HPLC technique requires post-column derivatization of the sample. This is generally time-consuming and not ideally suited for in-field application. Moreover, HPLC, electrochemical and colorimetric techniques are only restricted to *in-vitro* studies.[12] Considering these, reagents that allow the detection and estimation of Cys based on luminescence ON response have a distinct edge. Such probes offer higher sensitivity in the detection process as well as the possibility to use them in an imaging application and *in-vivo* studies. Among various methodologies, one that involves the use of chemodosimetric reagents is found to be most efficient.[4, 12-31] The structural similarities between Cys, Homocysteine (Hcy) and GSH add to the challenge in developing a chemodosimetric probe that is specific towards free Cys and such examples are rather limited in the contemporary literature.[32-47]

Peng *et al.* were first to report a chemodosimetric reagent that showed significant fluorescence enhancement on specific reaction with Cys.[48] Strongin group developed a novel acrylate based chemodosimetric probe that could discriminate between Cys and Hcy by the difference in the relative rate for the respective intramolecular cyclization reaction between acrylate and thiols.[49] Yoon *et al.* developed a near-infrared ratiometric fluorescent probe for Cys.[50]. Nevertheless, the possibility of using these reagents for probing the enzymatic process that leads to the release of intracellular Cys was not explored. Two recent reports from the group authoring this article have discussed such a possibility for two different Cys-specific reagents.[39,40] However, none of these two reagents were either utilized for monitoring the peroxide induced oxidative stress in live cells or for quantitative estimation of ACY-1 in human blood serum (HBS).

In our previous attempt, we reported a nitro-olefin based Cys specific probe[39] capable of detecting ACY-1 but the selectivity of the probe was dependent on pH. Moreover, this probe also known to bind to sulfhydryl groups of proteins. Both these properties lead to serious error in absolute quantification of the activity of the enzyme. So, to overcome these, we have designed a coumarin-based reagent (**CA**) having an acrylate functionality to develop a Cys-specific reagent that gives luminescence ON response on reaction with Cys. This luminescence ON response was utilized for evaluation of the specific rate constant for the reaction between Cys and **CA** following intracellular biochemical transformations induced by ACY-1, which opened up the possibility for quantifying the ACY-1 concentration in HBS. Further, this reagent could be utilized for monitoring the H_2O_2 mediated oxidative stress in living cells.

3.2. Experimental Section

3.2.1. Materials

4-bromophenol, triphenylphosphine, palladium acetate, triethylamine, acryloyl chloride Cysteine, Glutathione, Homocysteine, sodium acetate and Histidine, Leucine, Methionine, Phenylalanine, Tryptophan, Tyrosine, Valine , Alanine, Arginine, Glycine, Glutamine, Proline, Serine, Aspartic acid, Glutamic acid, Threonine, Isoleucine, Lysine, N-Acetylcysteine Ethylenediamine were purchased from Sigma Aldrich/Alfa Aesar and SD Fine chemicals.Dulbecco's Modified Eagle's Medium (DMEM) (Invitrogen), Fetal Bovine Serum (FBS) (Invitrogen), Penicillin-Streptomycin antibiotics (Invitrogen), Hct116 cell line (National Centre For Cell Science), trypsin-EDTA, MTT (3-(4,5-dimethylthiazol-2-yl)-2,5-diphenyltetrazolium bromide) (Sigma), Iso-propanol (Fischer Scientific) and Paraformaldehyde (Sigma) were used as received. Solvents were purchased from S.D. Fine Chemicals, India and were used without further purification unless mentioned otherwise. Silica gel 100-200 mesh was used for column chromatography. Analytical thin layer chromatography was performed using commercial silica plates (Merck, India).

3.2.2. Analytical Methods

^{1}H and ^{13}C NMR spectra were recorded on Bruker 400/500 MHz FT NMR (Model: Advance-DPX 400/500) using TMS as an internal standard. High-resolution mass spectra were recorded on JEOL JM AX 505 HA mass spectrometer. IR spectra were recorded on Bruker Alpha FT IR spectrometer. UV-Vis spectra were recorded using Shimadzu UV-1800 spectrometer. Fluorescence measurements were carried out on quanta master-400 fluorescence spectrometer. Lifetime data was acquired using Horiba TCSPC (Time-Correlated Single Photon Counting) system with excitation at 443 nm. 10000 counts were collected for each lifetime measurement, and all measurements were performed in triplicate using the DAS software to confirm the results. The calculation of the lifetimes was carried out with a single or biexponential decay function to each decay plot to extract the lifetime information using the DAS6 fluorescence decay analysis software. Confocal images were acquired in Olympus Fluoview microscope.

3.2.3. General experimental methods for UV-Vis and fluorescence studies

A stock solution of **CA** (5×10^{-3}M) was prepared in acetonitrile and the same solution was used for all the studies after appropriate dilution with aqueous buffer solution. Aqueous HEPES buffer: CH_3CN (98:2, v/v) solvent medium was used for

all spectroscopic measurements unless mentioned otherwise. All the amino acid solutions (1.0×10^{-1}M) were prepared in aq. HEPES buffer (pH 7). For spectroscopic measurements, a stock solution of the probe was further diluted by using aq. HEPES buffer: CH_3CN (98:2, v/v) mixture and the effective final concentration was made as 10 μM. All luminescence measurements were done using λ_{Ext} = 450 nm with an emission slit width of 1 nm. Quantum yield was determined according to literature method using fluorescein (in 0.1M aqueous NaOH) as the reference standard (Φ_f = 0.92). Quantum yield was calculated by formula,

$$\Phi_f = \Phi_f' \ (I_{sample}/I_{std})(A_{std}/A_{sample})(\eta^2_{sample}/\eta^2_{std}) \qquad \text{Eq. 1}$$

Where, Φ_f' was the absolute quantum yield for the rhodamine B and was used as a reference; I_{sample} and I_{std} are the integrated emission intensities; A_{sample} and A_{std} are the absorbances at the excitation wavelength, and η_{sample} and η_{std} are the respective refractive indices.

3.2.4. General procedure for enzymatic study

N-Acetylcysteine (mucinac 600) tablets (Cipla made) were purchased from commercially available sources. Based on the quantity of NAC present in the tablet, 1.0×10^{-1}M tablet solution was prepared in 10 mM aq. HEPES buffer solution (pH7). ACY-1 was purchased from Sigma Aldrich. The enzyme solution was prepared by dissolving 1mg/ml in aq. HEPES buffer solution. A fixed concentration (200 equiv.) of N-Acetylcysteine (NAC) was added to the 10 μM probe in aq. HEPES buffer: CH_3CN (98:2, v/v). 1.0 mg of solid enzyme contained 3301 units of protein, and 1 unit of ACY-1 could hydrolyse 1.0 μM of the substrate. Accordingly, the enzyme concentration was varied with respect to the substrate concentration. All the experiments were performed by incubating the solutions at 37^{o}C. EDTA solution was prepared by dissolving sodium salt of EDTA in aq. HEPES buffer medium.

3.2.5. General procedure for kinetic studies

Time-dependent studies of probe CA (10 μM) with 1 mM of different analytes like Cys, Hcy, GSH, and NAC were carried out by mixing the reactants and monitored by fluorescence measurements in aq-HEPES-CH_3CN (98:2, v/v) medium of pH 7 at 27^{o}C. λ_{Ext} = 450 nm. λ_{Ems} = 520 nm. Data were collected under pseudo-first-order conditions. The pseudo-first order rate constant for the reaction was determined by fitting the fluorescence intensity changes of the samples to the pseudo-first-order equation:

$\ln[(I_{max}-I_t)/I_{max}] = -k_{obs}\, t$

Where I_t and I_{max} represent the fluorescence intensities at times t and the maximum value obtained after the reaction was complete. k_{obs} is the observed rate constant of the reaction. From the slope we get k_{obs} value for each reaction.

3.2.6. General procedure for Michaelis constant calculation for aminoacylase 1

Michaelis constant was evaluated by using series of enzyme assay by varying N-acetylcysteine (NAC) concentration from (0.1 – 0.4 mM) with a fixed enzyme concentration of 20 Units/mL. Initial rates were evaluated from the plot of Log $[F_t - F_0]$ vs. time (in a sec), where F_t is the luminescence intensity for **CA** at 520 nm (λ_{Ext} = 450 nm) at time t and I_0 is the initial luminescence intensity. Linear plots were obtained for N-acetylcysteine concentration (0.1 – 0.4 mM). A plot of 1/V vs. 1/[S] would give intercept of $1/k_2[E]_0$ and slope of $K_m/k_2[E]_0$. Thus, {slope/intercept} would result K_m.

3.2.7. Cell-culture and Confocal microscopy experiments

Human colorectal adinocarcinoma cells (SW480 cells) (3×10^5) were seeded on coverslips placed in 6 well plates. After 24 hours, live cells were treated with **CA** (10 μM) for 30 minutes to detect the intracellular cysteine. After 30 minutes, cells were washed 3 times with Phosphate buffered saline (PBS), and images were captured. The same procedure was followed for the detection of intracellular Cys in normal HEK 293T cells as well. For control experiment with NEM, cells were pre-incubated with 2 mM of N-Ethyl Maleimide (NEM, a thiol-specific blocking reagent) for 30 minutes prior to the addition of **CA** (10 μM). For GSH inhibition experiment, live cells were incubated with 1mM of L-buthionine sulfoximine (BSO) (two sets for 2 hr and 24 hr respectively) to inhibit the GSH synthesis. Cells were washed and further incubated with **CA** (10 μM) for 30 minutes and images were captured. For co-staining studies with DAPI, cells were mounted with a well-known nucleus staining dye DAPI (4', 6-diamidino-2-phenylindole) containing mounting media. Co-staining studies were also performed by incubating the cells with Mito-Tracker orange (M7510) (500 nM) for 15 minutes. For H_2O_2 experiments, SW480 cells were pre-treated with different concentrations of hydrogen peroxide (0.5 mM, 1 mM & 2 mM) for 30 minutes followed by the incubation with **CA** (10 μM). A control experiment was also performed by incubating the H_2O_2 treated cells with N-acetyl cysteine (NAC) tablet solution 0.5 mM. All the images were acquired in Olympus Fluoview Microscope.
The *in vitro* cytotoxicity of **CA** on HEK 293T cells and SW480 cells were determined by MTT (3-(4, 5-Dimethylthiazol-2-yl)-2, 5-diphenyltetrazolium bromide, a yellow tetrazole)

assay. HEK 293T cells and SW480 cells (7 x 10^3) were seeded in each well of a 96 well plate and cultured in an incubator supplied with 5% CO_2 maintained at 37°C. Cells were maintained in DMEM medium, supplemented with 10% Foetal Bovine Serum and 100 Units of Penicillin-Streptomycin antibiotics. After 24 hours, the cells were treated with different concentrations of the **CA** in triplicates for 12 hours. Cells were then treated with 0.5 µg/ml of MTT reagent. The plate was then incubated for 4 hours at 37°C. 100 µl of isopropyl alcohol was added to each well. Optical density was measured at 570 nm using Multiskan Go (Thermo Scientific) to find the concentration of the cell inhibition. IC_{50} value has been calculated to be 300 µM.

The formula used for the calculation of the MTT assay for evaluation of the cell viability was as follows:

Cell viability (%) = (means of Absorbance values of treated group/ means of Absorbance values of untreated control) ×100.

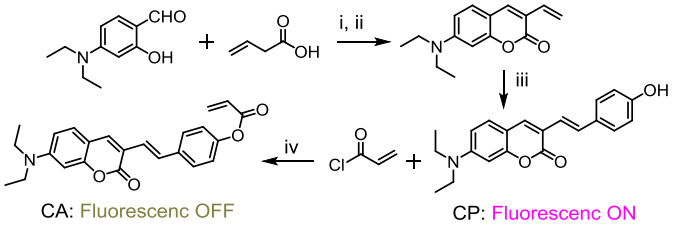

i: DCC, DMAP, 0°C, 4h; ii: Cs_2CO_3,12h; iii: 4-bromophenol, $Pd(OAc)_2$, PPh_3, NaOAc, DMF, 80°C,16h; iv: Et_3N, 0°C - RT, 12h.

Scheme 3.1. Methodologies adopted for the synthesis of **CA**.

3.3. Synthesis and Characterization

3.3.1. Synthesis of compound II

Vinyl coumarin, an intermediate that was used for this synthesis was prepared by following our previous report.[39] This (75 mg, 0.30 mmol) was dissolved in dry DMF and to this solution, 4-bromophenol (64 mg, 0.36 mmol), sodium acetate (28 mg, 0.33 mmol) and triphenylphosphine (64.67 mg, 0.24 mmol) were added. The resulting solution was purged with nitrogen gas and was added $Pd(OAc)_2$ (14 mg, 0.06 mmol). The reaction mixture was heated to 80° C and maintained at the same temperature for 12 hr under a nitrogen atmosphere. The progress of the reaction was monitored by TLC. Upon completion, the reaction was quenched with H_2O and extracted with EtOAc. The organic layer was washed with brine solution, dried with Na_2SO_4 and subsequently concentrated under vacuum. The crude product was purified by flash column chromatography to give hydroxyl compound as a yellow solid. Yield: 40%. IR (film) ν_{max} (cm^{-1}): 1696 (-CHO), 1612 (C=C), 3021 (-C=C-H). ^{1}H NMR (DMSO-d_6, 400 MHz) δ (ppm): 1.12 (6H, t, CH_3),

3.43 (4H, q, CH_2), 6.53 (1H, d, *J* = 1.7 Hz), 6.72 (1H, dd, *J* = 9.0 Hz), 6.77 (2H, d, *J* = 8.5 Hz), 6.90 (1H, d, *J* = 16.3 Hz), 7.38 (3H, dd, *J* = 8.5 Hz), 7.44 (1H, d, *J* = 8.8 Hz), 7.97 (1H, s), 9.64 (1H, s, OH). ^{13}C NMR (DMSO-d_6, 100 MHz): δ (ppm) 12.62, 44.39, 96.56, 108.77, 109.62, 115.97, 117.01, 120.21, 128.00, 128.71, 129.46, 138.25, 150.42, 155.26, 157.58, 160.81, 163.79. HRMS (ESI-Ms), m/z: calculated for $C_{21}H_{21}NO_3$ [M+H] 336.1594 found 336.1591.

3.3.2. Synthesis of CA

Compound **II** (70 mg, 0.20 mmol) was dissolved in dry dichloromethane. It was cooled to 0^{o}C and triethylamine (81.3 µl, 0.62 mmol) was added and stirred for 10 minutes. To this mixture, acryloyl chloride (22 µL, 0.26 mmol) was slowly added at the same temperature. The reaction mixture was further stirred at 25^{o}C for 12 hr. Upon completion of the reaction, it was washed with H_2O and extracted with dichloromethane. The organic layer was separated, dried and concentrated under reduced pressure. The crude product was purified by flash column chromatography to give yellow solid. Yield: 76%. ^{1}H NMR ($CDCl_3$, 400 MHz): δ (ppm)1.23 (6H, t, CH_3), 3.44 (4H, q, CH_2), 6.04 (1H, d, *J* = 10.5 Hz), 6.34 (1H, dd, *J* = 10.5 Hz), 6.51 (1H, d, *J* = 2.2 Hz), 6.60 (2H, m), 7.07 (1H, d, *J* = 16.3 Hz), 7.14 (2H, d, *J* = 8.5 Hz), 7.31 (1H, d, *J* = 8.8 Hz), 7.49 (1H, d, *J* = 16.3 Hz), 7.68 (1H, s). ^{13}C NMR ($CDCl_3$, 100 MHz): δ (ppm) 12.47, 44.84, 97.13, 109.09, 117.55, 121.67, 123.39, 127.44, 127.90, 128.79, 129.01, 132.60, 135.49, 138.24, 149.90, 150.44, 155.58, 161.41, 164.50. HRMS (ESI-Ms), m/z: calculated for $C_{24}H_{23}NO_4$ [M+H] 390.1700 found 390.1696.

3.4. Results and Discussions

Synthetic route adopted for **CA** is shown in scheme 1. Vinyl coumarin was coupled with 4-bromophenol following the Heck reaction in the presence of $Pd(OAc)_2$ as a catalyst to yield the corresponding hydroxyl compound (**II**). Acylation of the hydroxyl group was carried out using acryloyl chloride, and this resulted in the final compound **CA** with relatively good yield. Final compound and all the intermediates were appropriately characterized using standard analytical techniques. Reagent **CA**, on reaction with Cys, resulted in the formation of corresponding coumarin derivative (**CP**) in a nearly quantitative yield. This coumarin derivative (**CP**) was isolated in pure form and subjected to various spectroscopic and analytical studies. All such results confirmed the generation of the **CP** in a near quantitative yield.

Formation of **CP** was attributed to the conjugate addition of Cys with sulfhydryl functionality as the nucleophile to α, β-unsaturated carbonyl moiety to form a thioether. This participated in a cyclisation reaction involving $–NH_2^{Cys}$ moiety as the nucleophile and $–C=O^{acrylate}$ as the electrophilic center. This eventually led to the release of a cyclic 7-membered thiazepine type by product and **CP** (Figure 3.1). Formation of thiazepine as the byproduct was additionally confirmed by ^{1}H NMR and HRMS spectral data (Figures 3.2 and 3.3). In the case of Hcy, intermediate thioether was formed, but the subsequent cyclization process was not favourable, as this would have led to the formation of a kinetically unfavourable 8-membered ring with high activation barrier. GSH being a tripeptide failed to participate in the cyclization reaction. These helped in achieving the desired specificity for the reaction with Cys.

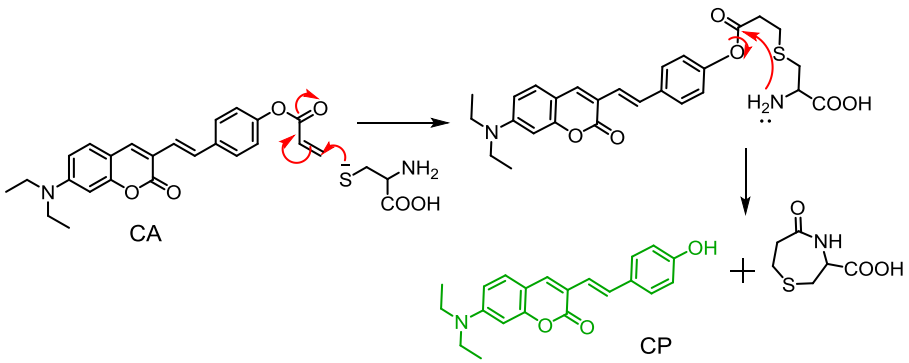

Figure 3.1. Proposed mechanism for the reaction of Cys with the probe **CA.**

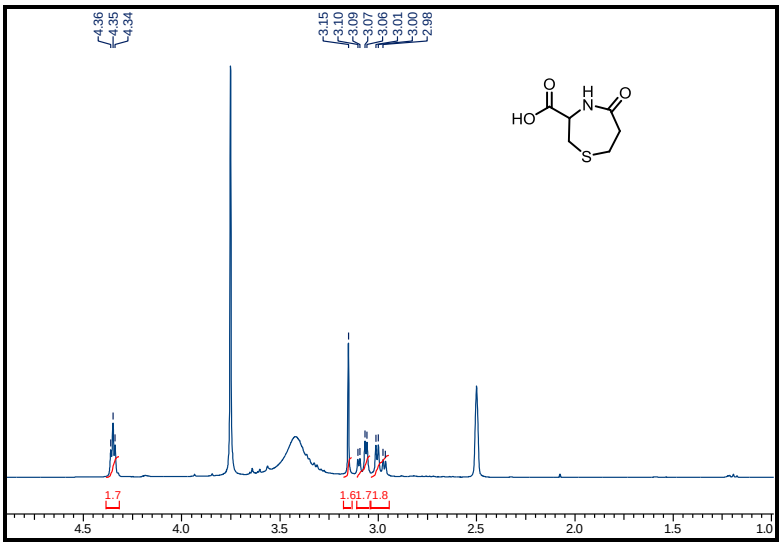

Figure 3.2. ^{1}H NMR spectrum of cyclised by-product in DMSO-d_6.

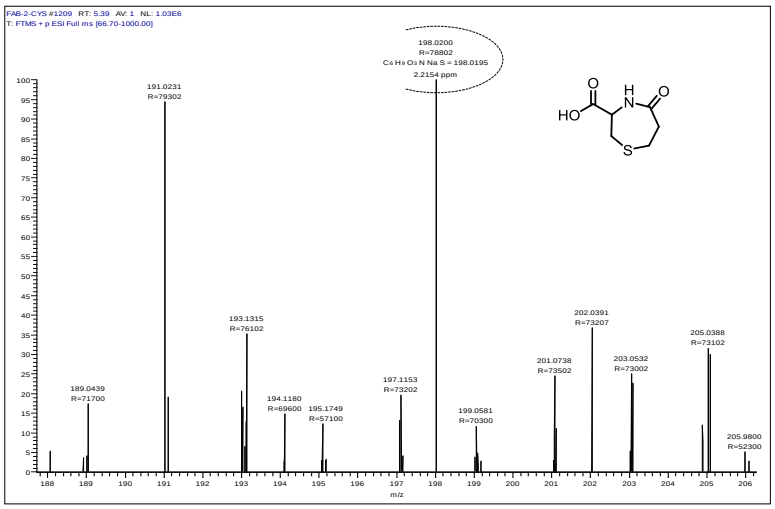

Figure 3.3. HRMS spectrum of cyclized by-product.

The electronic spectrum of **CA** (10 μM) in an essentially aq. HEPES buffer medium (aq. HEPES buffer: CH_3CN, 98:2 (v/v); pH 7.0) showed an absorption band maximum at 432 nm [Figure 3.4 (A)], which could be attributed to a coumarin-based π-π* transition. No significant change in the electronic spectrum was observed when **CA** was treated with large excess (100 equiv.) of all natural amino acids (AAs: Tryptophan (Trp), Leucine (Leu), Isoleucine (Ile), Methionine (Met), Threonine (Thr), Tyrosine (Tyr), Valine (Val), Alanine (Ala), Serine (Ser), Glycine (Gly), Cysteine (Cys), Glutathione (GSH), Homocysteine (Hcy), Proline (Pro) and Arginine (Arg)), all common anions and cations that could have biological relevance. Common anions (X: F^-, Cl^-, Br^-, CH_3COO^-, HSO_4^-, SCN^-, ClO_4^-, CN^-, SH^-) and cations (Na^+, Ca^{2+}, Mg^{2+}, Fe^{3+}, Cu^{2+}, Cr^{3+}, Ni^{2+}, Zn^{2+}, Hg^{2+}, Pb^{2+}) also failed to induce any detectable change in solution luminescence under similar experimental condition [Figure 3.5 (A)].

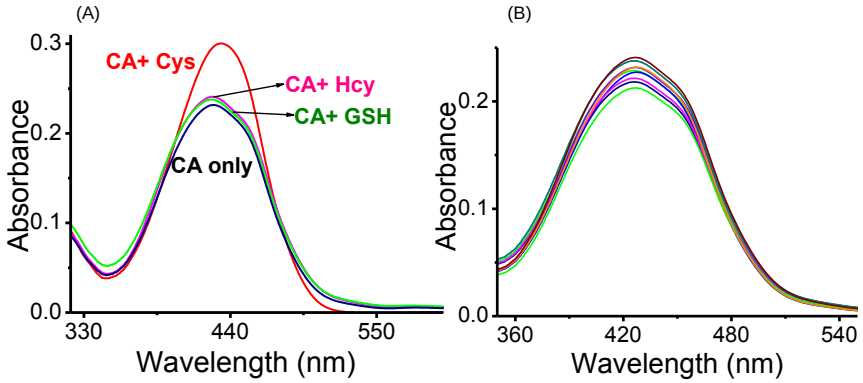

Figure 3.4. (A) UV-Vis response of **CA** in the presence of Cys, Hcy, and GSH. (B) UV-Vis response of **CA** in the presence of a mixture of different aminoacids, cations, and anions of biological relevance. in 10 mM HEPES: CH_3CN (98:2) v/v at pH7.

These results confirmed that the luminescence ON response was solely due the specific reaction of **CA** with Cys, which led to the formation of **CP** (Figure 3.1). Emission quantum yield for the reagent **CA** (10 μM) was evaluated (Φ_f^{CA} ~ 0.02 for λ_{Ext} = 450 nm), and low Φ_f^{CA} was attributed to an efficient photoinduced electron transfer (PET) process involving $-NMe_2$ as the donor and acryl moiety as quencher fragment. Upon reaction with Cys, **CP** is produced, and this showed a strong emission band (Φ_f^{CP} = 0.2, λ_{Ext} = 450 nm; fluorescein was used as reference) with a maximum at 520 nm [Figure. 3.5 (A) and 3.6].

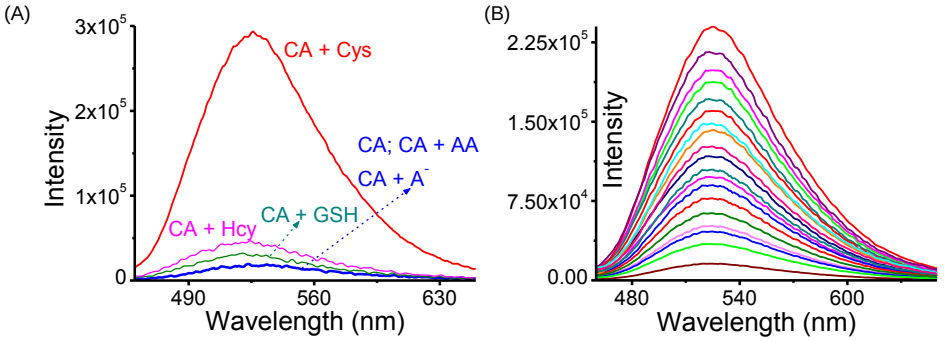

Figure 3.5. (A) Emission response of **CA** (10 μM) in the presence of Cys (150 μM), Hcy, GSH (300 μM each), other AA and anions (B) after the hydrolysis of NAC by ACY-1. Studies were performed in aq. HEPES buffer: CH_3CN, 98:2 (v/v) medium (pH 7.0) using λ_{Ext}: 450 nm.

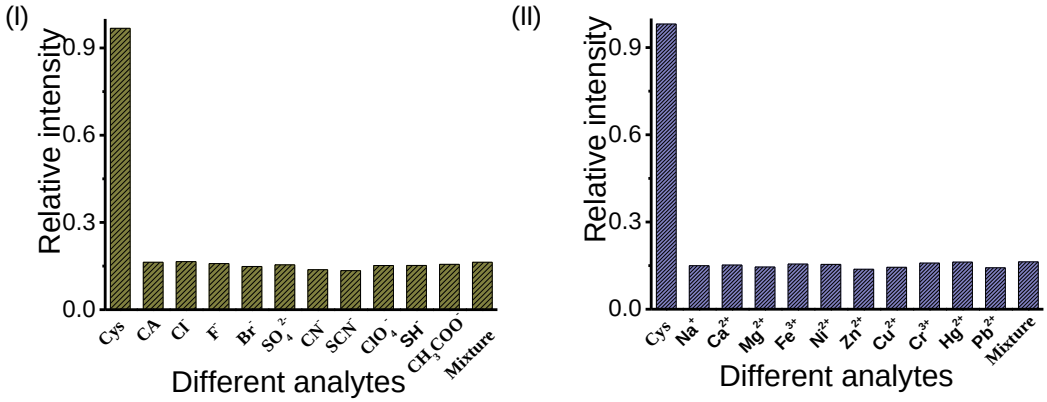

Figure 3.6. (i) Interference studies with different anions. (ii) Interference studies with different cations.

Since **CP** has a diethylamino rotor, the possibility of any twisted intramolecular charge transfer (TICT) state was thoroughly examined. A gradual increase in Φ_f^{CP} was observed with increase in solvent polarity, a situation that was contrary to the TICT process (Table 3.1). Time-resolved emission studies for **CP** were performed in solvents of varying

polarity following excitation with a 443 nm laser source, which revealed that there was no significant change in average lifetimes. These observations, together with the increase in radiative decay rates with increase in solvents polarity (e.g. n-C_6H_{14} to CH_3CN) confirmed that TICT process had no contribution to the luminescence spectrum of **CP.**[51,52]

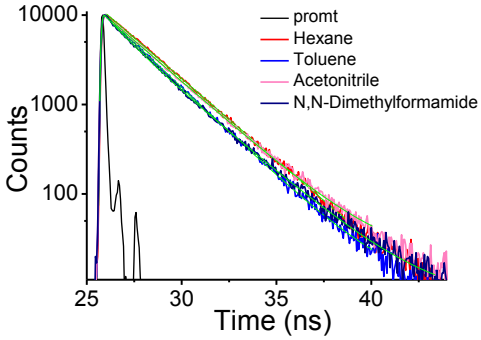

Figure 3.7. Emission decay traces of probe in different solvents (red-hexane, blue-toluene, magenta-acetonitrile, navy blue-N,N-Dimethylformamide)

Pseudo first order rate constant (k_{obs}) for the reaction between Cys and **CA** was evaluated from the slope of the plot $-\ln[I_{max} - I_t] / [I_{max}]$ *vs.* time (in s) (I_{max} maximum emission intensity; I_t emission intensity at time t, λ_{Ems}: 520 nm & λ_{Ext}: 450 nm) [Figure 3.8 (B)]. A linear dependency of the pseudo first order rate constants (k_{obs}) with varying [Cys] ($k_{obs} = k_c[Cys] + c$, where k_c is intrinsic rate constant for the reaction and c is the intercept) helped us in evaluating k_c as $(2.13 \pm 0.06).10^{-3} s^{-1}$[Figure 3.8 (A)].

Solvent	**Quantum Yield (Φ) @520 nm**	**Lifetime (ns)**	**Radiative Rate Constant (k_r) $10^7 s^{-1}$**	**Non-Radiative Rate Constant (k_{nr}) $10^7 s^{-1}$**
Hexane	0.26	2.38	0.26	2.38
Toluene	0.71	2.19	0.71	2.19
DMF	0.86	2.06	0.86	2.06
Acetonitrile	0.91	2.35	0.91	2.35

Table 3.1. Quantum yield, lifetime, radiative and nonradiative rate constant of **CP** in solvents of varying polarity

Linear dependency of k_{obs} on [Cys] confirmed that the rate determining step for this reaction involved Cys. Negligible intercept (3.1×10^{-4} s^{-1}) also suggested the absence of any detectable side reaction that could contribute to this observed luminescence changes.

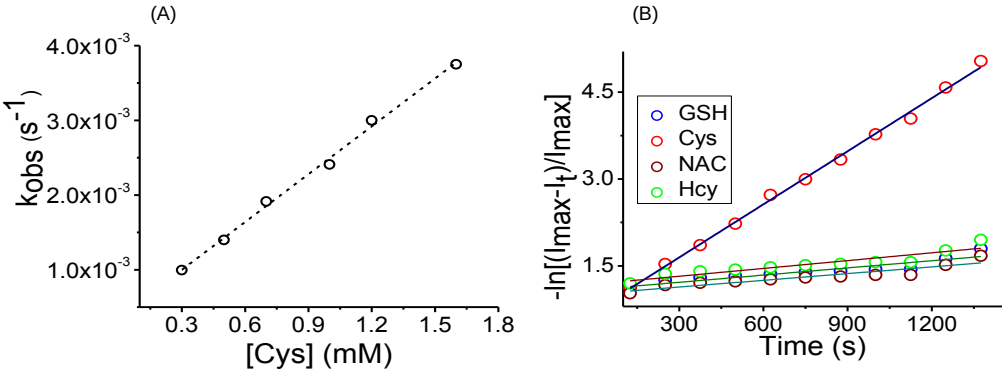

Figure 3.8. (A) The plot of k_{obs} vs. [Cys] to evaluate overall rate constant for the reaction between **CA** and Cys. (B) The plot of $-\ln[(I_{max}-I_t)/I_{max}]$ v/s time to evaluate k_{obs} for reactions with Cys, Hcy, GSH and NAC (1mM), respectively. These plots revealed that no change in luminescence was observed for Hcy/GSH/NAC. Studies were performed in 10mM aq. HEPES buffer: CH_3CN (98:2, v/v; pH 7.0) medium at 298 k. λ_{Ext} = 450 nm.

3.4.1. Enzymatic studies

This ACY-1 is a binuclear Zn(II)-based enzyme that hydrolyses the acetylated amino acid (NAC) and releases free Cys (Figure 3.9 B). Cys generated *in-situ*, was utilized for specific reaction with **CA** and this led to the generation of **CP** with associated luminescence ON response (Figure 3.5 B). Being an amide derivative, NAC lacks free -NH_2 functionality and thus fails to participate in cyclisation reaction with **CA**. Analyzing changes in luminescence responses on the generation of **CP** as a function of time or [Cys] or [ACY-1] helped us (Figure 3.9 A) in monitoring the enzymatic process and develop a fluorescence-based assay for ACY-1. The methodology adopted for this study is provided in the experimental section. Initially, a control experiment was performed by incubating aq. HEPES buffer: CH_3CN (98:2 v/v, pH 7.0) solution of NAC (100 μM) with **CA** (10 μM) at 37°C and as anticipated, no change in fluorescence intensity was observed at 520 nm (Figure 3.9 A). A similar reaction was performed after the addition of ACY-1 (200 units) and a significant increase in the luminescence intensity with λ_{Max}^{Ems} of 520 nm was observed (Figure 3.9 A), which can be attributed to the formation of **CP**. This was generated by the reaction between **CA** and *in-situ* generated Cys through enzymatic hydrolysis of NAC by ACY-1.

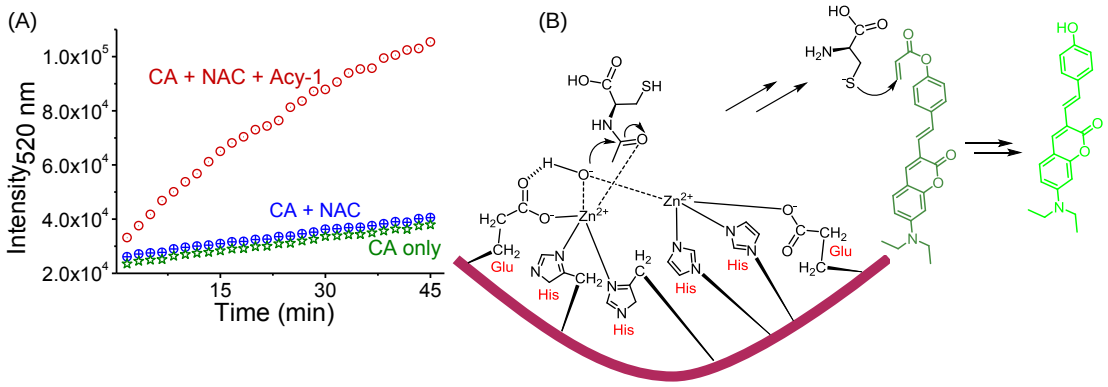

Figure 3.9. Emission response of **CA** (10 μM) monitored at 520 nm (A) as a function of time in the presence or absence of NAC (100 μM) and ACY-1 (200 units); (B) Cartoon representation of the active site for ACY-1 for the generation of Cys through the hydrolysis of NAC and the conversion of **CA** to a strongly luminescent **CP** by *in-situ* generated Cys. For all studies, λ_{Ext} = 450 nm; [NAC] = 100 μM in aq. HEPES buffer: CH_3CN (98:2 v/v, pH 7.0) medium at 37 ^oC were maintained.

Michaelis constant (K_m) for this enzymatic process was evaluated from time-dependent steady-state emission studies using fixed [**CA**] (10 μM) and [ACY-1] (20 units/mL) with varying [NAC] (0.1-0.4 mM). Initial rates (v) were calculated for the first 15 minutes, and K_m was determined from the slope of 1/v vs. 1/[NAC] (Figure 3.10 A). Evaluated value for K_m was 4.575 x 10^{-3}, which agreed well with the reported value.[7] It has been argued by several research groups that Zn(II) in the active site of ACY-1 plays crucial role in the hydrolysis of NAC.[53-56] It is argued that Zn(II)I-centre helps in polarizing the carbonyl group of -$CONH_{NAC}$ and catalyzes the hydrolysis reaction (Figure 3.9 B).[57] To examine this, enzymatic reactions were performed in absence and presence of varying concentration of an inhibitor, ethylenediaminetetraacetic acid (EDTA). A fixed concentration of ACY-1 (200 units) was incubated with varying [EDTA] (0-2 mM) in aq. HEPES-CH_3CN medium (98:2, v/v; pH 7) at 37°C for 15 min and then the resultant solution was further treated with **CA** (10 μM) and NAC (100 μM) for additional 45 minutes. A substantial decrease in the fluorescence intensity was observed for samples that were treated with EDTA (Figure 3.10 B), confirming the inhibitory role of EDTA on enzymatic activity. The high binding affinity of EDTA to Zn(II)[56] was accounted for the effective removal of Zn(II) from the active site and the inhibition of the activity.

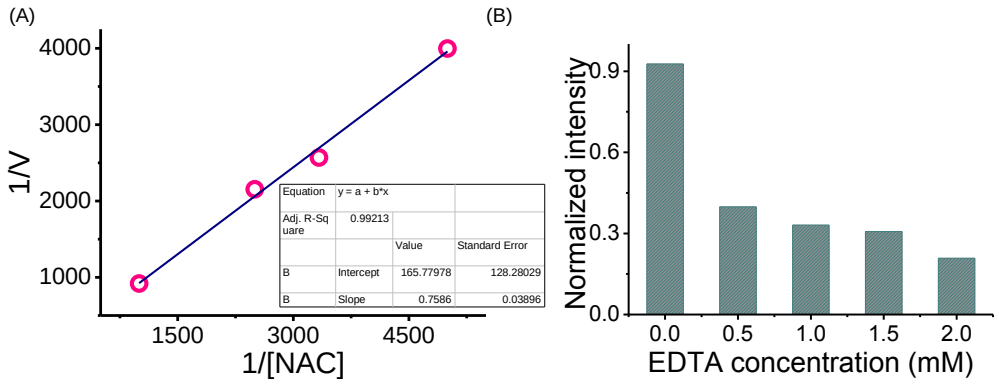

Figure 3.10. (A) The plot of 1/V vs. 1/[NAC] to determine K_m. (B) Emission response of **CA** (10 μM) at 520 nm as a function of [EDTA] (0 - 2 mM). Maintaining [ACY-1] = 200 units; λ_{Ext} = 450 nm; [NAC] = 100 μM in aq. HEPES buffer: CH_3CN (98:2 v/v, pH 7) at 37° C.

3.4.2. Cytotoxicity studies and imaging

The toxicity of the reagent was evaluated in healthy human Embryonic Kidney 293T cells (HEK 293T) and colon cancer cells (SW480) using conventional MTT assay method (MTT = (3-(4,5-dimethylthiazol-2-yl)-2,5-diphenyltetrazoliumbromide). MTT studies revealed insignificant toxicity of the reagent ($IC_{50} \geq 300$ μM) towards both the cell lines (Figure 3.11).

To test the efficacy of probe **CA** for imaging endogenous cysteine present in living cells, confocal laser scanning microscopic (CLSM) studies were carried out with healthy as well as cancerous cell lines (HEK 293T cells and SW480 cells, respectively). Standard protocols are provided in the experimental section. Living cells were incubated with **CA** (10 μM) for 30 min at 37° C in aq. HEPES-CH_3CN medium (98:2, v/v; pH 7.0).

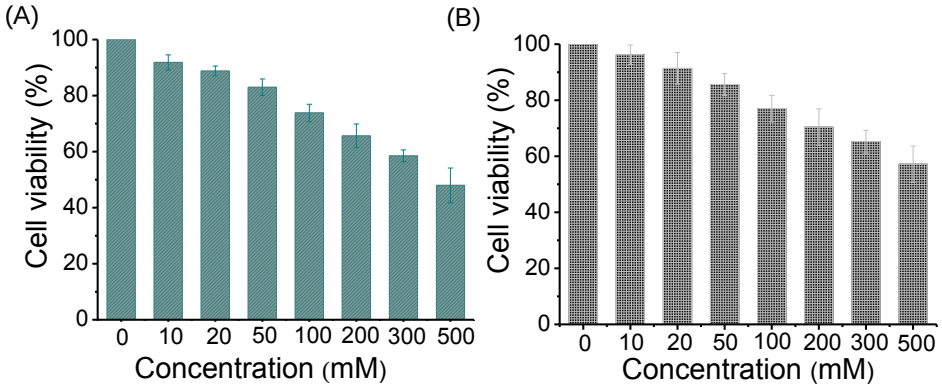

Figure 3.11. MTT assay to determine the cell viability percentage in the presence of **CA** in (A) HEK 293T cells and (B) SW480 cells.

Bright green fluorescence was observed from the cells. These images confirmed the cell membrane permeability of **CA** and its ability to react with intracellular Cys [Figure 3.12 (a)].

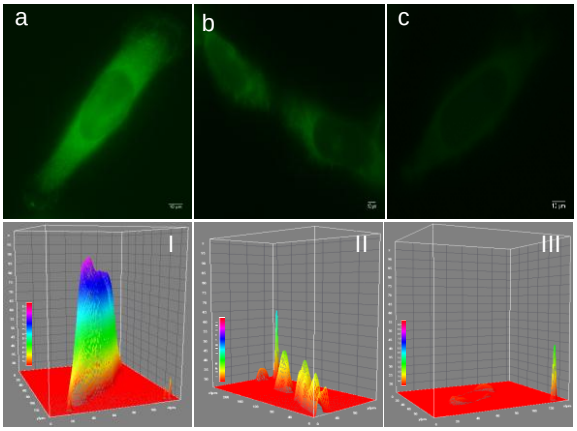

Figure 3.12. Confocal laser scanning microscopic (CLSM) images of (a) SW480 cells incubated with 10 μM of **CA** for 30 min. (b) HEK 293T cells incubated with 10 μM of **CA** for 30 min. (c) SW480 cells pre-treated with 2 mM of NEM for 30 minutes followed by further incubation with 10 μM of **CA** for 30 min. (i-iii) Corresponding 3D surface intensity plots of (a-c) respectively. For confocal microscopic studies, 495 nm excitation source was utilized, and emission was monitored in the green channel. Scale bar 10 μm.

Interestingly, fluorescent intensity was found to be less in healthy HEK 293T cells compared to that of cancerous SW480 cells (Figure 3.12 b). The membrane repair mechanism is less effective in cancerous SW480 cells, this would have resulted in better permeabilization of the probe in malignant cells compared to normal cells.[58] The result obtained here suggest that the probe is sensitive enough to report the small variation in the Cys level.

To confirm that the fluorescence responses in CLSM images were solely due to the reaction between **CA** and intracellular Cys, control experiments were also performed by pre-incubating the SW480 cancer cells with 2 mM of NEM (a known thiol blocking agent) for 30 minutes prior to the incubation with **CA.** A significant decrease in intensity of the intracellular fluorescence was observed in NEM treated cells, which could be attributed to the preferential reaction between endogenous Cys and NEM (Figure 3.12 c), rather than with **CA**.

In general, cancer cells are known to possess the higher concentration of GSH rather than Cys. We have done a control experiment to inhibit the GSH synthesis in cells. For this, SW480 cells were treated with L-buthionine sulfoximine (BSO), a well-known

inhibitor of the enzyme glutamate cysteine ligase (one of the enzymes required for GSH synthesis in cells).[59] Upon treating the cells with BSO is expected to inhibit the GSH synthesis and thus deplete the GSH concentration in cells. BSO treated cells were further incubated with **CA** for 30 minutes. BSO treatment failed to induce any appreciable change in fluorescence images (Figure 3.13).

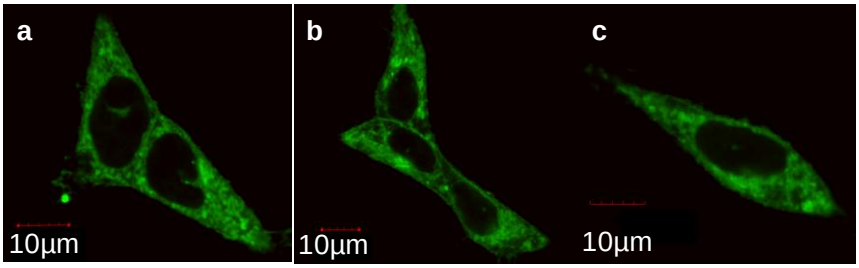

Figure 3.13. CLSM images of SW480 cells. (a) Cells incubated with **CA** for 30 minutes; (b) Cells incubated with BSO for 2hr followed by the incubation with **CA** for 30 minutes; (c) Cells incubated with BSO for 24 hr followed by the incubation with CA for 30 minutes. For all these studies, 10 µM **CA** was used. Scale bar 10 µm.

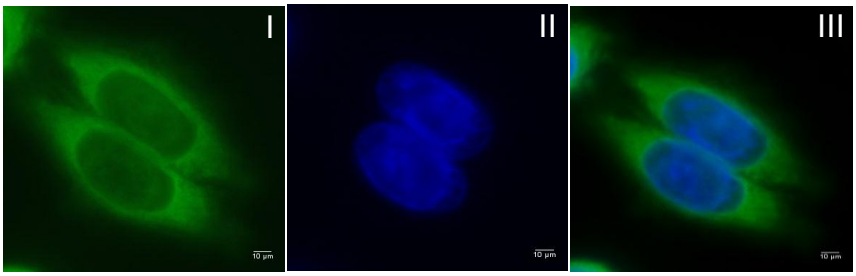

Figure 3.14. CLSM images of SW480 cells stained with (I) **CA** (10 µM); co-stained with nucleus staining dye DAPI (II); (III) merged images of I & II). For confocal microscopic studies with **CA**, 495 nm excitation source was utilized, and emission was monitored in the green channel. For DAPI, 359 nm laser was used as the excitation source, and emission was monitored in the blue channel. Scale bar 10 µm.

These results confirmed the potential utility of **CA** as a viable cellular imaging agent for the detection of intracellular Cys. Moreover, it could distinguish the difference in Cys concentration in normal and cancer cell lines. Co-staining experiment with a well-known nucleus staining dye DAPI indicates the preferential localization of the reagent **CA** in the cytoplasm of SW480 cells (Figure 3.14).

3.4.3. Peroxide induced oxidative stress

Literature reports suggest that reactive oxygen species (ROS), like H_2O_2 can induce oxidative stress in cells, which alters the Cys levels inside the cells.[2,6] Intracellular build-up of H_2O_2 could happen through some enzymatic process involving D-amino acid

oxidase, uric acid oxidase etc. or through disproportionation of superoxide ($O_2^{\bullet-}$).[2,60-66] It is reported that a low level of H_2O_2 can oxidize Cys-thiols into sulfenic acid (SOH) (Scheme 3.2).[6] For higher doses of H_2O_2, sulfenic acid further oxidizes to sulfinic acid (SO_2H), sulfonic acid (SO_3H) and disulfides.

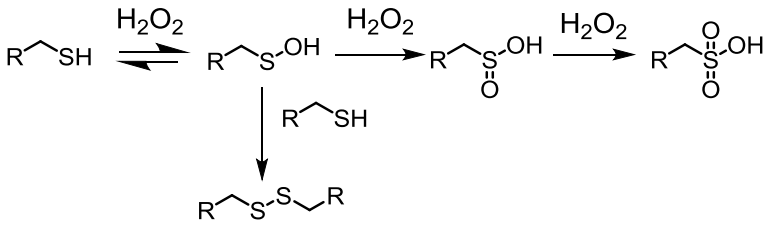

Scheme 3.2. Hydrogen peroxide-mediated oxidation of thiols.

Literature reports also suggest that H_2O_2 mediated reversible oxidation of Cys residues plays a crucial role in intracellular redox signaling.[2] Thus, monitoring the Cys levels in cells is vital for understanding the signaling mechanism and to get an overall idea about the redox environment. Insignificant toxicity and cell membrane permeability of **CA** helped us to explore further the possibility of using this reagent to monitor the H_2O_2 induced oxidative stress in living SW480 cells. Initially, the cells were incubated with **CA** in the absence of H_2O_2, wherein bright green fluorescence was observed from the cells indicating the presence of intracellular Cys (Figure 3.15 a). Later, these cells were pre-treated with different concentrations of H_2O_2 to induce oxidative stress and then further incubated with **CA**. Fluorescence intensity was dramatically decreased in the H_2O_2 pre-treated cells (Figure 3.15 b). This could be attributed to the H_2O_2 mediated oxidation of Cys to other forms (Scheme 3.2), which failed to participate in the conjugate addition with **CA**. This process was more efficient at higher concentration of H_2O_2, and intracellular fluorescence was completely quenched (Figures 3.15 c & d). It has been known from the literature that, NAC is a powerful radical scavenger and capable of reducing hydroxyl radicals and hydrogen peroxide.[55-56]

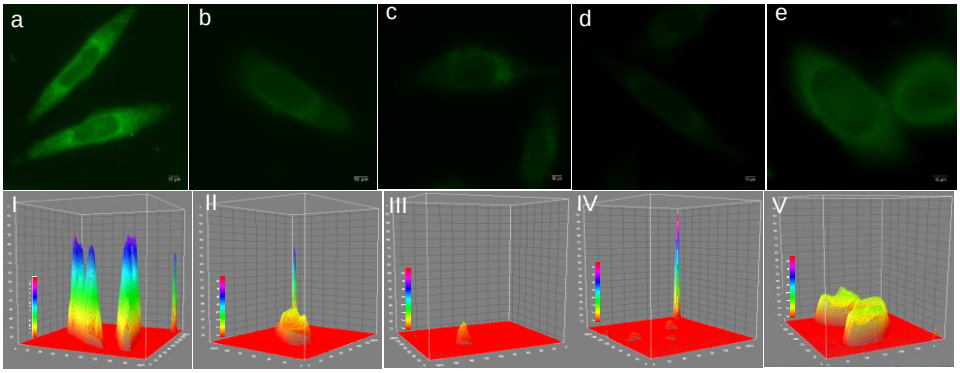

Figure 3.15. CLSM images of SW480 cells (a) incubated with 10 μM **CA** for 30 min; (b, c, d) treated with 0.5 mM, 1mM and 2mM H_2O_2, respectively for 30 min and then incubated with 10 μM **CA** for 30 min; (e) treated with 1 mM H_2O_2 and then incubated with 0.5 mM of NAC for 45 min and finally treated with 10 μM **CA** for 30 min. (I-V) Corresponding 3D intensity profile plots of (a-e), respectively. For CLSM studies 495 nm excitation source was used, while the emission was monitored in the green channel. Scale bar 10 μm.

It is also well documented that NAC undergoes enzymatic deacetylation process and releases Cys in cells where Cys is known to scavenge ROS.[53.54] On further treatment with excess NAC, live cells that are pre-treated with H_2O_2 are expected to show lesser H_2O_2 induced stress and a subsequent higher intracellular fluorescence recovery. To verify this fact, the cells that were previously under stress (due to exposure to H_2O_2) were further incubated with 0.5 mM of aqueous tablet solution of NAC for 45 minutes and subsequently with **CA** for 30 minutes. A partial resurgence in the fluorescence intensity was observed indicating the reduction in oxidative stress and Cys release from NAC (Figure 3.15 e). H_2O_2 mediated Cys oxidation is argued as the reversible process and the major mechanism for intracellular signaling, and this supports the present observation of the fluorescence recovery.[60,63] These results suggest the possibility of using **CA** as a fluorescent switch to monitor the H_2O_2 induced oxidative stress and in turn to understand the thiol-redox chemistry linked to intracellular signaling events in living cells.

3.4.4. Estimation of [ACY-1] in blood serum by standard addition method[69]

ACY-1 levels in blood serum markedly increase in patients with DGF after renal transplantation, and it is being considered as an important biomarker for monitoring the recovery of such patients.[11] As discussed earlier, ACY-1 catalyses the hydrolysis of NAC and releases Cys. We explored the possibility of using **CA** to quantify the ACY-1 present in blood serum (BS). Serum samples were prepared according to the literature procedure.[70] Diluted serum (100 μl) was spiked with an unknown quantity of ACY-1 to mimic the real clinical samples. It was added to a solution containing NAC (50 nM) and **CA** (10 μM) in HEPES: CH_3CN (98:2 v/v, pH 7) and incubated at 37^o C for 45 minutes. A control experiment was also performed without ACY-1 in order to nullify the background signal which arose from the reaction between Cys present in serum and **CA.** Unknown [ACY-1] present in blood serum was determined from the graphs by standard addition method by following the standard protocols (Figure 3.16), and the obtained values were tabulated in table 3.2.

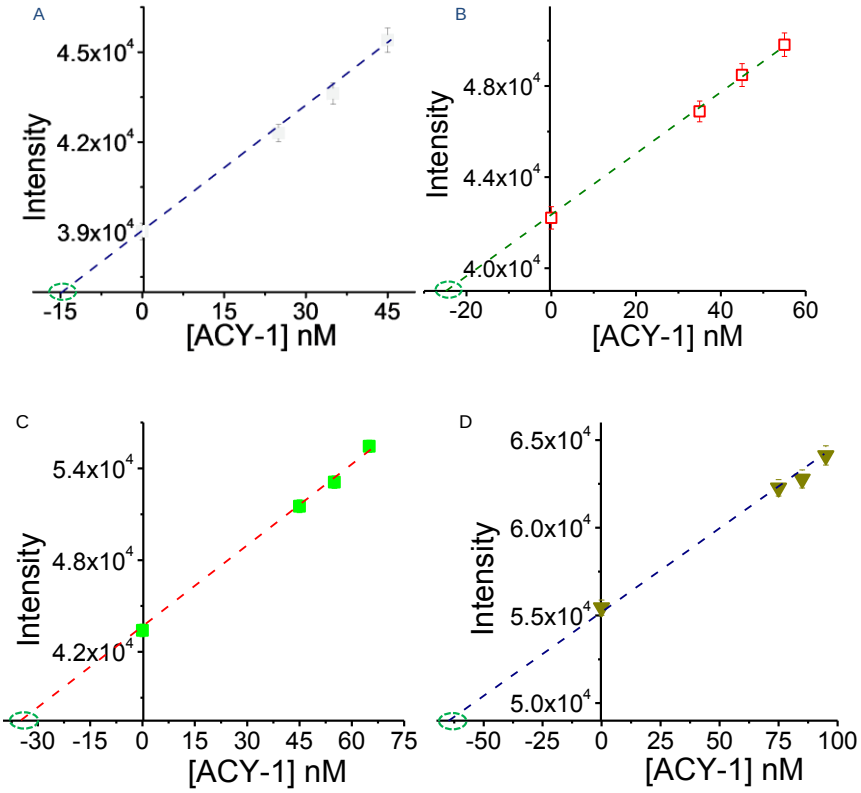

Figure 3.16. Determination of unknown concentration of ACY-1 present in blood serum by standard addition method by using reagent **CA**. The unknown [ACY-1] obtained from these graphs were given in the table below. (A standard solution of enzyme was prepared by dissolving solid enzyme in HEPES buffer).

The standard addition is a technique in which an analytical signal due to an unknown is first measured. Then a known quantity of analyte is added, and the increase in signal is recorded. Increase in signal intensity was plotted as a function of concentration. The curve obtained was extrapolated to zero intensity (Y=0) to get a negative value (on X-axis), and the magnitude of this will give the unknown concentration of analyte present in sample.[69]

S.No	[ACY-1] present in blood serum estimated by reagent CA (nM)
A	14.71
B	24.75
C	35.00
D	64.56

Table 3.2. Unknown [ACY-1] present in different blood serum samples determined by reagent **CA.**

Further, recovery studies were also performed in order to check the efficacy of our method to quantify the ACY-1. The results are provided in table 3.3.

ACY-1 Spiked (in nM)	Found (in nM)*	% Recovery
15	14.89	99.20
35	34.83	99.51
25	24.79	99.16
65	64.93	99.89

Table 3.3. Recovery studies of serum samples spiked with different concentration of ACY-1. * Average of three independent measurements.

3.4.5. Comparative studies with fluorescamine assay method[68]

In order to validate our method, we have compared our results with existing fluorescamine based assay method. Fluorescamine assay is a well established method used for the measurement of ACY-1. Fluorescamine assay involves the measurement of reaction product of the reaction between N-acyl amino acids and ACY-1. The free amine which is released after enzymatic de-acetylation reacts with fluorescamine reagent and gives turn-on fluorescence signal. Fluorescamine assay was performed for four different unknown samples in HEPES buffer by following the standard protocols reported elsewhere.[67,68] For fluorescamine assay, fluorescamine was excited at 390 nm and emission was recorded at 475 nm. Concentration of unknown sample was determined by using the calibration curve as per the standard protocols (Figure 3.17 and 3.18).

Fluorescamine assay studies were performed in buffer solution. Fluorescamine is known to react with the free amines present in proteins and peptides, leading to serious errors in measurement. So, it cannot be used for the analysis complex biological fluids like blood serum. Fluorescamine assay was performed in order to compare the efficacy of our reagent CA in quantifying ACY-1. Unknown concentrations of ACY-1 determined from the graph were given in the table 3.4.

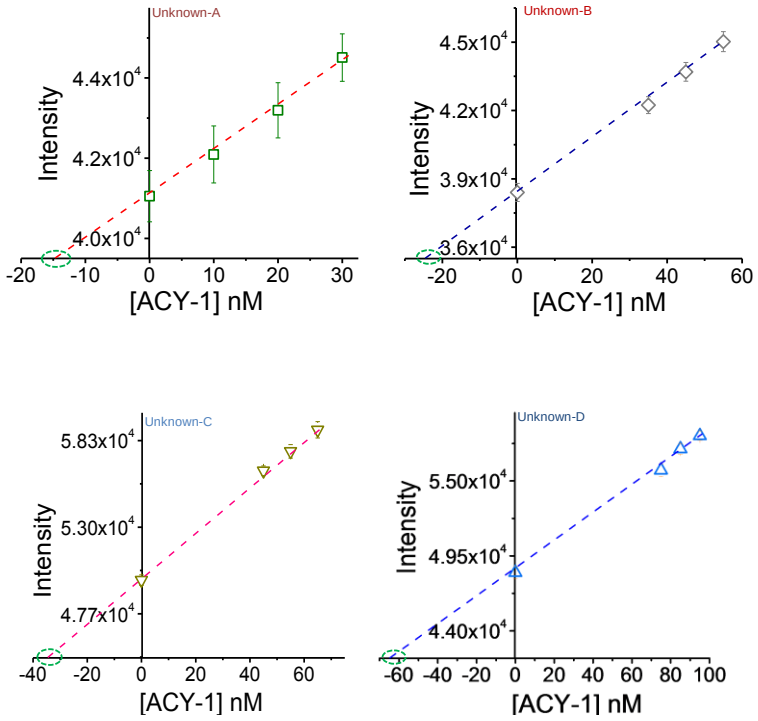

Figure 3.17. Determination of unknown concentration of ACY-1 in different samples (Unknown A, B, C & D) by reagent **CA**.

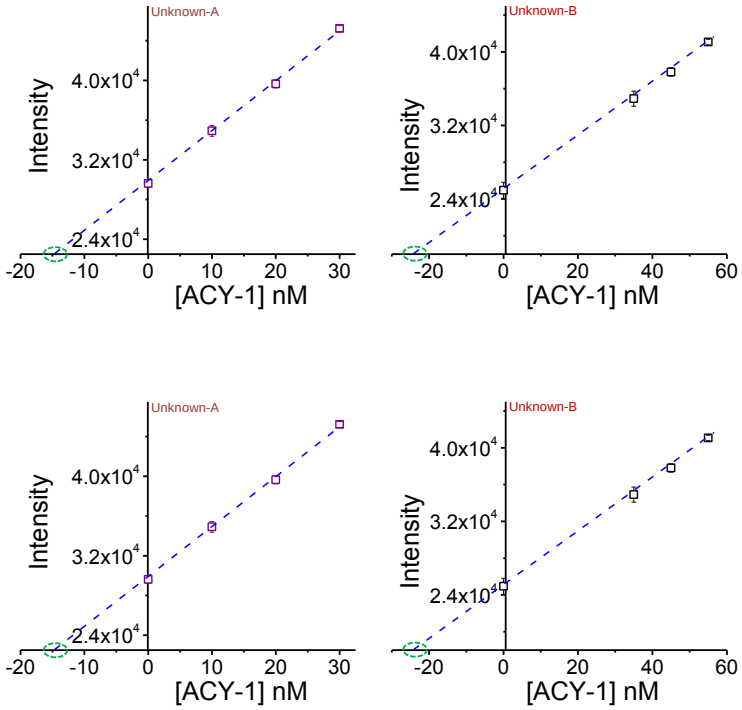

Figure 3.18. Determination of unknown concentration of ACY-1 in different samples (Unknown A, B, C & D) by fluorescamine assay method.

Unknown ACY-1 samples	ACY-1 (in nM) quantified by reagent CA	ACY-1 (in nM) quantified by fluorescamine method
Unknown-A	14.73	14.79
Unknown-B	24.83	24.68
Unknown-C	34.89	34.90
Unknown-D	64.88	64.80

Table 3.4. Unknown [ACY-1] samples (A, B, C & D) quantified by reagent **CA** and fluorescamine assay method.

3.4.6. Estimation of [ACY-1] in blood serum by kinetic method

We have also explored the possibility of using observed rate constants to quantify the ACY-1 present in serum samples. Serum samples were as mentioned in the standard addition method. A control experiment was also performed without ACY-1 to nullify the background signal which arose from the reaction between Cys present in serum and **CA.** (Figure 3.19 B). Rate constants were evaluated from the plot of log F_t-F_0 vs. time for each solution, and a calibration curve was obtained by plotting k_{obs} vs. [ACY-1] (Figure 3.19 A). Serum samples were spiked with different [ACY-1], and their rate constants were determined. These rate constants were fitted in standard calibration curve (Figure 3.19 C). From the calibration plot, unknown concentration of ACY-1 was determined. The background signal was subtracted from each experimental data to nullify the contribution from the background reaction. Rate constants were evaluated as $k_{obs}^{ACY\text{-}1@BS[15nM]}$ = 1.19×10^{-3} s^{-1}, $k_{obs}^{ACY\text{-}1@BS[25nM]}$ = 2.26×10^{-3} s^{-1}, $k_{obs}^{ACY\text{-}1@BS[35nM]}$ = 3.37×10^{-3} s^{-1} and $k_{obs}^{ACY\text{-}1@BS[55nM]}$ = 5.39×10^{-3} s^{-1}. To validate our method further, we have compared our results with the results of the fluorescamine-based assay (Table 3.4), a well-established methodology for the quantitative estimation of ACY-1.[67,68]

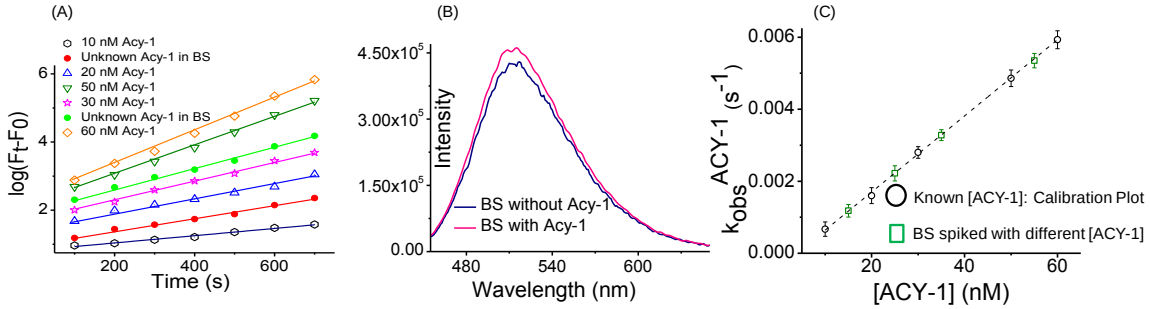

Figure 3.19. (A) Plot of log(F_t- F_0) vs. time for evaluating $k_{obs}^{ACY\text{-}1}$ (s^{-1}) for known, but different [Acy-1] (10 nM, 20 nM, 30 nM, 50 nM, 60 nM) in aq. buffer medium and unknown [Acy-1] (X_1 & X_2 nM) added to BS samples; (B) Fluorescence response of blood serum with **CA** (10 μM) and NAC (50 nM) in the presence and absence of ACY-1; (C) Calibration plot for plotting k_{obs} vs [ACY-1] to determine concentration of unknown ACY-1 in spiked blood serum sample.

Using these k_{obs} values and the calibration plot, respective [ACY-1] in BS samples were evaluated as 14.9 ± 0.1 nM, 24.9 ± 0.2 nM, 34.8 ± 0.2 nM and 54.7 ± 0.4 nM, respectively (Figure 3.19 C). This confirmed the feasibility of utilizing this methodology for evaluating the [ACY-1] in blood serum.

Concentration of ACY-1 in four different solutions (aq. HEPES buffer medium) was evaluated using the reagent **CA** and the present methodology as well as by fluorescamine assay (Figure 3.17 and 3.18). Results of these two independent experiments agree well, which confirmed that the present reagent (**CA**) is an effective one for quantification of ACY-1. Limited solubility and stability of fluorescamine in an aqueous medium, as well as its reactivity towards free amine(s) of proteins/peptides, limit its use for the analysis of ACY-1 in complex biological fluids like blood serum.[68] These offer a distinct edge to **CA** and the present methodology over fluorescamine assay. Since the quantification of ACY-1 is most important in patients with DGF after renal transplantation; reagent **CA** could be used for quantification of ACY-1 in clinical samples.

3.5. Conclusion

Fluorescence based technique for recognition of crucial biomarkers is one of the most promising tools in clinical diagnostics. In this contribution, we demonstrated that reagent **CA** could be used for selective detection of Cys in presence of the competing biothiols, cations and anions of biological relevance. This reagent is successfully utilized for monitoring the hydrolysis of an important commercial drug molecule NAC by an industrially and biologically important endogenous enzyme, aminoacylase-1 (ACY-1). Also, we demonstrated the possibility of quantification ACY-1 in blood serum samples. This has significance considering the fact that ACY-1 is an important biomarker with potential prognostic utility in patients with delayed graft function (DGF) following renal transplantation. MTT assay revealed the non-toxic nature of the compound even at higher concentrations (IC_{50} = 300 μM). This helped us in utilizing the reagent for intracellular detection of Cys. Moreover, this reagent could distinguish the Cys distribution in healthy and cancerous cells. Furthermore, we explored the possibility of using this reagent as a switch to monitor the peroxide-induced oxidative stress in living cells. To the best of our knowledge, the utility of such a Cys specific reagent as a switch to monitor the peroxide-induced oxidative stress as well as for the quantification ACY-1 in human blood serum is not discussed earlier.

3.6. References

1. S. M. Marino and V. N. Gladyshev, *J. Biol. Chem.*, 2012, **287**, 4419-4425.

2. S. García-Santamarina, S. Boronat and E. Hidalgo, *Biochemistry*, 2014, **53**, 2560-2580.

3. G, U. R.; Agarwalla, H.; Taye, N.; Ghorai, S.; Chattopadhyay, S.; Das, A. *Chem. Commun.* 2014, **50**, 9899-9902.

4. H. S. Jung, X. Chen, J. S. Kim and J. Yoon, *Chem. Soc. Rev.*, 2013, **42**, 6019-6031.

5. Z. A. Wood, L. B. Poole and P. A. Karplus, *Science*, 2003, **300**, 650-653.

6. J. M. Denu and K. G. Tanner, *Biochemistry*, 1998, **37**, 5633-5642.

7. V. Uttamsingh, D. A. Keller and M. W. Anders, *Chem. Res. Toxicol.*, 1998, **11**, 800-809.

8. Welberry Smith, M. P.; Zougman, A.; Cairns, D. A.; Wilson, M.; Wind, T.; Wood, S. L.; Thompson, D.; Messenger, M. P.; Mooney, A.; Selby, P. J.; Lewington, A. J. P.; Banks, R. E. *Kidney Int.,* 2013, **84,** 1214-1225.

9. Yarlagadda, S. G.; Coca, S. G.; Formica, R. N.; Poggio, E. D.; Parikh, C. R. *Nephrol. Dial. Transplant.,* 2009, **24,** 1039-1047.

10. Sola, R.; Alarcón, A.; Jiménez, C.; Osuna, A. *Nephrol. Dial. Transplant.,* 2004, **19,** iii32.

11. Smith, M. P. W.; Wood, S. L.; Zougman, A.; Ho, J. T. C.; Peng, J.; Jackson, D.; Cairns, D. A.; Lewington, A. J. P.; Selby, P. J.; Banks, R. E. *Proteomics,* 2011, **11,** 2222-2235.

12. W. Wang, O. Rusin, X. Xu, K. K. Kim, J. O. Escobedo, S. O. Fakayode, K. A. Fletcher, M. Lowry, C. M. Schowalter, C. M. Lawrence, F. R. Fronczek, I. M. Warner and R. M. Strongin, *J. Am. Chem. Soc.*, 2005, **127**, 15949-15958.

13. L.-Y. Niu, Y.-Z. Chen, H.-R. Zheng, L.-Z. Wu, C.-H. Tung and Q.-Z. Yang, *Chem. Soc. Rev.*, 2015, **44**, 6143-6160.

14. M. Isik, T. Ozdemir, I. S. Turan, S. Kolemen and E. U. Akkaya, *Org. Lett.*, 2012, **15**, 216-219.

15. Y.-Q. Sun, M. Chen, J. Liu, X. Lv, J.-f. Li and W. Guo, *Chem. Commun.*, 2011, **47**, 11029-11031.

16. X. Chen, S.-K. Ko, M. J. Kim, I. Shin and J. Yoon, *Chem. Commun.*, 2010, **46**, 2751-2753.

17. H. Kwon, K. Lee and H.-J. Kim, *Chem. Commun.*, 2011, **47**, 1773-1775.

18. M. Hu, J. Fan, H. Li, K. Song, S. Wang, G. Cheng and X. Peng, *Org. Biomol.Chem.*, 2011, **9**, 980-983.

19. P. Wang, J. Liu, X. Lv, Y. Liu, Y. Zhao and W. Guo, *Org. Lett.*, 2012, **14**, 520-523.

20. X. Liu, N. Xi, S. Liu, Y. Ma, H. Yang, H. Li, J. He, Q. Zhao, F. Li and W. Huang, *J. Mater. Chem.*, 2012, **22**, 7894-7901.

21. M. H. Lee, J. H. Han, P.-S. Kwon, S. Bhuniya, J. Y. Kim, J. L. Sessler, C. Kang and J. S. Kim, *J. Am. Chem. Soc.*, 2011, **134**, 1316-1322.

22. C. S. Lim, G. Masanta, H. J. Kim, J. H. Han, H. M. Kim and B. R. Cho, *J. Am. Chem. Soc.*, 2011, **133**, 11132-11135.

23. J. H. Lee, C. S. Lim, Y. S. Tian, J. H. Han and B. R. Cho, *J. Am. Chem. Soc.*, 2010, **132**, 1216-1217.

24. X.-F. Yang, Q. Huang, Y. Zhong, Z. Li, H. Li, M. Lowry, J. O. Escobedo and R. M. Strongin, *Chem. Sci.*, 2014, **5**, 2177-2183.

25. X. Zhou, X. Jin, G. Sun and X. Wu, *Chem.Eur. J.*, 2013, **19**, 7817-7824.

26. N. Shao, J. Y. Jin, S. M. Cheung, R. H. Yang, W. H. Chan and T. Mo, *Angew. Chem., Int. Ed.*, 2006, **118**, 5066-5070.

27. J. Liu, Y.-Q. Sun, H. Zhang, Y. Huo, Y. Shi and W. Guo, *Chem. Sci.*, 2014, **5**, 3183-3188.

28. P. Das, A. K. Mandal, U. Reddy G, M. Baidya, S. K. Ghosh and A. Das, *Org. Biomol.Chem.*, 2013, **11**, 6604-6614.

29. P. Das, A. K. Mandal, N. B. Chandar, M. Baidya, H. B. Bhatt, B. Ganguly, S. K. Ghosh and A. Das, *Chem.Eur. J.*, 2012, **18**, 15382-15393.

30. L.-Y. Niu, Y.-Z. Chen, H.-R. Zheng, L.-Z. Wu, C.-H. Tung and Q.-Z. Yang, *Chem. Soc. Rev.*, 2015*,* **44,** 6143-6160.

31. S. Sreejith, K. P. Divya and A. Ajayaghosh, *Angew. Chem., Int. Ed.*, 2008, **47**, 7883-7887.

32. H. S. Jung, J. H. Han, T. Pradhan, S. Kim, S. W. Lee, J. L. Sessler, T. W. Kim, C. Kang and J. S. Kim, *Biomaterials*, 2012, **33**, 945-953.

33. B. Liu, J. Wang, G. Zhang, R. Bai and Y. Pang, *ACS Appl. Mater. Interfaces*, 2014, **6**, 4402-4407.

34. H. Wang, G. Zhou, H. Gai and X. Chen, *Chem. Commun.*, 2012, **48**, 8341-8343.

35. X. Zhou, X. Jin, G. Sun, D. Li and X. Wu, *Chem. Commun.*, 2012, **48**, 8793-8795.

36. J. Zhang, J. Wang, J. Liu, L. Ning, X. Zhu, B. Yu, X. Liu, X. Yao and H. Zhang, *Anal. Chem.*, 2015, **87**, 4856-4863.

37. M. Zheng, H. Huang, M. Zhou, Y. Wang, Y. Zhang, D. Ye and H.-Y. Chen, *Chem.Eur. J.*, 2015, **21**, 10506-10512.

38. W. Niu, L. Guo, Y. Li, S. Shuang, C. Dong and M. S. Wong, *Anal. Chem.*, 2016, **88**, 1908-1914.

39. A. H. A, U. R. G, F. Ali, N. Taye, S. Chattopadhyay and A. Das, *Chem. Commun.*, 2015, **51**, 15592-15595.

40. F. Ali, A. H. A, N. Taye, R. G. Gonnade, S. Chattopadhyay and A. Das, *Chem. Commun.*, 2015, **51**, 16932-16935.

41. C. Han, H. Yang, M. Chen, Q. Su, W. Feng and F. Li, *ACS Appl. Mater. Interfaces*, 2015, **7**, 27968-27975.

42. Y. Liu, X. Lv, M. Hou, Y. Shi and W. Guo, *Anal. Chem.*, 2015, **87**, 11475-11483.

43. H. Zhang, R. Liu, J. Liu, L. Li, P. Wang, S. Q. Yao, Z. Xu and H. Sun, *Chem. Sci.*, 2016, **7**, 256-260.

44. X. Yang, Y. Guo and R. M. Strongin, *Org. Biomol.Chem.*, 2012, **10**, 2739-2741.

45. X. Dai, Q.-H. Wu, P.-C. Wang, J. Tian, Y. Xu, S.-Q. Wang, J.-Y. Miao and B.-X. Zhao, *Biosen.Bioelectron.*, 2014, **59**, 35-39.

46. B. Zhu, B. Guo, Y. Zhao, B. Zhang and B. Du, *Biosen.Bioelectron.*, 2014, **55**, 72-75.

47. Q. Han, Z. Shi, X. Tang, L. Yang, Z. Mou, J. Li, J. Shi, C. Chen, W. Liu, H. Yang and W. Liu, *Org. Biomol.Chem.*, 2014, **12**, 5023-5030.

48. H. Li, J. Fan, J. Wang, M. Tian, J. Du, S. Sun, P. Sun and X. Peng, *Chem. Commun.*, 2009, 5904-5906.

49. X. Yang, Y. Guo and R. M. Strongin, *Angew. Chem., Int. Ed.*, 2011, **50**, 10690-10693.

50. Z. Guo, S. Nam, S. Park and J. Yoon, *Chem. Sci.*, 2012, **3**, 2760-2765.

51. P. Mahato, S. Saha and A. Das, *J. Phys. Chem. C*, 2012, **116**, 17448-17457.

52. T. Debnath, P. Maity, H. Lobo, B. Singh, G. S. Shankarling and H. N. Ghosh, *Chem.Eur. J.*, 2014, **20**, 3510-3519.

53. J. Gordo, J. Avó, A. J. Parola, J. C. Lima, A. Pereira and P. S. Branco, *Org. Lett.*, 2011, **13**, 5112-5115.

54. S. V. Story, A. M. Grunden and M. W. W. Adams, *J. Bacteriol.*, 2001, **183**, 4259-4268.

55. Kiyoshima, T.; Enoki, N.; Kobayashi, I.; Sakai, T.; Nagata, K.; Wada, H.; Fujiwara, H.; Ookuma, Y.; Sakai, H. *Int. J. Mol. Med.,* 2012, **30,** 1007-1012.

56. S. C. De Rosa, M. D. Zaretsky, J. G. Dubs, M. Roederer, M. Anderson, A. Green, D. Mitra, N. Watanabe, H. Nakamura, I. Tjioe, S. C. Deresinski, W. A. Moore, S. W. Ela,

D. Parks, L. A. Herzenberg and L. A. Herzenberg, *Eur. J. Clin. Invest.*, 2000, **30**, 915-929.

57. V. Uttamsingh, R. B. Baggs, D. M. Krenitsky and M. W. Anders, *Drug Metab. Dispos.*, 2000, **28**, 625-632.

58. Frandsen, S. K.; McNeil, A. K.; Novak, I.; McNeil, P. L.; Gehl, J. *J. Membrane Biol.,* 2016, **249,** 569-576.

59. Anderson, M. E.; Meister, A. *Proc. Natl. Acad. Sci.,* 1983, **80,** 707-711.

60. Veal, E. A.; Day, A. M.; Morgan, B. A. *Molecular Cell,* 2007, **26,** 1-14.

61. M. Hernick and C. A. Fierke, *Arch. Biochem. Biophys.*, 2005, **433**, 71-84.

62. Mailloux, R. J.; Jin, X.; Willmore, W. G. *Redox Biol.,* **2014,** *2*, 123-139.

63. Conte, M. L.; Carroll, K. S., TIn *Oxidative Stress and Redox Regulation*, Jakob, U.; Reichmann, D., Eds. Springer Netherlands: Dordrecht, 2013; pp 1-42.

64. C. A. S. Regino and D. E. Richardson, *Inorg. Chim. Acta*, 2007, **360**, 3971-3977.

65. Trachootham, D.; Lu, W.; Ogasawara, M. A.; Valle, N. R.-D.; Huang, P. *Antioxid. Redox Signaling.* 2008, **10,** 1343-1374.

66. Filomeni, G.; De Zio, D.; Cecconi, F. *Cell Death Differ* 2015, **22,** 377-388.

67. Pushkin, A.; Kurtz, I. *Curr. Protoc. Toxicol*. John Wiley & Sons, Inc.2001.

68. Udenfriend, S.; Stein, S.; Böhlen, P.; Dairman, W.; Leimgruber, W.; Weigele, M. *Science* (New York, N.Y.), 1972, ***178,*** 871-872.

69. Harris, D. C., Quality assurance and calibration methods, *Quantitative chemical analysis*, 7th edn, Fiorillo J., Thorne A., Bleyer C., USA., 2007, 89.

70. Jia, M.-Y.; Niu, L.-Y.; Zhang, Y.; Yang, Q.-Z.; Tung, C.-H.; Guan, Y.-F.; Feng, L. *ACS Appl. Mater. Interfaces,* 2015, **7,** 5907-5914.

CHAPTER 4

POLYSULFIDE-TRIGGERED FLUORESCENT INDICATOR SUITABLE FOR SUPER-RESOLUTION MICROSCOPY AND APPLICATION IN IMAGING

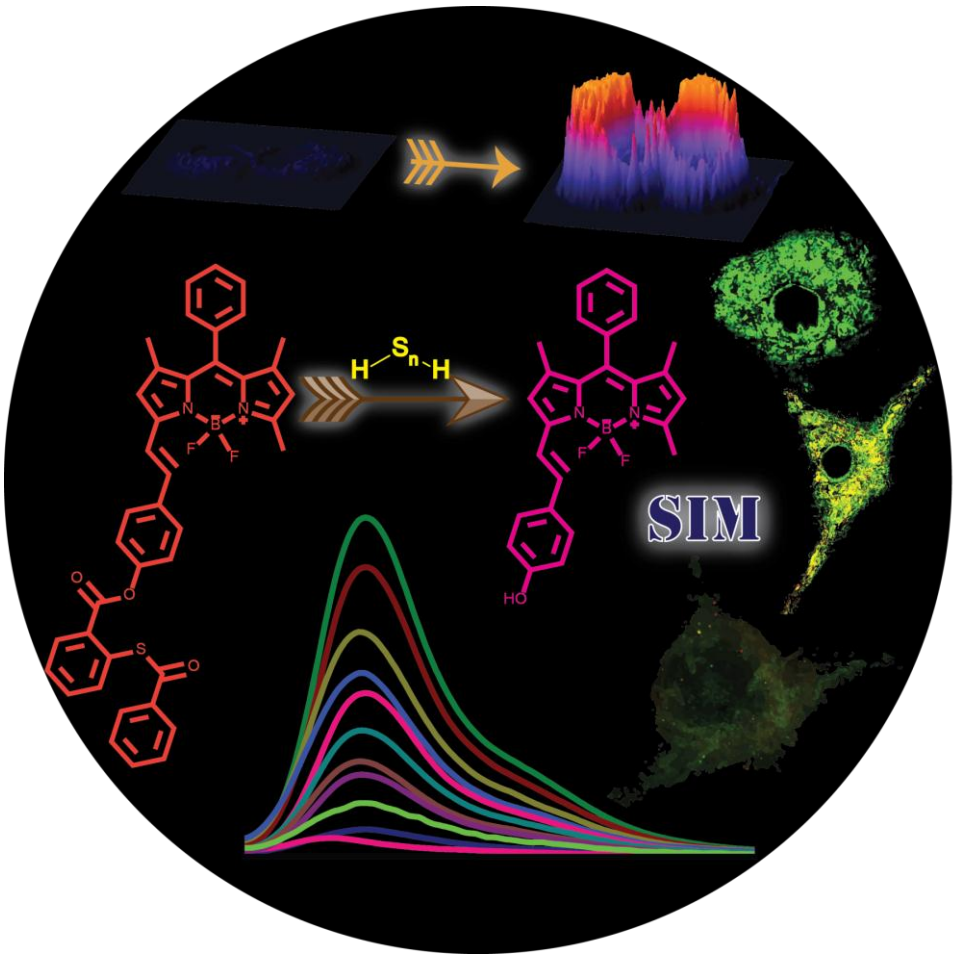

Chem. Commun., 2018, 54, 3735.

4.1. Introduction

Hydrogen polysulfide (H_2S_n, n > 1) is one of the reactive sulphur species (RSS), recently identified as an important signaling molecule. H_2S_n is produced in cells by the enzyme 3-mercaptopyruvate sulfurtransferase from 3-mercaptopyruvate.[1] It may also be produced by the reaction of H_2S with NO.[1] H_2S_n regulates many important biological functions. Recent studies suggest that many biological activities associated H_2S were driven by H_2S_n. One such function is Protein sulfuration, wherein a sulphur atom is added to the thiol group of cysteine in proteins causing the modification in protein conformation, and their activity.[2] H_2S_n induces Ca^{2+} influx in astrocytes more efficiently than H_2S by activating the transient receptor potential (TRP) A1 channels.[3,4] H_2S_n is a potent signaling molecule that regulates the activity of tumor suppressors, transcription factors.[3] These reports suggest that the active species in signaling is H_2S_n rather than H_2S.

So, to better understand the regulatory role of H_2S_n, there is an urgent need to develop some tools for the sensitive detection and tracking of this species in biosystems. Traditional spectroscopic method to detect H_2S_n is measuring the absorbance at 290-300 nm and 370 nm.[7] However, this method is not sensitive. Some mass spectrometric method by derivatization of the samples with monobromobimane is available, but these derivatives are unstable leading to the error in measurement.[3] Moreover, these methods are not suitable for biological studies suggesting the need of fluorescent probes. Fluorescence-based detection method could be the better alternative because of the sensitivity and its utility in biological imaging.[5,6] Even though many fluorescent probes were developed for other biothiols such as Cysteine, glutathione, and H_2S in recent years[8-13], but probes for the polysulfides are rather scanty because of the limited understanding of its chemistry and reactivity. Development of fluorescent probes for H_2S_n is rapidly growing, and it is an attractive area of research. Currently, there are mainly three types of probes available for H_2S_n sensing. Most of the polysulfide probes rely on the aromatic nucleophilic substitution reactions of polysulfides with 2-fluoro-5-nitro benzoate recognition moiety followed by spontaneous cyclization to release the fluorophore.[14-23] However, these probes can also undergo nucleophilic substitution in the presence of biothiols, which results in probe consumption and hence, a large amount of probe loading is required. Another type of probe based on specific aziridine ring opening by H_2S_n was reported.[24] Aziridine based probes showed good selectivity to H_2S_n. However, their utility is limited to solution studies only. These limitations were resolved by the pioneering work from Prof. Xian's group wherein they developed 2-(benzoylthio)

benzoate functionalized probes by taking advantage of dual reactivity of H_2S_n. Nevertheless, such reports are only a few in the literature.[25-29] So, an ideal probe should show high specificity to H_2S_n and it should be capable of detecting H_2S_n inside the living cells, precisely, at sub-cellular organelles.

Fluorescence microscopy is an invaluable tool to image as well as to study the functions of specific analytes in living systems.[5,6] Unfortunately, their applicability is hindered by the spatial resolution.[30] Recently, this problem was resolved by the discovery of super-resolution microscopy techniques that breaks the diffraction limit and provides resolution up to 20 nm. Among the super-resolution techniques, STED and STORM provide very high resolution, but these techniques demand exceptionally photostable dyes, longer acquisition times and intense laser irradiations of 10^3 to 10^8 W/cm^2.[31] One exception is Structured Illumination Microscopy (SIM) wherein, resolution of 100 - 120 nm could be achieved.[30,31] Even though this technique gives moderate resolution, nevertheless it offers high-speed data acquisition with low illumination intensities when compared to STORM and STED.[32,33]

By considering these facts, we have developed a BODIPY based probe **MB-S_n**, capable of specific detection H_2S_n in an aqueous solution as well as inside the living cells. Moreover, this non-toxic, cell-permeable probe is capable of detecting H_2S_n in the endoplasmic reticulum of cells, and it is compatible with super-resolution Structured Illumination Microscopy (SIM), which resulted in high-resolution images.

4.2. Experimental Section

4.2.1. Materials

Benzoyl Chloride, 2,4-Dimethylpyrrole, 4-Hydroxybenzaldehyde, Boron trifluoride diethyl etherate, Triethylamine, Piperidine, Glacial acetic acid, Thiosalicylic acid, *N,N'*-Dicyclohexylcarbodiimide (DCC), 4-Dimethylaminopyridine (DMAP), K_2HPO_4, Cetyltrimethylammonium bromide (CTAB) were obtained from Sigma Aldrich and were used as received. Na_2S_2 was purchased from Dojindo molecular technologies Inc. Japan. Solvents used for the synthesis of various intermediates and final compounds were of AR grade (S.D. Fine Chemicals) and were used as received without further purification unless mentioned otherwise. HPLC grade (S.D. Fine Chemicals) solvents were used for various spectroscopic studies.

4.2.2. Analytical Methods

^{1}H and ^{13}C NMR spectra were recorded on Bruker 400/500 MHz FT NMR (Model: Advance-DPX 400/500) using TMS as an internal standard. High-resolution mass spectra were recorded on JEOL JM AX 505 HA mass spectrometer. UV-Vis spectra were recorded using Shimadzu UV-1800 spectrometer. Fluorescence measurements were carried out on quanta master-400 fluorescence spectrometer. [2] All the Structured Illumination Microscopy (SIM) and wide-field Fluorescence Microscopy experiments were performed by using Delta Vision OMX-SIM (GE Healthcare). The Post-processing SIM reconstructions were performed by using Soft Worx software. Images were analyzed and processed using ImageJ software.

4.2.3. General Methodology Adopted for Spectroscopic Studies

A stock solution of **MB-S_n** (5×10^{-3}M) was prepared in HPLC grade acetonitrile, and the same solution was used for all the studies after appropriate dilution with 20 mM Phosphate buffer solution (pH 7.4). For spectroscopic measurements, a stock solution of the probe was diluted by using phosphate buffer:CH_3CN (9:1 v/v) mixture and the effective final concentration of the probe was made as 10 µM. CTAB (5 mM) was prepared in ethanol and 50 µM of CTAB was used for all the studies. After a thorough screening of the different solvent/buffer combinations, we found that 10 µM of **MB-S_n** in Phosphate buffer: CH_3CN (9:1 v/v) and 50 µM of CTAB provided the best results. Hence, this combination was used for all the spectral measurements. Emission measurements were done using λ_{Ext}= 530 nm with the emission slit widths of 4/4 nm.

All the ROS, RNS used in the study was freshly prepared. Hydroxyl radicals were generated *in-situ* by the Fenton reaction of $FeSO_4$ with H_2O_2. $^{1}O_2$ was generated by the reaction of NaOCl with H_2O_2. Superoxide was prepared by adding 1mg of KO_2 to 1ml of dry DMSO followed by vigorous stirring. Na_2S_2 stock solution (5 mM) was prepared in phosphate buffer. Na_2S_2 is highly unstable and readily decomposes in the buffer, so solutions were freshly prepared as and when required and used immediately. CTAB is necessary to ensure the stability of Na_2S_2. Hence, 50 µM of CTAB was used for the spectroscopic measurements.[24]

4.2.4. Structured Illumination Microscopy Experiments with MB-S_n probe

Structured Illumination diffracts the beam into three parallel beams, and they are combined by the objective to produce 3D interference fringe patterns in the sample.

Multiple images are obtained by adjusting the fringe pattern and by slicing through the sample with respect to different focal planes generating a series of images of the sample and this image volume is known as Z-stack. Each frame of the Z-stack is reconstructed so that it could provide definitive information of the details of the sample which we are imaging thereby improving the resolution close to two-fold, which is not achieved by using conventional light microscopy.

4.2.5. Sample preparation (SIM and Wide-field Microscopy)

RAW 264.7 cells were seeded on cover slips (22 mm X 22 mm, 170 ± 5 µm square Cover glasses) placed in six-well plates in DMEM culture medium containing (10% FBS and 1% Penicillin-Streptomycin) for 24 hours at 37°C, 4% CO_2. After 24 hours when 70% confluency was achieved the cells were washed with DMEM culture medium then cells were treated with **MB-S_n** (10 µM) for 25 minutes. Cells were then washed thrice with culture medium and further treated with different Na_2S_2 for 20 minutes. After that cells were washed again with Phosphate Buffer Saline (2X PBS). After carrying out the Live cell uptake of the **MB-S_n** probe and Na_2S_2, the cells were fixed with 4% PFA for 15 minutes and then washed thrice with PBS and then the coverslips were mounted using the mounting medium (Vectashield h-1000).The coverslips were then sealed using nail varnish, and the sample was then imaged by Structured Illumination Microscopy and also wide-field Fluorescence Microscopy. For the endogenous detection, cells were pre-treated with various concentrations of (0-2500 nano grams/ml) Lipopolysccharides (16 hours). (LPS is known to stimulate H_2S_n production in cells through CSE pathway). Cells were washed and further treated with **MB-S_n** (10 µM) for 25 minutes. And images were captured by following the same procedure mentioned above.

4.2.6. Instrument Specification

The Delta Vision OMX system is a Microscope which surpasses normal microscopy resolution limits. It allows to image beyond the surface of the coverslips by using multiple probes to retrieve exhaustive biological information from all directions. This Instrument's Structured Illumination Microscopy technology enables to image deeply the biology and resolves features which are literally close to invisible through traditional light microscopy. Delta Vision OMX is a flexible microscope and it works well with all kinds of probes including conventional fluorophores to artificially engineered fluorochromes.

4.2.7. Data Processing

Structured Illumination Microscopy (SIM) carried out by us using the Delta Vision OMX is a wide-field Microscopy technique based on Moire's effect. The Resolution improvement is achieved based on the Reconstruction of the acquired image by using the inbuilt software namely Soft Worx. The Z stacks acquired during the Imaging are post-processed by using the reconstruction option of Soft Worx. SIM acquisition is dependent mainly on the imaging parameters and acquisition parameters, and this varies depending on the sample and in particular on the nature of the probe. The **MB-S_n** probe was Excited at 568 nm, and the emission was collected at 586 nm (Alexa Flour 568 Channel of the Delta Vision OMX). In the case of **MB-S_n** probe, the Structured Illumination experimental conditions for single colour experiments were mainly dependent on the thickness of the Z stack (sections 80 to 100), section spacing (0.125 to 0.150), and thickness of the sample (8 to 10). As **MB-S_n** probe is a very bright probe, for the SIM acquisition, we needed to vary the %T and exposure time. Therefore in all our Single colour experiments exposure time was between 3 to 10, and the %T was in the range of 10 to 50. The Colocalization experiments were performed with ER-Tracker Green. The Dual colour experiments were performed with Hoechst. In both of these experiments the SIM conditions of these Co-staining agents were maintained in accordance with the **MB-S_n** probe which would be discussed in the later sections.

4.2.8. 3D SIM Projection

The off line processing of Structured Illumination Microscopy (SIM) images was carried out by using ImageJ software. The option Stacks (3D project) was employed in obtaining a 3D projection of the Structured Illumination Microscopy images obtained by using the Delta Vision OMX-SIM Microscope.

4.2.9. Colocalization Experiments with ER Tracker Green

The Co-staining experiments with ER Tracker Green was carried out by Incubating the ER Tracker Green (1 μM) further for 30 minutes after incubating the RAW cells with **MB-S_n** (10 μM) for 25 minutes probe (10 μM) initially for 25 minutes and Na_2S_2 (12.5 μM) for a further 20 minutes. The Cells were washed regularly three times with DMEM culture media and PBS. The Cellular uptake of both the probes are carried out in live cells and then the cells were fixed with 4% PFA and mounted and navigated initially for proper cell morphology by using Light Microscope and then imaged by using Structured Illumination Microscopy (SIM) and wide-field Microscopy (WF).The **MB-S_n** (10 μM) for 25 minutes

probe was excited at 568 nm, and the emission was collected in the Alexa Fluor Channel (570 nm to 620 nm) and the ER-Tracker Green was excited at 488 nm, and the Emission was collected in the FITC Channel (500 nm to 550 nm). The SIM imaging conditions maintained are, For **MB-S_n** probe: Thickness of the Z stack (sections 50 to 100), section spacing (0.125 to 0.150), Thickness of the sample (8 to 11), Exposure time was between 3 to 30, and the %T was in the range of 10 to 50. For ER Tracker Green: Thickness of the Z stack (sections 50 to100), section spacing (0.125 to 0.150), thickness of the sample (8 to 11), exposure time was between 10 to 50, and the %T was in the range of 10 to 50. The WF imaging conditions maintained are, For **MB-S_n** probe: Thickness of the Z stack (Sections 40 to 80), Section spacing (0.250 to 0.500), thickness of the sample (8 to 11), exposure time was between 1 to 30and the %T was in the range of 2 to 30. For ER Tracker Green: thickness of the Z stack (sections 40 to 80), section spacing (0.250 to 0.500), thickness of the sample (8 to 11), exposure time was between 10 to 50 and the %T was in the range of 2 to 30.

4.2.10. Dual Colour SIM and wide-field Microscopy Experiments

The Dual colour experiments with Hoechst as the nuclear stain was carried out by Incubating the Hoechst (500 nM) for 30 minutes after incubating the RAW cells with **MB-S_n** (10 μM) for 25 minutes. The cells were washed regularly three times with DMEM culture media and PBS. The cellular uptake of both the probes are carried out in live cells, and then the cells were fixed with 4% PFA and mounted and navigated initially for proper cell morphology by using a light microscope and then imaged by using Structured Illumination Microscopy (SIM) and wide-field Microscopy (WF). Hoechst was excited at 405 nm, and the emission was collected in the DAPI channel (420 nm to 500 nm). The SIM imaging conditions maintained are, For **MB-S_n** probe: Thickness of the Z stack (Sections 40 to 80), Section spacing (0.125 to 0.150), Thickness of the sample (5 to 8), Exposure time was between 10 to 50, and the %T was in the range of 10 to 50. The SIM imaging conditions maintained are, For Hoechst: Thickness of the Z stack (Sections 40 to 80), Section spacing (0.125 to 0.150), thickness of the sample (5 to 8), exposure time was between 50 to 100 and the %T was in the range of 10 to 50. The WF imaging conditions maintained are, For SF-1 probe: thickness of the Z stack (Sections 20 to 50), section spacing (0.250 to 0.500), thickness of the sample (5 to 9), exposure time was between 10 to 50 and the %T was in the range of 2 to 30. The WF imaging conditions maintained are, For Hoechst: Thickness of the Z stack (Sections 20 to 50), Section spacing (0.250 to 0.500), thickness of the sample (5 to 9), Exposure time was between 10 to 50 and the %T was in the range of 2 to 30.

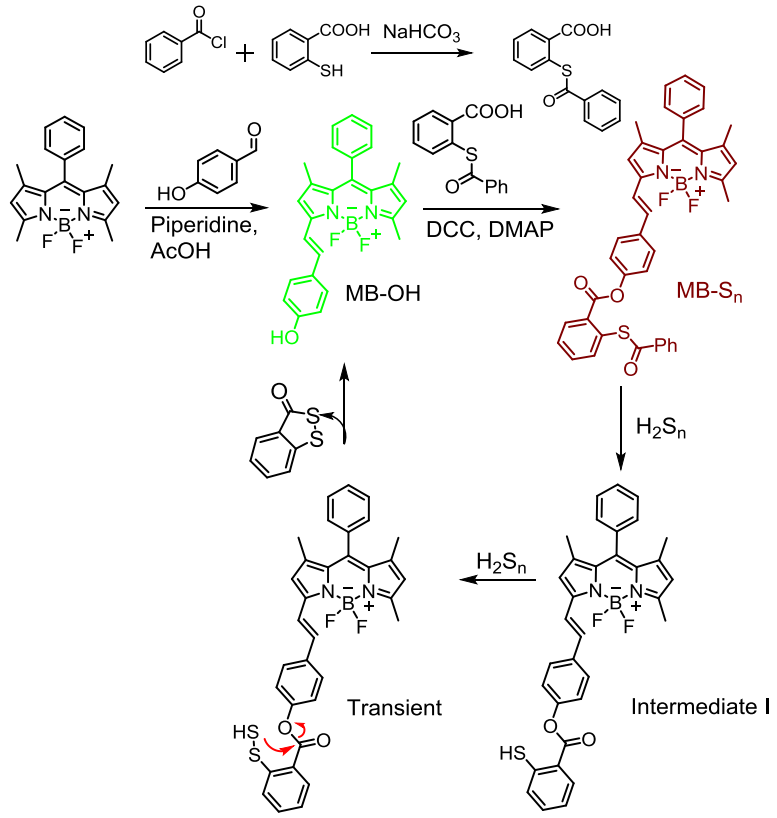

Scheme 4.1. Synthetic route adopted for **MB-S$_n$** and its reaction with H_2S_n

4.3. Synthesis and Characterization

4.3.1. Synthesis 2-(benzoylthio)benzoic acid

Thiosalicylic acid (1.5 g, 9.72 mmol) was dissolved in 25 ml of sodium bicarbonate (3 g, 35.71 mmol). The mixture was cooled to 0^{o}C and benzoyl chloride (1.15 ml, 9.72 mmol) and solid sodium carbonate (1.5 g, 14.15 mmol) was added. Reaction mass was stirred at 0^o C for 30 minutes and then allowed to warm to room temperature. Reaction was stirred at room temperature for 1 hour. It was acidified with conc. HCl, which resulted in pure white precipitate. It was filtered and washed with water to afford 2-(benzoylthio)benzoic acid as white solid 72% Yield. ^{1}H NMR (DMSO-d_6, 500 MHz): δ (ppm) 7.95 (2H, d, J = 7.63 Hz), 7.91 (1H, d, J = 7.25 Hz), 7.73-7.70 (1H, t) , 7.63-7.57 (5H, m). ^{13}C NMR (DMSO-d_6, 125 MHz): δ (ppm) 189.33, 167.94, 137.48, 136.54, 136.38, 134.74, 132.28, 130.88, 130.42, 129.75, 127.54, 126.86. HRMS (ESI): m/z calculated for $C_{14}H_{11}O_3S$ [M+H] 259.0423 found 259.0419.

4.3.2. Synthesis of MB-S_n

Bodipy core and MB-OH were prepared by following our previous reports.[10,34] 2-(benzoylthio)benzoic acid (150 mg, 0.58 mmol) was dissolved in 20 ml of dry CH_2Cl_2 . It was cooled to 0^{o}C and *N,N'*-Dicyclohexylcarbodiimide (DCC) (121 mg, 0.58 mmol) was added. It was stirred at the sam temperature for 1 hour. Then BODIPY-OH (200 mg) and catalytic amount of 4-Dimethylaminopyridine (DMAP) was added. Reaction mass was allowed to warm to room temperature and stirred overnight. Reaction mass was filtered in order to remove the urea impurity and subsequently concentrated under reduced pressure. Crude was purified by silica gel flash column chromatography using EtOAc and hexane. Compound was eluted at 13% EtOAc. Off-pink solid yield 18%. ^{1}H NMR ($CDCl_3$, 400 MHz): δ (ppm) 1.41 (3H, s), 1.45 (3H, s), 2.62 (3H, s), 6.03 (1H, s), 6.63 (1H, s), 7.23 (2H, d, *J* = 6.71 Hz), 7.32 (3H, d, *J* = 7.32 Hz), 7.37-7.41 (1H, m), 7.50-7.56 (6H, m), 7.66-7.71 (5H, m), 8.22-8.24 (3H, m). ^{13}C NMR ($CDCl_3$, 100 MHz): δ (ppm) 14.42, 14.57, 29.72, 117.51, 119.38, 121.55, 122.00, 127.60, 127.90, 128.14, 128.46, 128.83, 129.01, 129.15, 129.64, 133.84, 134.46, 137.23, 142.35, 152.23, 155.87, 164.60, 189.36. HRMS (ESI): m/z calculated for $C_{40}H_{31}N_2O_3BF_2S$ [M+Na] 691.2009 found 691.2003.

4.3.3. Reaction of MB-S_n with Na_2S_2

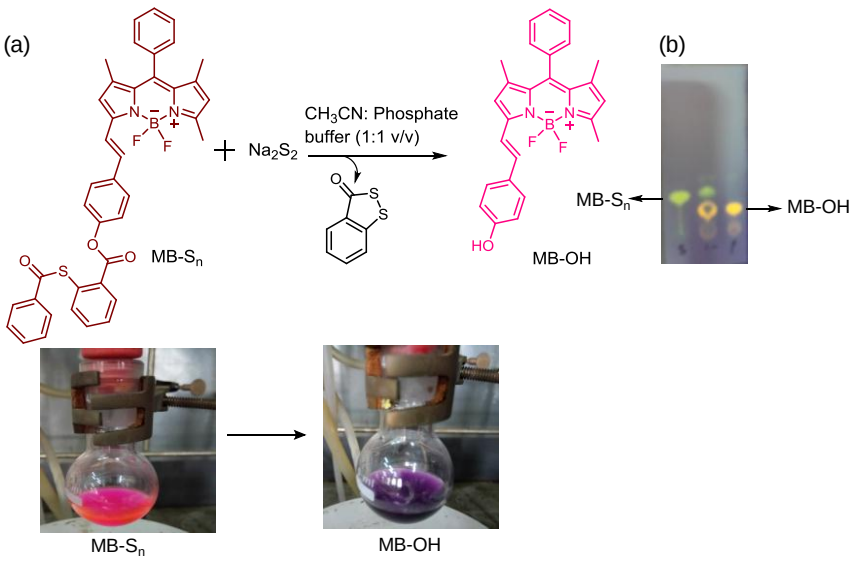

Scheme 4.2. (a) Reaction of **MB-S_n** with Na_2S_2. (b) Thin layer chromatography analysis under hand held 365 nm UV-lamp showing the formation of **MB-OH**. (c) Corresponding colour change in the reaction mass observed after the addition of Na_2S_2.

MB-S_n (0.015 mmol) was dissolved in 2 ml CH_3CN and 2 ml of Phosphate buffer (pH 7.4) containing 200 µM of CTAB. To this Na_2S_2 (0.15 mmol) was added. Immediate change in the colour from pale pink to purple was observed. Reaction mass was further stirred for

30 minutes, and it was monitored by TLC. The reaction mass was diluted with EtOAc organic layer was separated and dried over Na_2SO_4 and concentrated. It was purified by preparatory chromatography method. ^{1}H NMR ($CDCl_3$, 400 MHz): δ (ppm) 1.39 (3H, s), 1.42 (3H, s), 2.60 (3H, s), 6.00 (1H, s), 6.58 (1H, s), 6.81 (2H, d, *J* = 8.51 Hz), 7.22 (1H, d, *J* = 16.52 Hz), 7.31 (2H, m), 7.33-7.52 (6H, m). HRMS (ESI): m/z calculated for $C_{26}H_{24}N_2OBF_2$ [M+H] 429.1944 found 429.1945.

4.4. Results and Discussion

We have chosen borondipyromethane (Popularly known as BODIPY), as a fluorescent reporter because of its excellent photophysical properties such as high brightness, tunable emission, excellent photostability, narrow emission bandwidth and high quantum yield etc.[10,34,35]

We have designed our probe by taking advantage of the dual-reactivity of H_2Sn. Our probe design involves a BODIPY signaling unit functionalized with benzothioester polysulfide recognition site. Polysulfide trigger group was synthesized by the reaction of thiosalicylic acid with benzoyl chloride (scheme 4.1). The absorption and emission of the BODIPY core were extended to the red region by Knoevenagel type condensation of the acidic methyl group of the BODIPY core with electron-rich para-hydroxybenzaldehyde (Scheme 4.1). Condensation product, **MB-OH** was further functionalized with thiobenzoate trigger group by following the DCC coupling, which gave the final probe **MB-S_n**. All the products were characterized by standard analytical techniques.

From our previous studies, we understand that modulation of the hydroxyl group of the staryl BODIPYs results in the complete quenching of the fluorescence through photoinduced electron transfer.[10,34] So, **MB-S_n** is expected to be non-fluorescent. We anticipate that the reaction of H_2S_n with thioester trigger, followed by spontaneous cyclization releases free hydroxyl fluorophore (**MB-OH**) with desired fluorescence turn ON response. With the probe in hand, first we checked the absorption and emission response of **MB-S_n** in 20 mM phosphate buffer medium, pH 7.4 (9:1 Phosphate buffer: CH_3CN) containing 100 µM CTAB. Absorption spectra of **MB-S_n** showed an absorption band in the red region with an absorption maximum around 570 nm.

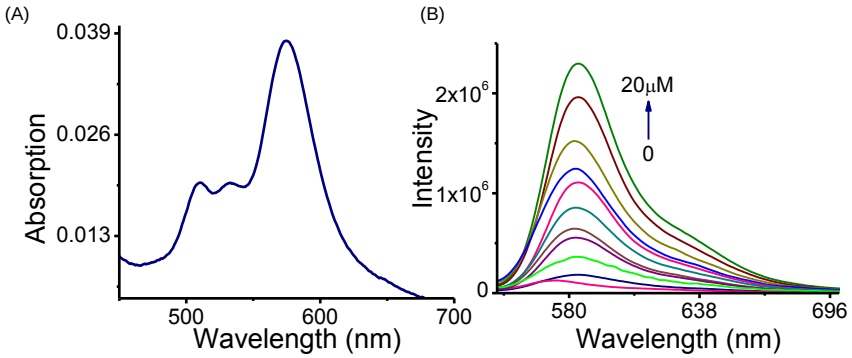

Figure 4.1. (A) Absorption spectra of **MB-S_n** (10 μM) in phosphate buffer (20 mM): CH_3CN (9:1 v/v), at pH7.4 containing 50 μM of CTAB. (B) Emission response of **MB-S_n** (10 μM) in the presence of varying concentration of Na_2S_2 (0-20 μM).

As anticipated, the probe was poorly emissive (Φ_f=0.007). Upon addition of Na_2S_2 (H_2Sn donor), a remarkable increase in the fluorescence (Figure 4.1B) was observed indicating the release of the free probe, **MB-OH**. A 22 fold increase in the fluorescence intensity was observed upon increasing the concentration of Na_2S_2 (0-20 μM, Figure 4.1B) and a significant elevation in the quantum yield (Φ_f=0.125) was also observed. Moreover, the emission intensity of **MB-S_n** reached the maximum level within 10 minutes signifying the fast response of the probe to H_2S_n (Figure 4.2A). Fluorescence intensity of **MB-S_n** at 584 nm was increased linearly with increase in the concentration of Na_2S_2 (0-10 μM). The detection limit of the probe was determined by 3 σ method and it was found to be 26.01 nM (Figure 4.2B) suggesting the high sensitivity of **MB-S_n** to H_2S_n.

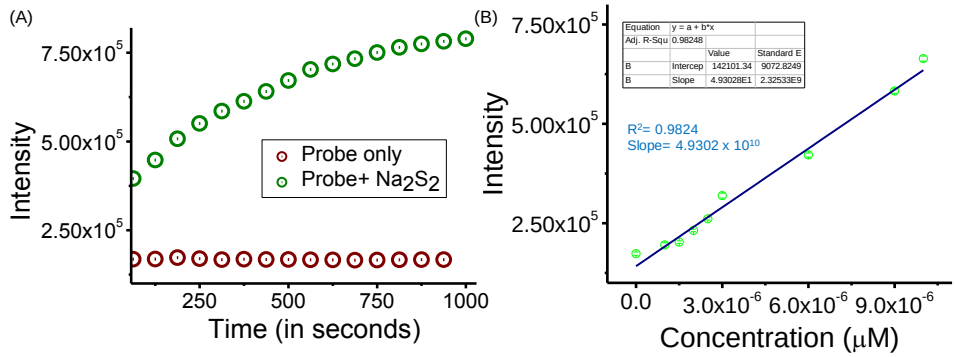

Figure 4.2. (A) Time-dependent emission response of **MB-S_n** (10 μM) in the absence or presence of Na_2S_2 (10 μM). (B) Intensity v/s concentration plot. Experimental condition: 20 mM phosphate buffer: CH_3CN (9:1 v/v), at pH7.4 containing 50 μM of CTAB. λ_{Ext} = 530 nm. Emission was monitored at 584 nm.

The detection limit was calculated based on the fluorescence titration. The standard deviation of the blank was determined by measuring the emission spectra of **MB-S_n** 7 times without the addition of Na_2S_2.

The detection limit (DL) of **MB-S_n** was determined from the following equation:

DL = K * Sb1/S.....Equation 4.1

Where K = 2 or 3 (we took 3 in this case);

Sb1 is the standard deviation of the blank;

S is the slope of the calibration curve.

From the graph, we get slope = 4.93028 x 10^{10}, and Sb1 value was found to be 427.5843.

Thus, using the above formula, we get the Detection Limit = 23.65x 10^{-9} M.

Turn ON emission response was due to the cleavage of thioester group by the nucleophilic attack from H_2S_n and the resulting thiolate again reacts with H_2S_n, followed by spontaneous cyclization releases benzodithiolone and free fluorophore **MB-OH** (Scheme 4.1). To provide the evidence for the proposed mechanism, we have carried out a separate reaction between **MB-S_n** and Na_2S_2 in acetonitrile: phosphate buffer medium (Scheme 4.2). Upon addition of Na_2S_2, a prominent change in colour from pale pink to purple was observed (See Scheme 4.2). The reaction was monitored by TLC, and the product was isolated and characterized by ^{1}H NMR and HRMS. Both the data suggest the formation of **MB-OH** and thus, supports the proposed mechanism.

Selectivity is a key criterion to assess the efficacy of any fluorescent probe. To evaluate the selectivity of the probe, we have compared the emission response of **MB-S_n** to H_2S_n over various reactive oxygen species (ROS) such as, $^{\cdot}OH$, H_2O_2, $^1O_2$, O_2^- , HOCl, anions such as NO_2^-, NO_3^- , SO_4^{2-}, SO_3^-, $S_2O_3^-$ and biothiols like H_2S, cysteine, Glutathione.The probe showed excellent selectivity to H_2Sn whereas the other analytes failed to induce any significant change in the fluorescence (Figure 4.3A). It has been known from the literature that H_2Sn could be generated in situ from the reaction of H_2S with ROS.[3,36] To verify this fact, we have mixed the aqueous solution of H_2S (100 µM) with different ROS and then recorded the emission spectra with **MB-S_n**. Among the various ROS, only HOCl with H_2S showed significant enhancement in the fluorescence indicating that H_2S_n may be generated in situ by the reaction of hypochlorite with H_2S (Figure. 4.3A). So, our probe is

also capable of detecting the H_2S_n generated in situ. Effect of pH was also examined and the results suggest that **MB-S$_n$** works well under physiological conditions (Figure. 4.3B).

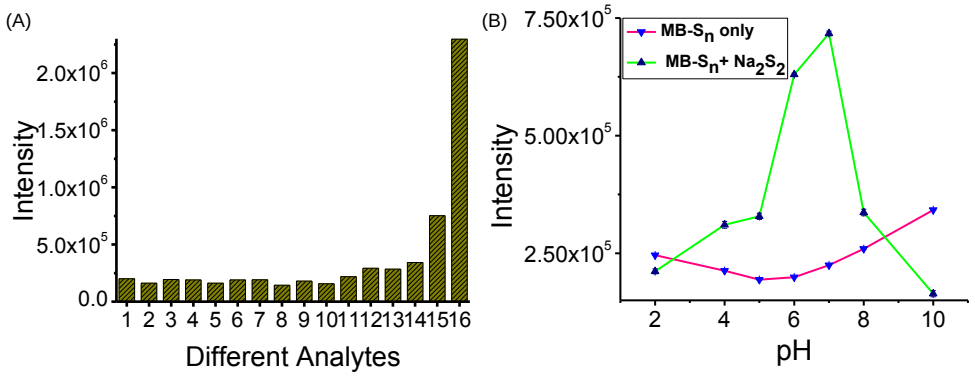

Figure 4.3. (A) Emission response of **MB-S$_n$** (10 µM) in the presence of various analytes (1) **MB-S$_n$** only, (2) H_2O_2 (200 µM), (3) HOCl (50 µM), (4) $^{\cdot}OH$ (50 µM), (5) $^1O_2$ (50 µM), (6) O_2^- (50 µM), (7) NO_2^- (50 µM), (8) NO_3^- (50 µM), (9) Cys, (100 µM), (10) GSH, (100 µM), (11) Na_2S, (100 µM), (12) $^{\cdot}OH$ + Na_2S (50 µM + 100 µM), (13) $^1O_2$ + Na_2S (50 µM + 100 µM), (14) H_2O_2 + Na_2S (200 µM + 100 µM), (15) HOCl + Na_2S (50 µM + 100 µM), (16) Na_2S_2 (20 µM). (B) Emission response of **MB-S$_n$** (10 µM) at different pH in the absence or presence of Na_2S_2 (10 µM). λ_{Ext} = 530 nm.

Since thioester groups are known to react with the biothiols, this may lead to large probe consumption as the biothiols like Cysteine and Glutathione present in a millimolar concentration in the biological system. So, selectivity studies at higher concentrations of biothiols are essential. If the biothiols react with the thioester group of **MB-S$_n$**, the product should further react with elemental sulphur (S_8) which in turn should result in the fluorescence ON response. To validate this fact, we have evaluated the emission response of **MB-S$_n$** (10 µM) with higher concentrations of Cysteine and GSH (1 mM each) in the presence or absence of S_8 (50 µM). To our delight, negligible change in the emission was observed (Figure 4.4A) suggesting the remarkable selectivity of the probe towards H_2S_n in the presence of competing biothiols.

These results suggested that **MB-S$_n$** has exceptional selectivity and sensitivity to H_2Sn with the desired turn ON fluorescence response. These results encouraged us to test its efficacy in monitoring and imaging H_2S_n in living cells. Initially, we have evaluated the cytotoxicity of **MB-S$_n$** towards RAW 264.7 macrophages using conventional MTT assay. MTT result showed negligible toxicity even at higher doses (Figure 4.4 B).

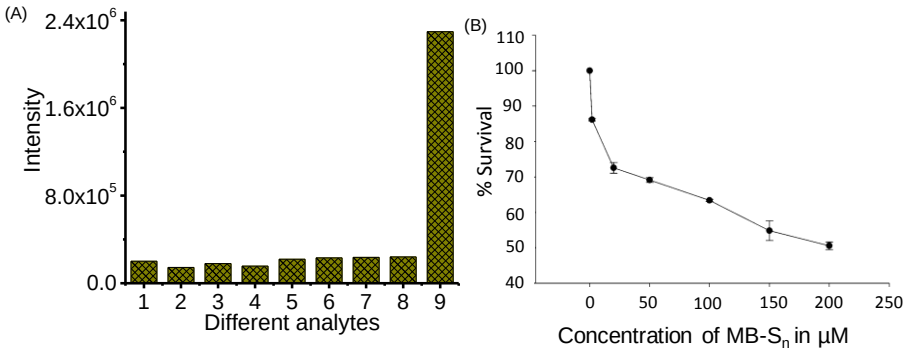

Figure 4.4. (A) Emission response of **MB-S_n** (10 µM) in the presence of biothiols and S_8. (From 1-9 **MB-S_n** only; Cys; Homocysteine, GSH, H_2S; S_8; Cys+ S_8; GSH+ S_8; **MB-S_n**+ Na_2S_2. (B) MTT assay to determine cytotoxicity of **MB-S_n.**

Next, we have carried out wide-field fluorescence microscopy experiment to check the efficacy of **MB-S_n** to visualize exogenous H_2S_n in RAW 264.7 macrophages. Cells were first incubated with **MB-S_n** (10 µM) for 25 minutes. No significant fluorescence was observed from the cells. Further, cells were incubated with different concentrations of Na_2S_2 (2.5, 5, 12.5 µM respectively). Bright fluorescence was observed from the cells indicating the cell permeability and capability of **MB-S_n** to detect H_2S_n inside the living cells (Figure 4.5).

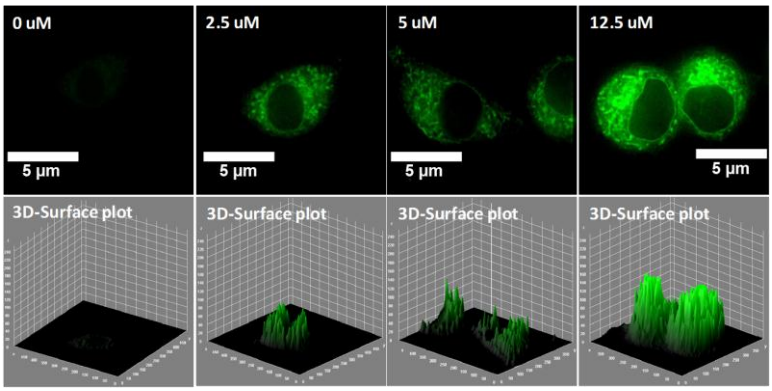

Figure 4.5. Wide-field fluorescence microscopy images of RAW 264.7 macrophages incubated with **MB-S_n** (10 µM) and various concentration of Na_2S_2. Bottom row indicates the corresponding 3D intensity profile plots.

This result motivated us to explore the possibility of using **MB-S_n** in super-resolution imaging, particularly, structured Illumination Microscopy (SIM). SIM experiment with **MB-S_n** in Na_2S_2 treated cells produced striking images (Figure 4.6). Interestingly, the emission intensity from the cells was increased with respect to H_2S_n concentration signifying the capability of **MB-S_n** to monitor the change in H_2S_n levels inside the cells (Figure 4.6). These studies suggested that **MB-S_n** has a great potential to be used as a probe in super-resolution microscopy. Moreover,

MB-S_n was stable enough to withstand the prolonged laser irradiation needed for SIM**.** In addition to this, we have also checked the time dependent response of **MB-S_n** in cells.

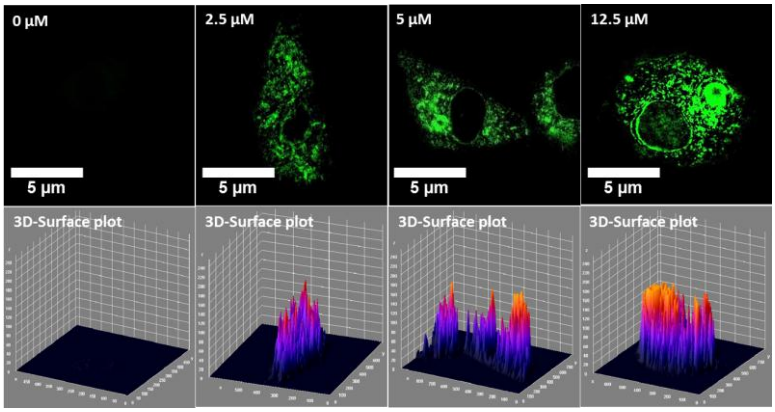

Figure 4.6. SIM images of exogenous H_2S_n in RAW 264.7 macrophages. Cells were incubated with **MB-S_n** (10 µM) for 25 minutes and then incubated with different Na_2S_2 for 20 minutes. Bottom row-corresponding 3D profile plots.

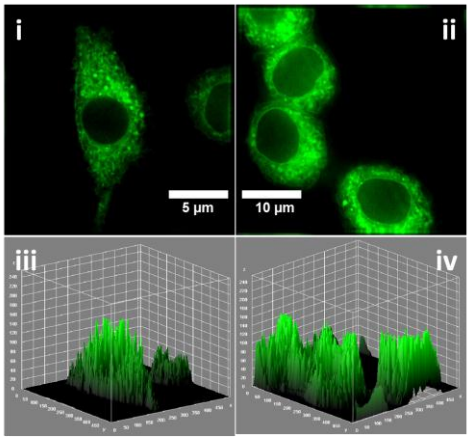

Figure 4.7. Wide-field images of RAW 264.7 macrophages with **MB-S_n** (10 µM) recorded after the addition of 20 µM Na_2S_2 (i) 2 minutes and (ii) 20 minutes. (iii & iv) corresponding 3D profile plots.

Bright fluorescence from the cells were observed within 2 minutes after the addition of Na_2S_2 indicating the quick response of the probe (Figure 4.7).

Inspired by these results, we wondered whether **MB-S_n** could be used for imaging endogenous H_2S_n in cells. Literature reports suggest over-expression of Cystathionine γ-lyase (CSE) in cells leads to the significant elevation in the polysulfide level.[4] So, we have stimulated the cells with Lipopolysaccharides (LPS) to induce the over-expression of CSE. Living cells were supplied with different concentration of LPS (0-2500 nanograms/ml) and maintained for 16 hours in DMEM culture medium with 10% FBS and then further treated with **MB-S_n** (10 µM)

for 25 minutes. SIM imaging showed bright fluorescence from the cells confirming the generation of polysulfides and efficacy of **MB-S_n** to detect endogenous H_2S_n (Figure 4.8).

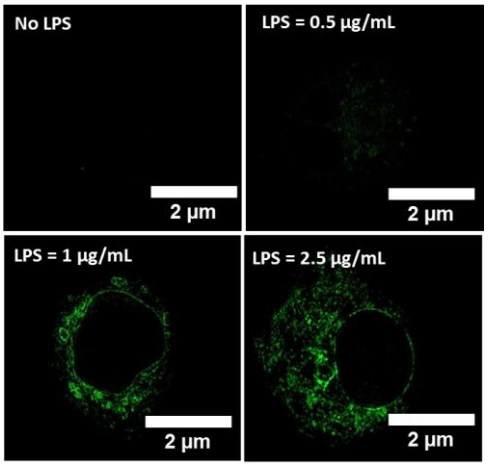

Figure 4.8. Endogenous H_2S_n detection by SIM. RAW 264.7 cells were treated with different concentration of LPS for 16 hours followed by incubation with **MB-S_n** (10 µM) for 25 minutes.

By looking at the images, it suggests that **MB-S_n** is not localizing in the nucleus. To determine the exact location, we have further carried out the co-localization experiment with ER-tracker. A Pearson's correlation coefficient (PCC) of 0.944 confirmed the precise localization of **MB-S_n** in Endoplasmic reticulum of the cells. We have further utilized **MB-S_n** for 3D-SIM imaging (Figure 4.9).

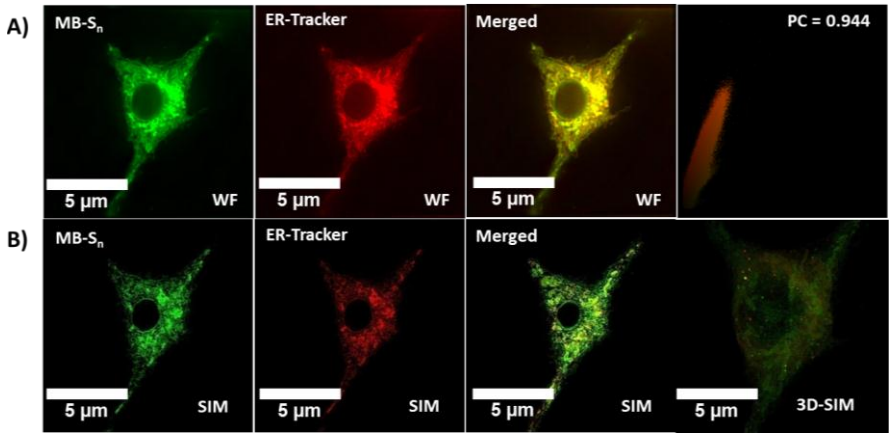

Figure 4.9. Colocalization experiments (Cells were pre-treated with LPS, 2500 ng/mL before **MB-S_n** and ER-Tracker incubation): (A) Wide-field images of **MB-S_n**, ER-tracker green, merged image and Pearson's profile plot indicating maximum colocalization (0.944), confirming the preferential colocalization in the Endoplasmic reticulum. (B) Corresponding SIM images of **MB-S_n**, ER-tracker green, merged image and 3D-SIM image.

Multicolour imaging is a powerful tool to simultaneously monitor the various cellular processes in different cell organelles. We wondered whether our ER-specific probe **MB-S_n** is useful for dual colour imaging. To realize this, we have performed SIM

imaging (Figure 4.10) with a nuclear staining dye Hoechst in LPS treated cells. The clear-cut images suggest the usefulness of the probe in dual-color imaging.

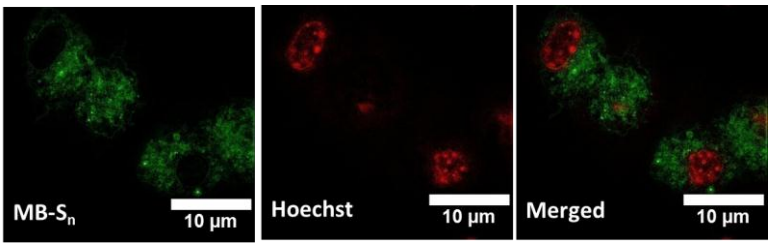

Figure 4.10. Dual colour SIM using **MB-S_n** in the presence of LPS and Hoechst.

4.5. Conclusion

We have designed and synthesized a BODIPY based probe **MB-S_n** capable of specific detection of H_2S_n in the aqueous solution as well inside the living cells. H_2Sn mediated thioester cleavage followed by spontaneous cyclization released free fluorophore with turn ON emission response. The probe showed excellent selectivity to H_2S_n over other competing analytes. Non-toxic nature and cell membrane permeability allowed us to utilize it for imaging both exogenous and endogenous H_2S_n in living cells. Co-localization studies with ER tracker confirmed the precise localization of the probe in ER. Furthermore, we have demonstrated the utility of the probe in super-resolution Structured Illumination Microscopy. In addition to this, we have demonstrated the applicability of the probe in dual colour imaging as well as 3D-SIM imaging. We believe this will open up a new window to develop SIM compatible probes for other analytes as well.

4.6. References

1. H. Kimura, *Proc. Jpn. Acad., Ser. B*, 2015, **91**, 131.

2. A. K. Mustafa, M. M. Gadalla, N. Sen, S. Kim, W. Mu, S. K. Gazi, R. K. Barrow, G. Yang, R. Wang and S. H. Snyder, *Sci. Signal.*, 2009, **2**, ra72.

3. Y. Kimura, Y. Mikami, K. Osumi, M. Tsugane, J.-i. Oka and H. Kimura, *FASEB J.,* 2013, **27**, 2451.

4. T. Ida, T. Sawa, H. Ihara, Y. Tsuchiya, Y. Watanabe, Y. Kumagai, M. Suematsu, H. Motohashi, S. Fujii, T. Matsunaga, M. Yamamoto, K. Ono, N. O. Devarie-Baez, M. Xian, J. M. Fukuto and T. Akaike, *Proc. Natl. Acad. Sci. U.S.A*, 2014, **111**, 7606.

5. A. S. Klymchenko, *Acc. Chem. Res*., 2017, **50**, 366.

6. D. Wu, A. C. Sedgwick, T. Gunnlaugsson, E. U. Akkaya, J. Yoon and T. D. James, *Chem. Soc. Rev.,* 2017, **46**, 7105.

7. R. Greiner, Z. Pálinkás, K. Bäsell, D. Becher, H. Antelmann, P. Nagy and T. P. Dick, *Antioxid. Redox Signal.,* 2013, **19**, 1749.

8. V. S. Lin, W. Chen, M. Xian and C. J. Chang, *Chem. Soc. Rev.,* 2015, **44,** 4596.

9. L.-Y. Niu, Y.-Z. Chen, H.-R. Zheng, L.-Z. Wu, C.-H. Tung and Q.-Z. Yang, *Chem. Soc. Rev.,* 2015, **44**, 6143.

10. F. Ali, A. H. A, N. Taye, R. G. Gonnade, S. Chattopadhyay and A. Das, *Chem. Commun.,* 2015, **51**, 16932.

11. A. H. A, F. Ali, S. Kushwaha, N. Taye, S. Chattopadhyay and A. Das, *Anal. Chem.,* 2016, **88**, 12161.

12. A. H. A, U. R. G, F. Ali, N. Taye, S. Chattopadhyay and A. Das, *Chem. Commun*., 2015, **51**, 15592.

13. H. S. Jung, X. Chen, J. S. Kim and J. Yoon, *Chem. Soc. Rev.,* 2013, **42**, 6019.

14. C. Liu, W. Chen, W. Shi, B. Peng, Y. Zhao, H. Ma and M. Xian, *J. Am. Chem. Soc.,* 2014, **136**, 7257.

15. W. Chen, X. Yue, H. Zhang, W. Li, L. Zhang, Q. Xiao, C. Huang, J. Sheng and X. Song, *Anal. Chem.,* 2017, **89**, 12984.

16. M. Gao, R. Wang, F. Yu, J. You and L. Chen, *Analyst,* 2015, **140**, 3766.

17. M. Gao, F. Yu, H. Chen and L. Chen, *Anal. Chem.,* 2015, **87**, 3631.

18. L. Zeng, S. Chen, T. Xia, W. Hu, C. Li and Z. Liu, *Anal. Chem.*, 2015, **87**, 3004.

19. Q. Han, Z. Mou, H. Wang, X. Tang, Z. Dong, L. Wang, X. Dong and W. Liu, *Anal. Chem.,* 2016, **88**, 7206.

20. Y. Huang, F. Yu, J. Wang and L. Chen, *Anal. Chem.,* 2016, **88**, 4122.

21. K.-B. Li, F.-Z. Chen, Q.-H. Yin, S. Zhang, W. Shi and D.-M. Han, *Sens. Actuators, B*, 2018, **254**, 222.

22. J. Ma, J. Fan, H. Li, Q. Yao, F. Xu, J. Wang and X. Peng, *J. Mater. Chem. B*, 2017, **5**, 2574.

23. H. Shang, H. Chen, Y. Tang, R. Guo and W. Lin, Sens. Actuators, B, 2016, **230**, 773.

24. W. Chen, E. W. Rosser, D. Zhang, W. Shi, Y. Li, W.-J. Dong, H. Ma, D. Hu and M. Xian, *Org. Lett.,* 2015, **17**, 2776.

25. W. Chen, A. Pacheco, Y. Takano, J. J. Day, K. Hanaoka and M. Xian, *Angew. Chem., Int. Ed.,* 2016, **55**, 9993.

26. W. Chen, E. W. Rosser, T. Matsunaga, A. Pacheco, T. Akaike and M. Xian, *Angew. Chem., Int. Ed*., 2015, **54**, 13961.

27. W. Chen, C. Liu, B. Peng, Y. Zhao, A. Pacheco and M. Xian, *Chem. Sci.,* 2013, **4**, 2892.

28. Y. Fang, W. Chen, W. Shi, H. Li, M. Xian and H. Ma, *Chem. Commun.,* 2017, **53**, 8759.

29. J. Guo, S. Yang, C. Guo, Q. Zeng, Z. Qing, Z. Cao, J. Li and R. Yang, *Anal. Chem.,* 2018, **90,** 881.

30. M. Gustafsson, *Proc. Natl. Acad. Sci. U.S.*A, 2005, **102**, 13081.

31. D. Li, L. Shao, B.-C. Chen, X. Zhang, M. Zhang, B. Moses, D. E. Milkie, J. R. Beach, J. A. Hammer, M. Pasham, T. Kirchhausen, M. A. Baird, M. W. Davidson, P. Xu and E. Betzig, *Science*, 2015, **349**, aab3500.

32. S. Sreedharan, M. R. Gill, E. Garcia, H. K. Saeed, D. Robinson, A. Byrne, A. Cadby, T. E. Keyes, C. Smythe, P. Pellett, J. Bernardino de la Serna and J. A. Thomas, *J. Am. Chem. Soc.,* 2017, **139**, 15907.

33. E. Sezgin, F. Schneider, V. Zilles, E. Garcia, D. Waithe, A. S. Klymchenko and C. Eggeling, *bioRxiv*.

34. F. Ali, S. Sreedharan, A. H. Ashoka, H. K. Saeed, C. G. W. Smythe, J. A. Thomas and A. Das, *Anal. Chem*., 2017, **89**, 12087.

35. N. Boens, V. Leen and W. Dehaen, *Chem. Soc. Rev.*, 2012, **41**, 1130.

36. P. Nagy and C. C. Winterbourn, *Chem. Res. Toxicol.,* 2010, **23**, 1541.

CHAPTER 5A

SILICON-RHODAMINE BASED NEAR-INFRARED FLUOROGENIC PROBES FOR MEMBRANE IMAGING

Manuscript under preparation….

5A.1. Introduction

Small molecule fluorophores are indispensable tools for biological imaging. Fluorescence imaging opens up the possibilities for non-invasive detection techniques which are of high interest both in research and diagnostics.[1] Fluorescence bio-probes are well-established tools for bioimaging and monitoring biological species and processes in living systems.[1,2] Among various biological targets, the cell membrane is the one with utmost importance. The cell membrane is composed of lipid bilayers along with many ion channels and some surface proteins. Being the outer envelope of cells, it regulates the movement of various ions or molecules in and outside the cells. The cell membrane is the first barrier which is exposed to the extracellular environment and it is a prime target for many drugs.[1,3] Membrane imaging with fluorescent probes gives an overall idea about the membrane surface chemistry and structural heterogeneity, which in turn is crucial for drug design and therapeutic applications.[4] Membrane probes are useful reporters to monitor the processes which are happening at the cell surface. A general strategy to target the membrane is the conjugation of long-chain hydrocarbons of different chain lengths to fluorescent probes, which partition into hydrophobic membrane surface and helps in probe binding.[5] Based on this strategy, several different dyes have been reported in the literature for the targeted imaging of cell membrane. Probes based on pyrene[6], diphenylhexatriene (DHP), laurdan, 7-nitrobenz-2-oxa-1,3diazol-4yl (NBD)[7] were reported in the literature. But most of these dyes require washing steps to avoid background signals. Also, because of the long hydrophobic chains, water solubility is the major problem. In our laboratory, we have developed some new concepts for imaging biological membranes. We designed the solvatochromic dyes bearing hydrophobic chain and zwitterionic group, which enabled the specific staining of the outer membrane leaflet.[8,9] These probes found applications for the detection of apoptosis[10]and detection of lipid rafts.[9,10] Moreover, these amphiphilic probes self-assemble in aqueous medium, resulting in self quenching.[9] This phenomenon is useful for imaging the membranes under 'no-wash' conditions.[8-10] However, most of the environment sensitive probes require excitation in the blue part of the visible spectrum, which is less suitable for biological studies because of the photo-damage and strong auto-fluorescence. Moreover, the brightness and photo stability of these probes are limited. Thus, environment-sensitive fluorescent turn-on probes that show far red/NIR emission with high brightness, stability and quantum yield are much significant.[3,9] Autofluorescence from biological samples at NIR window is negligible and NIR probes are useful for deep tissue imaging. Recently, a new class of environment-sensitive NIR dyes based on silicon-rhodamine (SiR) scaffold

were reported.[11,12] The absorption and emission behaviour of SiR are completely dependent on the surrounding environment. In the polar, hydrophilic environment, SiR exists in fluorescent-zwitterionic form whereas in the non-polar, hydrophobic environment, SiR predominantly exists in non-fluorescent, spirocyclic form. Unlike the trivial rhodamines, SiR shows a higher propensity to exist spirocyclic form. Along with the NIR emission, these dyes show much photostability and high quantum yield in aqueous medium and are excellent tools for imaging.[13-15]

Based on this specific ON/OFF switching behaviour of SiR, we have designed and synthesized a series of new environment sensitive, NIR membrane probes, **SiR-C12**, **SiR-C18** and **SiR-C12DA**. To achieve the cell membrane specificity, SiR fluorophore scaffold was modified with membrane-specific zwitterionic anchor groups having different alkyl chain lengths without affecting the environment-sensitivity of the parent fluorophore. Among the synthesized probes, **SiR-C18** and **SiR-C12DA** showed excellent membrane binding with negligible background signal. Live-cell imaging demonstrated application potential of these probes in cell membrane imaging under 'no wash' conditions using fluorescence microscopy.

5A.2. Experimental Section

5A.2.1. Materials

All the chemicals and solvents were procured from Sigma Aldrich or TCI and used as received without further purification. Dioleoylphosphatidylcholine (DOPC), dioleoylphosphatidylserine (DOPS), and cholesterol were purchased from Sigma-Aldrich. Bovine brain sphingomyelin (SM) was from Avanti Polar Lipids (Alabaster, AL).

5A.2.2. Analytical Methods

^{1}H NMR and ^{13}C NMR spectra were recorded on Bruker Avance III 400/500 MHz spectrometer. Mass spectra were obtained using Agilent Q-TOF 6520 spectrometer and JEOL JM AX 505 HA mass spectrometer. Absorption spectra were recorded on a Cary 4000 spectrophotometer (Varian). Fluorescence spectra were recorded on a Fluoromax-4 (Jobin Yvon, Horiba) spectrofluorometer. Emission measurements were systematically done at 20^{o}C, unless indicated otherwise. All the spectra were corrected from the fluorescence of the corresponding blank (suspension of lipid vesicles without the probe) and for the wavelength-dependent response function of the detector. Relative fluorescence quantum yields for **SiR-C12**, **SiR-C18,** and **SiR-C12DA** were measured using DiD in Methanol (QY = 0.33) as standard. Large unilamellar vesicles (LUVs) were

prepared Lipex Biomembranes extruder (Vancouver, Canada).Preparative thin layer chromatography was performed on a silica pre-coated plates.

5A.2.3. Large unilamellar vesicles (LUVs) preparation

Dioleoylphosphatidylcholine (DOPC), dioleoylphosphatidylserine (DOPS), and cholesterol were purchased from Sigma-Aldrich. Bovine brain sphingomyelin (SM) was from Avanti Polar Lipids (Alabaster, AL). Large unilamellar vesicles (LUVs) were obtained by the extrusion method as described in the literature[7]. Briefly, a suspension of multilamellar vesicles was extruded by using a Lipex Biomembranes extruder (Vancouver, Canada). The size of the filters was first 0.2 μM (7 passages) and after that 0.1 μm (10 passages). Mean diameter of the monodisperse vesicles were measured with a Malvern Zetamaster 300 (Malvern, U.K.) and it was found to be 0.11 to 0.12 µm. LUVs were labelled with 1 μM of the probe in dimethyl sulfoxide to 1mL solutions of vesicles. A 20 mM phosphate buffer, pH 7.4, was used in these experiments. The fluorescence experiments were performed 10 minutes after addition of the aliquot. Concentrations of the probes and lipids were generally 1 μM and 200 μM, respectively.

5A.2.4. Giant unilamellar vesicles (GUVs) preparation

Giant unilamellar vesicles (GUVs) were generated by electro-formation in a home-built liquid cell (University of Odense, Denmark), using previously described procedures.[8] A 1 mM solution of lipids in chloroform was deposited on the platinum wires of the chamber, and the solvent was evaporated under vacuum for 30 min. The chamber, thermostatted at 55 °C, was filled with a 300 mM sucrose solution, and a 2-V, 10-Hz alternating electric current was applied to this capacitor-like configuration for ca. 2 h. Then, a 50 μL aliquot of the obtained stock solution of GUVs in sucrose (cooled down to room temperature) was added to 200 μL of 300 mM glucose solution to give the final suspension of GUVs used in microscopy experiments. The staining of GUVs was performed by addition of an aliquot of the probe stock solution in DMSO to obtain a 0.1 μM final probe concentration (final DMSO volume <0.25%).

5A.2.5. Cell culture preparation

KB cells were grown in minimum essential medium (MEM, Gibco-Invitrogen) with 10% fetal bovine serum (FBS, Lonza), 1% nonessential amino acids (Gibco- Invitrogen), 1% MEM vitamin solution (Gibco-Invitrogen), 1% L-Glutamine (Sigma-Aldrich), and 0.1% antibiotic solution (gentamicin, Sigma-Aldrich) at 37 °C in humidified atmosphere

containing 5% CO_2. Cells were seeded onto a chambered coverglass (IBiDi) at a density of 5 × 104 cells/well and treated with Actinomycin-D (10 µM/mL) for 18 hours to induce apoptosis. For imaging, the culture medium was removed and the attached cells were washed with Opti-MEM (Gibco−Invitrogen). Next, the cells were incubated in Opti-MEM with **SiR-C12**, **SiR-C18** and **SiR-C12DA** (20 nM). And images were captured under 'no wash' condition. For the Co-staining experiment, nuclear staining dye Hoechst was used.

5A.2.6. General experimental methods for UV-Vis and fluorescence studies

Stock solutions of **SiR-C12**, **SiR-C18,** and **SiR-C12DA** (5×10^{-3}M) were prepared in DMSO, and the same solution was used for all the studies after appropriate dilution with aqueous buffer solution. A 20 mM phosphate buffer (pH 7.4) was used for all the spectroscopic measurements unless mentioned otherwise. The effective final concentration of the probes used for spectroscopic measurements was 1 µM. All luminescence measurements were done using λ_{Ext} = 620 nm with an emission slit width of 2 nm.

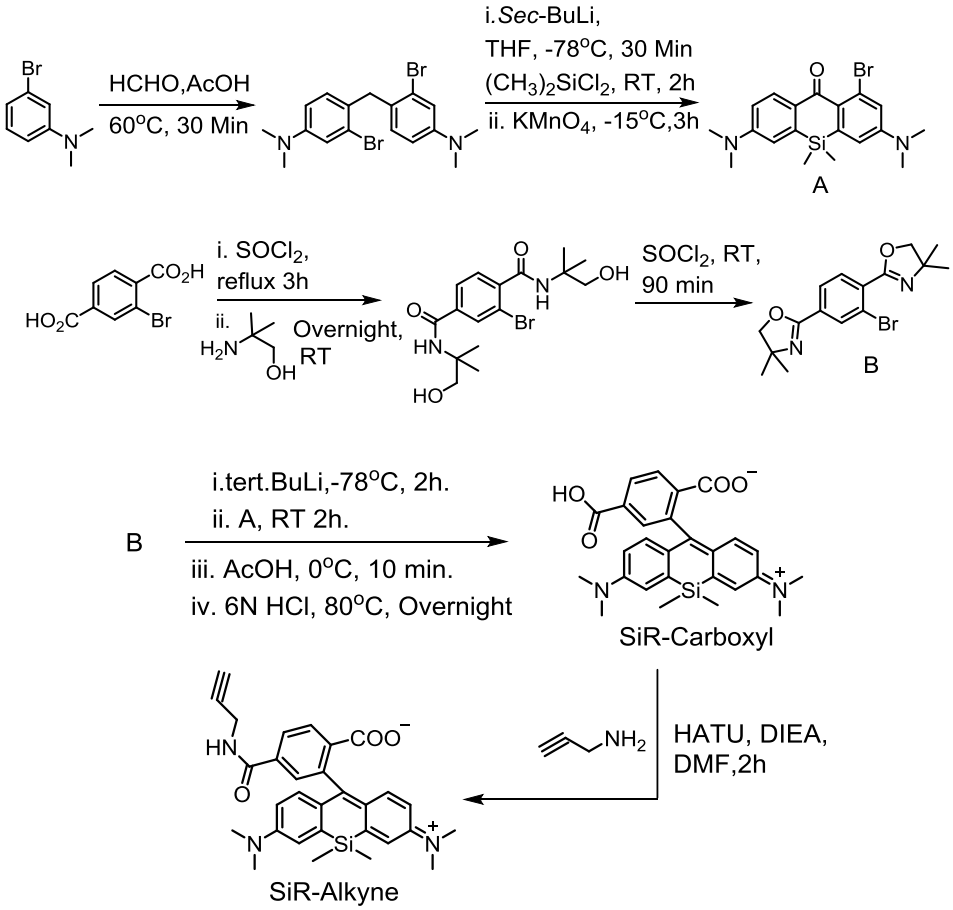

Scheme 5A.1. The synthetic route towards **SiR-Alkyne.**

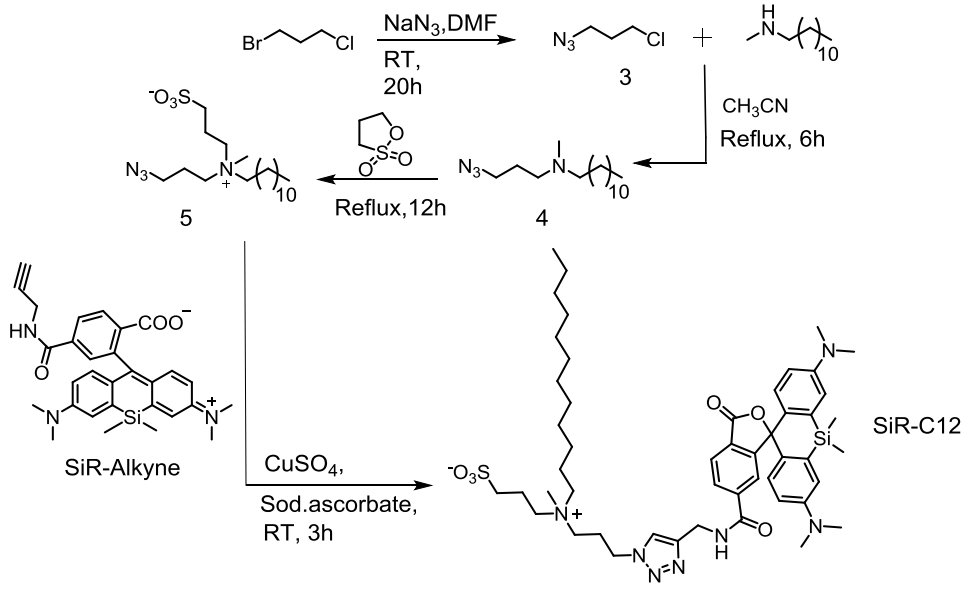

Scheme 5A.2. The synthetic route towards **SiR-C12**.

5A.3. Synthesis and Characterisation

5A.3.1. Synthesis of 1

SiR-carboxyl was synthesized by following the literature method.[11]

3-bromo N,N-dimethylaniline (4 g, 19.99 mmol) and formaldehyde (4 ml) was dissolved in acetic acid (40 ml). It was heated to 60^{o}C for 30 minutes. After cooling, acetic acid was evaporated with reduced pressure and the reddish residue was neutralized with saturated $NaHCO_3$ solution. It was extracted with dichloromethane and the organic layer was washed with H_2O and brine. Organic layer was dried over Na_2SO_4, filtered and concentrated under reduced pressure. The product was purified by silica gel column chromatography by using heptanes and ethyl acetate as eluents. Compound was isolated as a white crystalline solid.Yield = 50%. ^{1}H NMR (400 MHz, CHLOROFORM-d) δ = 7.03 (br. s., 2 H), 6.88 (d, *J* = 8.4 Hz, 2 H), 6.69 (br. s., 2 H), 4.03 (s, 2 H), 2.95 (s, 12 H).

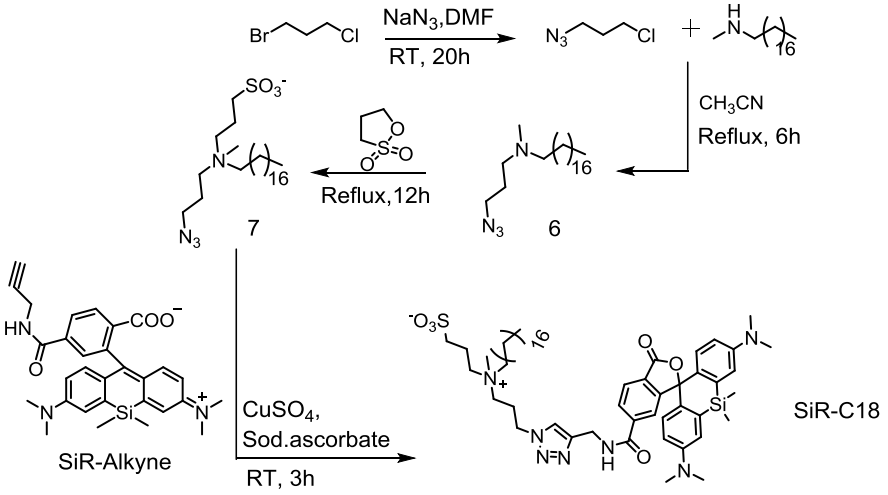

Scheme 5A.3. Synthetic route towards **SiR-C18**.

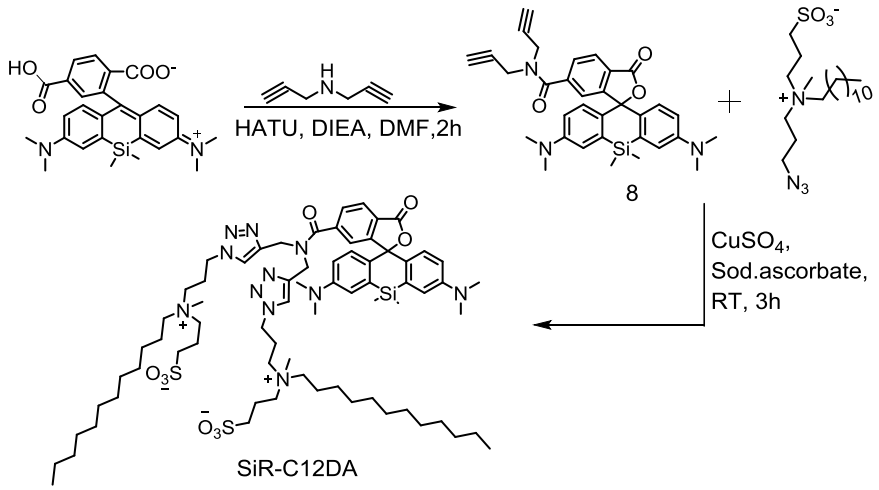

Scheme 5A.4. The synthetic route towards **SiR-C12DA**.

5A.3.2. Synthesis of A

In a two neck, round bottom flask flushed with argon, Bis-bromo compound (2g, 4.85 mmol) was added and it was dissolved in dry THF under argon atmosphere. The solution was cooled to -78 ^{o}C with dry ice and acetone. To this Sec-BuLi (1.4 M solution in hexane 10.4 ml, 3 equiv.) was slowly added drop by drop for 30 minutes. It was stirred at same temperature for 2 hours. To this dichlorodimethylsilane (1.06 ml, (4 g, 1.8 equiv., 8.78 mmol) was slowly added and the resulting solution was stirred at room temperature for additional 2hours. During this time, the colour of the solution gradually turns to greenish blue. Reaction mixture was quenched by the addition of 1N HCl. THF was evaporated and the aqueous layer was extracted with ethyl acetate washed with saturated $NaHCO_3$, water and brine. Organic layer was dried over Na_2SO_4, filtered and concentrated under

reduced pressure. This crude product was prone to undergo oxidation in presence of oxygen. So, it was immediately taken for the next step. Crude mixture was dissolved in acetone and it was cooled to -15^{o}C. $KmnO_4$ powder (766.83 mg, 4.85 mmol) was added portion wise (6 lots) and the mixture was stirred at same temperature for 2 hours. Purple coloured suspension was filtered through celite bed the greenish yellow filtrate was concentrated and purified by silica gel column chromatography using heptane and ethyl acetate. After the isolation compound was stored in an airtight vial. Yield=32%.^{1}H NMR (400 MHz, CHLOROFORM-d) δ = 8.41 (d, *J* = 8.9 Hz, 2 H), 6.95 - 6.76 (m, 4 H), 3.10 (s, 12 H), 0.48 (s, 6 H).

5A.3.3. Synthesis of 2

3-bromoterephthalic acid (1 g, 4.03 mmol) was suspended in $SOCl_2$ (7 ml), and 2 to 3 drops of DMF was added (catalytic amount), and it was refluxed for 3hours. After cooling, $SOCl_2$ was evaporated, and the residue was dried in high vacuum. It was purged with argon for 15 minutes and dissolved in dry dichloromethane. It was added to a mixture of 2-amino-2-methyl-1-propanol (982 mg, 11.01 mmol) and diisopropylethylamine and stirred at room temperature overnight. The reaction was quenched with a saturated $NaHCO_3$ solution, extracted 3 times with ethyl acetate, washed with water and brine, dried over Na_2SO_4, filtered and concentrated to get the white solid. Yield=72%. ^{1}H NMR (400 MHz, DMSO-d_6) δ = 8.03 (s, 1 H), 7.85 (s, 1 H), 7.81 (d, *J* = 7.9 Hz, 1 H), 7.72 (s, 1 H), 7.42 (d, *J* = 7.8 Hz, 1 H), 4.86 (t, *J* = 6.1 Hz, 1 H), 4.81 (t, *J* = 6.0 Hz, 1 H), 3.50 (t, *J* = 6.1 Hz, 4 H), 1.30 (s, 12 H). ^{13}C NMR (100 MHz, DMSO-d_6) δ = 167.1, 164.9, 142.2, 137.7, 131.6, 128.8, 126.9, 119.1, 67.8, 67.5, 60.1, 55.7, 23.9.

5A.3.4. Synthesis of B

Compound **2** (1 g, 2.57 mmol) was dissolved in $SOCl_2$ and this was stirred at room temperature for 90 minutes. Thionyl chloride was evaporated and the residue was neutralized by adding saturated $NaHCO_3$ solution, extracted 3 times with ethyl acetate, dried over Na_2SO_4, filtered and concentrated. The mixture was purified by silica-gel column chromatography by using ethyl acetate and dichloromethane as eluents. Column fractions were concentrated and kept at 4^{o}C overnight to get the white solid. Yield=60%. ^{1}H NMR (400 MHz, DMSO-d_6) δ = 7.98 (s, 1 H), 7.86 (d, *J* = 7.8 Hz, 1 H), 7.42 (d, *J* = 7.8 Hz, 1 H), 4.14 (s, 2 H), 4.01 (s, 2 H), 1.38 (s, 6 H), 1.29 (s, 6 H). ^{13}C NMR (100 MHz, DMSO-d_6) δ = 167.1, 159.4, 142.2, 131.8, 130.1, 129.5, 127.2, 119.3, 79.2, 68.1, 54.6, 51.2, 28.6, 25.1.

5A.3.5. Synthesis of SiR-Carboxyl

In an argon-flushed 50 ml round bottom flask fitted with a septum, compound **B** (150 mg, 2 equiv. 0.46 mmol) was dissolved in dry THF under argon atmosphere. It was cooled to -78^{o} C using dry ice and acetone bath. *tert*.BuLi (300 µL, 2 equiv.) was slowly added dropwise. It was stirred at same temperature for 1hour. Compound **A** (70 mg, 0.14 mmol) was dissolved in dry THF and it was slowly added to the reaction mixture. After the addition, the temperature was gradually increased to room temperature and it was stirred at room temperature for 2 hours. Again the mixture was cooled to 0^{o}C in an ice bath and acetic acid (1ml) was added and stirred for 1o minutes. The reaction mass was immediately turned to deep blue colour. The solution was evaporated under reduced pressure and the residue was used for the next step without further purification. The blue residue was dissolved in 6N HCl (15 ml) and heated to 80^{o}C overnight. The resulting pale yellow coloured solution was cooled and added slowly to the saturated $NaHCO_3$ solution and the pH was adjusted 1 to 2. The aqueous layer was extracted with dichloromethane (3 times) and the organic layer was washed with 0.1 N HCl (3 times), brine and it was dried over Na_2SO_4, filtered and concentrated under reduced pressure. The crude product was purified by silica-gel column chromatography using CH_2Cl_2 and CH_3OH. Yield=46%. ^{1}H NMR (400 MHz, METHANOL-d_4) δ = 8.20 (d, *J* = 7.9 Hz, 1 H), 7.95 (d, *J* = 7.9 Hz, 1 H), 7.85 (s, 1 H), 7.04 (br. s., 2 H), 6.72 (d, *J* = 8.7 Hz, 2 H), 6.62 (d, *J* = 9.3 Hz, 2 H), 2.95 (s, 12 H), 0.66 (s, 3 H), 0.56 (s, 3 H).LRMS (ESI) (M+ H)-473.132.

5A.3.6. Synthesis of SiR-Alkyne

SiR-Carboxyl (50 mg, 0.10 mmol) was dissolved in 2ml of dry DMF. To this DIEA (36.8 µL, 2 equiv.) was added and stirred at room temperature for 10 minutes. To the above mixture, propargylamine (10.16 µL, 1.5 equiv.) HATU (48.22 mg, 0.12 mmol, 1.2 equiv.) were added and it was stirred at room temperature for two hours. Reaction was monitored by TLC. Upon completion, DMF was evaporated completely and the crude product was purified by silica gel column chromatography using CH_2Cl_2 and CH_3OH. Yield=28%. ^{1}H NMR (400 MHz, METHANOL-d_4) δ = 8.02 (br. s., 2 H), 7.69 (s, 1 H), 7.03 (br. s., 2 H), 6.76 - 6.67 (m, 2 H), 6.66 - 6.57 (m, 2 H), 4.10 (br. s., 2 H), 3.02 - 2.87 (m, 12 H), 2.80 (s, 1 H), 0.65 (s, 3 H), 0.55 (s, 3 H). HRMS (M+H) calculated for $C_{30}H_{31}N_3O_3Si$ 509.2128. Found- 510.2201.

5A.3.7. Synthesis of 4 and 6

Compound **3** was synthesized according to the literature report.[8] Anchor groups having 12-Carbon and 18-Carbon alkyl chains were synthesized by following the common synthetic procedure.

3-chloropropylazide (500 mg, 4.15 mmol, 1 equiv.) and N-methldodecylamine or N-methyloctadecylamine (1.17 g, 4.15 mmol, 1 equiv.) was dissolved in 15 ml acetonitrile. It was heated to reflux at 60^{o} C in a sealed tube for 6 hours. (Note- N-methyloctdecylamine is sparingly soluble in acetonitrile, it dissolves completely in the reflux condition). After cooling, acetonitrile was evaporated and the compound was purified by silica gel column chromatography using CH_2Cl_2 and CH_3OH. Yield=30%. Compound **6**- ^{1}H NMR (400 MHz, CHLOROFORM-d) δ = 3.32 (br. s., 2 H), 2.52 - 2.37 (m, 1 H), 2.37 - 2.09 (m, 4 H), 1.85 - 1.66 (m, 2 H), 1.53 - 1.38 (m, 2 H), 1.34 - 1.05 (m, 22 H), 0.87 (br. s., 3 H). ^{13}C NMR (100 MHz, CHLOROFORM-d) δ = 57.9, 54.5, 49.6, 42.1, 31.9, 29.7, 29.4, 27.5, 26.9, 22.7, 14.1.

5A.3.8. Synthesis of 5 and 7

Compound **5** was synthesized by following our previous report.[8]

Azide (60 mg, 0.16mmol, 1 equiv.) and 1,3-propanesultone (100 mg, 0.8 mmol, 5 equiv.) was dissolved in acetonitrile (3 ml). It was refluxed for 12 hours. White precipitate formed was filtered and washed several times with acetonitrile and dried. Yield=56%. Compound **7**- ^{1}H NMR (400 MHz, METHANOL-d_4) δ = 3.51 (br. s., 4 H), 3.43 - 3.34 (m, 2 H), 3.06 (br. s., 3 H), 2.87 (br. s., 2 H), 2.17 (br. s., 2 H), 2.02 (br. s., 2 H), 1.77 (br. s., 2 H), 1.47 - 1.21 (m, 31 H), 0.90 (br. s., 3 H). ^{13}C NMR (100 MHz, METHANOL-d_4) δ = 61.9, 31.7, 29.4, 29.2, 29.1, 29.1, 28.8, 26.0, 22.3, 21.7, 18.1, 13.0. HRMS (M+H) calculated for $C_{25}H_{52}N_4O_3S$ 488.3760. Found- 489.3840.

5A.3.9. Synthesis of 8

Carboxy-SiR (10 mg, 0.02 mmol) was dissolved in 2ml of dry DMF. To this DIEA (11.1 µL, 3 equiv.) was added and stirred at room temperature for 10 minutes. To the above mixture, dipropropargylamine (2 equiv.) HATU (9.65 mg, 1.2 equiv.) were added and it was stirred at room temperature two hours. Reaction was monitored by TLC. Upon completion, DMF was evaporated completely. Reaction mass was acidified with dilute HCl. It was extracted with ethylacetate, washed with saturated $NaHCO_3$ and H_2O and

dried over $MgSO_4$ and concentrated under reduced pressure. It was directly taken for the next step without further purification.

5A.3.10. General procedure for the click reaction

SiR-alkyne (1 equiv.) and corresponding zwitterionic anchor (C12 or C18) (1.2 equiv.) was dissolved in DMF. $CuSO_4$ (5 mg) and sodium ascorbate (5 mg) was dissolved separately in H_2O. Both the solutions were mixed and vortexed for 2 minutes. Once the colour changes from black to orange, it was added to the reaction mixture and stirred for 2 hours at room temperature. Reaction was monitored by TLC. Upon completion, solvents were evaporated completely and the product was purified by silica gel preparatory TLC method using CH_2Cl_2 and CH_3OH as eluents.

SiR-C12: ^{1}H NMR (400MHz ,METHANOL-d_4) δ = 8.08 (d, *J* = 1.0 Hz, 1 H), 8.01 (d, *J* = 1.0 Hz, 1 H), 7.97 (br. s., 1 H), 7.71 (s, 1 H), 7.02 (br. s., 2 H), 6.75 - 6.66 (m, 2 H), 6.65 - 6.56 (m, 2 H), 4.59 (br. s., 2 H), 4.46 (br. s., 2 H), 3.53 - 3.41 (m, 2 H), 3.27 - 3.18 (m, 2 H), 2.99 (br. s., 3 H), 2.94 (s, 12 H), 2.85 - 2.74 (m, 2 H), 2.36 (br. s., 2 H), 2.05 (br. s., 2 H), 1.62 (br. s., 2 H), 1.26 (br. s., 23 H), 0.94 - 0.84 (m, 4 H), 0.64 (s, 3 H), 0.55 (s, 3 H). ^{13}C NMR (100 MHz ,METHANOL-d_4) δ = 173.0, 169.5, 157.9, 152.2, 147.6, 142.1, 139.0, 133.2, 131.1, 130.4, 127.8, 125.9, 125.8, 118.9, 116.0, 95.6, 93.0, 60.6, 60.5, 49.0, 41.6, 37.4, 34.1, 31.8, 31.7, 31.6, 31.5, 31.3, 30.6, 28.4, 25.1, 24.8, 24.1, 20.5, 15.5, 2.0, -0.5. HRMS calculated for $C_{49}H_{71}N_7O_6SSi$ 913.4955 (M+H). Found- 914.5026.

SiR-C18: ^{1}H NMR (400 MHz, METHANOL-d_4) δ = 8.01 - 7.95 (m, 1 H), 7.94 - 7.90 (m, 1 H), 7.88 (s, 1 H), 7.61 (s, 1 H), 6.93 (d, *J* = 2.8 Hz, 1 H), 6.63 - 6.56 (m, 1 H), 6.56 - 6.49 (m, 1 H), 4.50 (s, 3 H), 4.38 (t, *J* = 6.3 Hz, 2 H), 3.45 - 3.32 (m, 4 H), 3.31 - 3.24 (m, 1 H), 3.16 - 3.09 (m, 2 H), 2.95 (s, 1 H), 2.92 - 2.82 (m, 11 H), 2.77 (t, *J* = 6.7 Hz, 1 H), 2.73 - 2.66 (m, 2 H), 2.33 - 2.20 (m, 2 H), 2.08 (br. s., 1 H), 2.00 - 1.85 (m, 3 H), 1.66 (br. s., 1 H), 1.52 (br. s., 2 H), 1.29 (br. s., 2 H), 1.19 (br. s., 41 H), 0.83 - 0.76 (m, 4 H), 0.55 (s, 3 H), 0.45 (s, 1 H). ^{13}C NMR (100 MHz, METHANOL-d_4) δ = 170.6, 167.9, 166.7, 149.8, 148.7, 136.5, 130.8, 127.9, 125.3, 123.4, 116.4, 113.5, 100.5, 96.0, 80.6, 39.1, 35.0, 31.7, 29.4, 29.0, 28.8, 27.3, 26.0, 22.3, 21.7, 18.0, 17.3, 13.6, 3.1, 0.6, -1.1, -2.6.

SiR-C12DA was synthesized according to the general procedure. ^{1}H NMR (400MHz, METHANOL-d_4) δ = 8.23 - 7.88 (m, 3 H), 7.78 - 7.61 (m, 1 H), 7.05 (d, *J* = 6.6 Hz, 1 H), 6.94 (d, *J* = 8.8 Hz, 1 H), 6.72 - 6.46 (m, 1 H), 6.41 - 6.13 (m, 1 H), 4.65 (br. s., 2 H), 4.59 - 4.37 (m, 4 H), 3.68 - 3.48 (m, 3 H), 3.08 (br. s., 3 H), 3.01 - 2.90 (m, 5 H), 2.90 - 2.62 (m, 6 H), 2.50 - 2.24 (m, 3 H), 2.23 - 1.99 (m, 3 H), 1.75 (br. s., 2 H), 1.28 (br. s., 44 H), 0.74 - 0.58 (m, 3 H), 0.62 - 0.47 (m, 3 H).HRMS calculated for $C_{71}H_{113}N_{11}O_9S_2Si$ 677.8966 (m/2). Found- 678.9035.

5A.4. Results and Discussion

Our design strategy involves silicon-rhodamine reporter unit which is expected to give reversible ON/OFF switching with respect to the surrounding environment. Reporter unit is covalently linked to a zwitterionic anchor groups having long alkyl chains of different length. Anchor group helps to specifically localise the probes in membrane.[8]

One of the key intermediates, SiR-Carboxyl was synthesized by following the literature methods. It was further coupled with propargylamine to obtain SiR fluorophore with a clickable alkyl handle.

Zwitterionic membrane anchor groups with different alkyl chain lengths (C12 and C18) were synthesized in 3 steps. Azidification of 1-bromo-3-Chloropropane followed by SN2 substitution with N-methylalkylamines (C12 and C18) and quaternization with propane sultone resulted in zwitterionic anchor groups.

Click reaction of the SiR-alkynes with azide functionalized zwitterionic anchor groups resulted in final compounds **SiR-C12**, **SiR-C18** and **SiR-C12DA**. All the final compounds and intermediates were characterized by standard analytical techniques.

We hypothesize that silicon rhodamine appended with zwitterionic anchor group helps in the localization of the probe in the membrane. Unbound probes are expected to self-assemble in the aqueous solution because of the aliphatic long carbon chains aggregate and in turn, converted to non-fluorescent spirocyclic form. Probes which are inside the membrane are expected to be in the OFF state due to the hydrophobic membrane environment and a fraction of the probes which are on the surface of the membrane is expected to be in the ON state.

In order to evaluate the ON/OFF switching behaviour of the probes, absorption spectra of **SiR-C18**, **SiR-C12DA** and **SiR-C12** (1μM) was recorded in dioxane and phosphate buffer (in the presence or absence of anionic surfactant 0.5% SDS). In a medium with low dielectric constant such as dioxane, all the probes exist in non-fluorescent spirocyclic form. Absorption spectra showed an absorption peak at 280 nm which corresponds to a ring closed form of SiR (Figure 5A.1).

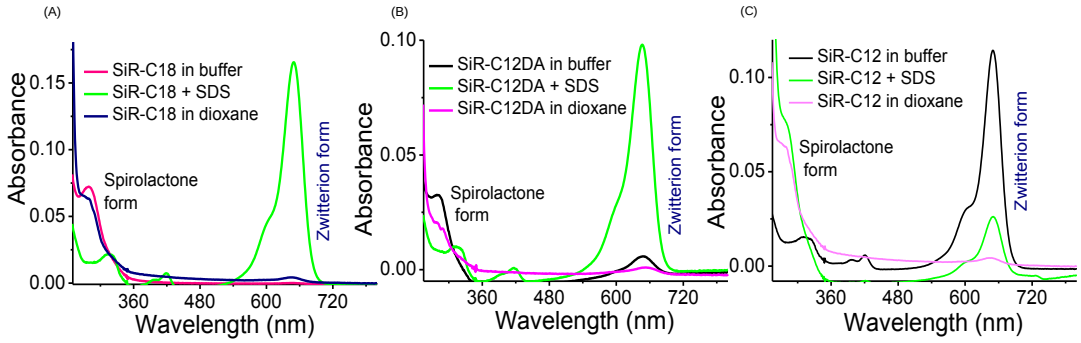

Figure 5A.1. Absorption spectra of (A) **SiR-C18**, (B) **SiR-C12DA** and (C) **SiR-C12** (1μM) in dioxane and phosphate buffer in the presence or absence of 0.5% SDS.

In phosphate buffer medium, **SiR-C12** shows a strong absorption band at 650 nm, corresponds to fluorescent zwitterion form of silicon rhodamine. On the contrary, **SiR-C18** in buffer shows almost no absorption at 650 nm whereas **SiR-C12DA** shows only a small absorption band at 650 nm. This is due to the fact that **SiR-C18** and **SiR-C12DA** have anchor groups with long carbon chains (C-18 and two C-12 carbon chains respectively). These carbon chains help to aggregate the dye in the aqueous medium and keep them predominantly in the spirocyclic ring-closed form. Whereas in the case of **SiR-C12,** a single C12-carbon chain is not sufficient to aggregate the probe in the aqueous medium, so **SiR-C12** probe predominantly exists in fluorescent zwitterionic form. This observation is well supported by the absorption spectra of compounds in buffer medium wherein a peak 280 nm corresponds to spirocyclic form was observed in the case of **SiR-C18** and **SiR-C12DA** whereas this peak was absent in **SiR-C12** suggesting the presence of only zwitterionic form. This was also evident from the quantum yield measurements wherein **SiR-C12** showed high quantum yield (Φ_f=0.26) in the aqueous medium whereas it was much lower in case of **SiR-C18** (Φ_f=0.0057) and **SiR-C12DA** (Φ_f=0.077). It has been known from the literature that addition of anionic surfactant like SDS switch the equilibrium of SiR to zwitterionic ring opened form[10]. Addition of 0.5% SDS to the aqueous solutions of **SiR-C18** and **SiR-C12DA** showed a dramatic increase in the absorption at 650 nm and a concomitant decrease in the absorption at 280 nm suggesting the formation of the zwitterionic form (Figure 5A.1 A & B). This OFF/ON switching behaviour resulted in the large increase in the fluorescence quantum yields to 0.33 and 0.32 for **SiR-C18** and **SiR-C12DA** respectively. Since **SiR-C12** already exists in the ring-opened form in aqueous buffer, no such increase was observed.

Probe	In buffer	SDS	DOPC	DOPC/cholesterol	SM/cholesterol
SiR-C12	0.28	-	0.062	0.09	-
SiR-C18	0.0057	0.33	0.014	0.024	0.023
SiR-C12DA	0.077	0.32	0.042	0.046	-

Table 5A.1. Relative quantum yields of probes in vesicles, buffer and SDS.

Probe	In buffer	DOPC	DOPC/cholesterol	SM/cholesterol
SiR-C18	1.7	4.2	7	6.9
SiR-C12DA	24	13	14	-

Table 5A.2. Percentage of zwitterionic form in vesicles and buffer. (Note-calculated by comparing the quantum yield of fully opened form of probes with the quantum yield in membranes).

After confirming the ON/OFF switching behaviour of SiR probes with respect to the surrounding environment, we were interested to see the switching behaviour in the hydrophobic membrane environment. We have prepared the LUVs of various compositions to represent ordered and disordered phases of the membrane. DOPC and DOPC/cholesterol represent liquid disordered phase (Ld phase). Sphingomyelin(SM)/cholesterol represent liquid ordered phase (Lo phase). We first tested the response of **SiR-C12** in lipid vesicles. In Ld phase (DOPC and DOPC/cholesterol) **SiR-C12** showed a significant decrease in the absorbance at 650 nm and a sharp increase in the absorbance at 280 nm indicating the formation of the spirocyclic form (OFF state) in the hydrophobic membrane environment. Emission spectra of **SiR-C12** also showed a notable decrease in the fluorescence intensity at 667 nm upon interaction with DOPC and DOPC/cholesterol vesicles [Figure 5A.2(B)]. However, **SiR-C12** showed no change in the absorption of liquid-ordered phases, SM/cholesterol [Figure 5A.2 (A)]. A possible explanation for this poor affinity to ordered phases is due to two reasons. Lo domains (SM/cholesterol) forms tightly packed, rigid structure, hence it does not allow the dye to penetrate into the Lo phase. Moreover, the anchor group with 12-Carbon alkyl chain is not sufficient to localize the probe on the surface of SM/cholesterol.

SiR-C12 remained highly fluorescent in buffer medium as the 12-carbon alkyl chain in the anchor group is not enough to aggregate the dye in the aqueous medium, which resulted in very high background signal, which is not suitable for membrane imaging (Figures 5A.1C and 5A. 2).

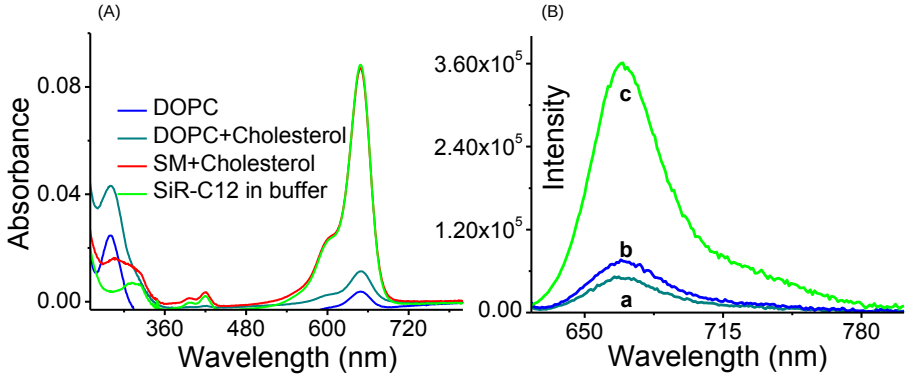

Figure 5A.2. Absorption (A) and emission (B) spectral response of **SiR-C12** (1 µM) in LUVs (DOPC, DOPC+ Cholesterol, SM+ Cholesterol 200 µM each) in phosphate buffer medium pH 7.4. (a, b & c in figure B represents DOPC, DOPC+ Cholesterol, and **SiR-C12** in buffer respectively) Excitation-610 nm.

This observation was further evidenced by the membrane staining experiments wherein the KB-cells treated with **SiR-C12** (20 nM) probe failed to stain the cell membrane. Only the background signal was observed (Figure 5A. 3). Due to this, the cell membrane is indistinguishable from the background signal (Figure 5A.3).

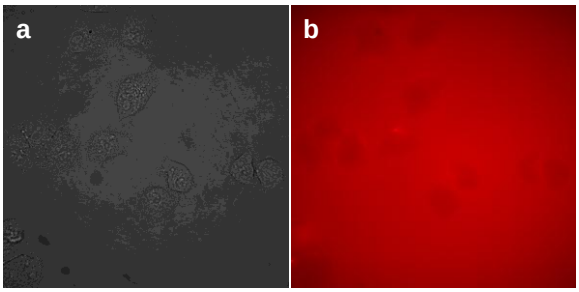

Figure 5A.3. Fluorescence images of living KB cells (a) stained with 20 nM of **SiR-C12** (b) represent the KB cells without probe. λ_{max} excitation= 640 nm. Photons were collected at red channel.

SiR-C12 showed both absorption and emission spectral changes to Ld phases by the internalization of the probe inside the hydrophobic pockets of the vesicles. However, an anchor group with a single 12-carbon alkyl chain failed to localize the probe on the membrane surface, which resulted in the poor signal from the membrane. Also, a single 12-carbon alkyl chain is not sufficient to aggregate the dye in the aqueous medium to transform the dye into spirocyclic form, which resulted in high background noise.

To overcome these issues, we have modified the probe with the anchor group having 18-carbon long alkyl chain, **SiR-C18.** We have also synthesized one more probe **SiR-C12DA**

with two zwitterionic C-12 anchor groups to increase the binding affinity. These structural modifications dramatically altered the absorption and emission behaviour.

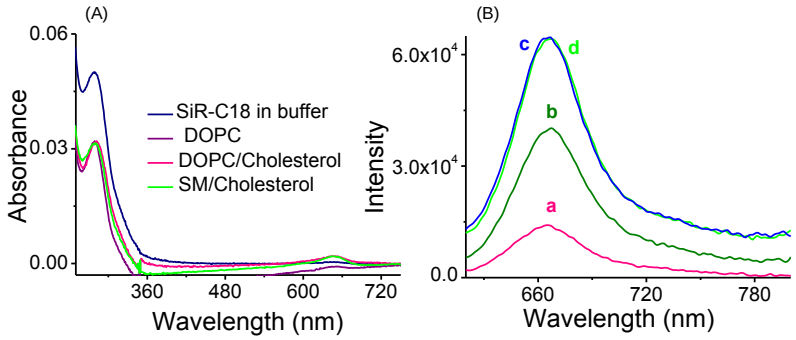

Figure 5A.4. Absorption (A) and emission (B) spectral response of **SiR-C18** (1 µM) in LUVs (DOPC, DOPC+ Cholesterol, SM+ Cholesterol 200 µM each) in phosphate buffer medium pH 7.4. (a, b, c & d in figure B represents **SiR-C18** in buffer, DOPC, DOPC/Cholesterol and SM/cholesterol respectively). Excitation- 610 nm.

SiR-C18 in the aqueous medium showed almost no absorption at 650 nm and a prominent absorption band at 280 nm suggesting the presence spirocyclic OFF form (Figure 5A.1A) and a small absorption band at 650 nm was observed in the case of **SiR-C12DA** (Figure 5A.1B), suggesting the aggregation of the dyes and subsequent formation of the spirocyclic form in the aqueous medium.We have further tested the affinity of these probes to model membranes. **SiR-C18** in Ld phases showed a small absorption peak at 650 nm, suggesting that a small fraction of dye was in the zwitterionic form (Figure 5A. 3). Emission response also showed 3 fold and 4.8 fold increase in the fluorescence intensity. Surprisingly, **SiR-C18** also showed 4.8 fold enhancement in Lo phases (SM/cholesterol) (Figure 5A.4). Silicon-rhodamine in hydrophobic membrane environment should be in the spirocyclic-OFF state. So what is the reason behind fluorescence enhancement? To explain this phenomenon, we have proposed a membrane model (Figure 5A. 5).

SiR-C18 upon interaction with Ld phases most of the dye molecule internalized in the membrane and converted to OFF state whereas a small fraction of the dye (about 7%, Table 1) which stick to the surface of the membrane is in the ON state. 18-carbon long alkyl chain helps to penetrate into the rigid structures of Lo phase and localize the dye molecule on the surface and showed enhancement in the fluorescence intensity. Unbound dye molecules in the aqueous solution form aggregate due to long hydrophobic alkyl chains and converted to spirocyclic-OFF state (Figure 5A. 5). This explanation is in agreement with the observed absorption and emission spectral response of **SiR-C18** in vesicles as well as in the aqueous buffer.

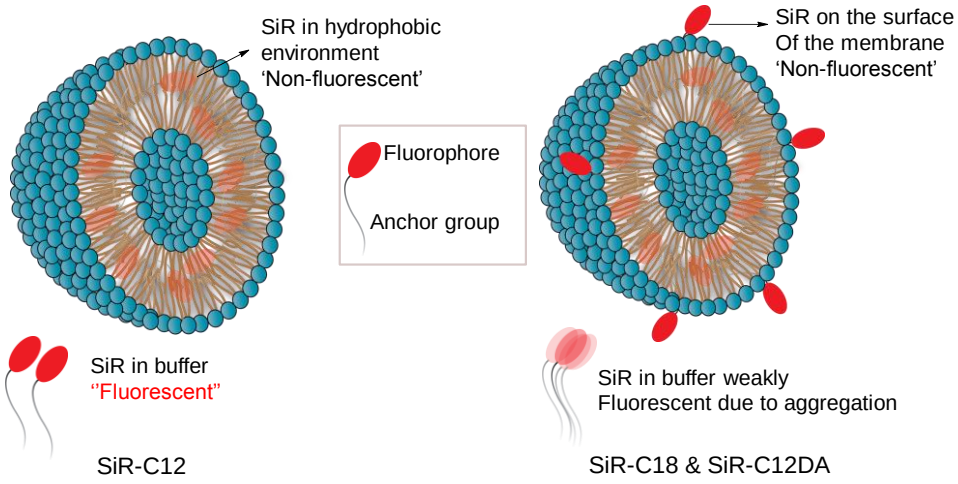

Figure 5A.5. Proposed membrane model to explain the behaviour of **SiR** probes in the membrane environment.

Negligible fluorescence quantum yield for **SiR-C18** in the aqueous buffer (Φ_f=0.0057) and an increase in the quantum yield both in Ld and Lo phases DOPC/cholesterol (Φ_f=0.024) and SM/cholesterol (Φ_f=0.023) further support the proposed model. Moreover, negligible quantum yield of **SiR-C18** in the aqueous medium should result in very low background signal; this would help to visualize the cell membrane under wash-free conditions.

On the other hand, **SiR-C12DA** with two 12-carbon anchor groups showed some background signal in the aqueous medium but it was significantly less (Φ_f=0.077) when compared to single 12-carbon anchor (Φ_f=0.26). In the presence of LUVs, **SiR-C12DA** also showed a small absorption band at 650 nm in Ld vesicles indicating the fraction of probe in the ON state in the hydrophobic membrane environment (Figure 5A.6).

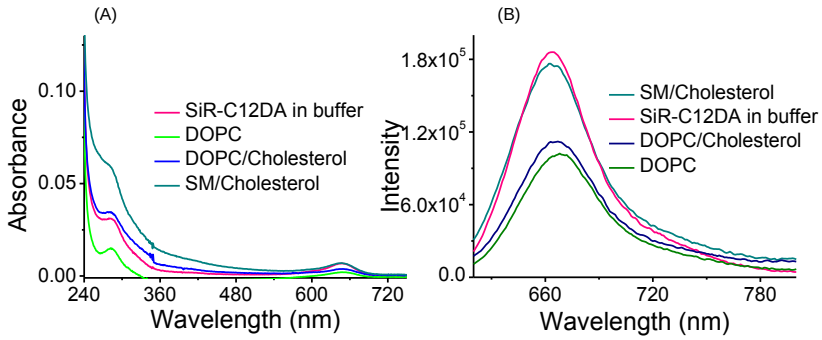

Figure 5A.6. Absorption (A) and emission (B) spectral response of **SiR-C12DA** (1 µM) in LUVs (DOPC, DOPC+ Cholesterol, SM+ Cholesterol 200 µM each) in phosphate buffer medium pH 7.4. Excitation-610 nm.

The presence of two 12-carbon anchor groups helps to stick the dye on the surface of the membrane. However, this probe showed less affinity to Lo phases. Absorption and emission spectra in Lo vesicles remain almost identical as that of probe in buffer except a small change in the fluorescence (Figure 5A.6).

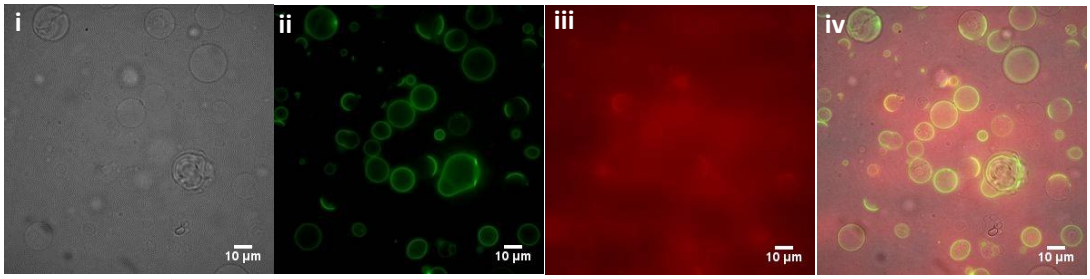

Figure 5A.7. Fluorescence microscopic images of GUVs (i) composed of SM/cholesterol treated with (ii) **SiR-C12DA** 20 nM and (iii) NR12S 50 nM. (iv) Merged image. Scale bar 10 µm.

This observation was further confirmed by co-staining experiment with a commercial probe NR12S, which is known to bind to Lo phases. The giant unilamellar vesicles (GUVs) composed of Lo phase (SM/cholesterol) were stained with 20 nM **SiR-C12DA** and 50 nM of NR12S and images were captured in green and red channels. NR12s showed strong affinity to Lo vesicles and uniform staining was observed where as **SiR-C12DA** showed poor affinity to Lo phases (Figure 5A.7). Bulky structure of the **SiR-C12DA** and short length 12-carbon alkyl chains could be the reason for the low affinity of this probe to tightly packed Lo phases.

Further, we have carried out membrane staining experiment with **SiR-C18, SiR-C12DA** to check the efficacy of probes to stain the cell membranes in living cells. KB-cells were incubated with 20 nM of the probe stock solution in DMSO.

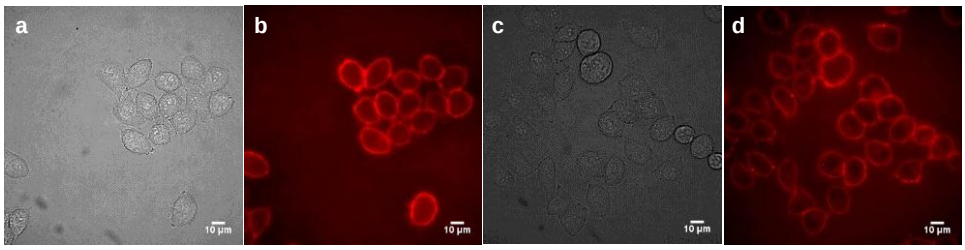

Figure 5A.8. Fluorescence images of living KB cells stained with 20 nM of (b)**SiR-C18,** (d) **SiR-C12DA** and (f) **SiR-C12**. (a & c) represent the KB cells without probe. λ_{max} excitation=640 nm. Photons were collected at red channel. Scale bar 10 µm.

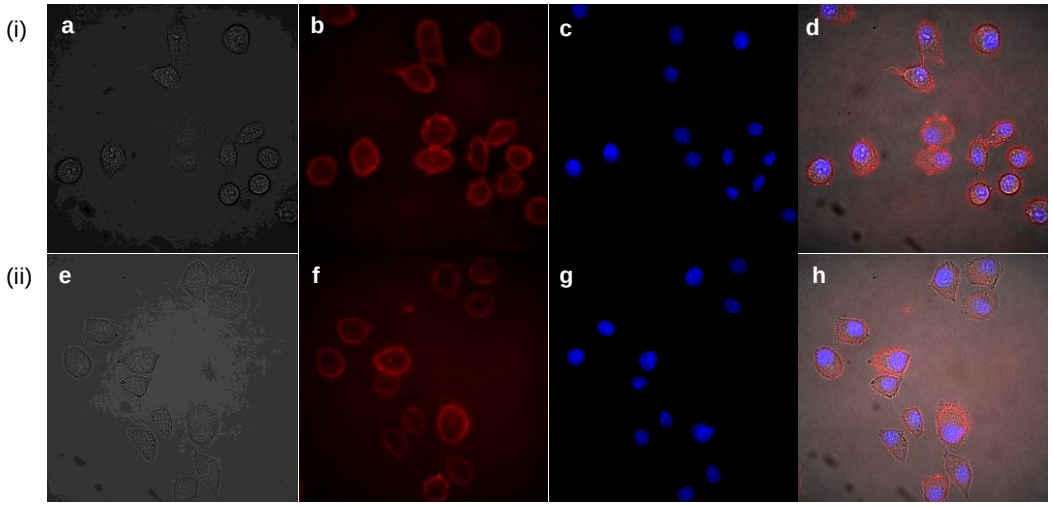

Figure 5A.9. (i) & (ii) Fluorescence images of living KB cells stained with SiR**-C18** & **SiR-C12DA.** (i) and 20 nM of (b) **SiR-C18,** (e) **SiR-C12DA** and co-stained with Hoechst (c&g).(d & h) are merged images. (a & e) represent the KB cells without probe. Photons were collected at the blue and red channel.

SiR-C18, SiR-C12DA showed strong affinity to the cell membrane and uniform staining of the membrane was observed. Moreover, cell membrane imaging under 'no wash' condition was achieved with both **SiR-C18 and SiR-C12DA** probes nevertheless; former showed negligible background signal compare to the latter ones. Moreover, these probes did not show any internalization into the cell even after 30 minutes of incubation, suggesting the strong affinity of the probes to the cell membrane.

We have also carried co-staining experiment with a nuclear staining dye Hoechst. Dual-colour overlay images (Figure 5A. 9) clearly distinguish the cell membrane and intracellular regions, which further confirmed the affinity of these probes to membranes.

5A.5. Conclusion

In Summary, We have successfully developed cell membrane probes based on silicon-rhodamine fluorophore. We have demonstrated the specific ON/OFF switching behaviour of the probes in the hydrophobic membrane environment due to the reversible switching from fluorescent zwitterionic form to non-fluorescent spirocyclic form. Among the probes, **SiR-C12** with a single zwitterionic anchor group showed poor affinity to the membrane with a lot of background signal. **SiR-C12DA** having two zwitterionic anchor groups showed strong affinity to the liquid disordered phase of the membrane with less background signal. However, the bulky nature and 12-C chains hinder the efficient localization this probe in the liquid ordered (Lo) domains. **SiR-C18** with an anchor group having 18-C alkyl chain

showed strong affinity to both Ld and Lo phases of the membrane. 18-C, long-alkyl chain helped the un-bound probe to aggregate in the solution, which resulted in the negligible background signal. Further, we have successfully demonstrated the application of **SiR-C18** and **SiR-C12DA** for imaging plasma membrane in living cells under 'no wash' conditions. Future studies will be focused on the utilization of the ON/OFF switching behaviour of these probes in super-resolution microscopy.

5A.6. References

1. A. S. Klymchenko*, Acc. Chem. Res*., 2017*,* **50***,* 366-375.

2. I. A. Karpenko, M. Collot, L. Richert, C. Valencia, P. Villa, Y. Mély, M. Hibert, D. Bonnet and A. S. Klymchenko, *J. Am. Chem. Soc.*, 2015, **137**, 405-412.

3. K. R. Kampen, *J. Membr. Biol*, 2011, **242**, 69-74.

4. L. D. Bergelson, J. G. Molotkovsky and Y. M. Manevich, *Chemistry and Physics of Lipids*, 1985, **37**, 165-195.

5. Y. Niko, P. Didier, Y. Mely, G.-i. Konishi and A. S. Klymchenko, *Sci. Rep.*, 2016, **6**, 18870.

6. L. M. S. Loura, F. Fernandes, A. C. Fernandes and J. P. P. Ramalho, *Biochim. Biophys. Acta.*, 2008, **1778**, 491-501.

7. I. A. Karpenko, R. Kreder, C. Valencia, P. Villa, C. Mendre, B. Mouillac, Y. Mély, M. Hibert, D. Bonnet and A. S. Klymchenko, *ChemBioChem*, 2014, **15**, 359-363.

8. O. A. Kucherak, S. Oncul, Z. Darwich, D. A. Yushchenko, Y. Arntz, P. Didier, Y. Mély and A. S. Klymchenko, *J. Am. Chem. Soc.*, 2010, **132**, 4907-4916.

9. M. Collot, R. Kreder, A. L. Tatarets, L. D. Patsenker, Y. Mely and A. S. Klymchenko, *Chem. Commun.*, 2015, **51**, 17136-17139.

10. 10. V. V. Shynkar, A. S. Klymchenko, C. Kunzelmann, G. Duportail, C. D. Muller, A. P. Demchenko, J.-M. Freyssinet and Y. Mely, *J. Am. Chem. Soc.*, 2007, **129**, 2187-2193.

11. G. Lukinavičius, K. Umezawa, N. Olivier, A. Honigmann, G. Yang, T. Plass, V. Mueller, L. Reymond, I. R. Corrêa Jr, Z.-G. Luo, C. Schultz, E. A. Lemke, P. Heppenstall, C. Eggeling, S. Manley and K. Johnsson, *Nat Chem*, 2013, **5**, 132-139.

12. G. Lukinavičius, L. Reymond, K. Umezawa, O. Sallin, E. D'Este, F. Göttfert, H. Ta, S. W. Hell, Y. Urano and K. Johnsson, *J. Am. Chem. Soc.*, 2016, **138**, 9365-9368.

13. J. B. Grimm, B. P. English, H. Choi, A. K. Muthusamy, B. P. Mehl, P. Dong, T. A. Brown, J. Lippincott-Schwartz, Z. Liu, T. Lionnet and L. D. Lavis, *Nat Meth*, 2016, **13**, 985-988.

14. S.-n. Uno, M. Kamiya, T. Yoshihara, K. Sugawara, K. Okabe, M. C. Tarhan, H. Fujita, T. Funatsu, Y. Okada, S. Tobita and Y. Urano, *Nat Chem*, 2014, **6**, 681-689.

15. H. Takakura, Y. Zhang, R. S. Erdmann, A. D. Thompson, Y. Lin, B. McNellis, F. Rivera-Molina, S.-n. Uno, M. Kamiya, Y. Urano, J. E. Rothman, J. Bewersdorf, A. Schepartz and D. Toomre, *Nat Biotech*, 2017, **35**, 773-780.

CHAPTER 5B

A FLUOROGENIC BODIPY MOLECULAR ROTOR AS APOPTOSIS MARKER

To be communicated….

5B.1. Introduction

The lipid bilayer of the mammalian plasma membrane is made up different polar lipids and proteins. Plasma membrane shows the asymmetric distribution of the polar lipids in the bilayer wherein the zwitterionic phosphatidylcholine (PC) is present in the outer leaflet of the bilayer and the anionic phosphatidylserine (PS) exclusively located in the inner leaflet.[1,2] This asymmetric distribution is maintained by the intracellular translocases. During the early stages of apoptosis, translocases activity is diminished leading to the exposure of PS on the cell surface.[2] The presence of anionic PS on the cell surface is a hallmark of apoptosis. The presence of anionic PS on the cell surface plays many important roles. It is responsible for the daily clearance of dead cells from the body by phagocytes.[3,4] Moreover, the therapeutic efficacy of the anticancer drugs could be determined by monitoring the apoptosis.[3,4] Hence, apoptosis detection is very important from the biological and clinical standpoint.

Methods such as monitoring the caspase activation,[6] DNA fragmentation[7] were developed for apoptosis detection. One of the most widely used methods for apoptosis monitoring is Annexin V assay. Annexin V reagent is a fluorescently labeled is 35 KDA protein specifically binds to negatively charged PS on the apoptotic cell surface.[3,4] Even though Annexin V is extensively used as apoptosis marker, but it has many limitations. Annexin V has a very short shelf life and its binding requires millimolar concentration of extracellular Ca^{2+}. In addition to this, Annexin V binding is very slow; it needs up to 1 hour incubation time for complete binding.[3-5] Because of these limitations, research was focused on the development of alternative methods or reagents for apoptosis detection.

Recently, fluorescently labeled cationic Zn-dipicolylamine (DPA) complexes were reported as the alternatives for Annexin V reagents.[3]These Zn-DPA complexes forms a strong association with anionic PS-rich membranes and are useful in the apoptosis detection. However, most of these probes suffer from intrinsic fluorescence[8-11] and the probes that turn ON fluorescence upon PS binding are rare in the literature.[5,12]

Fluorogenic probes that turn ON the fluorescence upon interaction with the target are very useful in imaging with minimum background signal. One such approach to get turn ON signal is to use the molecular rotors.[13-15] Molecular rotors are a group

of twisted intramolecular charge transfer (TICT) molecules wherein the deexcitation from the photoexcited state occurs through nonradiative manner.[13,14] Molecular rotors are highly sensitive to surrounding viscosity; their emission is completely dependent on solvent viscosity.[13-15] Molecular rotors were successfully used as viscosity probes in cells, turn on probes for membranes and protein aggregation.[16-21] One way to modify the molecular rotors for practical application is the attachment of target-specific ligands to parent probe without modifying its photophysical behavior.[13] However, probes based on receptor-ligand interaction are scarce in the contemporary literature. Recently, one such probe was reported for oxytocin receptor.[22]

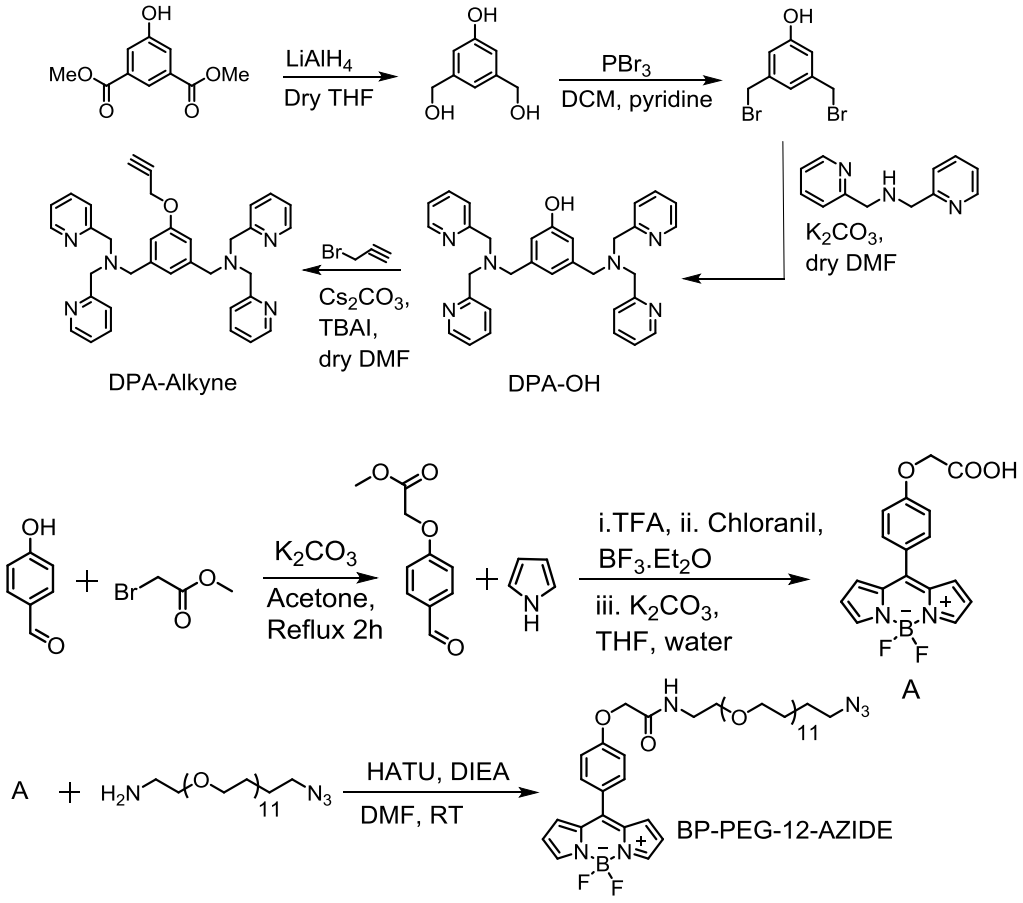

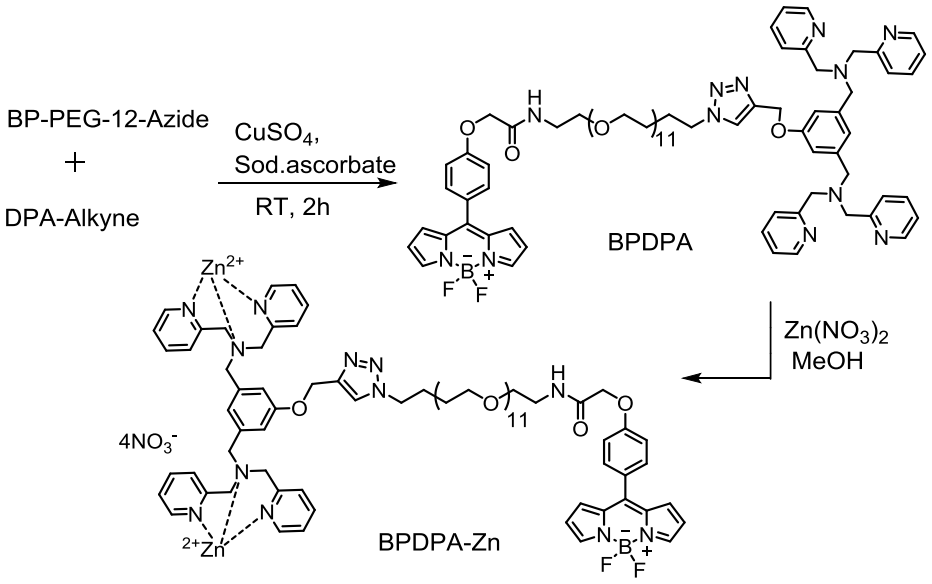

Scheme 5B.1. Synthetic route adopted for **BPDPA-Zn**.

Herein we report a BODIPY molecular rotor **BPDPA-Zn**, as a fluorogenic probe for apoptosis detection. **BPDPA-Zn** showed turn ON fluorescence response upon binding to negatively charged PS-rich membranes. Moreover, this reagent was successfully applied to detect the early stages of apoptosis in HeLa cells.

5B.2. Experimental Section

5B.2.1. Materials

All the chemicals and solvents were procured from Sigma Aldrich or TCI and used as received without further purification. Actinomycin D, Hank's balanced salt solution (HBSS) was from Gibco and Annexin V-FITC Kit was obtained from Immunotech. Egg yolk phosphatidyl-choline, bovine brain phosphatidylserine were obtained from Sigma-Aldrich

5B.2.2. Analytical Methods

^{1}H and ^{13}C NMR spectra were recorded on Bruker Avance III 400 MHz spectrometer. Mass spectra were obtained using Agilent Q-TOF 6520 spectrometer and JEOL JM AX 505 HA mass spectrometer. Absorption spectra were recorded on a Cary 4000 spectrophotometer (Varian). Fluorescence spectra were recorded on a Fluoromax-4 (Jobin Yvon, Horiba) spectrofluorometer. Emission measurements were systematically done at 20^{o}C, unless indicated otherwise. All the spectra were corrected from the

fluorescence of the corresponding blank (suspension of lipid vesicles without the probe) and for the wavelength-dependent response function of the detector. Lifetime data was acquired using Horiba TCSPC (Time-Correlated Single Photon Counting) system with excitation at 443 nm. 10000 counts were collected for each lifetime measurement, and all the measurements were performed in triplicate using the DAS software to confirm the results. The calculation of the lifetimes was carried out with a single or biexponential decay function to each decay plot to extract the lifetime information using the DAS6 fluorescence decay analysis software. Relative fluorescence quantum yields were measured using fluorescein in 0.1 M aqueous NaOH (QY = 0.92) as standard. Large unilamellar vesicles (LUVs) were prepared Lipex Biomembranes extruder (Vancouver, Canada).

5B.2.3. General experimental methods for UV-Vis and fluorescence studies

A stock solution of **BPDPA-Zn** (1×10^{-3}M) was prepared in DMSO and the same solution was used for all the studies after appropriate dilution with aqueous buffer solution. A 20 mM phosphate buffer (pH 7.4) was used for all the spectroscopic measurements, unless mentioned otherwise For spectroscopic measurements, the stock solution of the probe was further diluted by using phosphate buffer and the effective final concentration was made as 2 μM. All luminescence measurements were done using λ_{Ext} = 467 nm with an emission slit width of 2 nm.

5B.2.4. Lipid Vesicles preparation

Egg yolk phosphatidyl-choline, bovine brain phosphatidylserine were obtained from Sigma-Aldrich. Large unilamellar vesicles (LUVs) were obtained by the extrusion method as described in the literature[7]. Briefly, a suspension of multilamellar vesicles was extruded by using a Lipex Biomembranes extruder (Vancouver, Canada). The size of the filters was first 0.2 *μ*m (7 passages) and after that 0.1 *μ*m (10 passages). Mean diameter of the monodisperse vesicles were measured with a Malvern Zetamaster 300 (Malvern, U.K.) and it was found to be 0.11 to 0.12 μm. LUVs were labeled with 2 *μ*M of the the probe in dimethyl sulfoxide to 1-mL solutions of vesicles. A 20 mM phosphate buffer, pH 7.4, was used in these experiments. The fluorescence experiments were performed immediately after addition of the aliquot. Concentrations of the probes and lipids were generally 1 and 200 *μ*M, respectively.

5B.2.5. Cell culture preparation

HeLa cells were grown in minimum essential medium (MEM, Gibco-Invitrogen) with 10% fetal bovine serum (FBS, Lonza), 1% nonessential amino acids (Gibco- Invitrogen), 1% MEM vitamin solution (Gibco-Invitrogen), 1% L-Glutamine (Sigma-Aldrich), and 0.1% antibiotic solution (gentamicin, Sigma-Aldrich) at 37 °C in humidified atmosphere containing 5% CO_2. Cells were seeded onto a chambered coverglass (IBiDi) at a density of 5 × 104 cells/well and treated with Actinomycin-D (10 μM/mL) for 18 hours to induce apoptosis. For imaging, the culture medium was removed and the attached cells were washed with Opti-MEM (Gibco−Invitrogen). Next, the cells were incubated in Opti-MEM with **BPDPA-Zn** (2 μM) and Annexin V Alexafluor-568. The cells were washed two times with HBSS and visualized in HBSS.

5B.3. Synthesis and Characterization

BODIPY rotor and DPA-OH was synthesized by following the literature methods.[23]

5B.3.1. Synthesis of DPA-alkyne

DPA-OH (50 mg, 0.096 mmol) was taken in 3 ml of dry DMF. To this solution, CS_2CO_3 (75 mg, 0.230 mmol) and TBAI (17.85 mg) was added and stirred at room temperature for 10 minutes. Propargyl bromide (17.26 mg, 0.145 mmol) was added and it was stirred 80^o C for 20 hours. The solvent was evaporated completely and the crude product was purified by neutral alumina column using methanol and dichloromethane as eluents. Yield - 74%. ^{1}H NMR (METHANOL-d_4, 400 MHz): δ (ppm) 3.24 (1H, m), 3.61 (4H, s), 3.75 (8H, s), 4.72 (2H, s), 6.93 (2H, s), 7.03 (1H, s), 7.23 (4H, s), 7.64 (4H, d, *J* = 7.65 Hz), 7.72-7.76 (4H, t), 8.40 (4H, s). ^{13}C NMR (METHANOL-d_4, 100 MHz): δ (ppm) 55.24, 58.36, 59.51, 75.50, 78.64, 113.99, 122.37, 123.28, 137.23, 140.24, 148.03, 157.98, 159.17. LRMS (ESI): m/z [M+H] 555.223.

5B.3.2. Synthesis of BODIPY-PEG-12-Azide

BODIPY acid (100 mg, 1 equiv.) was dissolved in dry DMF 10 ml. To this mixture, DIEA (150 μl, 3 equiv.) was added and stirred for 10 minutes. Then PEG12-Azide (250 mg, 1.5 equiv.) and HATU (132 mg, 1.2 equiv.) was added and stirred at room temperature for 2 hours. Reaction was monitored by TLC. After completion, DMF was evaporated and compound was diluted with dichloromethane and purified by column chromatography

using CH_2Cl_2 and methanol as eluents to get orange gel. Yield = 62 %. ^{1}H NMR (METHANOL-d_4, 400 MHz): δ (ppm) 1.28 (2H, s), 3.35 (4H, s), 3.50 (2H, s), 3.61 (45H, s), 4.67 (2H, s), 6.63 (2H, s), 7.03 (2H, s), 7.20 (2H, d, *J* = 7.65 Hz), 7.61-7.63 (2H, d, *J* = 7.71 Hz), 7.94 (2H, s). ^{13}C NMR (METHANOL-d_4, 125 MHz): δ (ppm) 29.35, 38.72, 50.38, 66.91, 69.07, 69.70, 70.04, 114.83, 118.31, 127.00, 131.25, 132.40, 134.63, 143.53, 147.10, 160.35, 169.16. HRMS (ESI): m/z calculated for $C_{41}H_{61}N_6O_{13}BF_2Na$ [M+Na] 917.4250 found 917.4247.

5B.3.3. Synthesis of BPDPA

DP-alkyne (20 mg, 1 equiv.) and BODIPY-PEG12-AZIDE (38.65 mg, 1.2 equiv.) was dissolved in DMF (2 ml). $CuSO_4$ (5mg) and sodium ascorbate (5 mg) was dissolved separately in H_2O. Both these solutions were mixed and vortexed for 2 minutes. Once the colour changes from black to orange, it was added to the reaction mixture and stirred at room temperature for 2 hours. Reaction was monitored by TLC. Upon completion, solvents were evaporated completely and the product was purified by neutral alumina column chromatography using CH_2Cl_2 and CH_3OH as eluents. Yield = 58% ^{1}H NMR (400 MHz ,METHANOL-d_4) δ (ppm) 3.21-3.50 (2H, t), 3.51 (13H, s), 3.55 (18H, s), 3.59-3.61 (14H, d), 3.75 (8H, s), 3.85 (2H, s), 4.56 (2H, s), 4.66 (2H, s), 5.17 (2H, s), 6.60 (2H, s), 6.97-7.00 (4H, d, *J* = 10.04 Hz),, 7.05 (1H, s), 7.18-7.20 (2H, d, *J* = 7.78 Hz), 7.24 (4H, br), 7.58-7.60 (2H, d, *J* = 7.40 Hz), 7.64-7.66 (4H, d, *J* = 7.40 Hz), 7.74-7.78 (4H, t), 7.92 (2H, s), 8.11 (1H, s), 8.40 (4H, s). ^{13}C NMR (METHANOL-d_4, 100 MHz): δ (ppm) 38.74, 50.09, 58.13, 58.37, 59.49, 61.11, 66.91, 69.03, 70.13, 113.89, 114.81, 118.28, 121.88, 122.41, 123.27, 124.81, 126.98, 131.23, 132.37, 134.59, 137.31, 140.38, 143.50, 147.08, 148.06, 158.64, 159.15, 160.32, 169.13. LRMS (ESI): [M/2+H] 725.319.

5B.3.4. Synthesis of BPDPA-Zn

BPDPA (12 mg, 8.28 mmol) was taken in 3 ml of methanol: water mixture (1:1). To this $Zn(NO_3)_2$ (4.92 mg, 16.56 mmol) was added and stirred for 1 hour. Solvents were evaporated and dried to get BPDPA-Zn as brown solid with a quantitative yield. ^{1}H NMR (400 MHz, METHANOL-d_4) δ (ppm) 3.21-3.25 (3H, t), 3.47 (3H, s), 3.55-3.59 (40H, d), 3.78 (4H, s), 3.90-4.00 (6H, m), 4.31-4.35 (4H, d), 4.62-4.66 (4H, d), 5.25 (2H, s), 6.61 (2H, s), 6.73 (1H, s), 6.93 (2H, s), 7.02 (2H, s), 7.19-7.21 (2H, d, *J* = 7.15 Hz), 7.57-7.61 (6H, br), 7.67 (4H, br), 7.90 (2H, s) 8.11-8.13 (4H, m), 8.23 (1H, br), 8.68 (4H, br). HRMS (ESI): [M/4 + Na] 418.8782.

5B.4 Results and Discussion

Synthetic route adopted for **BPDPA-Zn** is given in the scheme 5B.1. BODIPY rotor was coupled with PEG-12 azide spacer to increase the water solubility of the probe and the azide group helped in further functionalization of the probe with target-specific ligand. Bis-dipicolylamine (bis-DPA) ligand was synthesized by following the literature method.[23] O-alkylation of bis-DPA with propargyl bromide provided a clickable alkyne handle. Azide-alkyne click reaction of the rotor and bis-DPA followed by complexation with $Zn(NO_3)_2$ in 1:1 methanol: water resulted in the final probe **BPDPA-Zn**. Products were characterized by standard analytical methods.

The absorption spectrum of **BPDPA-Zn** in 20 mM phosphate buffer shows a sharp absorption band at 498 nm due to Π- Π* transition of the BODIPY unit. Upon excitation at 467 nm, the probe shows an emission band at 514 nm (figure 5B.1). Viscosity effect on the emission behaviour of **BPDPA-Zn** conjugate was evaluated in glycerol and methanol binary mixture. The probe showed poor emission in pure methanol solvent (Φ_F = 0.009, Table 5B.1) suggesting the existence of TICT state.

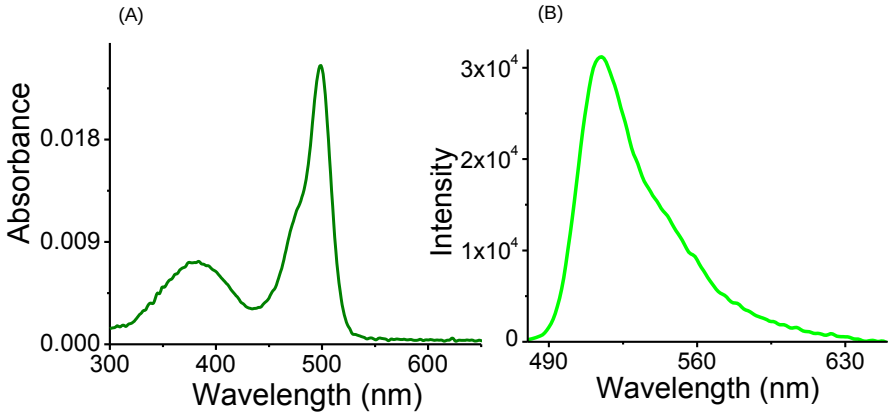

Figure 5B.1. (A) Absorption and (B) emission spectra of **BPDPA-Zn** in 20 mM phosphate buffer pH 7.4. Excitation – 467 nm.

The charge-separated TICT state was strongly stabilized by the polar solvent molecule, which resulted in the poor emission quantum yield in methanol. Emission intensity was gradually increased with the increase in the percentage of glycerol (Figure 5B.2) indicating the reduction in the non-radiative decay process with the increase in the solvent viscosity.

Percentage of methanol	Fluorescence quantum yield (Φ)
100	0.009
90	0.02
75	0.03
50	0.06
40	0.11
30	0.14
20	0.16
10	0.18
0	0.32

Table 5B.1. Quantum yield variation of **BPDPA-Zn** in glycerol: methanol mixture.

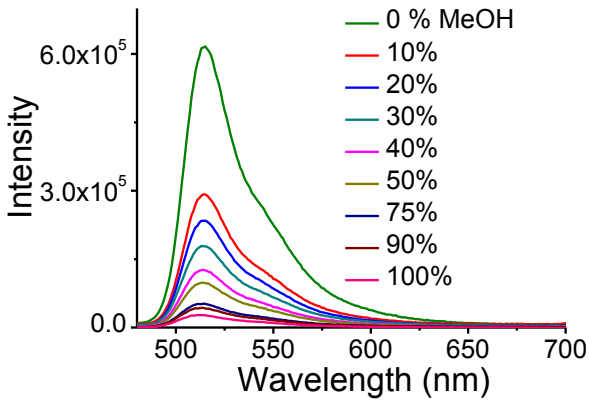

Figure 5B.2. Emission response of **BPDPA-Zn** in glycerol: methanol mixture (0-100%)

Φ_F increased dramatically with the increase in the ratio of glycerol/methanol (Table 5B.1). Overall a 35-fold increase in the quantum yield was observed when the percentage of glycerol was increased from 0-100%. These results suggested that the emission intensity and Φ_F of **BPDPA-Zn** were dependent on the viscosity of the solvent. Moreover, the molecular rotor properties of the BODIPY unit were retained even after the conjugation of the rotor with bis-DPA.

Next, we have measured the lifetime of **BPDPA-Zn** in glycerol/methanol binary mixture to determine the viscosity dependence on the lifetime of **BPDPA-Zn**. A linear increase in the lifetime from 0.3 ns-4.22 ns was observed with increase in the glycerol content from 0-99% (Figure 5B. 3 and Table 5B. 2). These results

confirmed that the emission, quantum yield and lifetime of **BPDPA-Zn** is strongly dependent on the viscosity of the solvent and it behaves as a molecular rotor.

After evaluating the molecular rotor properties of **BPDPA-Zn**, its efficacy as a fluorogenic probe for apoptosis detection were tested in lipid vesicles. To mimic the apoptotic cell membranes, large unilamellar vesicles (LUVs) having a different ratio of zwitterionic PC and anionic PS (PC: PS 0-50%) were prepared by the extrusion method. Liposomes were labeled with 2 μM of the **BPDPA-Zn** and emission spectra were recorded immediately after the addition of the probe. Initially, probe showed a weak emission at 514 nm.

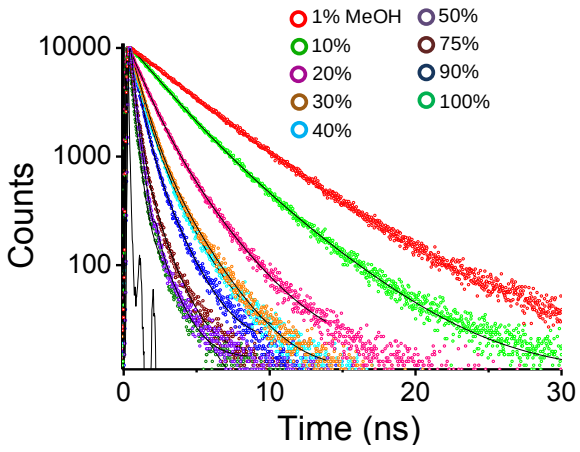

Figure 5B.3. Emission decay traces of **BPDPA-Zn** in glycerol: methanol mixture.

Percentage of methanol	Lifetime (in ns)
100	0.30
90	0.35
75	0.41
50	0.66
40	0.86
30	0.96
20	1.45
10	2.88
1	4.22

Table 5B.2. Lifetime data of **BPDPA-Zn** in glycerol: methanol mixture.

No significant change in the emission was observed in the samples containing 100 % zwitterionic PC suggesting the poor affinity of **BPDPA-Zn** to zwitterionic PC vesicles (Figure 5B. 4). A significant enhancement in the emission was observed in the samples containing anionic PS. Emission intensity was gradually increased with the increase in the concentration of PS (0-50%). This result confirmed that **BPDPA-Zn** binds to anionic PS with the turn ON emission response.

Remarkable selectivity of the **BPDPA-Zn** to anionic vesicles inspired us to explore the possibility of using the probe for apoptosis detection. First, HeLa cells were treated with Actinomycin D (10 µM/mL) for 18 hours to induce the apoptosis. The cells were subsequently stained with **BPDPA-Zn** (2 µM).

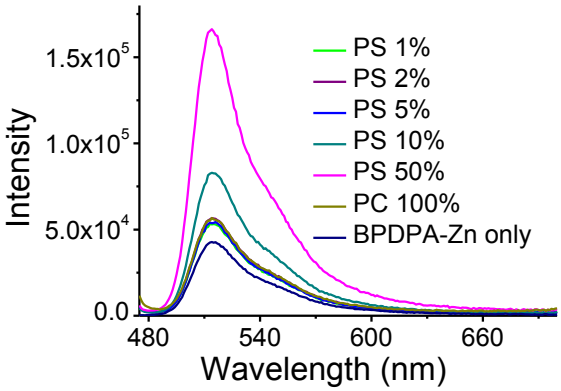

Figure 5B.4. Emission response of **BPDPA-Zn** in LUVs composed of a different percentage of PS.

As shown in the figure 5B.5a, bright green fluorescence was observed from the cell membranes indicating that the cells were in the early stages of the apoptosis and the probe **BPDPA-Zn** could efficiently bind to anionic PS on the cell membrane and light up the apoptotic cell membranes. Apoptotic cells were also stained with commercially available Annexin -V Alexafluor-568 (Figure 5B.5b) and compared with the **BPDPA-Zn**. Overlay image in the figures 5B and 5c confirmed that our probe could detect the apoptotic cells as efficiently as the commercially available Annexin V. Moreover, it works even in the absence of extracellular Ca^{2+}, a major limitation associated with Annexin V based probes.

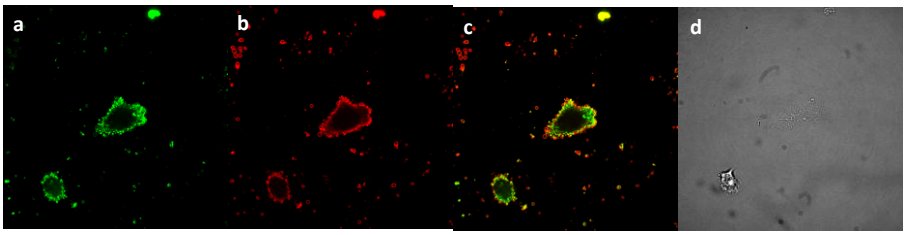

Figure 5B.5. Confocal micrographs of apoptotic HeLa cells treated with; (a) **BPDPA-Zn** (2 µM), (b) Annexin V-Alexafluor-568, (c) merged image of a & b, (d) bright filed image. Apoptosis was induced by treating the cells with Actinomycin D for 18 hours.

Further, we have carried out a control experiment in the normal cells (not treated with Actinomycin D) to verify the specificity of the reagent to apoptotic cells. As shown in figure 5B.6a, no specific membrane staining was observed in the normal HeLa cells treated with **BPDPA-Zn** as well as with Annexin V -Alexafluor-568 (figure 5B.6b). This result further confirmed the specificity and efficacy of **BPDPA-Zn** for the detection of apoptosis.

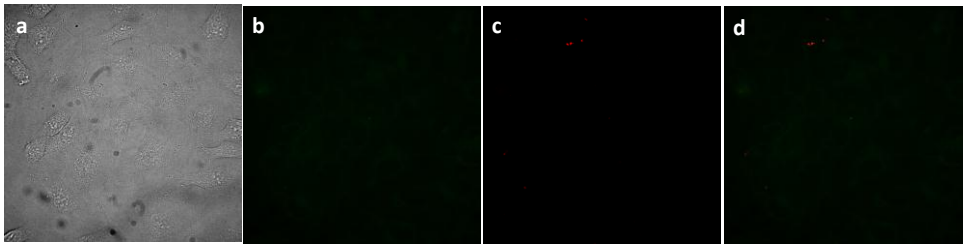

Figure 5B.6. Confocal micrographs of HeLa cells without Actinomycin D treatment; (a) bright field image, (b) Cells stained with **BPDPA-Zn** (2 µM), (c) Annexin V-Alexafluor-568, (d) Merged image of b & c.

5B.5. Conclusion

In summary, we have developed a BODIPY-DPA based molecular rotor **BPDPA-Zn,** as a fluorogenic probe for the detection of apoptosis. The emission, quantum yield and the lifetime of the probe showed a strong dependence on the viscosity of the solvent thus confirming the molecular rotor properties. The probe specifically binds to anionic phospholipid with turn ON emission response. The probe showed no interaction with the normal cells whereas it showed absolute specificity to apoptotic cells with bright green emission. Comparative studies with commercial apoptosis marker Annexin V, confirmed the efficiency of the probe to report early stages of apoptosis. Moreover, this is the first attempt to develop a molecular rotor for apoptosis imaging. Considering the remarkable specificity and turn ON

emission response, we believe this probe could be a better alternative to the Annexin V based reagents as apoptosis markers.

5B.6. References

1. O. A. Kucherak, S. Oncul, Z. Darwich, D. A. Yushchenko, Y. Arntz, P. Didier, Y. Mély and A. S. Klymchenko, *J. Am. Chem. Soc.*, 2010, **132**, 4907-4916.

2. M. Mourdjeva, D. Kyurkchiev, A. Mandinova, I. Altankova, I. Kehayov and S. Kyurkchiev, *Apoptosis*, 2005, **10**, 209-217.

3. D. R. Rice, K. J. Clear and B. D. Smith, *Chem. Commun.*, 2016, **52**, 8787-8801.

4. A. V. Koulov, K. A. Stucker, C. Lakshmi, J. P. Robinson and B. D. Smith, *Cell Death Differ*, 2003, **10**, 1357-1359.

5. V. V. Shynkar, A. S. Klymchenko, C. Kunzelmann, G. Duportail, C. D. Muller, A. P. Demchenko, J.-M. Freyssinet and Y. Mely, *J. Am. Chem. Soc.*, 2007, **129**, 2187-2193.

6. Y. Wu, D. Xing, S. Luo, Y. Tang and Q. Chen, *Cancer Lett.*, **235**, 239-247.

7. P. R. Walker, J. Leblanc, B. Smith, S. Pandey and M. Sikorska, *Methods*, 1999, **17**, 329-338.

8. K. J. Clear, K. M. Harmatys, D. R. Rice, W. R. Wolter, M. A. Suckow, Y. Wang, M. Rusckowski and B. D. Smith, *Bioconjugate Chem.*, **27**, 363-375.

9. R. G. Hanshaw, C. Lakshmi, T. N. Lambert, J. R. Johnson and B. D. Smith, *ChemBioChem*, 2005, **6**, 2214-2220.

10. R. G. Hanshaw and B. D. Smith, *Bioorg. Med. Chem.*, 2005, **13**, 5035-5042.

11. B. A. Smith, W. J. Akers, W. M. Leevy, A. J. Lampkins, S. Xiao, W. Wolter, M. A. Suckow, S. Achilefu and B. D. Smith, *J. Am. Chem. Soc.*, **132**, 67-69.

12. Q. Hu, M. Gao, G. Feng, X. Chen and B. Liu, *Acs Appl. Mater. Interfaces*, 2015, **7**, 4875-4882.

13. M. A. Haidekker and E. A. Theodorakis, *Org. Biomol.Chem.*, 2007, **5**, 1669-1678.

14. M. K. Kuimova, G. Yahioglu, J. A. Levitt and K. Suhling, *J. Am. Chem. Soc.*, 2008, **130**, 6672-6673.

15. A. S. Klymchenko, *Acc. Chem. Res*., 2017, **50**, 366-375.

16. M. t. KubA¡nkovA, I. LApez-Duarte, J. A. Bull, D. M. Vadukul, L. C. Serpell, M. de Saint Victor, E. Stride and M. K. Kuimova, *Biomaterials*, 2017, **139**, 195-201.

17. M. A. H. Alamiry, A. C. Benniston, G. Copley, K. J. Elliott, A. Harriman, B. Stewart and Y.-G. Zhi, *Chem. Mater.*, 2008, **20**, 4024-4032.

18. L. E. Shimolina, M. A. Izquierdo, I. Lapez-Duarte, J. A. Bull, M. V. Shirmanova, L. G. Klapshina, E. V. Zagaynova and M. K. Kuimova, *Sci. Rep.*, 2017, **7**, 41097.

19. T. T. Vu, R. Meallet-Renault, G. Clavier, B. A. Trofimov and M. K. Kuimova, *J. Mater. Chem. C*, 2016, **4**, 2828-2833.

20. P. S. Sherin, I. Lopez-Duarte, M. R. Dent, M. Kubankova, A. Vysniauskas, J. A. Bull, E. S. Reshetnikova, A. S. Klymchenko, Y. P. Tsentalovich and M. K. Kuimova, *Chem. Sci.*, 2017, **8**, 3523-3528.

21. JacekÂ T. Mika, AlexanderÂ J. Thompson, MichaelÂ R. Dent, NicholasÂ J. Brooks, J. Michiels, J. Hofkens and MarinaÂ K. Kuimova, *Biophys. J.*, 2016, **111**, 1528-1540.

22. I. A. Karpenko, Y. Niko, V. P. Yakubovskyi, A. O. Gerasov, D. Bonnet, Y. P. Kovtun and A. S. Klymchenko, *J. Mater. Chem. C*, 2016, **4**, 3002-3009.

23. D. Zamora-Olivares, T. S. Kaoud, K. N. Dalby and E. V. Anslyn, *J. Am. Chem. Soc.*, 2013, **135**, 14814-14820.

Conclusion of the Thesis

The thesis entitled "*Synthesis of Fluorescent Probes for Specific Recognition and Imaging Applications*" describes the design and synthesis of new fluorescent molecules that are capable of detecting and monitoring the various analytes having biological significance. Bioimaging applications of the probes were explored through modern microscopy techniques. The first chapter is the introductory chapter, which describes the importance of fluorescent probes in analyte monitoring and bioimaging. Some of the existing fluorescent probes in the literature for the detection of biologically important analytes and the reagents that are available for imaging are briefly described.

Chapter 2 describes a chemodosimetric reagent **L** capable of specific detection of Cys in an aqueous medium as well as in Hct116 living cells. This reagent is capable of specific detection of Cys in the presence of various amino acids, competing bio thiols and ions of biological significance with a visual colour change as well as turn ON fluorescence response. This colorimetric and fluorescence response was utilized to develop simple, cost-effective test strips for Cys detection. Moreover, **L** could monitor the Cys released from a commercial Cys supplement drug NAC in hepatocytes. In addition to this, the application of **L** in the fluorescence detection of Cys residues present in proteins was demonstrated by using whey proteins extracted from cow milk.

Chapter 3 describes a coumarin-acrylate based enzyme specific reagent **CA,** capable of specific detection and quantification an important enzyme and biomarker aminoacylase-1 (ACY-1). Moreover, this reagent is also capable of detecting Cys as well as reporting the oxidative stress induced by reactive oxygen species inside the living cells. Photophysical properties of the probe were studied in detail. Application of the probe in monitoring intracellular Cys levels in normal HEK 293T cells as well as in cancerous SW 480 cells was demonstrated by confocal imaging. Moreover, **CA** could detect and quantify the ACY-1 in an aqueous solution as well as in blood serum samples. ACY-1 is an important biomarker in patients with delayed DGF and the treatment is based on the quantity of the biomarker released. The possible application of CA in quantifying ACY-1 in stimulated blood serum samples was demonstrated and the results were compared with the existing commercial reagents.

Conclusion

Chapter 4 deals with a BODIPY based hydrogen polysulfide (H_2S_n, n>1) probe **MB-S_n** capable of specific detection of H_2S_n in an aqueous medium. Moreover, this reagent is specific to endoplasmic reticulum region of the cells and it could detect the H_2S_n localized in the sub-cellular organelle. In addition to this, an important feature of this probe is its compatibility with super-resolution microscopy, precisely structured illumination microscopy (SIM). Further, application of the probe in imaging intracellular H_2S_n in RAW 264.7 macrophages was demonstrated using super-resolution SIM and 3D-SIM microscopy.

Cell membrane is a foremost barrier responsible for the movement of ions or molecules in and outside of the cell. Cell membrane plays many important roles and it is the outer most layer accessible to drug targets. Chapter 5A describes the three near-infrared emissive silicon-rhodamine (SiR) based membrane probes **SiR-C12**, **SiR-C18** and **SiR-C12DA**. Reversible ON/OFF switching behaviour of SiR with respect to the surrounding environment was utilized to develop environment-sensitive membrane probes. Among the probes, **SiR-C18** and **SiR-C12DA** showed excellent affinity to model membranes with turn ON fluorescence response. Further application of the probes in imaging plasma membrane was demonstrated in live KB cells using fluorescence microscopy. Long chain hydrophobic carbon chains present on the probes helped the unbound probes to self-assemble in the aqueous medium, and in turn, converted to non-fluorescent form. This helped to carry out live cell imaging under 'no wash' conditions.

Apoptosis or 'programmed cell death' is an important phenomenon which is happening inside the body. Apoptosis has immense biological significance and it is one of the prime methods used to determine the efficacy of any cancer treatment. Chapter 5B deals with a BODIPY based molecular rotor BPDPA-Zn, capable of reporting apoptosis through turn ON fluorescence response. Cationic DPA-Zn ligand is linked with the probe to recognise the anionic phosphatidylserine present on the apoptotic membrane surface. Photophysical properties of the molecular rotor were studied in detail. BPDPA-Zn showed strong affinity to anionic membrane surface in model membranes with turn ON fluorescence response. Further application of the probe in imaging early stages of apoptosis was demonstrated using apoptotic HeLa cells. Efficacy of the reagent was compared with the commercially available Annexin V based apoptosis probe.

Overall an attempt has been made to develop new fluorescent probes for specific recognition and imaging. Analyte responsive probes for Cys, ACY-1, H_2S_n and imaging reagents for

apoptosis and cell membrane were developed and their optical responses with the targets were studied in detail. Along with the solution studies, application of the probes for biological imaging is also explored. Some of the probes could also be used for imaging without washing steps. Wherever is possible, the results were compared with the commercially available methods or toolkits. Optical properties of the probes were fine-tuned with the synthetic modifications and the turn-ON emission probes ranging from visible to near-infrared were achieved. Some of the probes also showed excellent compatibility with the modern microscopic techniques which demand more photostable fluorophores. So, the design strategies and the results discussed in this thesis are interesting and it will certainly be useful in designing better and efficient molecules for specific detection and imaging.

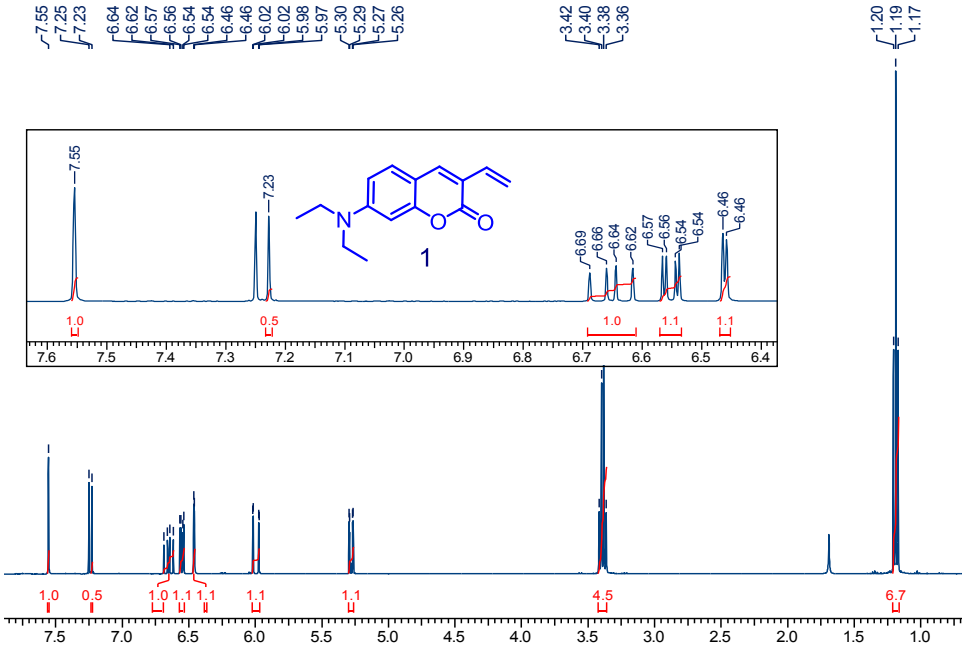

Figure 1. ^{1}H NMR spectrum of compound 1 recorded in $CDCl_3$.

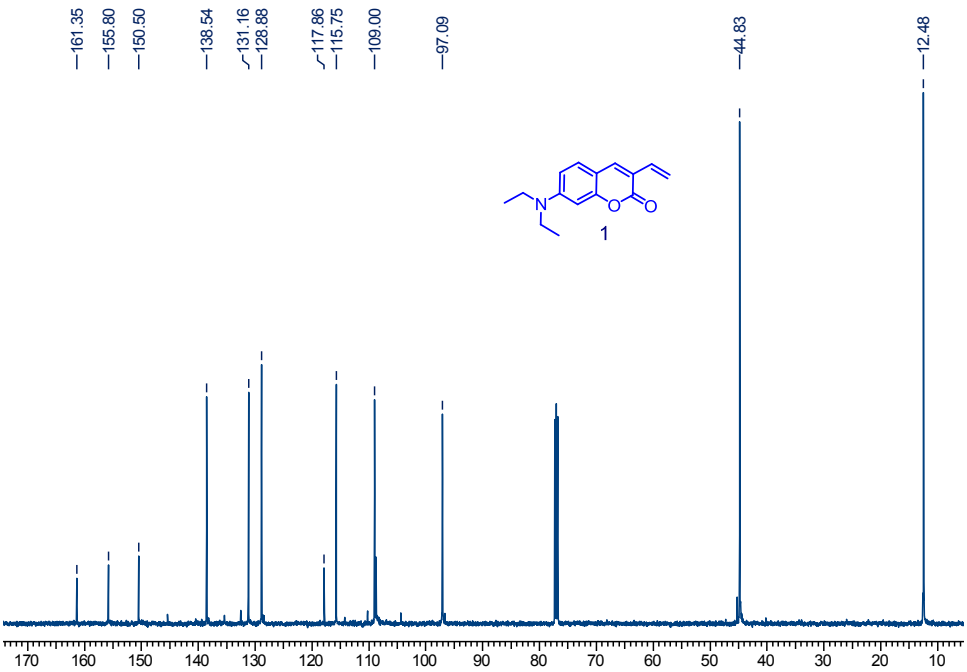

Figure 2. ^{13}C NMR spectrum of compound 1 recorded in $CDCl_3$.

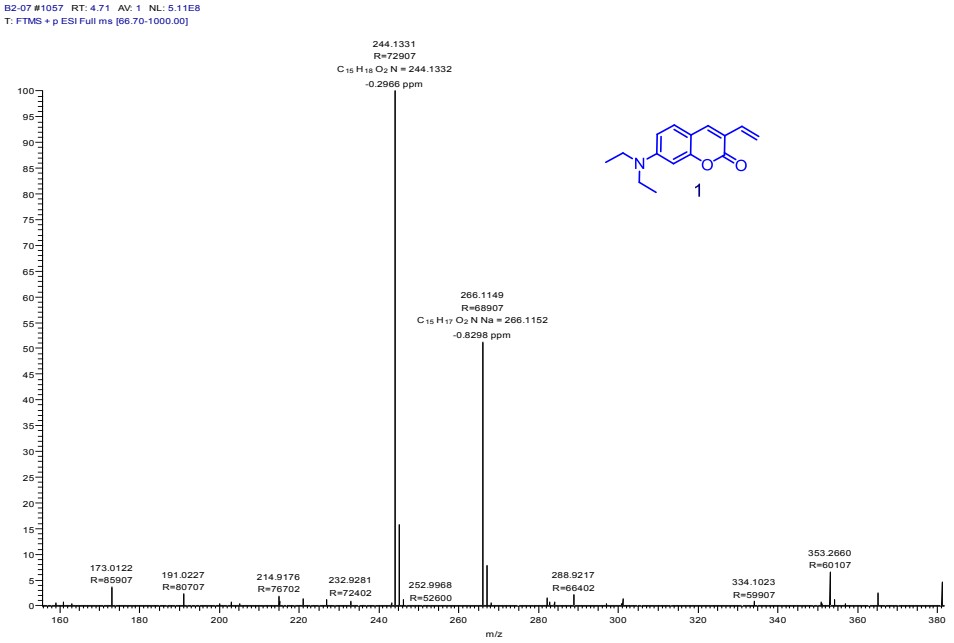

Figure 3. HRMS spectrum of compound 1.

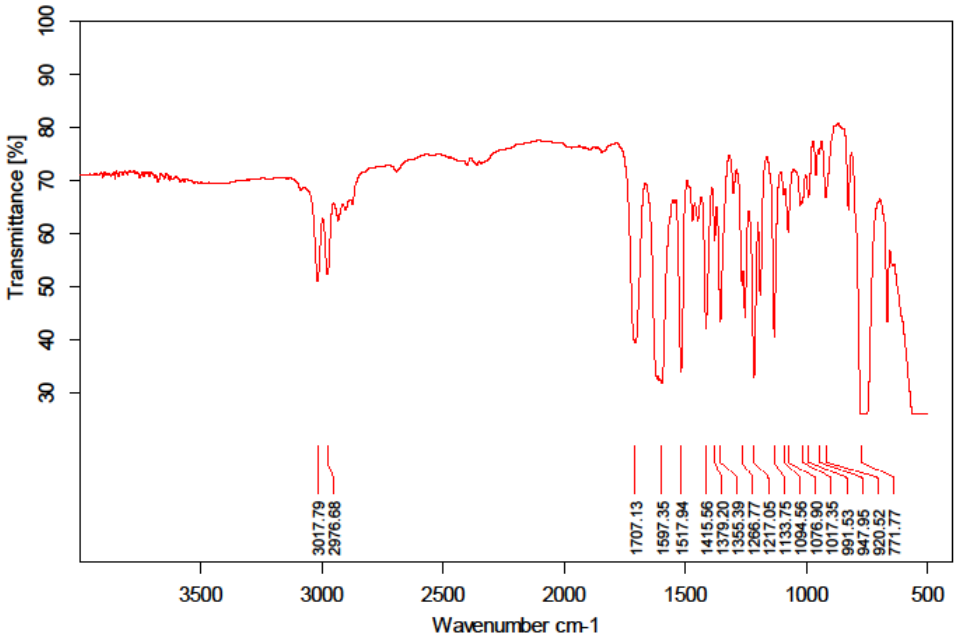

Figure 4. IR spectrum of compound 1.

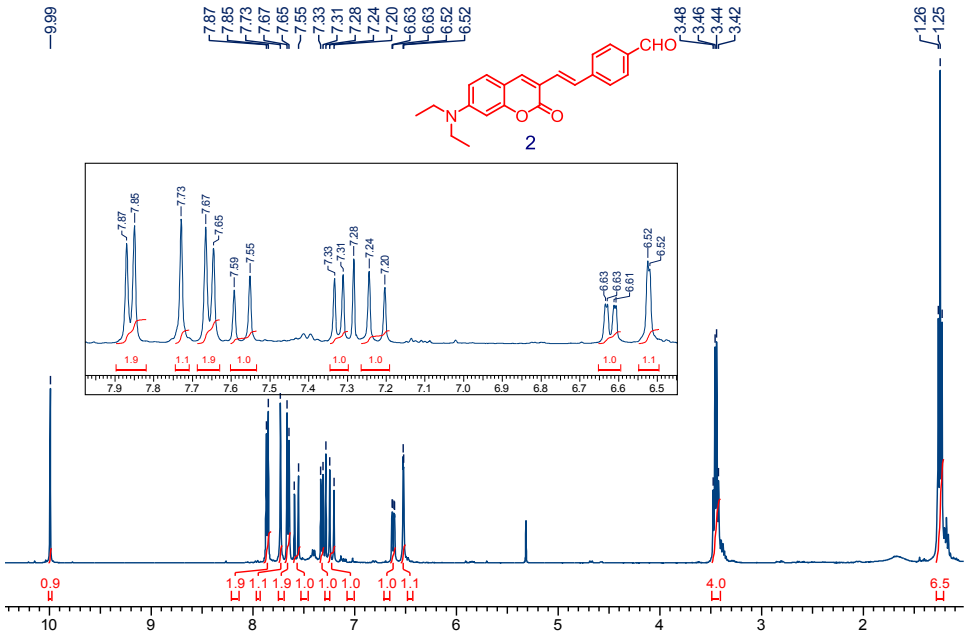

Figure 5. ^{1}H NMR spectrum of compound 2 recorded in $CDCl_3$.

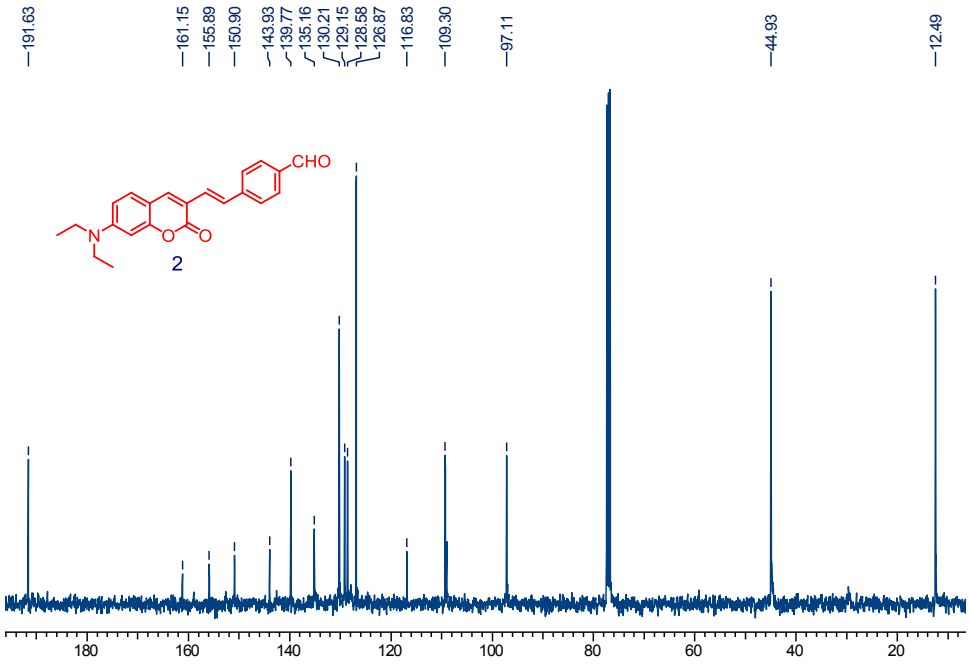

Figure 6. ^{13}C NMR spectrum of compound 2 recorded in $CDCl_3$.

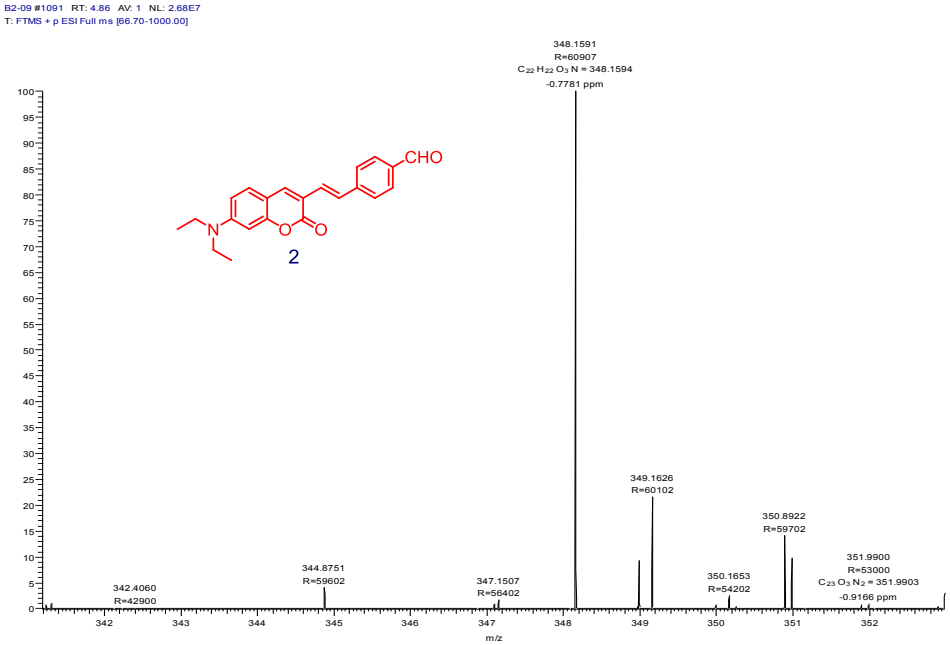

Figure 7. HRMS spectrum of compound 2.

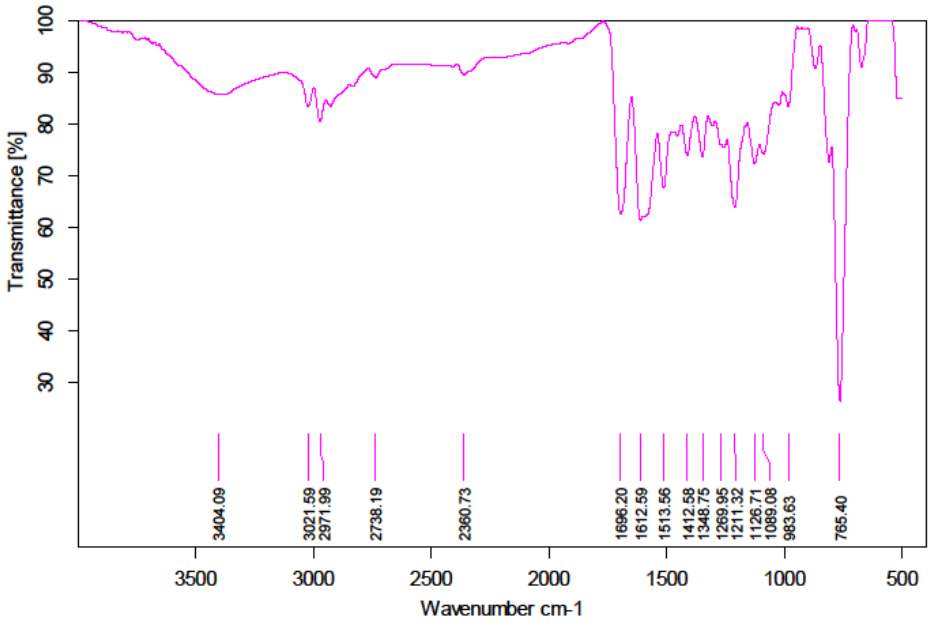

Figure 8. IR spectrum of compound 2.

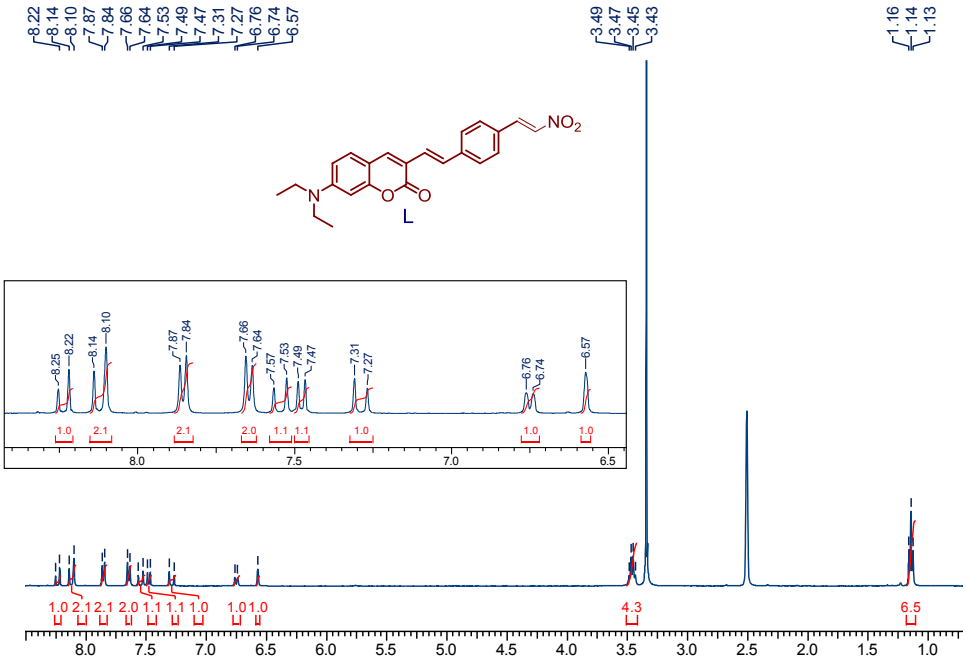

Figure 9. ^{1}H NMR spectrum of **L** recorded in DMSO-d_6.

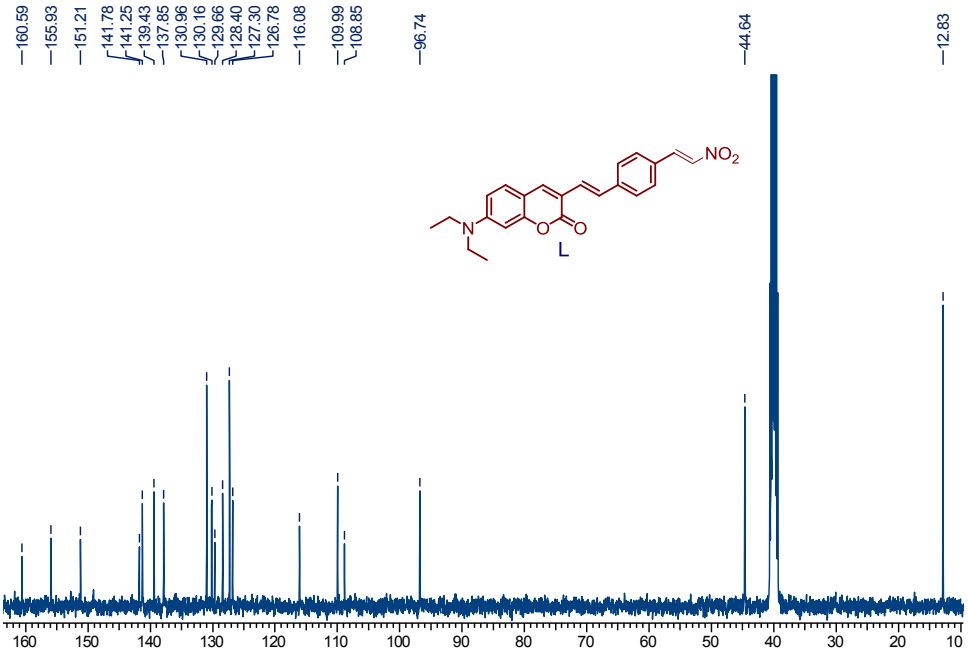

Figure 10. ^{13}C NMR spectrum of **L** recorded in DMSO-d_6.

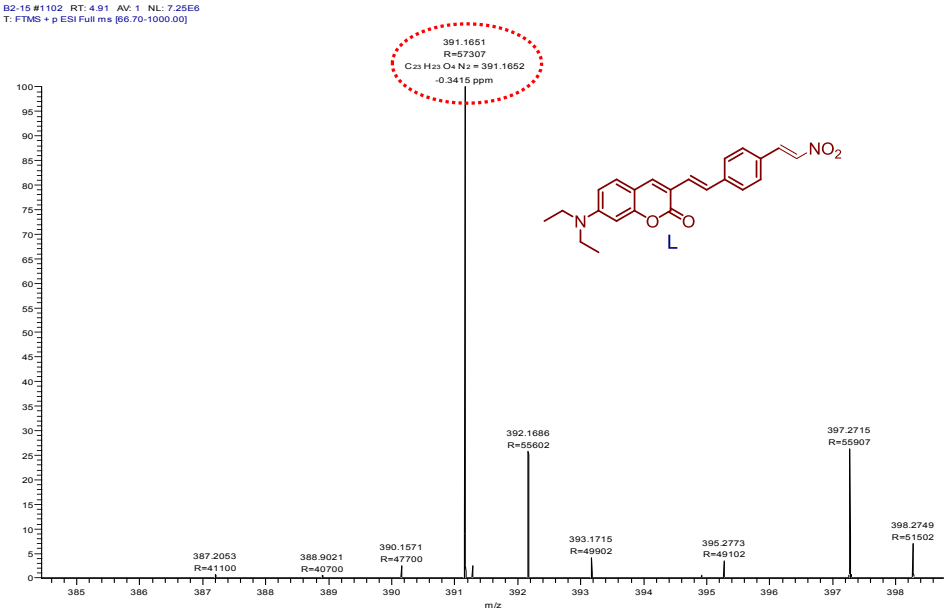

Figure 11. HRMS spectrum of **L**.

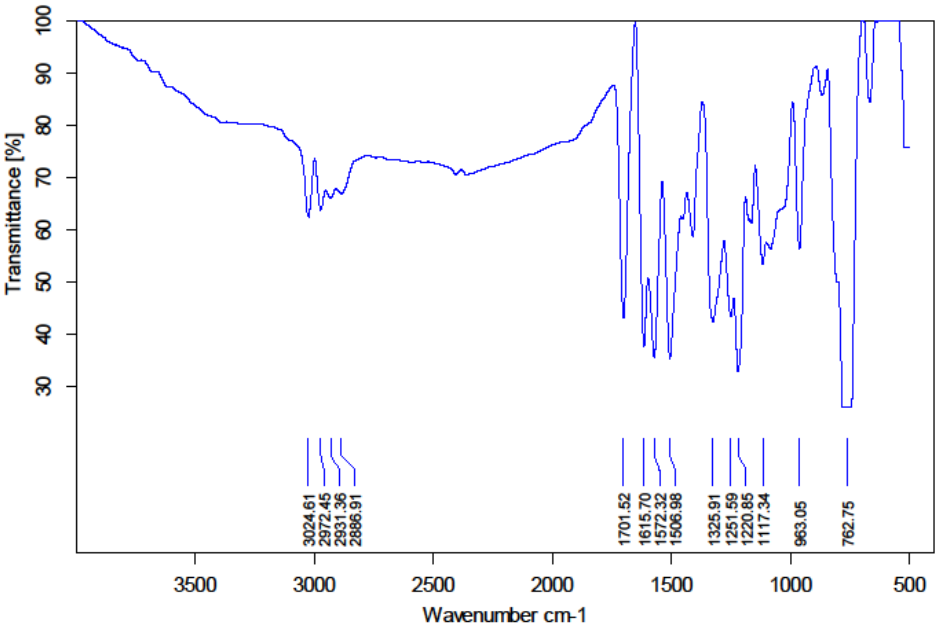

Figure 12. IR spectrum of **L**.

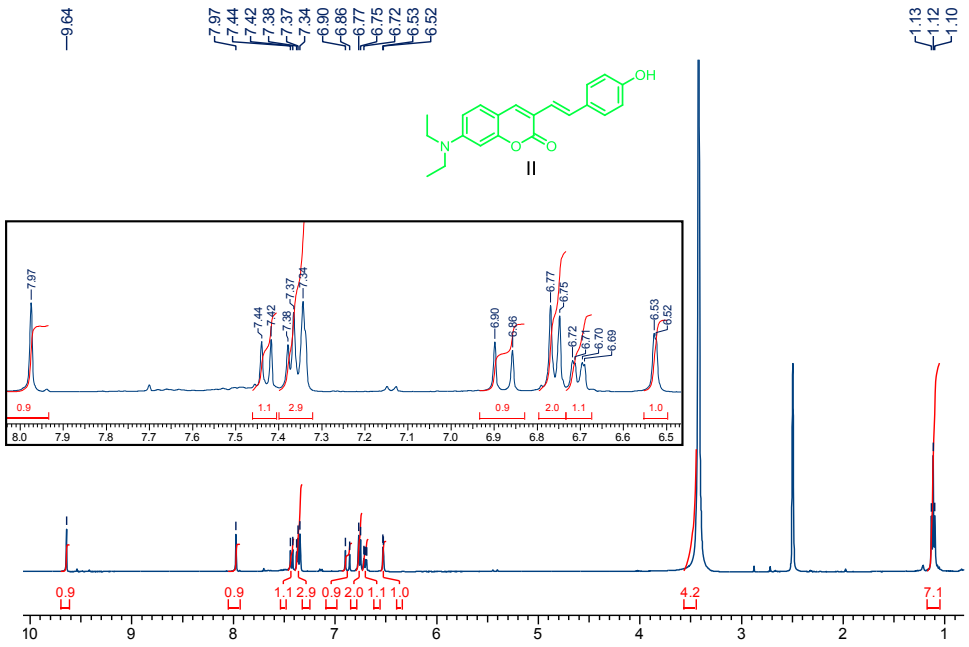

Figure 13. ^{1}H NMR spectrum of compound II recorded in DMSO-d_6.

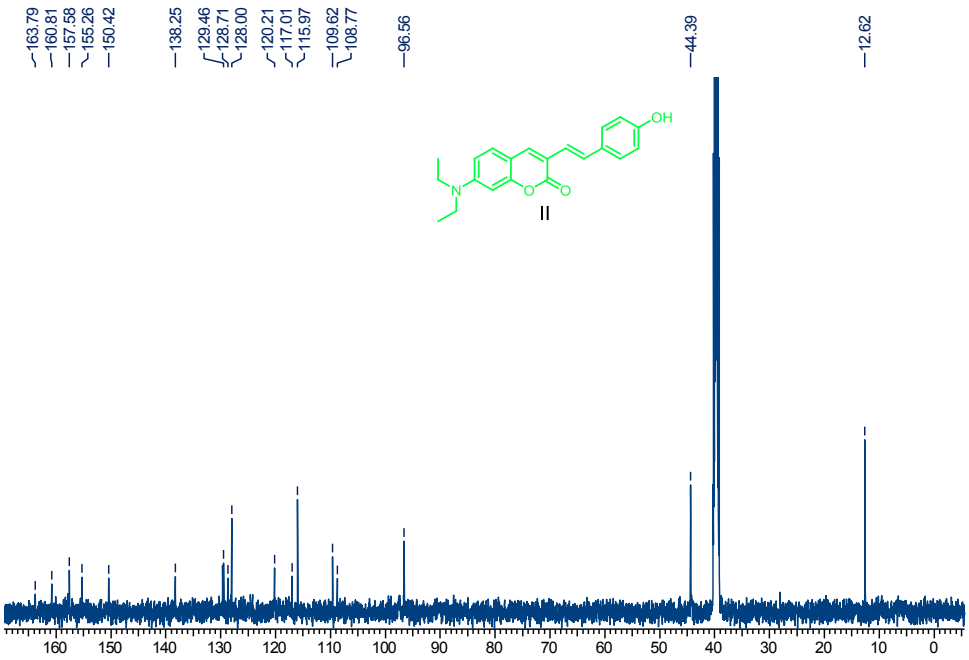

Figure 14. ^{13}C NMR spectrum of compound II recorded in DMSO-d_6.

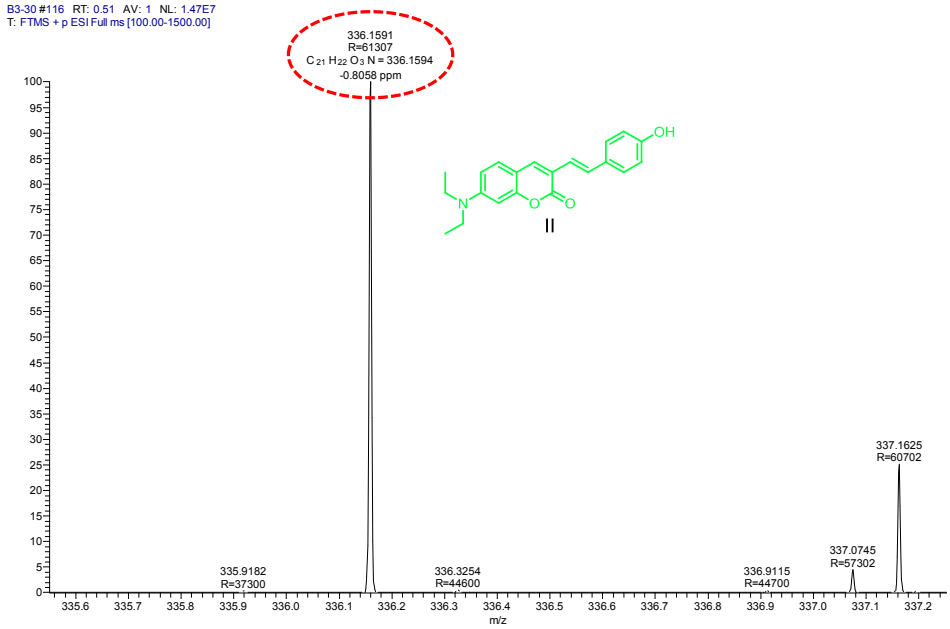

Figure 15. HRMS spectrum of compound II.

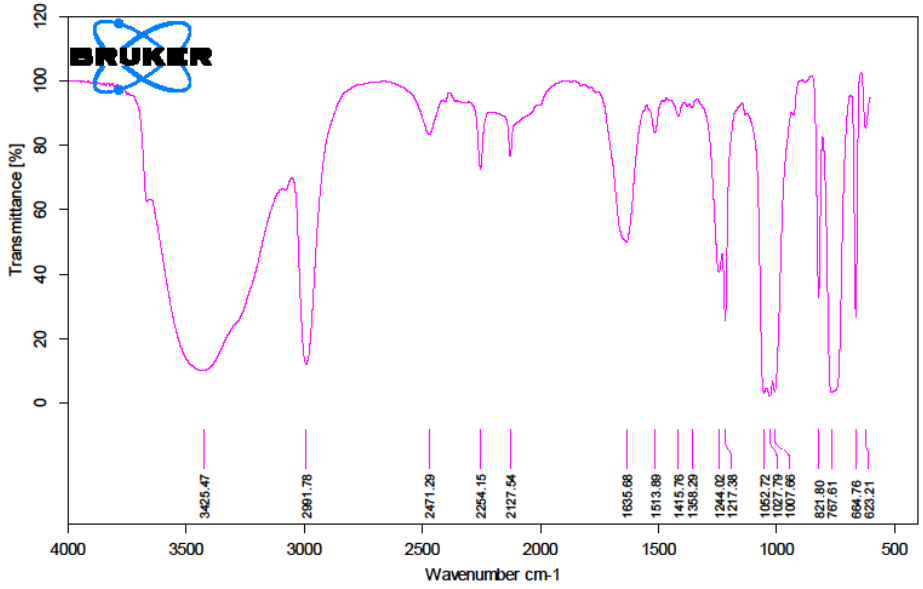

Figure 16. IR spectrum of compound II.

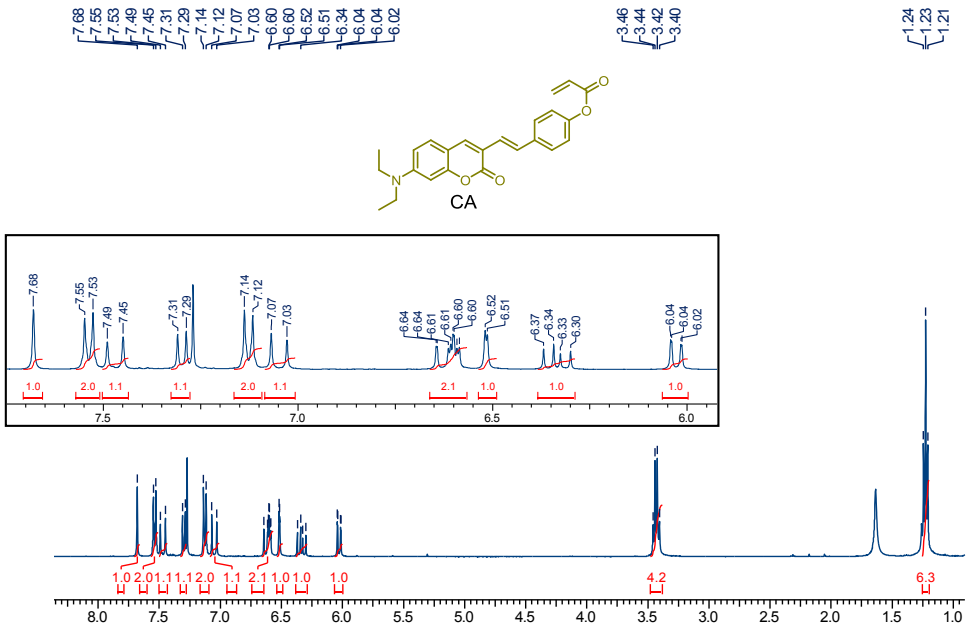

Figure 17. ^{1}H NMR spectrum of **CA** recorded in $CDCl_3$.

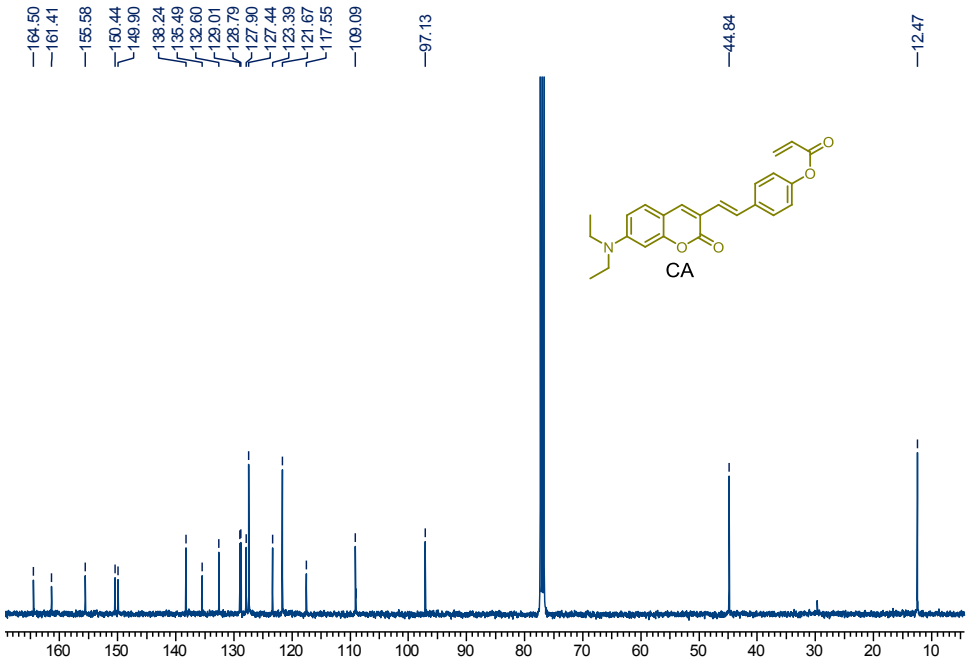

Figure 18. ^{13}C NMR spectrum of **CA** recorded in $CDCl_3$.

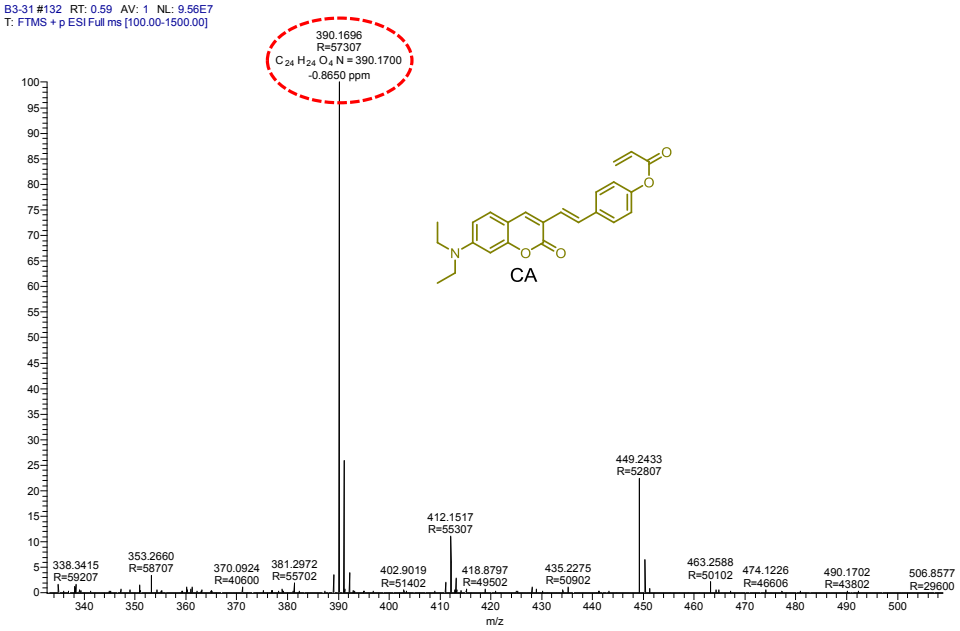

Figure 19. HRMS spectrum of **CA**.

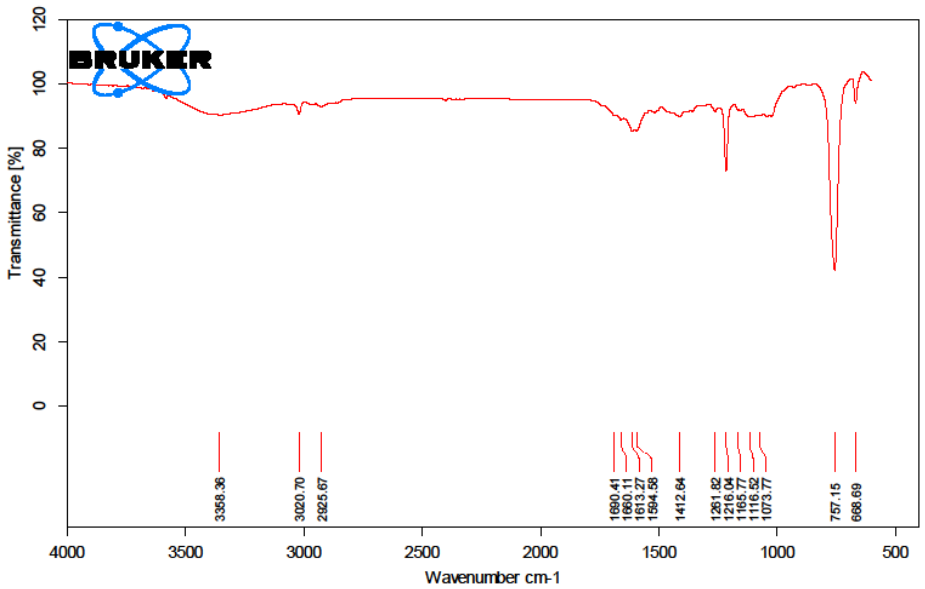

Figure 20. IR spectrum of **CA**.

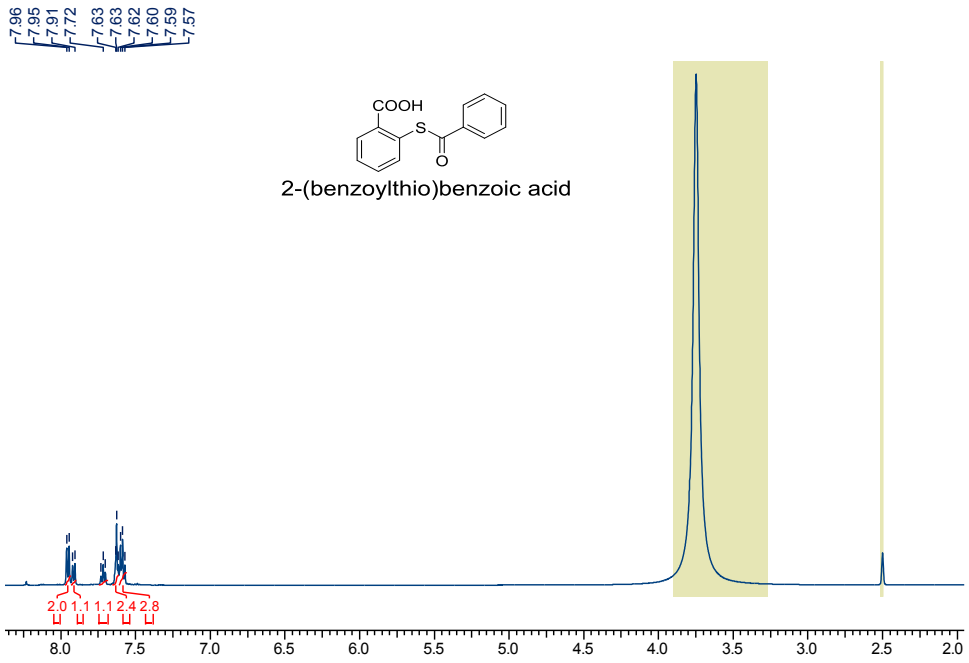

Figure 21. ^{1}H NMR spectrum of 2-(benzoylthio)benzoic acid recorded in DMSO-d_6.

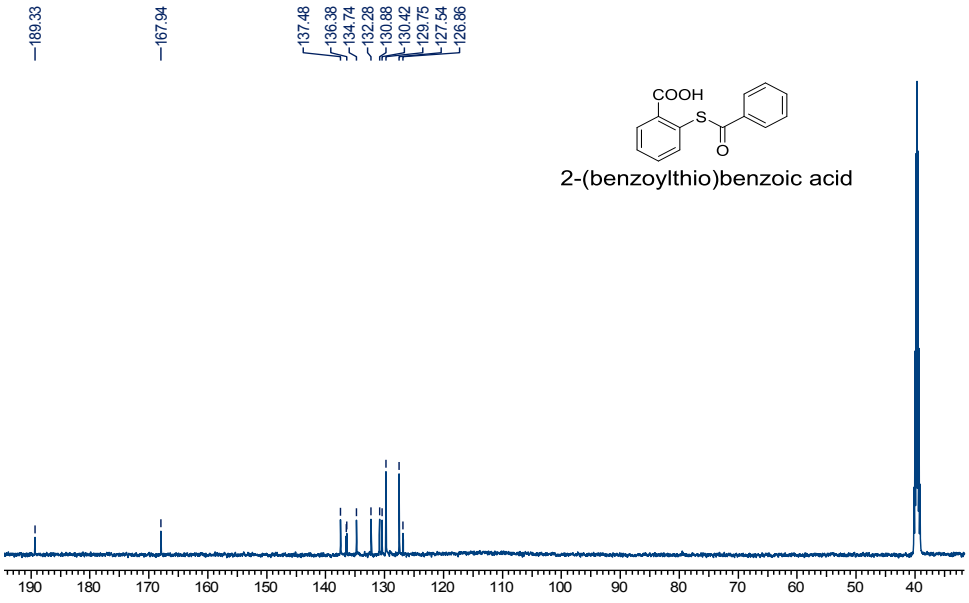

Figure 22. ^{13}C NMR spectrum of 2-(benzoylthio)benzoic acid recorded in DMSO-d_6.

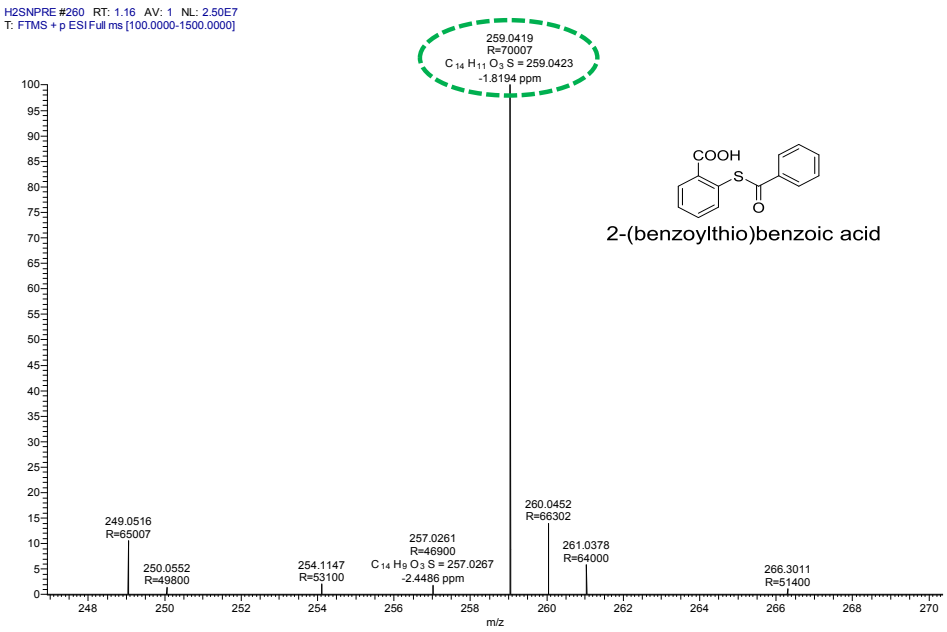

Figure 23. HRMS spectrum of 2-(benzoylthio) benzoic acid.

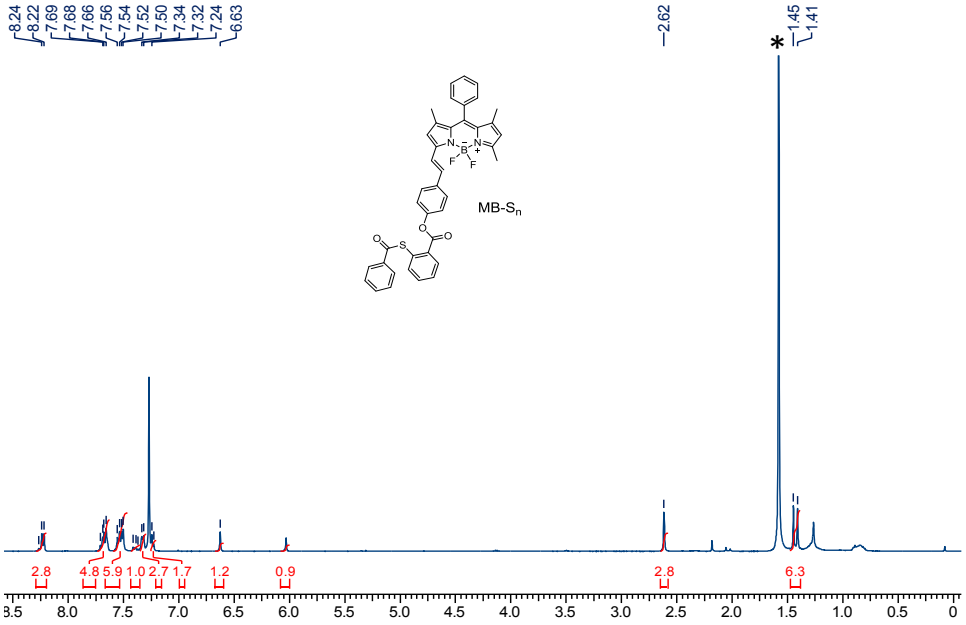

Figure 24. ^{1}H NMR spectrum of **MB-S$_n$** recorded in CD

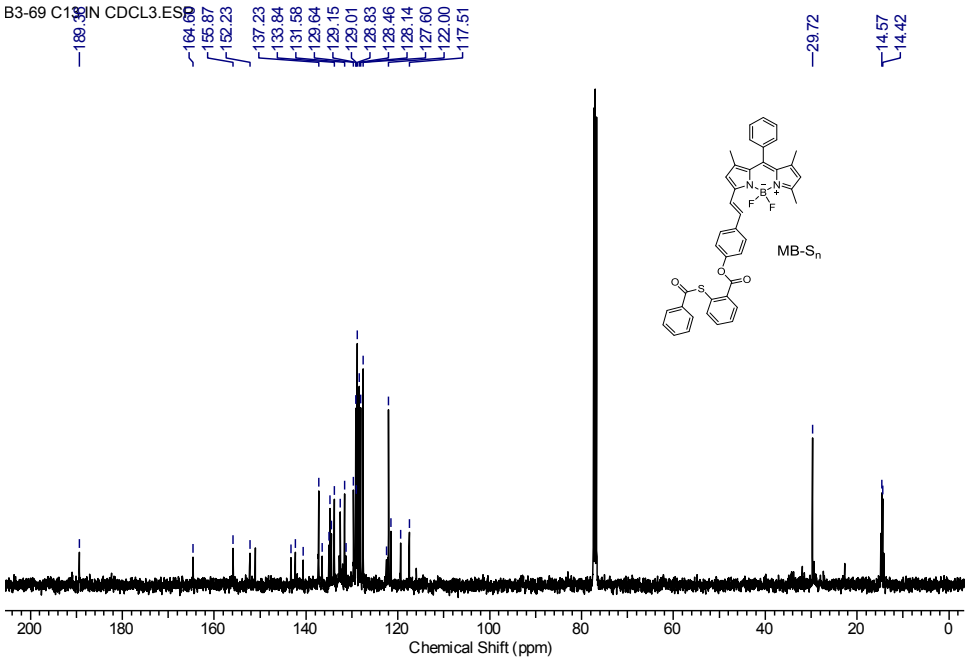

Figure 25. ^{13}C NMR spectrum of **MB-S$_n$** recorded in $CDCl_3$.

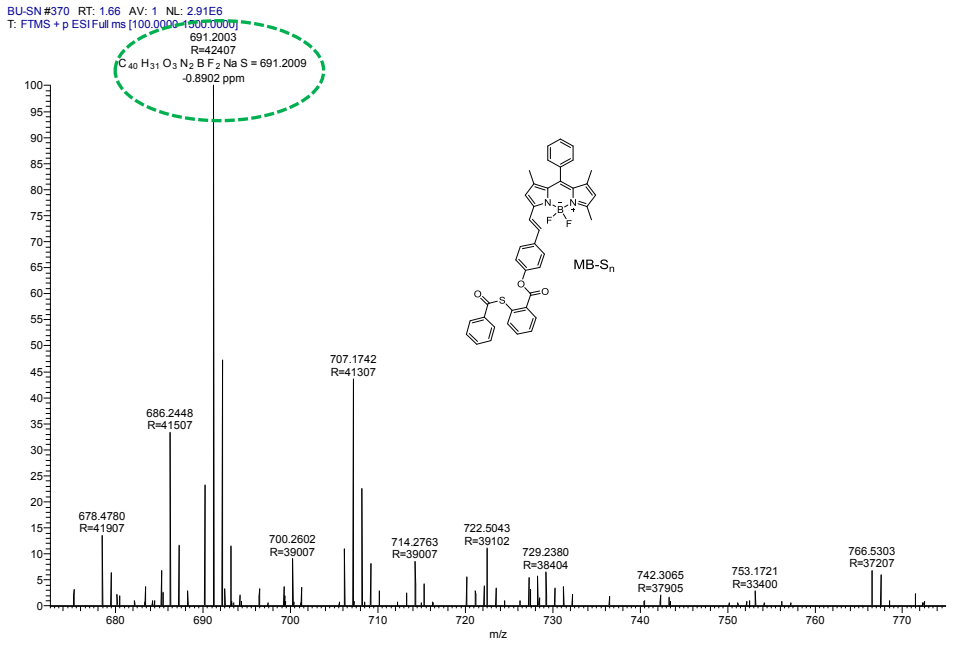

Figure 26. HRMS spectrum of **MB-S$_n$**.

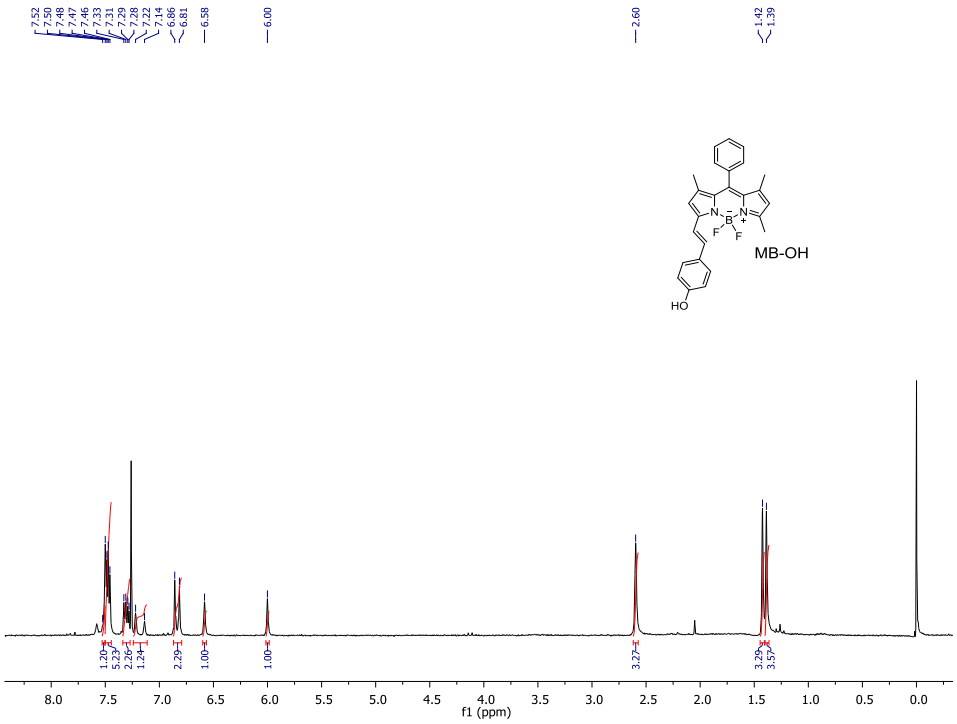

Figure 27. ^{1}H NMR spectrum of **MB-OH** recorded in $CDCl_3$.

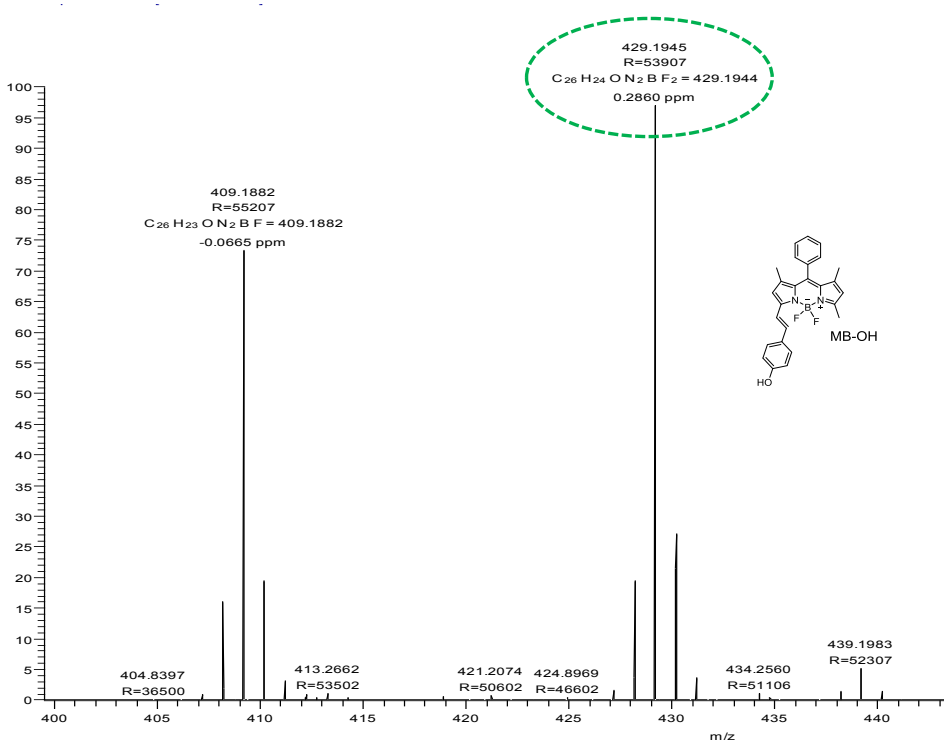

Figure 28. HRMS spectrum of **MB-OH**.

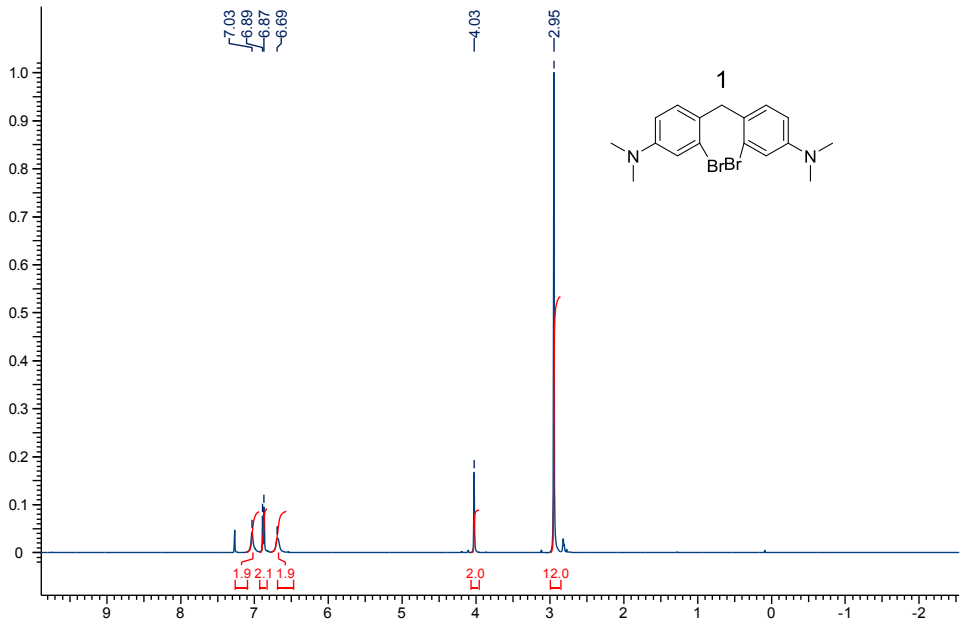

Figure 29. ^{1}H NMR spectrum of **1** recorded in $CDCl_3$.

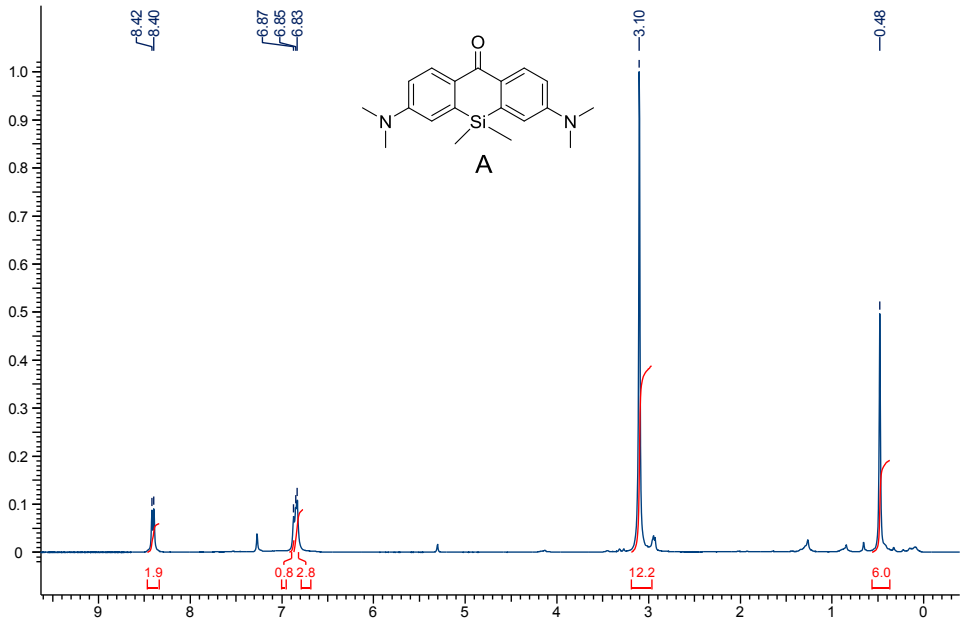

Figure 30. ^{1}H NMR spectrum of **A** recorded in $CDCl_3$.

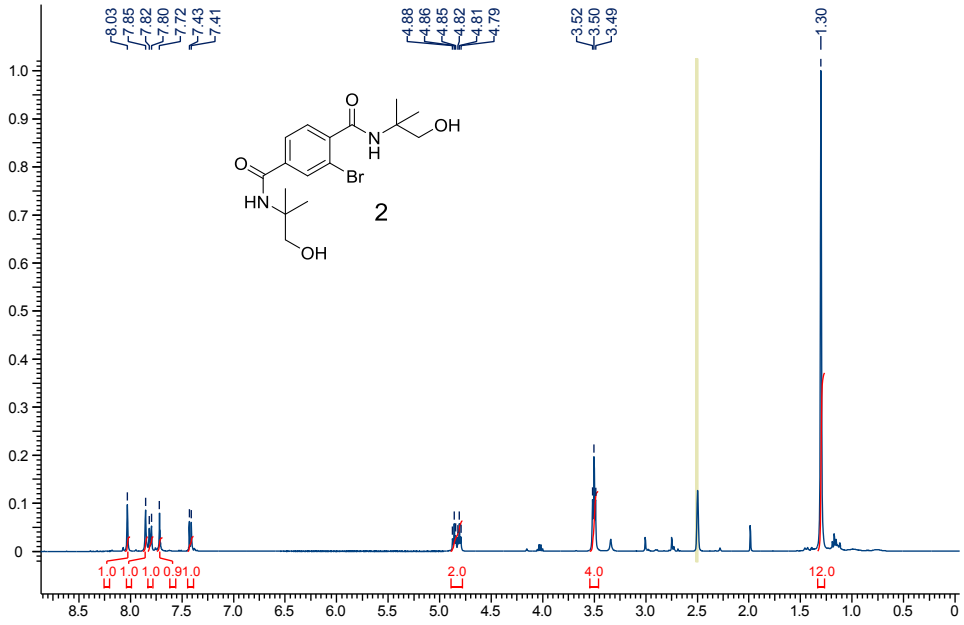

Figure 31. ^{1}H NMR spectrum of **2** recorded in DMSO-d_6.

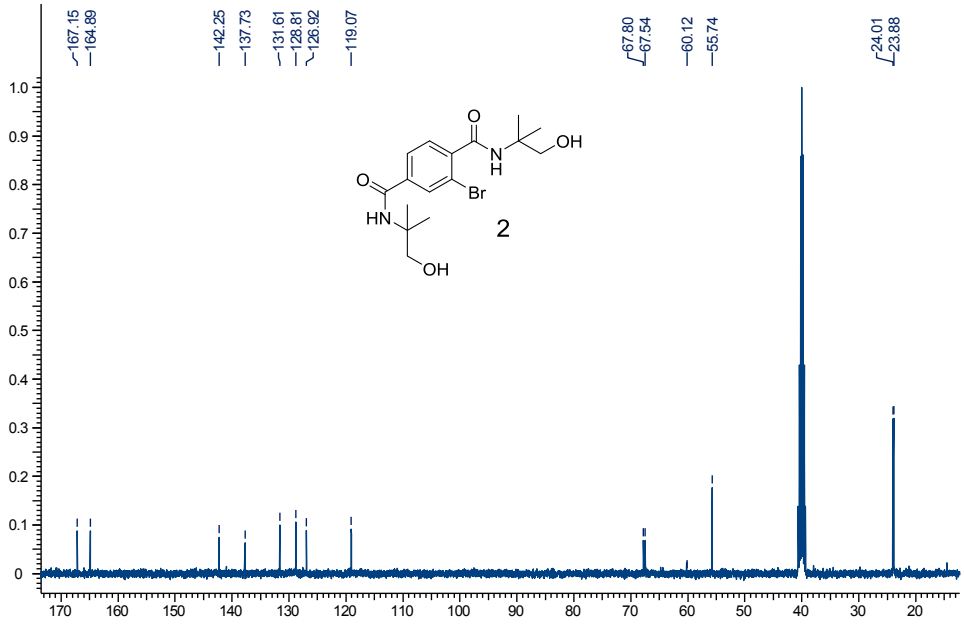

Figure 32. ^{13}C NMR spectrum of **2** recorded in DMSO-d_6.

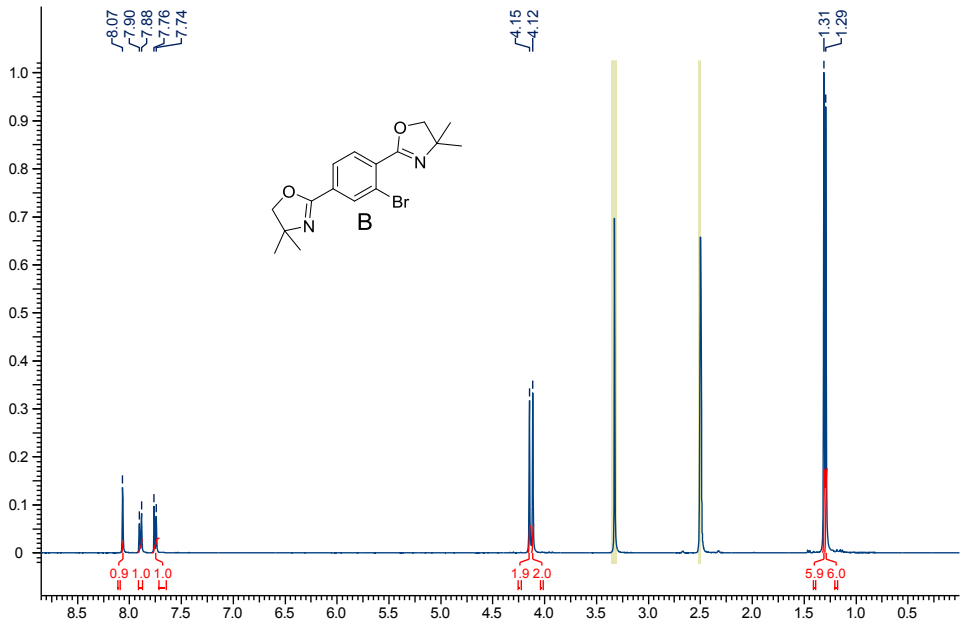

Figure 33. ^{1}H NMR spectrum of **B** recorded in DMSO-d_6.

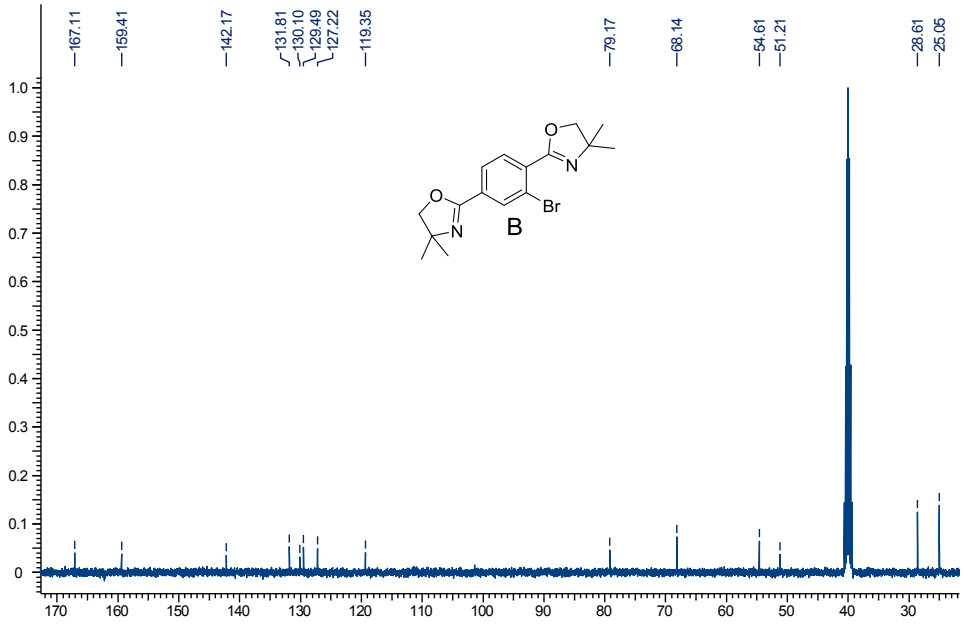

Figure 34. ^{13}C NMR spectrum of **B** recorded in DMSO-d_6.

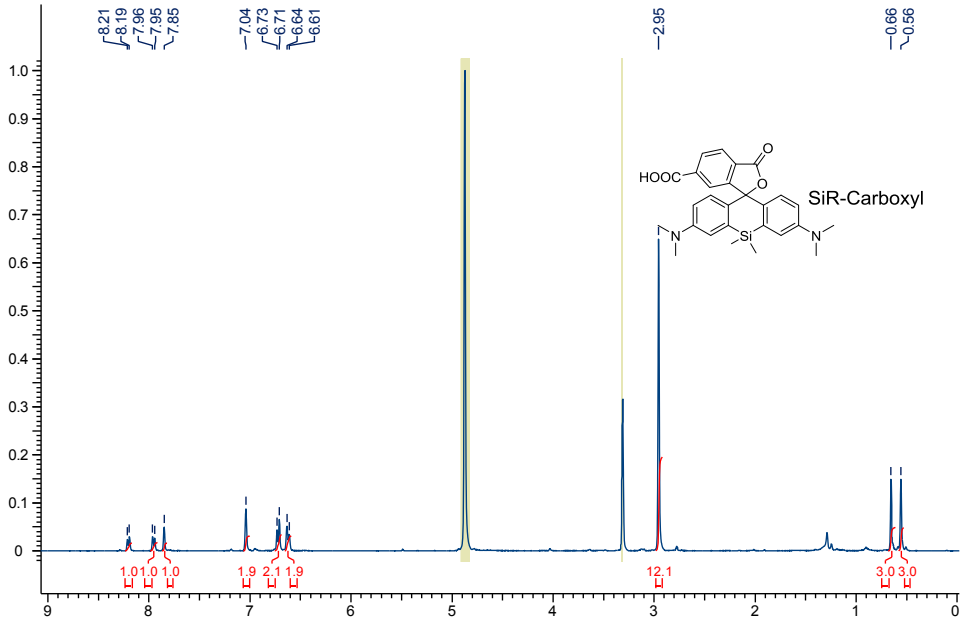

Figure 35. ^{1}H NMR spectrum of **SiR-Carboxyl** recorded in METHANOL-d_4.

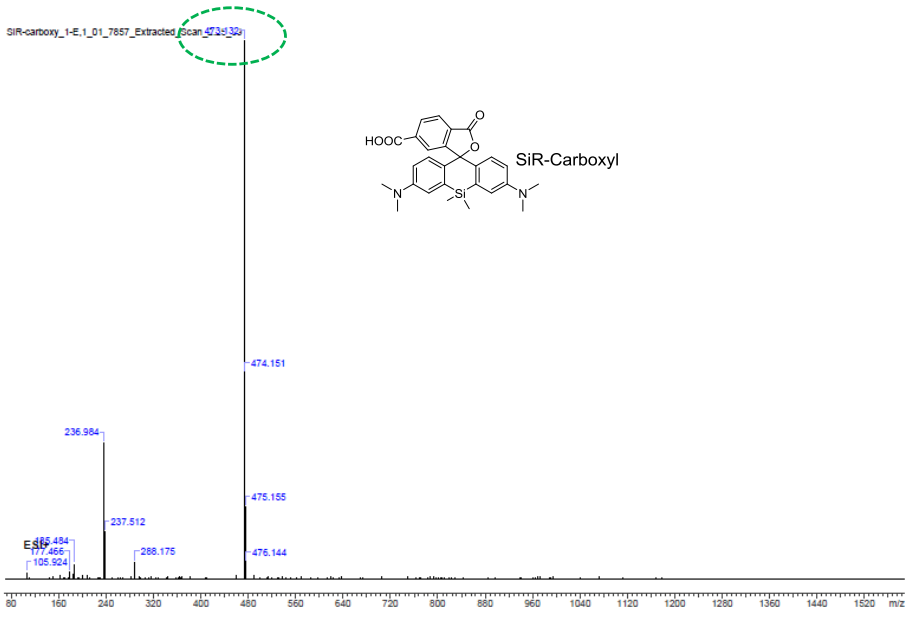

Figure 36. LRMS spectrum of **SiR-Carboxyl**.

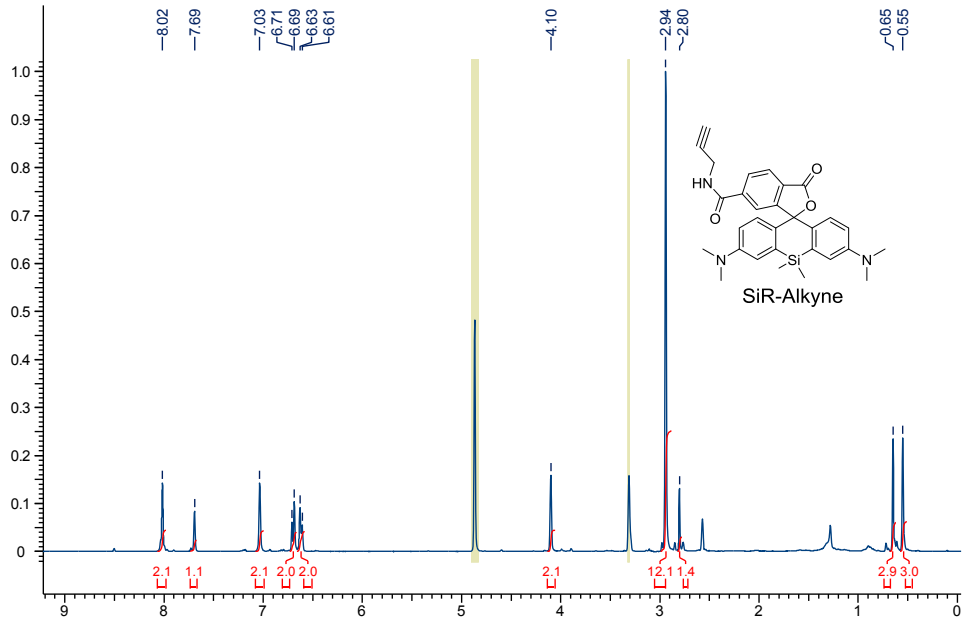

Figure 37. ^{1}H NMR spectrum of **SiR-Alkyne** recorded in METHANOL-d_4.

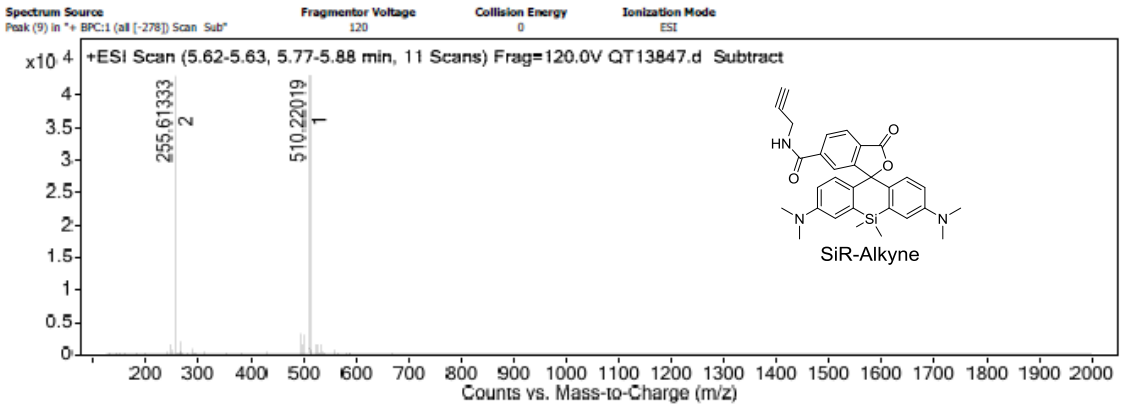

Figure 38. HRMS spectrum of **SiR-Alkyne**.

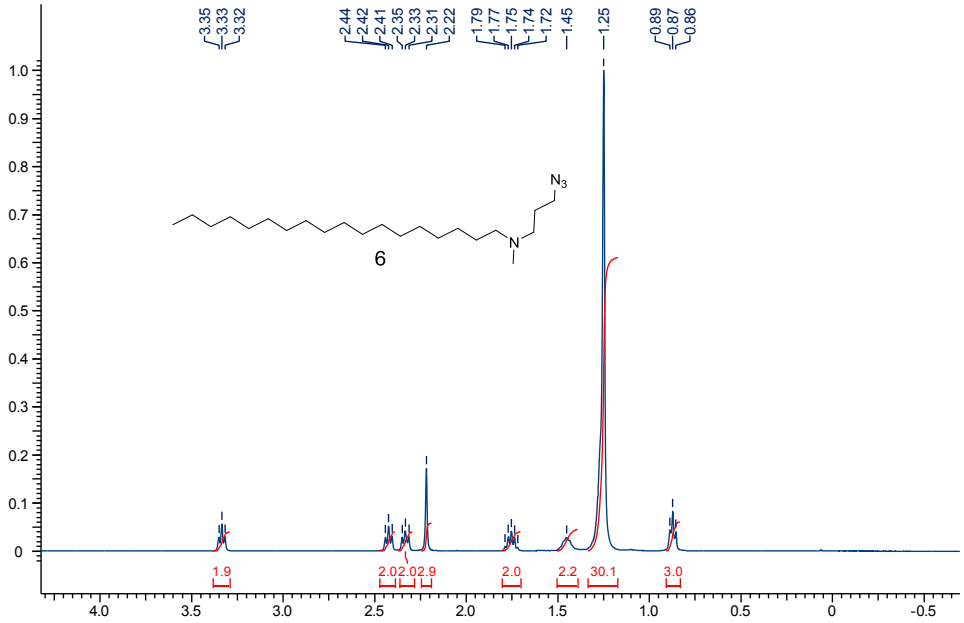

Figure 39. ^{1}H NMR spectrum of **6** recorded in $CDCl_3$.

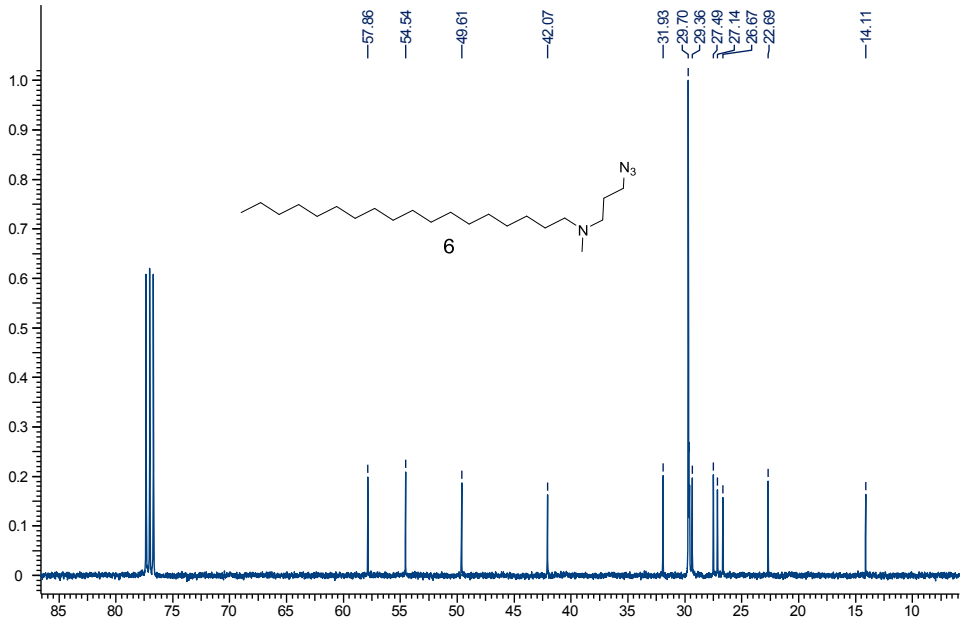

Figure 40. ^{13}C NMR spectrum of **6** recorded in $CDCl_3$.

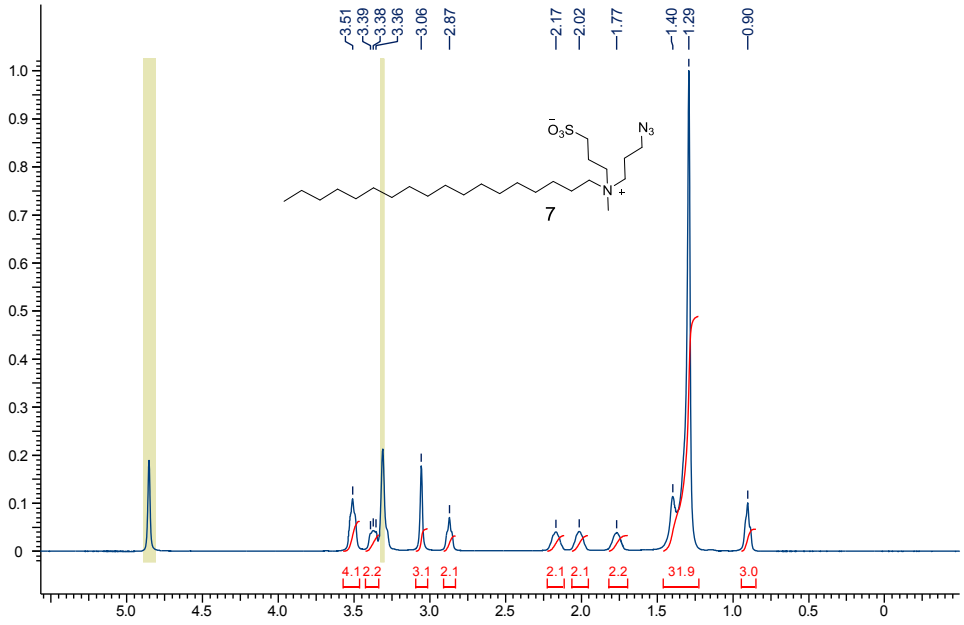

Figure 41. ^{1}H NMR spectrum of **7** recorded in METHANOL-d_4.

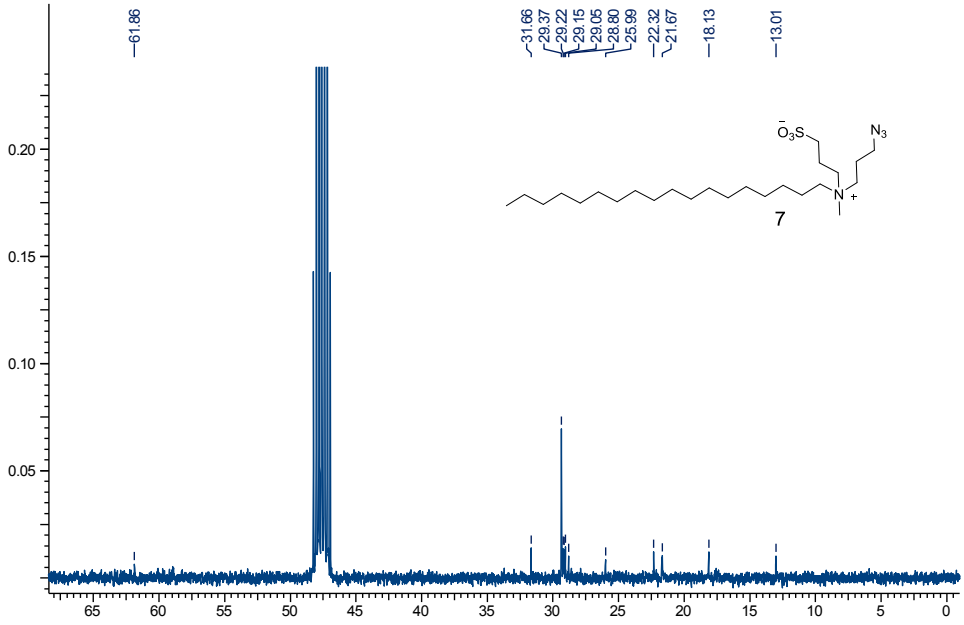

Figure 42. ^{13}C NMR spectrum of **7** recorded in METHANOL-d_4.

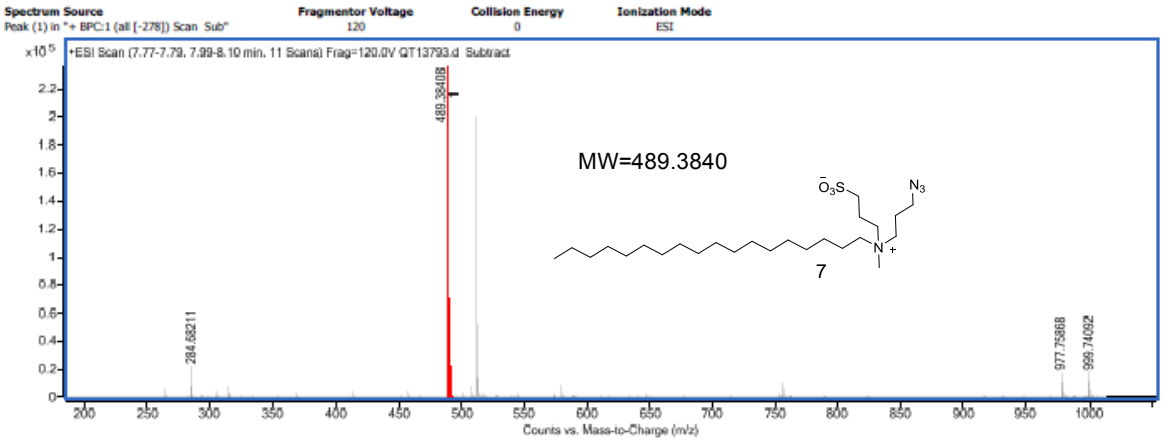

Figure 43. HRMS spectrum of **7**.

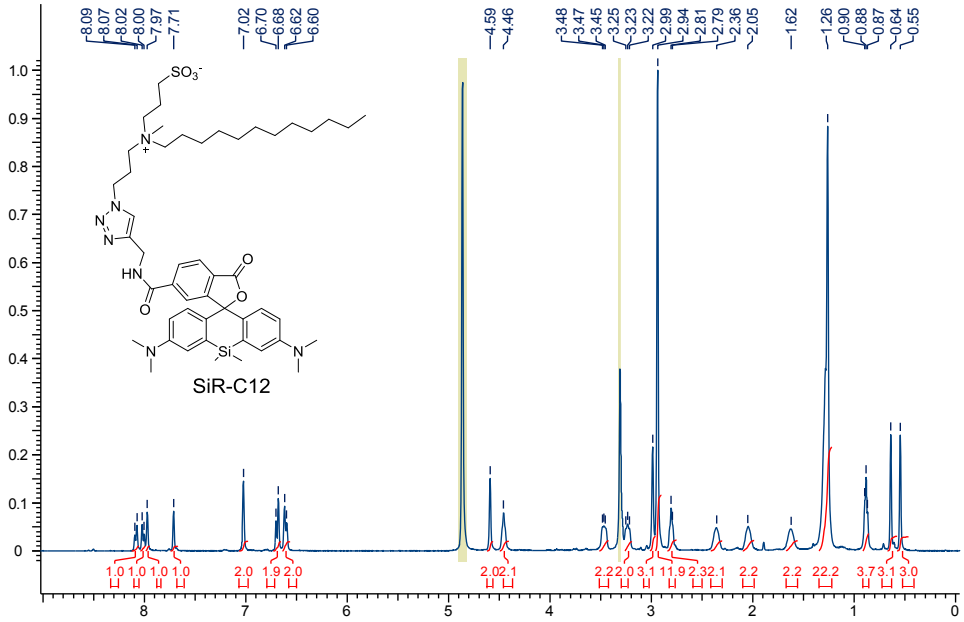

Figure 44. ^{1}H NMR spectrum of **SiR-C12** recorded in METHANOL-d_4.

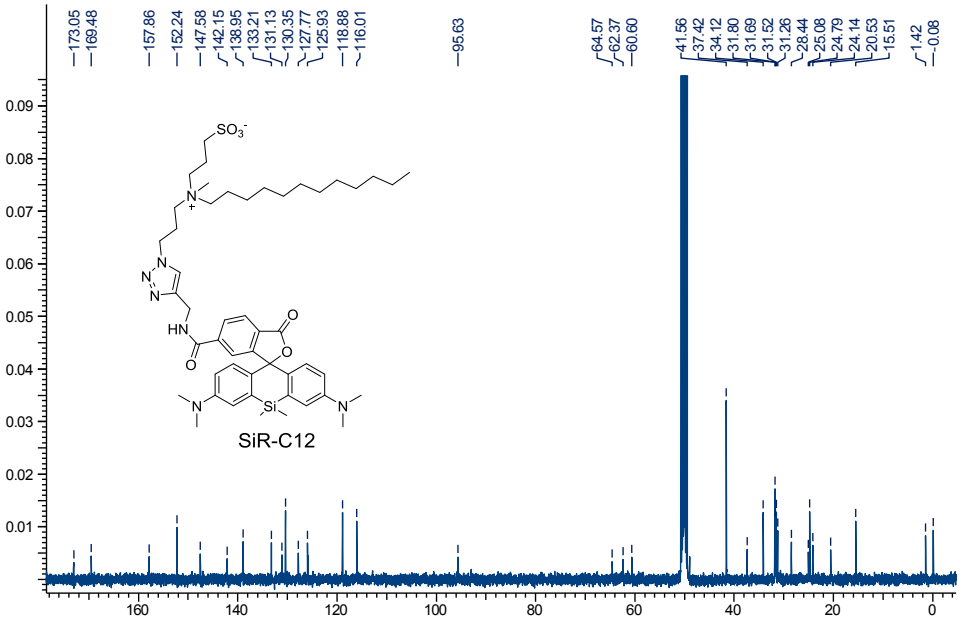

Figure 45. ^{13}C NMR spectrum of **SiR-C12** recorded in METHANOL-d_4.

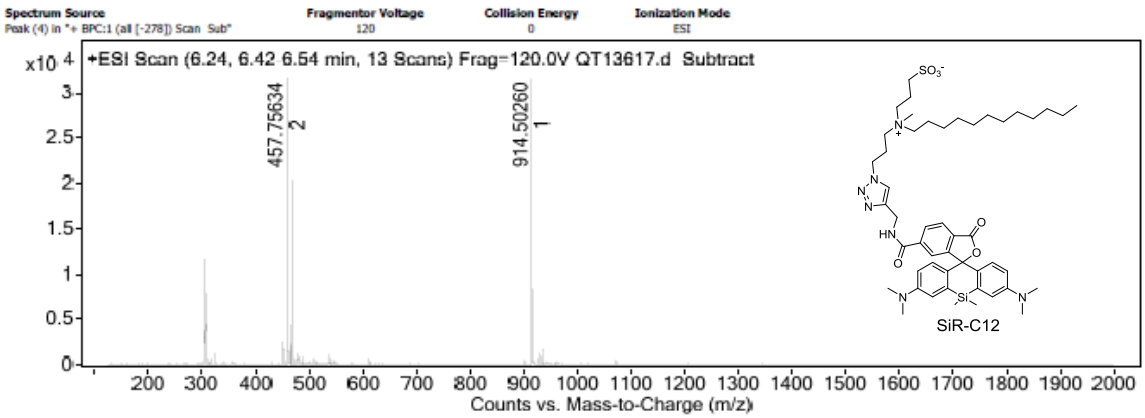

Figure 46. HRMS spectrum of **SiR-C12**.

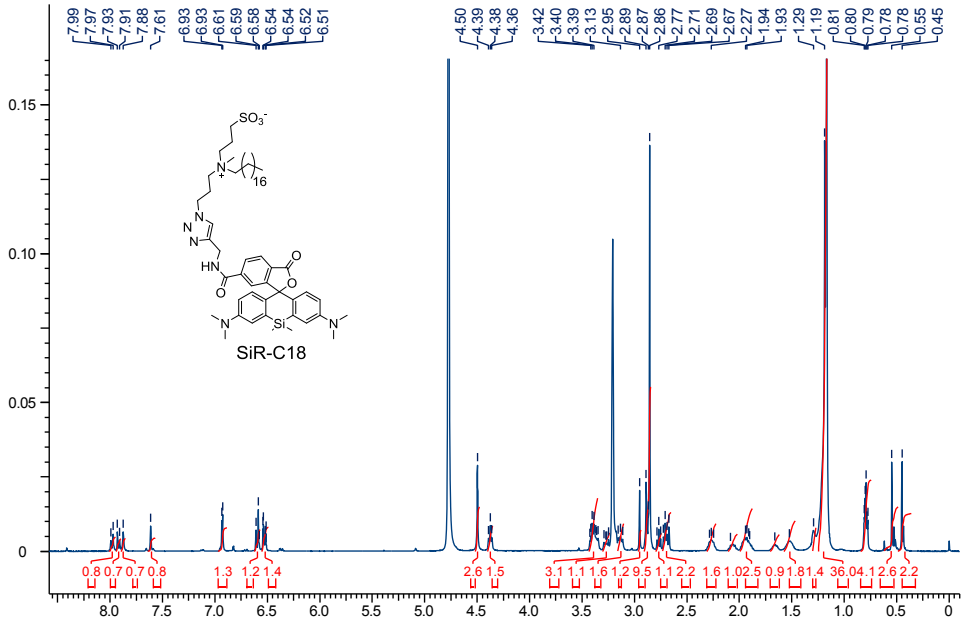

Figure 47. ^{1}H NMR spectrum of **SiR-C18** recorded in METHANOL-d_4

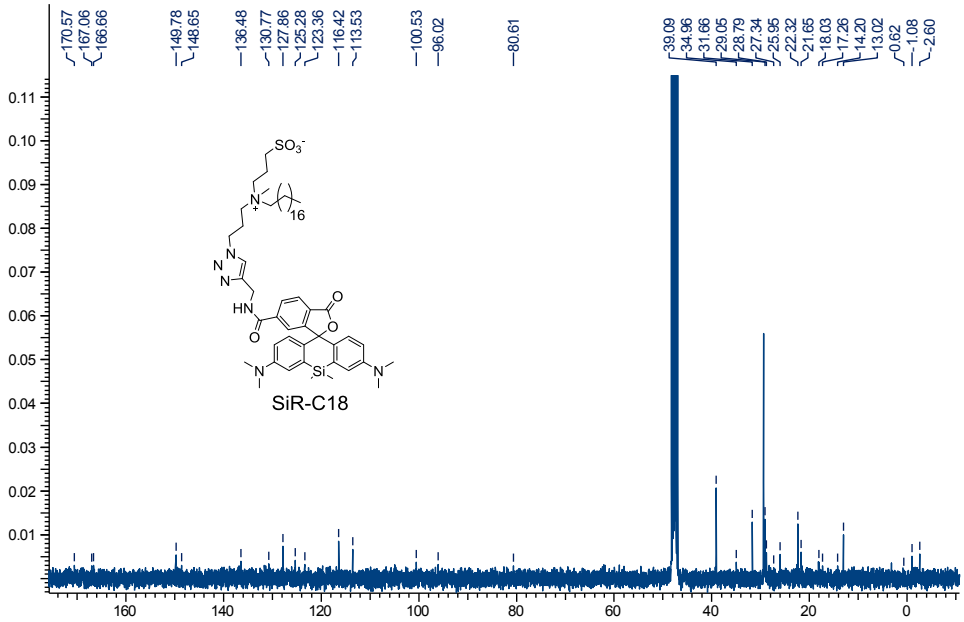

Figure 48. ^{13}C NMR spectrum of **SiR-C18** recorded in METHANOL-d_4.

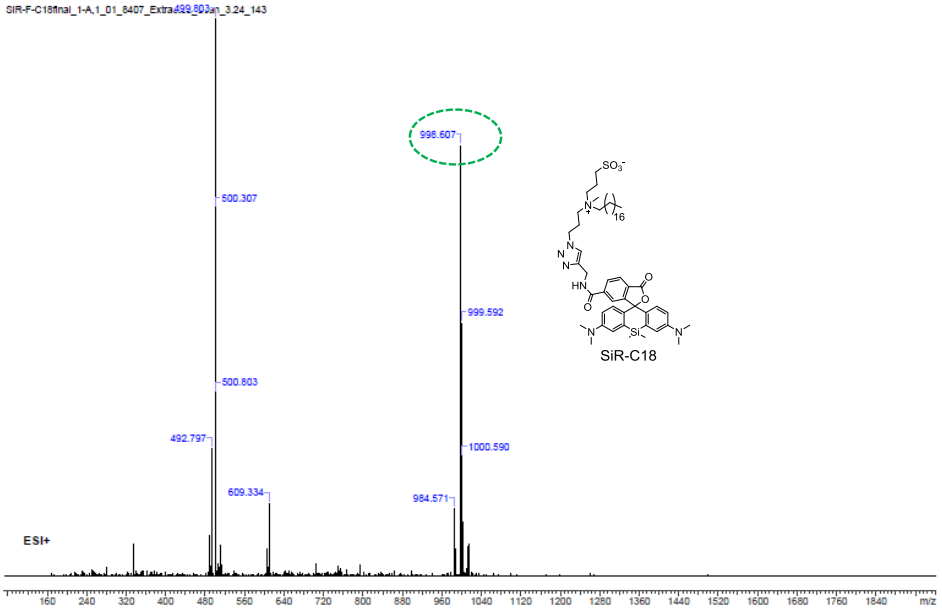

Figure 49. LRMS spectrum of **SiR-C18**.

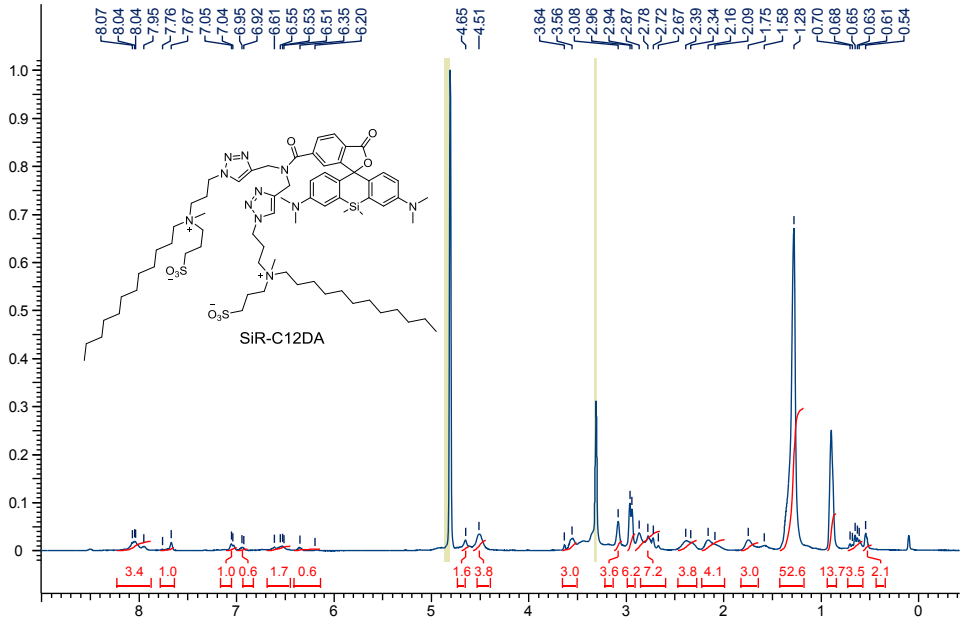

Figure 50. ^{1}H NMR spectrum of **SiR-C12DA** recorded in METHANOL-d_4.

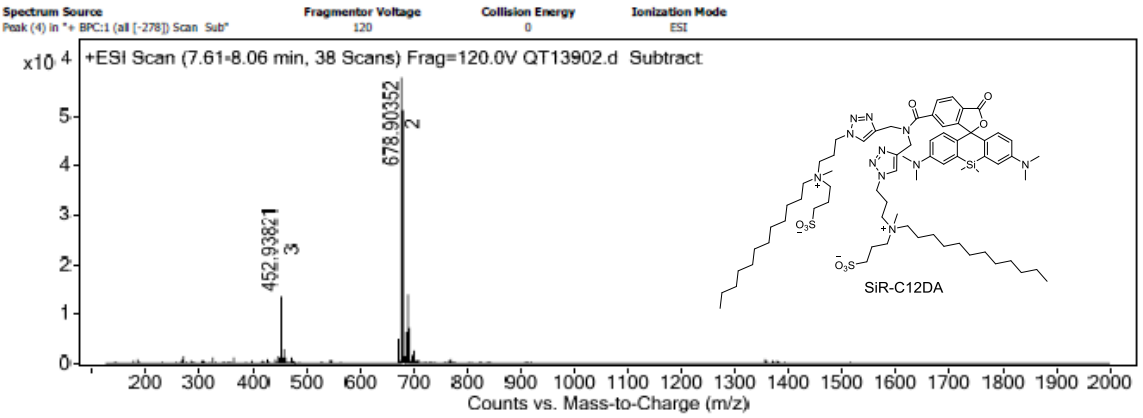

Figure 51. HRMS spectrum of **SiR-C12DA**.

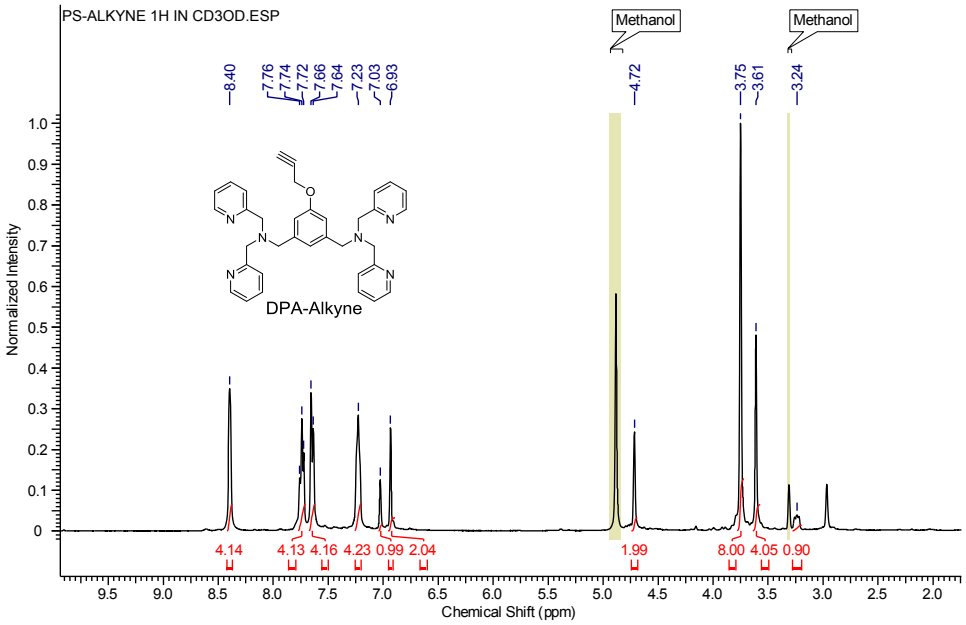

Figure 52. ^{1}H NMR spectrum of **DPA-Alkyne** recorded in METHANOL-d_4.

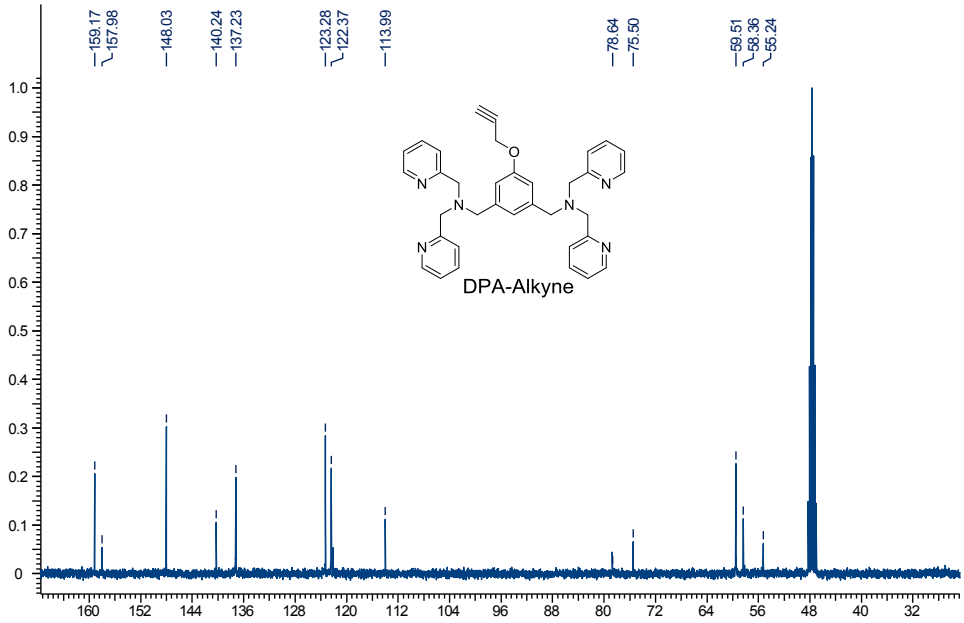

Figure 53. ^{13}C NMR spectrum of **DPA-Alkyne** recorded in METHANOL-d_4.

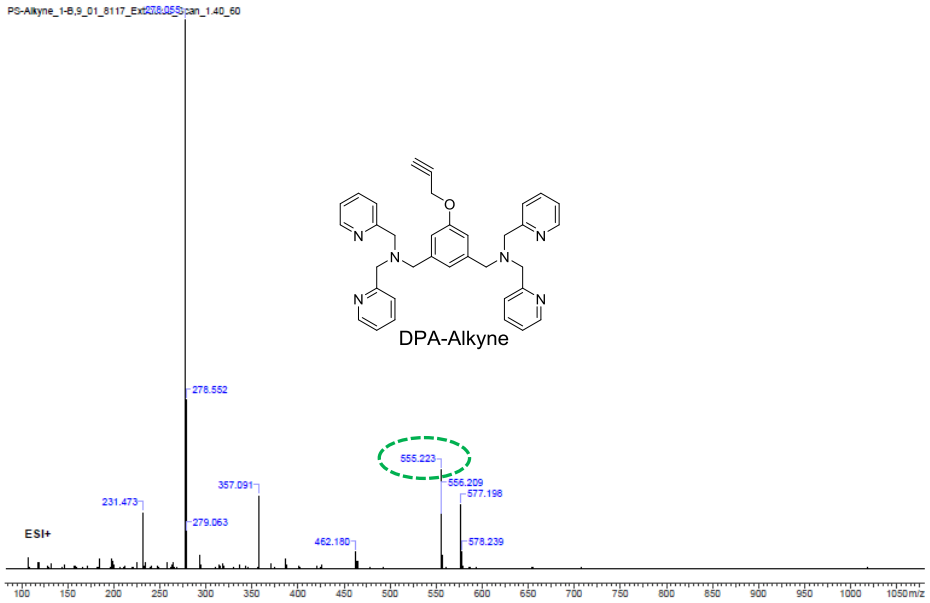

Figure 54. LRMS spectrum of **DPA-Alkyne**.

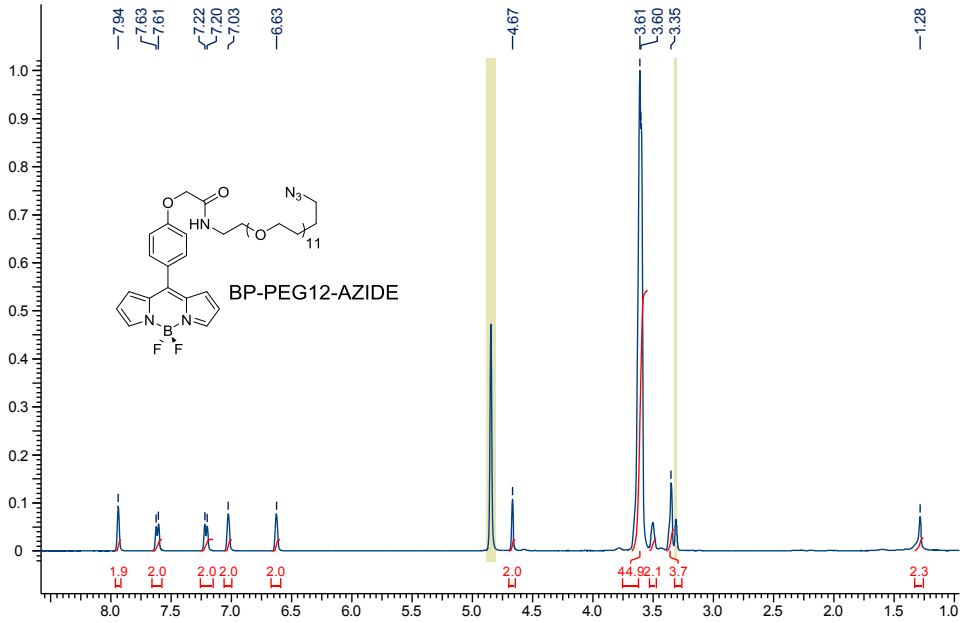

Figure 55. ^{1}H NMR spectrum of **BP-PEG12-Azide** recorded in METHANOL-d_4.

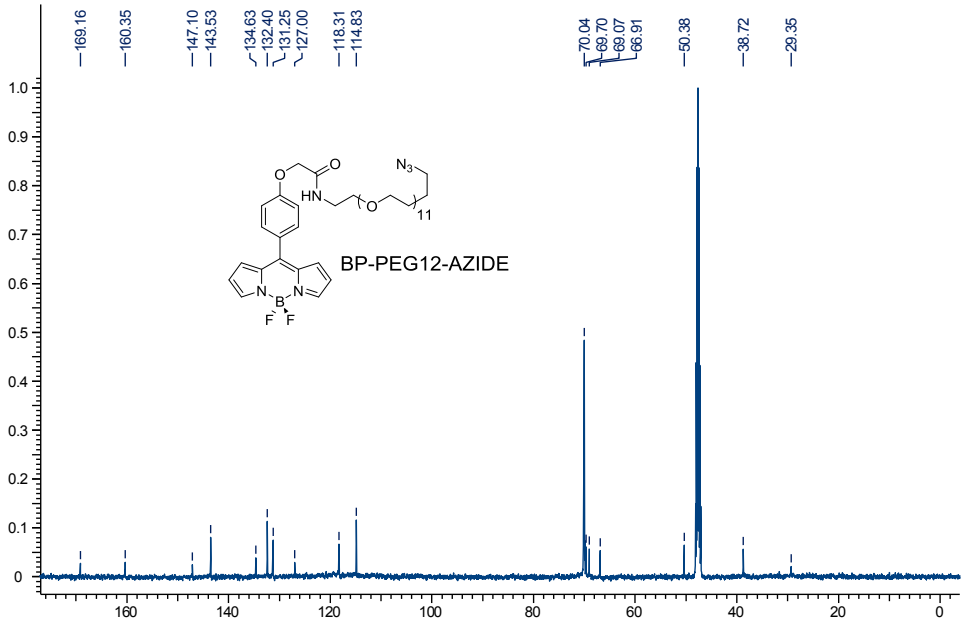

Figure 56. ^{13}C NMR spectrum of **BP-PEG12-Azide** recorded in METHANOL-d_4.

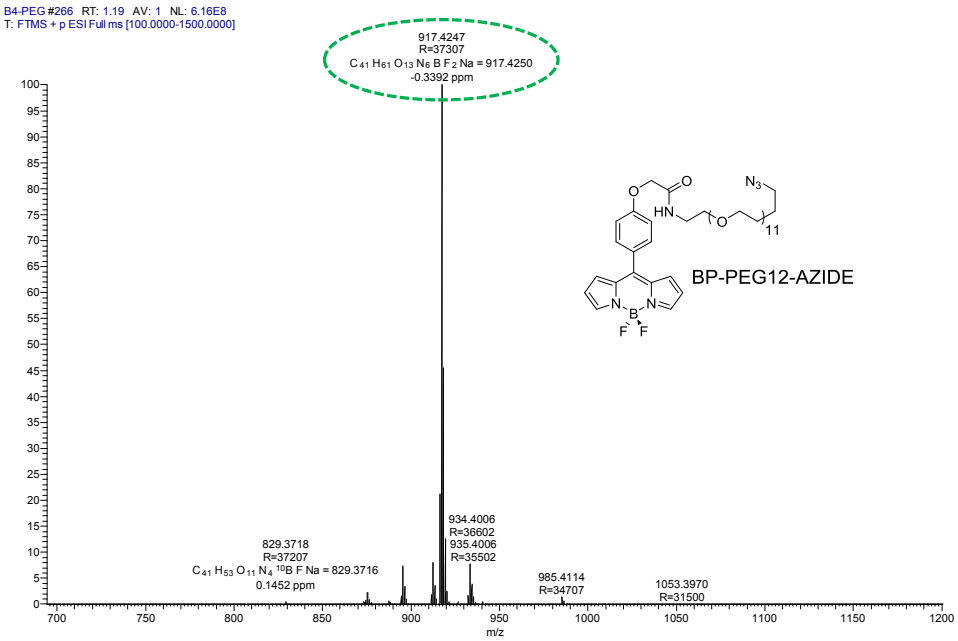

Figure 57. HRMS spectrum of **BP-PEG12-Azide**.

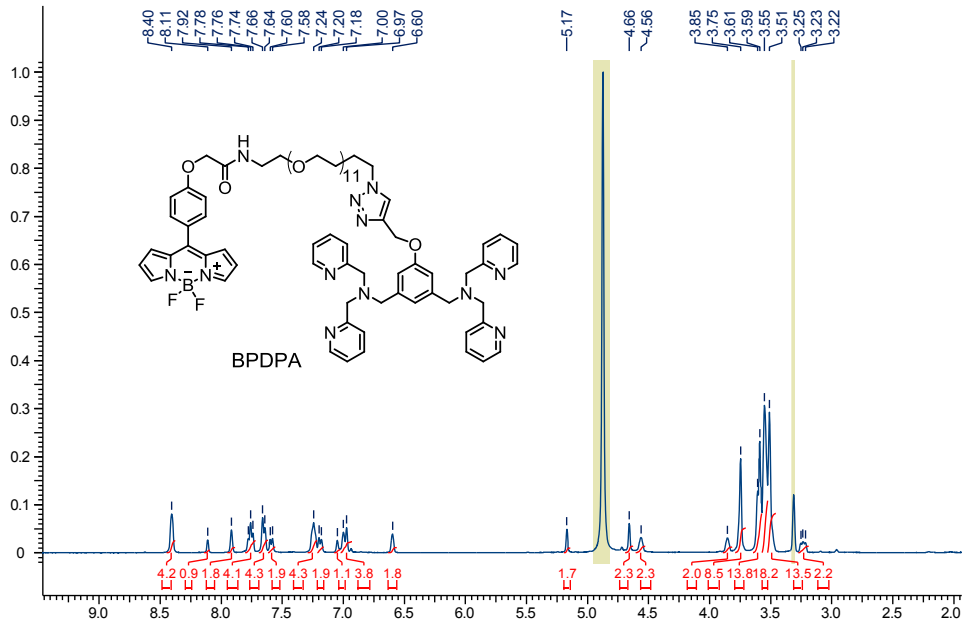

Figure 58. ^{1}H NMR spectrum of **BPDPA** recorded in METHANOL-d_4.

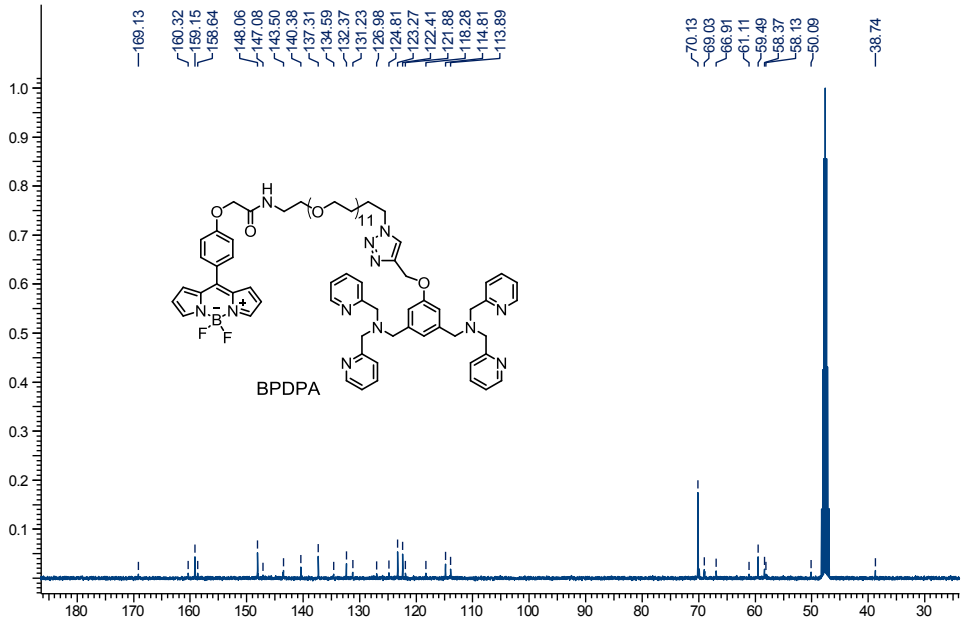

Figure 59. ^{13}CNMR spectrum of **BPDPA** recorded in METHANOL-d_4.

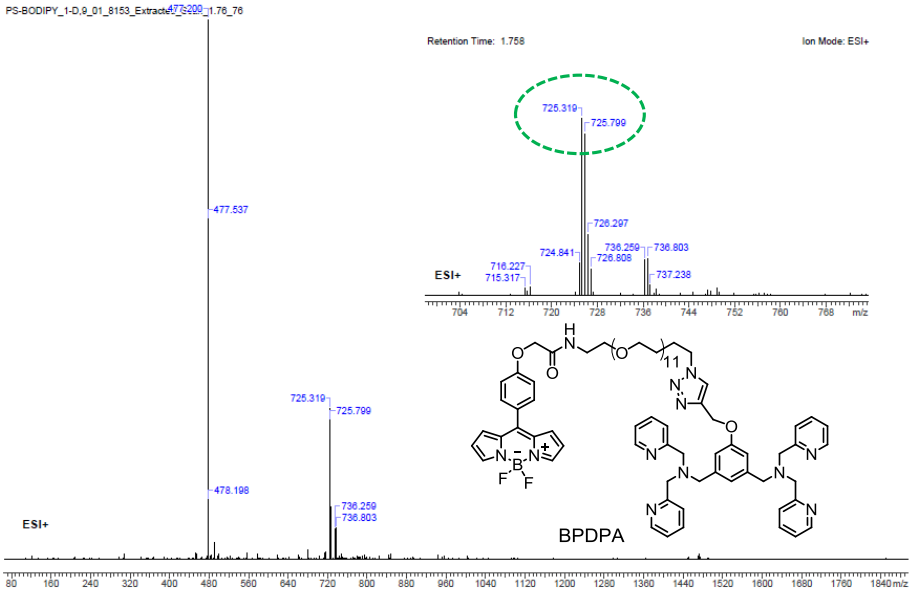

Figure 60. LRMS spectrum of **BPDPA**.

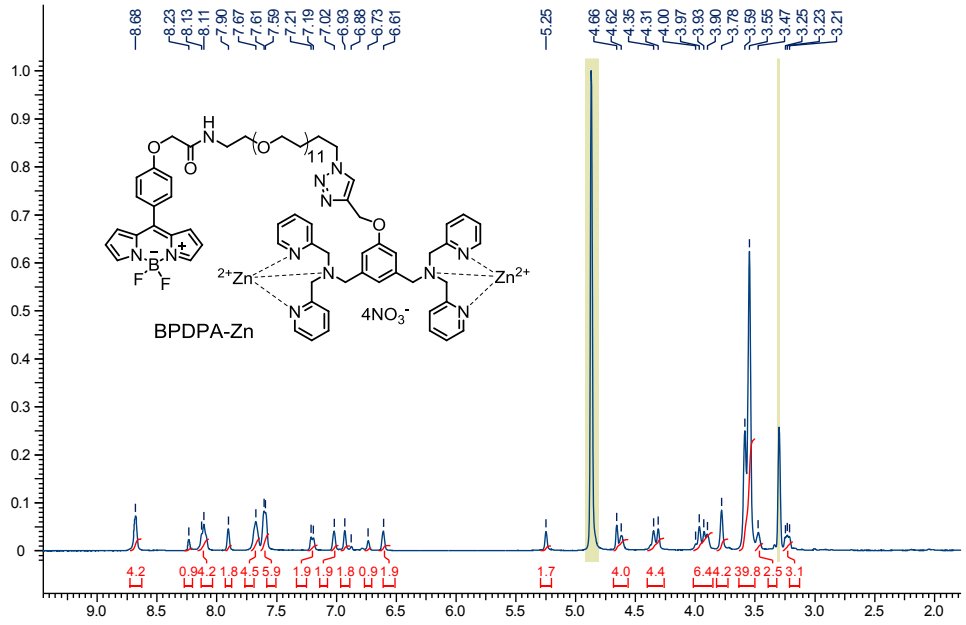

Figure 61. ^{1}H NMR spectrum of **BPDPA-Zn** recorded in METHANOL-d_4.

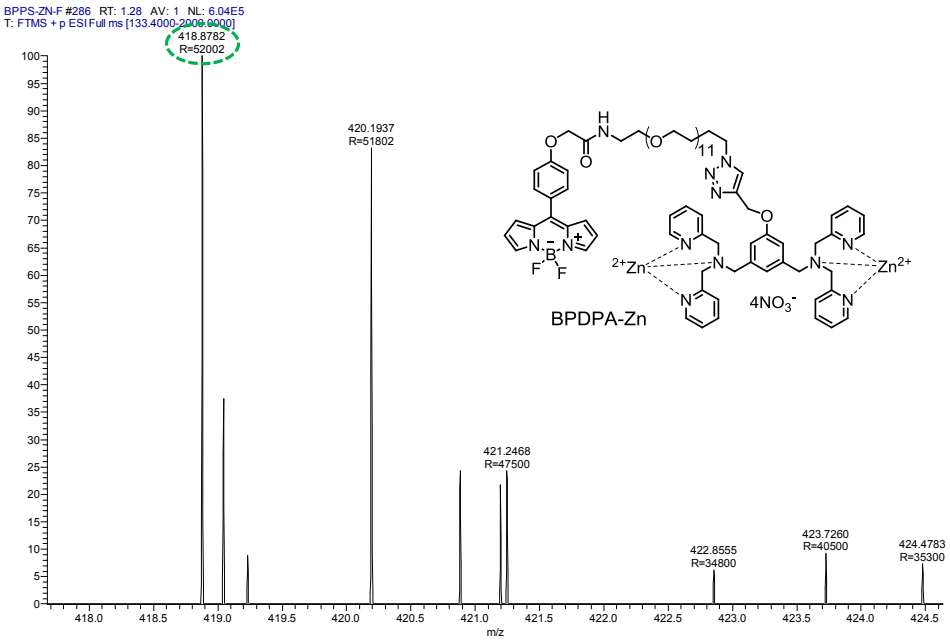

Figure 62. HRMS spectrum of **BPDPA-Zn**.

List of Publications

1. **Anila H. A**., Upendar Reddy G, Firoj Ali, Nandaraj Taye, Samit Chattopadhyay and Amitava Das, ***Chem. Commun***., *2015*, 51, 15592-15595**.**
2. **Anila H A**., Firoj Ali, Shilpi Kushwaha, Nandaraj Taye, Samit Chattopadhyay, and Amitava Das, ***Anal. Chem***., 2016, 88, 12161 −12168**.**
3. **Anila H. A**., Sreejesh Sreedharan, Firoj Ali, Carl G. W. Smythe, Jim A. Thomas and Amitava Das, ***Chem. Commun.,*** 2018, 54, 3735..
4. Upendar Reddy G, **Anila H. A**., Firoj Ali, Nandaraj Taye, Samit Chattopadhyay and Amitava Das, ***Org. Lett***., *2015,* 17*,* 5532-5535**.**
5. Firoj Ali, **Anila H. A**., Nandaraj Taye, Rajesh G. Gonnade, Samit Chattopadhyay and Amitava Das, ***Chem. Commun***, 2015*, 51,* 16932-16935.
6. Firoj Ali, **Anila H. A.**, Nandaraj Taye, Devraj G. Mogare, Samit Chattopadhyay and Amitava Das, ***Chem. Commun****.*, 2016*, 52,* 6166—6169.
7. Firoj Ali, Sreejesh Sreedharan, **Anila H. A**, Hiwa K. Saeed Carl G. W. Smythe, Jim A. Thomas and Amitava Das, ***Anal. Chem***., 2017, 89 (22), 12087-12093.
8. Firoj Ali, Sunil Aute, Sreejesh Sreedharan, **Anila H. A,** Hiwa K. Saeed Carl G. W. Smythe, Jim A. Thomas and Amitava Das. ***Chem. Commun.,*** 2018, 54, 1849.
9. Hridesh Agarwalla, **H. A. Anila**, Firoj Ali, Swaraj Rashmi Pradhan, Bishwajit Ganguly, Sumit Kumar Pramanik and Amitava Das, ***Chem. Commun.,*** 2018, 54, 9079.
10. **Anila H A**, Ashokkumar Pichandi, Mauyeul Collot, Amitava Das and Andrey Klymchenko. (*To be communicated).*
11. **Anila H A**, Ashokkumar Pichandi, Mauyeul Collot, Amitava Das and Andrey Klymchenko. (*Manuscript under preparation).*

Book Chapter:

Book: Comprehensive Supramolecular Chemistry II: 2017, 8. 319-349. Elsevier Ltd.; ISBN: 97801128031988. Title: Specific Receptors and Imaging Reagents for Certain Heavy Metal Toxins.

Anila H A and Firoj Ali and Amitava Das

List of Patents

1. New reagent for specific detection of Cysteine in physiological condition as well as by using modified silica coated test strip. Publication No: **US20180093963A1**

2. Selective determination of Free Cysteine. ***PCT/IN2016/050254***

3. New reagent as scavenger of Hydrazine in drug induced cytotoxicity and in vitro enzymatic assay. *Provisional Application No*: **2332/DEL/2015**, Provisional filing date: 30/7/2015.

4. An ER-Specific reagent for monitoring HNO in biological objects. ***PCT/IN2017/050571***.

5. A new reagent for specific detection of HOCl in physiological condition. *Provisional Application No*: **20171106120**, Provisional filing date: 08/05/2017.

List of Conferences attended

1. Presented poster in the sixth edition of Chemical Frontiers held at Goa on August 15-18, 2015 in India.
2. Presented poster in Optics Within Life Sciences (OWLS) 2016 held from March 16-19, 2016 at TIFR-Mumbai, India.
3. Attended International Conference on Structural and Inorganic Chemistry held from December 4-5, 2014 at CSIR-National Chemical Laboratory. Pune India.
4. Attended 17th CRSI-National Symposium in chemistry held from February 6-8, 2015 at CSIR-National Chemical Laboratory, Pune, India.
5. Attended 28th International Conference on Photochemistry (ICP 2017) held from July 16-21, 2017 at Strasbourg, France.
6. Presented poster in “National Science day 2015” at CSIR-NCL, Pune, India. February 25-28, 2015.

Awards and Recognition

1. **Best Poster award** in the sixth edition of Chemical frontiers held at Goa, India, during August 15-18, 2015.
2. **Best Poster award** in National Science Day-2015 held at National Chemical Laboratory Pune, India during February 25-28, 2015.
3. Awarded the **Raman-Charpak Fellowship-2016** under the area of Chemical Sciences

ChemComm

COMMUNICATION

View Article Online
View Journal | View Issue

Cite this: *Chem. Commun.*, 2015, **51**, 15592

Received 12th June 2015,
Accepted 26th August 2015

DOI: 10.1039/c5cc04876a

www.rsc.org/chemcomm

A reagent for specific recognition of cysteine in aqueous buffer and in natural milk: imaging studies, enzymatic reaction and analysis of whey protein†‡

Anila H. A.,[a] Upendar Reddy G.,[a] Firoj Ali,[a] Nandaraj Taye,[b] Samit Chattopadhyay*[b] and Amitava Das*[a]

We report a new chemodosimetric probe (L) for specific recognition of cysteine (Cys) in aqueous buffer and in whey protein isolated from fresh cow's milk. Using this reagent we could develop a luminescence-based methodology for estimation of Cys released from a commercially available Cys-supplement drug by aminoacylase-1 in live cells.

Post-translational modifications of specific amino acids play major roles in regulating protein functions.[1] The major functional sites of proteins that typically respond to redox perturbations contain cysteine (Cys) residues.[1] Glutathione (GSH) plays a pivotal role in maintaining the cellular antioxidant defence system.[1e,f,2a] Abnormal levels of GSH are linked to many diseases such as HIV, aging, neurodegenerative diseases and cancer.[2a] Cys is one of the three main precursors that are required for GSH synthesis.[1b,e,f] Apart from this crucial role in human physiology, deficiency of Cys also has adverse influences on child growth, depigmentation of hair, edema, liver damage, skin lesions and weakness.[1c,d] Literature reports also suggest that free Cys is not ideally suited for human physiology for its toxicity and facile oxidation.[2b] Thus, appropriate and stable Cys-derivatives are prescribed as supplements, which participate in enzymatic reactions to liberate Cys for maintaining its optimum concentration in human blood plasma (HBP). Whey protein (WP) concentrate is also used as an effective Cys supplement for GSH replenishment in its immune deficient state.[3a] Thus, specific detection and estimation of Cys and its derivatives have significance in clinical research and diagnostics. However, interference from Hcy (Homocysteine) and GSH makes it difficult owing to the similarities in structure and reactivity. Also, some of the reagents, which are commonly adopted for different types of chemodosimetric detection of Cys, also react with CN^-, an efficient nucleophile with relatively low hydration enthalpy.[3b,4] All these add to the challenge in designing a reagent for the specific detection and estimation of Cys in biofluids. HPLC is the most conventional methodology that is being adopted for Cys estimation in biofluids. However, such a procedure involves an intricate sample preparation process and more importantly requires a postcolumn derivatization technique.[4] Considering the complexity involved in such processes, recent efforts are focused on designing fluorescence-based molecular probes for selective estimation of Cys in biofluids as well as for use as an imaging reagent for detection of intracellular distribution of Cys.[1c,d] Strategies like chemodosimetric procedures or metal–Cys coordinations have been usually adopted for specific recognition of Cys in aqueous medium.[5] Barring some reports,[6] the examples of the specific detection of Cys or its residues in the presence of the above referred competing biothiols are limited. Moreover, none of these reagents were utilized for developing an assay for enzyme like aminoacylase-1 for *in situ* generation of Cys from a prescribed drug *N*-acetyl cysteine (NAC), which is generally used for treating psychiatric and many other disorders[7] or for the estimation of Cys/cystine residues in cow's milk whey.

Keeping these in mind, we have designed a chemodosimetric probe (**L**) for a specific reaction with Cys in the presence of all other amino acids (including Hcy and GSH), and all common anions and cations (alkali, alkaline earth and transition metal ions that are common in human physiology) in a physiologically relevant aq. medium. Using the specificity of this reagent **L** towards Cys, we could estimate Cys residues with free sulfhydryl functionality in whey protein as well as we could develop an efficient methodology for probing the release of Cys from NAC by aminoacylase-1, an important enzyme for human physiology. Such examples are scarce in the contemporary literature.

Kim and co-workers reported the role of pK_a in achieving the desired specificity to Cys (in the presence of Hcy & GSH) for participating in Michael-type reactions.[6d] We have adopted this methodology for designing an efficient chemodosimetric probe (**L**, Scheme 1) for Cys. The choice of nitro olefin not only helped in achieving a favourable intramolecular charge transfer (ICT) transition, but also offered us the desired functionality for participating in the Michael-type reaction.[5j]

[a] *Organic Chemistry Division, CSIR-National Chemical Laboratory, Pune - 411008, India. E-mail: a.das@ncl.res.in; Fax: +91 2025902629; Tel: +91 2025902385*

[b] *Chromatin and Disease Laboratory, National Center for Cell Science, Pune, 411007, India. E-mail: samit@nccs.res.in*

† Invention disclosure application no. 1061/DEL/2015.

‡ Electronic supplementary information (ESI) available: Experimental procedures and additional data. See DOI: 10.1039/c5cc04876a

analytical chemistry

Article

pubs.acs.org/ac

A Cysteine-Specific Fluorescent Switch for Monitoring Oxidative Stress and Quantification of Aminoacylase-1 in Blood Serum

Anila H A,[†] Firoj Ali,[†] Shilpi Kushwaha,[†] Nandaraj Taye,[‡] Samit Chattopadhyay,[*,‡,#] and Amitava Das[*,†,§]

[†]Organic Chemistry Division, CSIR-National Chemical Laboratory, Pune 411008, India

[§]CSIR-Central Salt and Marine Chemicals Research Institute, Bhavnagar 364002, Gujrat, India

[‡]Chromatin and Disease Laboratory, National Center for Cell Science, Pune 411007, India

[#]CSIR-Indian Institute of Chemical Biology, Kolkata 700032, India

Supporting Information

ABSTRACT: Reagents that allows detection and monitoring of crucial biomarkers with luminescence ON response have significance in clinical diagnostics. A new coumarin derivative is reported here, which could be used for specific and efficient chemodosimetric detection of cysteine, an important biomarker. The probe is successfully used for studying the biochemical transformation of N-acetylcysteine, a commonly prescribed Cys supplement drug to Cys by aminoacylase-1 (ACY-1), an important and endogenous mammalian enzyme. The possibility of using this reagent for quantification of ACY-1 in blood serum samples is also explored. Nontoxic nature and cell membrane permeability are key features of this probe and are ideally suited for imaging intracellular Cys in normal and cancerous cell lines. Our studies have also revealed that this reagent could be utilized as a redox switch to monitor the hydrogen-peroxide-induced oxidative stress in living SW480 cell lines. Peroxide-mediated cysteine oxidation has a special significance for understanding the cellular-signaling events.

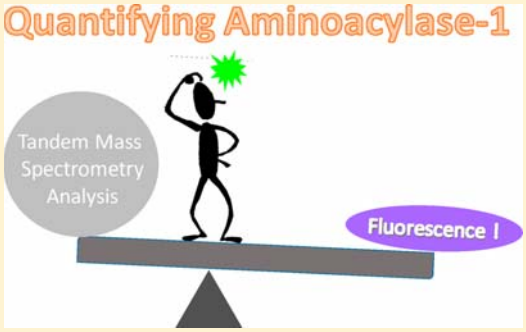

Recognition and visualization of molecular targets using fluorescent markers are vital in clinical diagnosis and real-time monitoring of analytes of biological importance. Cysteine (Cys) is one such analyte of interest because of its vital role in human physiology. Being one of the reactive sulfur species (RSS), Cys is often found in the majority of the proteins and is involved in various catalytic and regulatory functions.[1] Reversible oxidation of Cys residues is known to play a key role in intracellular-signaling mechanisms, and understanding the thiol-redox chemistry in cellular processes is crucial for developing a better insight into this issue.[2] The expected concentration of Cys in human blood plasma (HBP) sample for a healthy person is 240−360 μM.[3] Any abnormality in Cys level is a marker for many diseases. Deficiency of Cys has adverse influences on child growth, depigmentation of hair, edema, liver damage, skin lesions, and so on. Also Cys is responsible for maintaining the optimum glutathione (GSH) concentration in human physiology.[1] It is believed that the elevated level of Cys is responsible for neurotoxicity and Alzheimer's diseases.[4] Therefore, estimation of Cys in biofluids, like HBP is crucial for understanding the occurrence of many diseases. Reactive oxygen species (ROS) cause oxidative stress in cells. ROS like hydrogen peroxide (H_2O_2) causes oxidation of Cys residues into sulfenic acid intermediates or disulfides.[5,6] Cys residues not only act as an antioxidant but also regulate H_2O_2-induced signal transduction. It has been argued that understanding the reactivity of H_2O_2 with the sulfhydryl functionality of Cys is key to understand the thiol-mediated redox processes and how this species engages in signaling.[2]

ACY-1 is an important and endogenous mammalian enzyme that plays an important role in the hydrolysis of N-acetylcysteine and releases free Cys.[7] Interestingly, ACY-1 is also an important biomarker with potential prognostic utility in patients with delayed graft function (DGF) following renal transplantation.[8−10] ACY-1 level in serum samples of patients with DGF markedly increases after kidney transplantation, and its estimation in blood serum (BS) is decisive in clinical diagnosis for the recovery and treatment of such patients.[8−10] Such quantification in a serum sample is conventionally achieved by label-free single dimensional liquid chromatography-tandem mass spectrometry analysis.[11] Currently, no literature report suggests use of any optical spectroscopic method for such purpose.

From the past few decades, significant attention has been paid to develop methods for the detection/quantification of Cys either in biological fluids or for mapping distribution of

Received: August 7, 2016
Accepted: November 10, 2016
Published: November 10, 2016

DOI: 10.1021/acs.analchem.6b03066
Anal. Chem. 2016, 88, 12161−12168

ChemComm

COMMUNICATION

View Article Online
View Journal | View Issue

Cite this: *Chem. Commun.*, 2018, **54**, 3735

Received 15th February 2018,
Accepted 19th March 2018

DOI: 10.1039/c8cc01332b

rsc.li/chemcomm

Polysulfide-triggered fluorescent indicator suitable for super-resolution microscopy and application in imaging†

Anila Hoskere A.,[a] Sreejesh Sreedharan,[b] Firoj Ali,[a] Carl G. Smythe,[c] Jim A. Thomas *[b] and Amitava Das *[ad]

A new physiologically benign and cell membrane permeable BODIPY based molecular probe, MB-S_n, specifically senses intracellular hydrogen polysulfides (H_2S_n, $n > 1$) localized in the endoplasmic reticulum. This reagent is suitable for mapping the intracellular distribution of H_2S_n by wide-field as well as super-resolution Structured Illumination Microscopy (SIM).

Hydrogen polysulfide H_2S_n is one of the reactive sulphur species (RSS) and is primarily produced in cells from 3-mercaptopyruvate by the enzyme 3-mercaptopyruvate sulfurtransferase.[1] It is also produced by the reaction of H_2S with NO.[1] H_2S_n influences many important biological functions and activities associated with H_2S. For example, it induces sulfuration, wherein a sulphur atom is added to cysteine thiol groups within proteins, causing changes in conformation and the activity of the affected protein.[2] By activating transient receptor potential (TRP) A1 channels, H_2S_n induces Ca^{2+} influx in astrocytes more efficiently than H_2S.[3,4a] It is also a potent signaling molecule that regulates the activity of tumor suppressors and transcription factors.[3]

To develop a deeper understanding of the regulatory roles of H_2S_n, it is crucial to identify appropriate reagent and methodology for efficient detection and tracking of H_2S_n within cells. Traditional spectroscopic methods for the detection of H_2S_n rely on measuring characteristic absorbances at 290–300 nm and 370 nm[5] – a methodology of limited application due to its low sensitivity. Another methodology using mass spectroscopic technique requires derivatization of the sample with monobromobimane to produce chemically unstable derivatives that often lead to inaccurate results.[3] Moreover, none of these methods are suitable for studying *in vivo* biological processes or mapping the intracellular distribution of H_2S_n. Thus, there is clear scope to develop an efficient methodology for detection of H_2S_n using a fluorescence-based molecular probe.[4c] There are several literature reports for detection of other biothiols such as cysteine, glutathione, and H_2S using this approach.[6] However, such reports are scarce for H_2S_n due to the lack of proper understanding about its reactivity. Recent literature reports reveal that most polysulfide probes rely on a nucleophilic substitution reaction involving the polysulfide moiety and a 2-fluoro-5-nitro benzoate derivative, while the transient species undergo spontaneous cyclization to release the fluorophore in its "on state".[7] However, such probes also participate in nucleophilic substitution reaction with other biothiols, and this limits their application as a specific reagent for H_2S_n. Another approach involves the use of H_2S_n induced aziridine ring opening reactions.[8] Such probes show good selectivity for H_2S_n, however, their utility is largely limited to cell-free studies. Barring some recent reports from Xian and co-workers, H_2S_n specific probes are still very sparse in the literature.[9] However; there is no report on an organelle specific H_2S_n probe that is suitable for Structured Illumination Microscopy (SIM).[10a,b]

Fluorescence microscopy has proved to be an invaluable tool for imaging studies as well as for studying the functions of specific analytes in living systems.[4b,c] In many instances, the applicability of this technique is limited by its relatively poor spatial resolution.[10a] However, recent advances in super-resolution microscopy (SRM) have broken the diffraction limit of conventional optical-based techniques providing hitherto inaccessible imaging capabilities.[10b,d] One such SRM technique is SIM, which provides an appreciable increase in resolutions (100–120 nm)[10a,b] with minimal disruption of data acquisition rate. SIM requires considerably lower illumination intensities compared to other super-resolution microscopies like STORM and STED,[10c,d] making it particularly suited to live cell imaging.

With these facts in mind, we have developed a BODIPY based probe **MB-S_n** that could exclusively detect H_2S_n in physiological conditions as well as it could be used for mapping endogenous H_2S_n localized in the endoplasmic reticulum of cells. Importantly, the probe is also compatible for SIM studies.

[a] *Organic Chemistry Division, CSIR-National Chemical Laboratory, Pune-411008, India*
[b] *Department of Chemistry, University of Sheffield, Sheffield, S3 7HF, UK. E-mail: james.thomas@sheffield.ac.uk*
[c] *Department of Biomedical Science, University of Sheffield, Sheffield, S10 2TN, UK*
[d] *CSIR-Central Salt & Marine Chemicals Research Institute, Bhavnagar 364002, Gujarat, India. E-mail: a.das@csmcri.res.in*

† Electronic supplementary information (ESI) available. See DOI: 10.1039/c8cc01332b

Copyright Clearance Center RightsLink®

Home | Account Info | Help

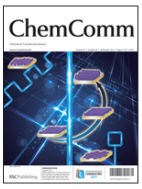

Title:	A fluorescent probe for specific detection of cysteine in the lipid dense region of cells
Author:	Firoj Ali,Anila H. A.,Nandaraj Taye,Rajesh G. Gonnade,Samit Chattopadhyay,Amitava Das
Publication:	Chemical Communications (Cambridge)
Publisher:	Royal Society of Chemistry
Date:	Sep 24, 2015

Logged in as:
Anila Ashoka
LOGOUT

This reuse request is free of charge. Please review guidelines related to author permissions here:
http://www.rsc.org/AboutUs/Copyright/Permissionrequests.asp

BACK | CLOSE WINDOW

Copyright Clearance Center RightsLink®

Home | Account Info | Help

Title:	A highly selective ratiometric near-infrared fluorescent cyanine sensor for cysteine with remarkable shift and its application in bioimaging
Author:	Zhiqian Guo,SeongWon Nam,Sungsu Park,Juyoung Yoon
Publication:	Chemical Science
Publisher:	Royal Society of Chemistry
Date:	Jun 13, 2012

Logged in as:
Anila Ashoka
LOGOUT

Order Completed

Thank you for your order.

This Agreement between Mr. Anila Ashoka ("You") and Royal Society of Chemistry ("Royal Society of Chemistry") consists of your license details and the terms and conditions provided by Royal Society of Chemistry and Copyright Clearance Center.

Your confirmation email will contain your order number for future reference.

printable details

License Number	4293450749751
License date	Feb 21, 2018
Licensed Content Publisher	Royal Society of Chemistry
Licensed Content Publication	Chemical Science
Licensed Content Title	A highly selective ratiometric near-infrared fluorescent cyanine sensor for cysteine with remarkable shift and its application in bioimaging
Licensed Content Author	Zhiqian Guo,SeongWon Nam,Sungsu Park,Juyoung Yoon

Copyright Clearance Center RightsLink®

Home | Account Info | Help

ACS Publications
Most Trusted. Most Cited. Most Read.

Title:	Highly Selective Two-Photon Fluorescent Probe for Ratiometric Sensing and Imaging Cysteine in Mitochondria
Author:	Weifen Niu, Lei Guo, Yinhui Li, et al
Publication:	Analytical Chemistry
Publisher:	American Chemical Society
Date:	Feb 1, 2016

Logged in as:
Anila Ashoka
LOGOUT

PERMISSION/LICENSE IS GRANTED FOR YOUR ORDER AT NO CHARGE

This type of permission/license, instead of the standard Terms & Conditions, is sent to you because no fee is being charged for your order. Please note the following:

- Permission is granted for your request in both print and electronic formats, and translations.
- If figures and/or tables were requested, they may be adapted or used in part.
- Please print this page for your records and send a copy of it to your publisher/graduate school.
- Appropriate credit for the requested material should be given as follows: "Reprinted (adapted) with permission from (COMPLETE REFERENCE CITATION). Copyright (YEAR) American Chemical Society." Insert appropriate information in place of the capitalized words.
- One-time permission is granted only for the use specified in your request. No additional uses are granted (such as derivative works or other editions). For any other uses, please submit a new request.

Order Completed

Thank you for your order.

This Agreement between Mr. Anila Ashoka ("You") and Royal Society of Chemistry ("Royal Society of Chemistry") consists of your license details and the terms and conditions provided by Royal Society of Chemistry and Copyright Clearance Center.

Your confirmation email will contain your order number for future reference.

printable details

License Number	4293451092348
License date	Feb 21, 2018
Licensed Content Publisher	Royal Society of Chemistry
Licensed Content Publication	Chemical Communications (Cambridge)
Licensed Content Title	A fluorescent chemodosimeter specific for cysteine: effective discrimination of cysteine from homocysteine
Licensed Content Author	Honglin Li,Jiangli Fan,Jingyun Wang,Maozhong Tian,Jianjun Du,Shiguo Sun,Pingping Sun,Xiaojun Peng

Order Completed

Thank you for your order.

This Agreement between Mr. Anila Ashoka ("You") and Royal Society of Chemistry ("Royal Society of Chemistry") consists of your license details and the terms and conditions provided by Royal Society of Chemistry and Copyright Clearance Center.

Your confirmation email will contain your order number for future reference.

printable details

License Number	4293451284388
License date	Feb 21, 2018
Licensed Content Publisher	Royal Society of Chemistry
Licensed Content Publication	Chemical Communications (Cambridge)
Licensed Content Title	A ratiometric fluorescent probe for specific detection of cysteine over homocysteine and glutathione based on the drastic distinction in the kinetic profiles
Licensed Content Author	Lin Yuan,Weiying Lin,Yueting Yang

Title: A cysteine-selective fluorescent probe for the cellular detection of cysteine

Author: Hyo Sung Jung,Ji Hye Han,Tuhin Pradhan,Sooyeon Kim,Seok Won Lee,Jonathan L. Sessler,Tae Woo Kim,Chulhun Kang,Jong Seung Kim

Publication: Biomaterials

Publisher: Elsevier

Date: January 2012

Order Completed

Thank you for your order.

This Agreement between Mr. Anila Ashoka ("You") and Elsevier ("Elsevier") consists of your license details and the terms and conditions provided by Elsevier and Copyright Clearance Center.

Your confirmation email will contain your order number for future reference.

printable details

License Number	4293460035752
License date	Feb 21, 2018
Licensed Content Publisher	Elsevier
Licensed Content Publication	Biomaterials
Licensed Content Title	A cysteine-selective fluorescent probe for the cellular detection of cysteine
Licensed Content Author	Hyo Sung Jung,Ji Hye Han,Tuhin Pradhan,Sooyeon Kim,Seok Won Lee,Jonathan L. Sessler,Tae Woo Kim,Chulhun Kang,Jong Seung Kim

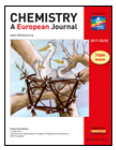

Title: A Sensitive and Selective Fluorescent Probe for Cysteine Based on a New Response-Assisted Electrostatic Attraction Strategy: The Role of Spatial Charge Configuration

Author: Xin Zhou,Xuejun Jin,Guangyan Sun,Xue Wu

Publication: Chemistry - A European Journal

Publisher: John Wiley and Sons

Date: Apr 17, 2013

Order Completed

Thank you for your order.

This Agreement between Mr. Anila Ashoka ("You") and John Wiley and Sons ("John Wiley and Sons") consists of your license details and the terms and conditions provided by John Wiley and Sons and Copyright Clearance Center.

Your confirmation email will contain your order number for future reference.

printable details

License Number	4293460447556
License date	Feb 21, 2018
Licensed Content Publisher	John Wiley and Sons
Licensed Content Publication	Chemistry - A European Journal
Licensed Content Title	A Sensitive and Selective Fluorescent Probe for Cysteine Based on a New Response-Assisted Electrostatic Attraction Strategy: The Role of Spatial Charge Configuration
Licensed Content Author	Xin Zhou,Xuejun Jin,Guangyan Sun,Xue Wu
Licensed Content Date	Apr 17, 2013
Licensed Content Pages	8

Order Completed

Thank you for your order.

This Agreement between Mr. Anila Ashoka ("You") and John Wiley and Sons ("John Wiley and Sons") consists of your license details and the terms and conditions provided by John Wiley and Sons and Copyright Clearance Center.

Your confirmation email will contain your order number for future reference.

printable details

License Number	4293441037136
License date	Feb 21, 2018
Licensed Content Publisher	John Wiley and Sons
Licensed Content Publication	Angewandte Chemie International Edition
Licensed Content Title	The Development of Fluorescent Probes for Visualizing Intracellular Hydrogen Polysulfides
Licensed Content Author	Wei Chen,Ethan W. Rosser,Tetsuro Matsunaga,Armando Pacheco,Takaaki Akaike,Ming Xian
Licensed Content Date	Sep 18, 2015

Order Completed

Thank you for your order.

This Agreement between Mr. Anila Ashoka ("You") and Royal Society of Chemistry ("Royal Society of Chemistry") consists of your license details and the terms and conditions provided by Royal Society of Chemistry and Copyright Clearance Center.

Your confirmation email will contain your order number for future reference.

printable details

License Number	4293441422869
License date	Feb 21, 2018
Licensed Content Publisher	Royal Society of Chemistry
Licensed Content Publication	Chemical Communications (Cambridge)
Licensed Content Title	A near-infrared fluorescence off–on probe for sensitive imaging of hydrogen polysulfides in living cells and mice in vivo
Licensed Content Author	Yu Fang,Wei Chen,Wen Shi,Hongyu Li,Ming Xian,Huimin Ma

Title: Fluorescent Biomembrane Probe for Ratiometric Detection of Apoptosis

Author: Vasyl V. Shynkar, Andrey S. Klymchenko, Corinne Kunzelmann, et al

Publication: Journal of the American Chemical Society

Publisher: American Chemical Society

Date: Feb 1, 2007

PERMISSION/LICENSE IS GRANTED FOR YOUR ORDER AT NO CHARGE

This type of permission/license, instead of the standard Terms & Conditions, is sent to you because no fee is being charged for your order. Please note the following:

- Permission is granted for your request in both print and electronic formats, and translations.
- If figures and/or tables were requested, they may be adapted or used in part.
- Please print this page for your records and send a copy of it to your publisher/graduate school.
- Appropriate credit for the requested material should be given as follows: "Reprinted (adapted) with permission from (COMPLETE REFERENCE CITATION). Copyright (YEAR) American Chemical Society." Insert appropriate information in place of the capitalized words.
- One-time permission is granted only for the use specified in your request. No additional uses are granted (such as derivative works or other editions). For any other uses, please submit a new request.